ROBUST AUTOLANDING SYSTEM DESIGN FOR A COMBAT AIRCRAFT ON THE GROUND

MUHARIP HAVA ARACI IÇIN YERDE GÜRBÜZ OTOMATIK INIŞ SISTEMI TASARIMI

SERDAR AVŞAR

ASST. PROF. DR. EMİR KUTLUAY

Thesis Supervisor

Submitted to
Graduate School of Science and Engineering of Hacettepe University
as a Partial Fulfillment of the Requirements
for the Award of the Degree of Master of Science
in Mechanical Engineering.

2023

ABSTRACT

ROBUST AUTOLANDING SYSTEM DESIGN FOR A COMBAT AIRCRAFT ON THE GROUND

Serdar AVŞAR

Master of Science, Department of Mechanical Engineering

Supervisor: Asst Prof. Dr. Emir KUTLUAY

January 2023, 162 pages

Within the scope of this thesis, a 6-degree-of-freedom model of a combat aircraft is created. Apart from the flight dynamics, landing gear dynamics on the ground are also modeled. After that, a robust autolanding system is designed for the autoland part after the main landing gears touch the ground until the aircraft stops. For the outer guidance loop line following guidance algorithms are compared and the linear sliding mode guidance algorithm is found to be the best in terms of the combination of line tracking and required control effort. For the inner autopilot loop sliding mode control (SMC) and proportional integral derivative (PID) control are used. Feedforward gains are also added for increased disturbance rejection. The designed autoland systems are tested against crosswind, brake failures, steering failure, and decreased cornering power factor for main landing gear tires. It has been found that SMC is as robust as PID control for inner loop applications.

Keywords: combat aircraft, autoland, robust control, sliding mode control, landing gear model

ÖZET

MUHARIP HAVA ARACI IÇIN YERDE GÜRBÜZ OTOMATIK INIŞ SISTEMI TASARIMI

Serdar AVŞAR

Yüksek Lisans, Makine Mühendisliği Bölümü

Tez Danışmanı: Dr. Öğretim Üyesi Emir KUTLUAY

Ocak 2023, 162 sayfa

Bu tez kapsamında muharip bir hava aracı 6 serbestlik dereceli olarak modellenmiştir. Havadaki dinamiğe ek olarak yerdeki dinamik için de 3 tekerlekli bir iniş takımı modeli oluşturulmuştur. Daha sonrasında bu model kullanılarak hava aracının iniş esnasında tekerleği yere koymasından durmasına kadar olan süreç için gürbüz bir otomatik iniş sistemi tasarlanmıştır. Literatürdeki çizgi takip algoritmaları karşılaştırılmış ve çizgi takip ve kontrol eforu birlikte değerlendirildiğinde doğrusal kayan kip güdüm kanununun en başarılı olduğu bulunmuştur. İç döngü otopilot tasarımı için kayan kip kontrol (SMC) ve doğrusal integral türev (PID) kontrol yöntemleri kullanılmıştır. Bozucu bastırma kapasitesini arttırmak için ileri besleme kazançları kullanılmıştır. Tasarlanan otomatik iniş sistemleri yan rüzgar, fren arızaları, direksiyon arızası ve ana iniş takımı tekerleklerinin yanal etkinliklerindeki değişimlere göre test edilmiştir. Sonuç olarak SMC denetleyicinin en az PID denetleyici kadar gürbüz olduğu bulunmuştur.

Anahtar Kelimeler: muharip hava aracı, otomatik iniş, gürbüz kontrol, kayan kip kontrol, iniş takımı modeli

ACKNOWLEDGMENTS

Firstly, I would like to thank my thesis supervisor Dr. Emir Kutluay for his guidance. His invaluable insight and feedback helped me endure the process of writing this Master's Thesis.

Secondly, I would like to thank my lovely wife Gözde for her tolerance and support during the late nights and holidays I spent writing this thesis.

I would also thank my mother, father, and sister for their continuous support during this journey.

I thank my colleague, friend, and mentor Hüseyin Aktan for his invaluable feedback during the thesis.

I thank all my colleagues for their support during this thesis. I especially thank my superiors Hüseyin Yağcı and Orkun Şimşek for helping to choose this topic as my field of expertise and thesis subject.

I thank my former and current chiefs Halit Oruç and Halil Kaya for their tolerance, support, and feedback and Hakan Tiftikçi for his feedback.

I would also like to thank Dr. Erhan Solakoğlu for his support and motivation that helped me finish this thesis.

Lastly, I would like to thank my company Turkish Aerospace for the academic permission opportunity that it provides to working graduate students.

TABLE OF CONTENTS

TABLE OF FIGURES

TABLE OF CHARTS

SIGNS AND ABBREVIATIONS

Signs

a_{ref}	Acceleration command
a_{tire}	Ratio of gross footprint area to net footprint area
a_y	Lateral acceleration
$a_{y_{ref}}$	Lateral acceleration reference
b	Wingspan of the aircraft
c	A constant in sliding mode example
C	Cornering power factor
$\bar{c}$	Mean aerodynamic chord of the aircraft
c_c	A tire coefficient
C_{corr}	Corrected cornering power factor value
c_{strut}	Strut damping coefficient
c_{tire}	Tire damping coefficient
$C_{y,z}$	Lateral force coefficient of the tire
c_z	A nondimensional tire coefficient
c_1	A constant in sliding mode example
d	Distance of the aircraft from the path for optimal guidance
d_b	Minimum distance from the path for optimal guidance
d_{tire}	Diameter of the tire
e	Error between position reference and position output
$\dot{e}$	Error between velocity reference and velocity output
f_{acc}	Tire acceleration factor
F_{brake}	Brake force

f_{corr}	Cornering power factor correction coefficient
F_{c_tire}	Tire damping force
$\vec{F}_{landing\_gear}$	Landing gear forces and moments
F_{k_tire}	Tire spring force
F_{strut}	Resultant force on the strut
F_{tire}	Resultant force on the tire
F_{x_tire}	Longitudinal force of the tire
F_{y_tire}	Lateral force of the tire
F_{z_tire}	Vertical force of the tire
g	Gravitational acceleration
G_{ad}	Transfer function of air data sensors
G_{at}	Transfer function of attitude sensors
G_{cs}	Transfer function of control surface actuators
G_{ra}	Transfer function of rate sensors
$h_{runway/lg}$	Altitude of the runway at the position of the landing gear
I_{xx}	Roll moment of inertia
I_{yy}	Pitch moment of inertia
I_{zz}	Yaw moment of inertia
I_{xy}	Product moment of inertia in xy plane
I_{xz}	Product moment of inertia in xz plane
I_{yz}	Product moment of inertia in yz plane
k	Constant
k_1	Constant used in sliding mode control law
k_2	Constant used in sliding mode control law
k_{strut}	Strut stiffness coefficient
k_{tire}	Tire stiffness coefficient

L	Body axis moment component in x axis
L_1	Distance between the aircraft and the target for nonlinear guidance
m	Aircraft mass
M	Body axis moment component in y axis
m_{wheel}	Mass of the landing gear wheel
N	Body axis moment component in z axis
N_{PG}	Proportional guidance proportionality constant
p	Body axis angular velocity component in x axis
p_g	Tire gross footprint pressure
p_n	Tire net footprint pressure
p_r	Tire rated pressure
p_t	Tire pressure
$\vec{p}_{aircraft/earth}$	Position of the aircraft with respect to earth in NED axis
$\vec{p}_{lg}$	Position of the tire with respect to body axis with strut displacement
$\vec{p}_{lg0}$	Position of the tire with respect to body axis without strut displacement
$\vec{p}_{lg/aircraft}$	Position of the landing gear with respect to the aircraft in NED axis
$\vec{p}_{lg/earth}$	Position of the landing gear with respect to earth in NED axis
q	Body axis angular velocity component in y axis
r	Body axis angular velocity component in z axis
r_c	Radius of circles used in predictive guidance
$\vec{r}_{tire\_aircraft}$	Position of the tire with respect to aircraft
s	Strut position
S	Wing area of the aircraft
s_{lmg}	Strut position of left main landing gear
s_{mgavg}	Average of main gear strut displacements

s_{mgdiff}	Difference of main gear strut displacements
s_{ng}	Strut position of nose landing gear
s_{rmg}	Strut position of right main landing gear
s_{tire}	Tire displacement
s_1	Auxiliary sliding variable for sliding mode example
$\dot{s}$	Strut velocity
$\dot{s}_{lmg}$	Strut velocity of left main landing gear
$\dot{s}_{mgavg}$	Average of main gear strut velocities
$\dot{s}_{mgdiff}$	Difference of main gear strut velocities
$\dot{s}_{ng}$	Strut velocity of nose landing gear
$\dot{s}_{rmg}$	Strut velocity of right main landing gear
$\dot{s}_{tire}$	Tire velocity
$\ddot{s}$	Strut acceleration
t_r	Reaching time in sliding mode control
u	Body axis velocity component in x axis
u_{eq}	Equivalent control input in sliding mode
u_{ned}	Velocity component in north axis of NED coordinates
u_{tire}	Longitudinal velocity of the tire in tire axis
u_1	Force input in sliding mode example system
$\hat{u}_{eq}$	Estimated equivalent control input
v	Body axis velocity component in y axis
V	Speed of the aircraft
v_d	Normal velocity of the aircraft to the path for optimal guidance
V_L	Lyapunov function
v_{ned}	Velocity component in east axis of NED coordinates

v_{tire}	Lateral velocity of the tire in tire axis
V_{ref}	Reference velocity used in vector guidance law
v_1	New input for auxiliary sliding mode example
$\vec{v}_{aircraft}$	Velocity of the aircraft in body axis
$\vec{v}_{aircraft\_ned}$	Velocity of the aircraft in NED axis
$\vec{v}_{lg}$	Velocity of landing gear in body axis
$\vec{v}_{tire\_ned}$	Velocity of the tire in NED axis
w	Body axis velocity component in z axis
W	Weight of the aircraft
w_{ned}	Velocity component in down axis of NED coordinates
w_{tire}	Tire width
w_1	Input variable for sliding mode example
w_2	Input variable for sliding mode example
x	Longitudinal position
X	Body axis force component in x axis
x_{lg}^{ned}	North position of landing gear tire in NED axis
x_1	First state in sliding mode example system
x_2	Second state in sliding mode example system
y	Lateral position
Y	Body axis force component in y axis
y_{lg}^{ned}	East position of landing gear tire in NED axis
z	Vertical position
Z	Body axis force component in z axis
z_1	Estimation error of sliding mode observer
α	A constant in sliding mode example

β	Sideslip angle
β_{tire}	Lateral slip angle of the aircraft tire
γ	Flight path angle
δ_{ail}	Aileron input of the aircraft
δ_{ele}	Elevator input of the aircraft
$\delta_{left_{brake}}$	Left brake input
δ_{pedal}	Pedal input
$\delta_{right_{brake}}$	Right brake input
δ_{rud}	Rudder input of the aircraft
$\delta_{steering}$	Steering angle input
δ_{tire}	Tire compression
δ_{thr}	Throttle input of the aircraft
Δt	Specified time difference
ΔV	Speed of aircraft with respect to the target
Δx	Longitudinal position difference
ε	Infinitesimally small number
η	Arc angle for nonlinear guidance law
θ	Pitch Euler angle
$\dot{\lambda}$	Rate of change of line-of-sight angle
μ_{roll}	Rolling resistance coefficient
μ_{max}	Maximum coefficient of friction
ξ	Angle of the target with respect to the aircraft
ρ	Control gain sliding mode example
σ	Sliding surface equation
T_{a_y}	Time period of lateral acceleration dynamics

ϕ	Roll Euler angle
χ	Track angle
χ_{ref}	Reference track angle
χ^{d}	Track angle of the vector in the near field
χ^{∞}	Track angle of the vector in the far field
ψ	Yaw Euler angle
$\vec{\omega}_{aircraft}$	Angular velocity of the aircraft in body axis

Abbreviations

CG	Center of gravity
CP	Critical point used in predictive guidance
DOF	Degree of freedom
LOS	Line of sight
LP	Line point used in predictive guidance
LPF	Low pass filter
LQG	Linear quadratic gaussian
MP	Midpoint used in predictive guidance
NED	North-East-Down
PI	Proportional integral
PID	Proportional integral derivative
QFT	Quantitative feedback theory
SHSS	Steady heading steady sideslip
SLERP	Spherical linear interpolation
SMC	Sliding mode control
TAI	Turkish Aerospace Industries

TAS	True air speed
UAV	Unmanned aerial vehicle

1. INTRODUCTION

1.1 MOTIVATION

Landing is one of the most dangerous parts of the mission profile of an aircraft. Various accidents happen during landing. One of these types of accidents is runway excursions. Aircraft can get outside of the runway by diverging to one side. Examples can be seen in Figure 1.1 where a Pegasus Airlines aircraft had a runway excursion in 2017 in Trabzon Airport and Figure 1.2 where another aircraft had a runway excursion in Maastricht Aachen Airport.

Figure 1.1 Runway Excursion in Trabzon Airport [1].

Figure 1.2 Runway excursion in Maastricht Aachen Airport [2].

These types of accidents happen fairly frequently as can be seen in Figure 1.3 which shows the runway accident numbers for years between 2010 to 2014 and in Figure 1.4 where runway accident percentages by types of accidents can be found for the same period.

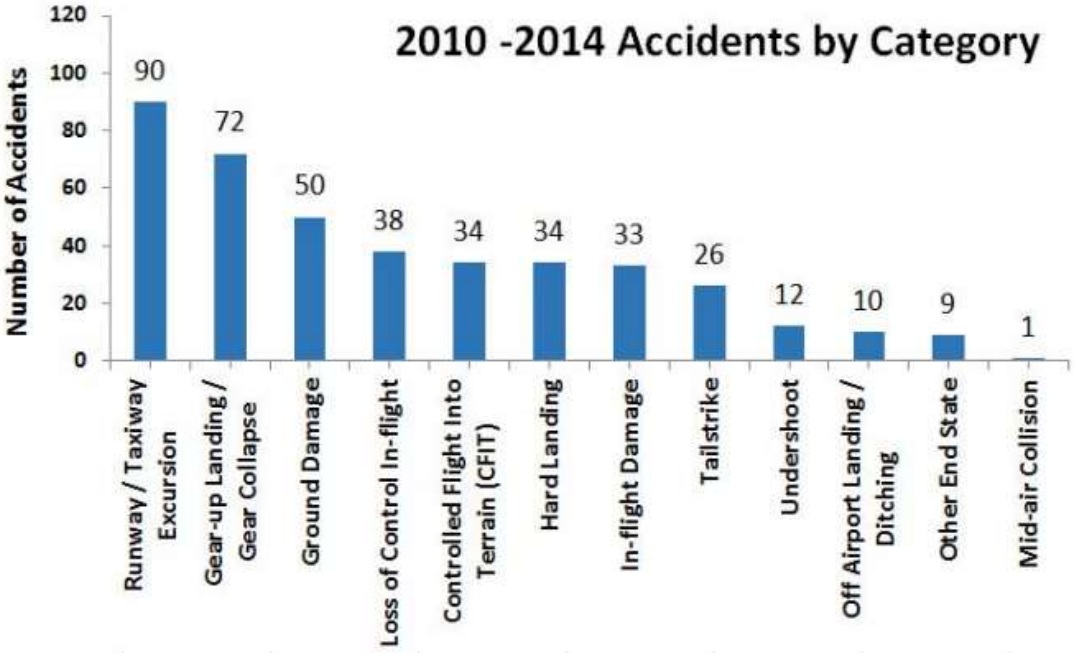

Figure 1.3 Number of runway accidents by category [3].

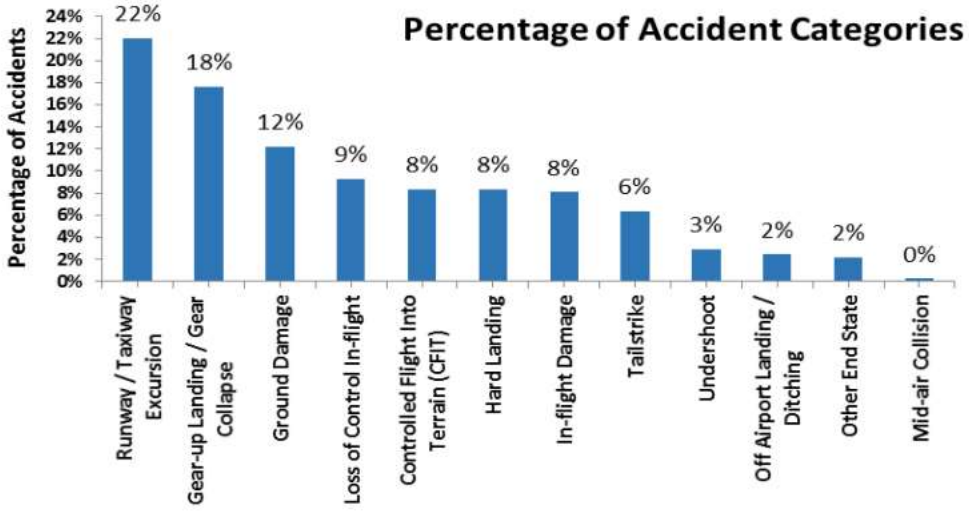

Figure 1.4 Percentage of runway accidents by category [3].

As can be seen from Figure 1.3 and Figure 1.4 excursions are the most common runway accidents. These runway excursions can occur because of severe crosswind and mechanical failures.

Autoland systems are getting widespread in recent years. They can be used in piloted or unmanned aircrafts. A few example applications in Türkiye include Anka and Aksungur (Figure 1.5) drones that use novel autoland systems. Hürjet (Figure 1.6) and TFX aircraft prototypes may also use autoland systems in the future.

Figure 1.5 a. TAI Anka drone [4] that use an autoland system, Figure 1.5 b. TAI Aksungur drone [5] also uses an autoland system.

Figure 1.6 TAI Hürjet [6] jet trainer and light combat aircraft may have an autoland system in the future.

Because of the widespread usage of autoland systems at the national level there is ongoing inflation in the literature about these systems. However, the recent literature mainly focuses on the landing approach and flare parts of the landing. The landing rollout phase in which the landing gears are on the ground is equally important for the landing of the aircraft. Robust control systems must be designed for the landing rollout phase of the aircraft. The controller must be robust mainly against crosswinds and brake failures. The literature about the autoland systems will be summarized in the literature review part.

Phases of the landing must be explained in this part for clarity.

- **Approach Phase**

In this phase the aircraft approaches the runway in a constant indicated airspeed and constant descent rate until the point it starts the landing flare maneuver.

- **Landing Flare Phase**

In this phase the aircraft makes a pull-up maneuver, decreases speed and decreases the descent rate such that it touches the ground more smoothly and with less speed.

- **Landing Rollout Phase**

In this phase landing gears of the aircraft touch the ground. The aircraft slows down and stops while trying to stay inside the runway.

Phases of landing is shown in Figure 1.7 in more detail.

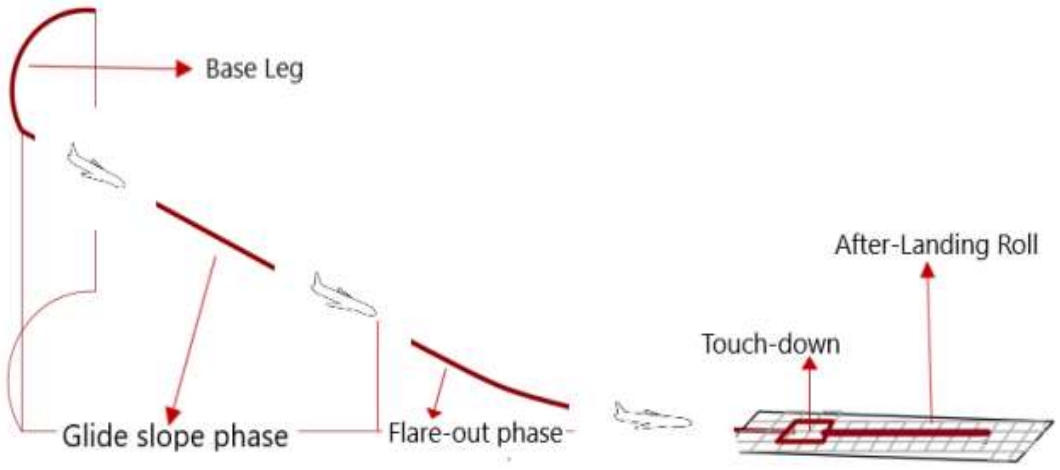

Figure 1.7 Phases of landing [7]

The motivation of this thesis is to design a robust autoland system for the landing rollout phase such that runway excursion risk is minimized.

1.2 STATE OF THE ART

In this part, state of the art is reviewed. Here, the topics that have been reviewed are aircraft models, landing gear models, aircraft trim, autoland systems, automotive lane-keeping systems, sliding mode control, autoland guidance algorithms and aircraft tire models.

1.2.1 AIRCRAFT MODELS

There are a lot of flight mechanics models for aircraft in literature. The aircraft with the most literature and data is the F-16. Thus, flight mechanics and landing gear dynamics for F-16 are used in this thesis.

The aerodynamic model of F-16 is available in the literature [8]. The parametric aerodynamics model of F-16 is presented and compared with wind tunnel data to show that they match. It is a model that have polynomial coefficients and validity of the model matches that of landing conditions. It can be used for aerodynamics calculations during landing.

The propulsion model of F-16 is also available [9]. A complete flight dynamics model of the F-16 is presented. Aerodynamics for longitudinal model and I_{yy} inertia term for the longitudinal model is also available.

Weight and geometry parameters for F-16 are also found in the literature [10]. All inertia parameters are included and equations of motion are also accessible.

1.2.2 LANDING GEAR AND AIRCRAFT TIRE MODELS

This study also includes a tricycle landing gear model. There are some papers in the literature including this in the modelling.

Georgieva et al. [11] presented a 3 degree of freedom aircraft lateral ground dynamics model. They used the data of a passenger aircraft. Brake force and crosswinds are neglected in their study.

Yin et al. [12] studied a 6 degree of freedom aircraft model and a tricycle landing gear model for a UAV application.

Bo et al. [13] studied a 6 degree of freedom aircraft model and a tricycle landing gear model for a combat aircraft application. In this study the landing gear strut states were neglected.

Coetzee et al. [14] studied a 6 degree of freedom aircraft model and a tricycle landing gear model including strut states. The dynamics are modeled using SimMechanics. An Airbus commercial airplane is modeled.

Pines et al. [15] studied a 6 degree of freedom aircraft model and a tricycle landing gear model including the strut states and the cornering power factor estimation.

For the parametric aircraft tire force modelling there is one frequently used paper [16]. Smiley et al. present empirical formulae for calculation of cornering power factor of different types of aircraft tires.

1.2.3 AIRCRAFT TRIM

Trimming and linear model derivation is necessary for controller synthesis and simulations. For this reason, aircraft trimming literature is covered.

De Marca et al. [17] investigated aircraft trimming. Two types of trim cost minimization methods have been explained. These are gradient-based minimization methods and gradient free direct search minimization methods.

Gradient-based minimization methods can also be divided into two categories named single-axis and multi-axis methods. an algorithm for aircraft trimming using multi axis Jacobian is introduced [18]. It is explained that the single axis methods are easier and used more often but multi-axis gradient search methods are faster at converging.

While most of the trimming algorithms work in the air, ground trimming is a different problem. Pashilkar [19] explained a step-by-step ground trimming procedure without an optimization scheme.

Gradient search algorithms can diverge from the solution. To cope with this problem some solutions can be used. Millidere et al. [20] improved convergence of Newton Raphson Algorithm by the addition of a line search algorithm.

1.2.4 AUTOLAND SYSTEMS

There are studies in literature about autoland systems. These mostly focus on the approach and flare phases of the landing.

Ismail et al. [21] studied a 6 degree of freedom aircraft model and an autoland controller for approach and flare phases using nonlinear direct inversion and control allocation optimization. It is also robust against control surface actuator failures and severe winds.

Lin et al. [22] studied a 6 degree of freedom aircraft model and an autoland controller for approach and flare phases using recurrent wavelet Elman neural network. The system is robust against wind turbulence.

Ismail et al. [23] studied a 6 degree of freedom aircraft model and an autoland controller for approach and flare phases using neural aided sliding mode fault-tolerant controller. The fault tolerance performance of the controller was improved using phase compensation and anti-windup schemes.

Xiong et al. [24] studied a 6 degree of freedom aircraft model including a tricycle landing gear model and an Autoland controller for approach, flare, and rollout phases using active disturbance rejection controller. The controller is robust against wind shear and wind turbulence.

Wagner et al. [25] studied a 6 degree of freedom aircraft model and an autoland controller for approach and flare phases using quantitative feedback theory (QFT) and direct digital design. QFT controller was compared against a proportional-integral (PI) controller in presence of wind disturbances.

Rao et al. [26] studied a 6 degree of freedom aircraft model and an autoland controller for approach and flare phases using SMC and PID. Simulations were started from the approach phase with a large offset from the nominal trajectory. The performance of the PID and SMC controllers was compared.

1.2.5 AUTOMOTIVE LANE KEEPING SYSTEMS

Relevant literature to the problem at hand is automotive lane keeping. While not the same, landing rollout phase is similar in terms of remaining inside a defined lane. That lane is the runway for the landing rollout phase.

There are a lot of different controller types and their comparisons in this literature.

Lee at al. [27] compared PID, linear quadratic gaussian (LQG) and H_∞ controllers for an automobile. 2 degree of freedom bicycle lateral model is used for controller synthesis and 4 degree of freedom vehicle lateral dynamics model is used for simulations. Simulations with different parameters were done and the sensitivity to parameters was estimated.

Yamamoto et al. [28] studied an optimal controller and a feedforward input by estimation of the external forces. A controller that is robust against road banks and crosswinds was developed.

Basjaruddin et al. [29] studied a Fuzzy logic controller for a lane-keeping assist system.

Sliding mode control and fuzzy logic are popular in recent automotive lane-keeping studies. Since it is easier to prove stability for a sliding mode controller this thesis will focus on sliding mode controllers.

1.2.6 SLIDING MODE CONTROL (SMC)

While there are many textbooks and papers in the subject of sliding mode control, one study is a guide to sliding mode control design [30]. As explained in detail in the paper; the main strength of the sliding mode control is its ability to reject disturbances. This is possible due to practically using infinite gain. While in theory this works flawlessly, in real life chattering and instability may occur due to unmodeled parasitic dynamics. These parasitic dynamics include delays, sensor dynamics, actuator dynamics, and noise. While there are ways to cope with this chattering and instability problems, the common solution of boundary layer control which involves using a linear gain inside a boundary [31], [32], [33] undermines the very fundamental advantage of sliding mode control which is disturbance rejection. The way to optimize the solution to the problem is to model the parasitic dynamics thoroughly such that the stability and the disturbance rejection performance of the controller is satisfied at the same time. Another method to deal with chattering phenomena is to use an observer-based sliding mode controller. In this method a high frequency bypass loop is created using an observer and the chattering phenomena are localized inside it [34], [35]. The block diagram of the observer-based SMC is shown in Figure 1.8.

Another method to deal with chattering phenomena is to use a sliding mode estimator for disturbance estimation and a classical feedback controller [36].

A part of the parasitic dynamics is actuators. Actuator bandwidths limit the bandwidth of the feedback system. Since the output of the actuator is continuous, sliding mode cannot occur. A proposition to deal with this problem is to use the actuator dynamics as a pre-filter. Another solution is to use the sliding mode estimator and linear feedback system as

explained earlier (Figure 1.9). While there are many applications of the sliding mode estimator configuration [37], [38], they are mostly basic systems with low number of states and degrees of freedom. It is questionable if it can work for a complex system of an aircraft on a runway with 14 active states, 9 degrees of freedom, and uncountable numbers of parameter uncertainties and disturbances.

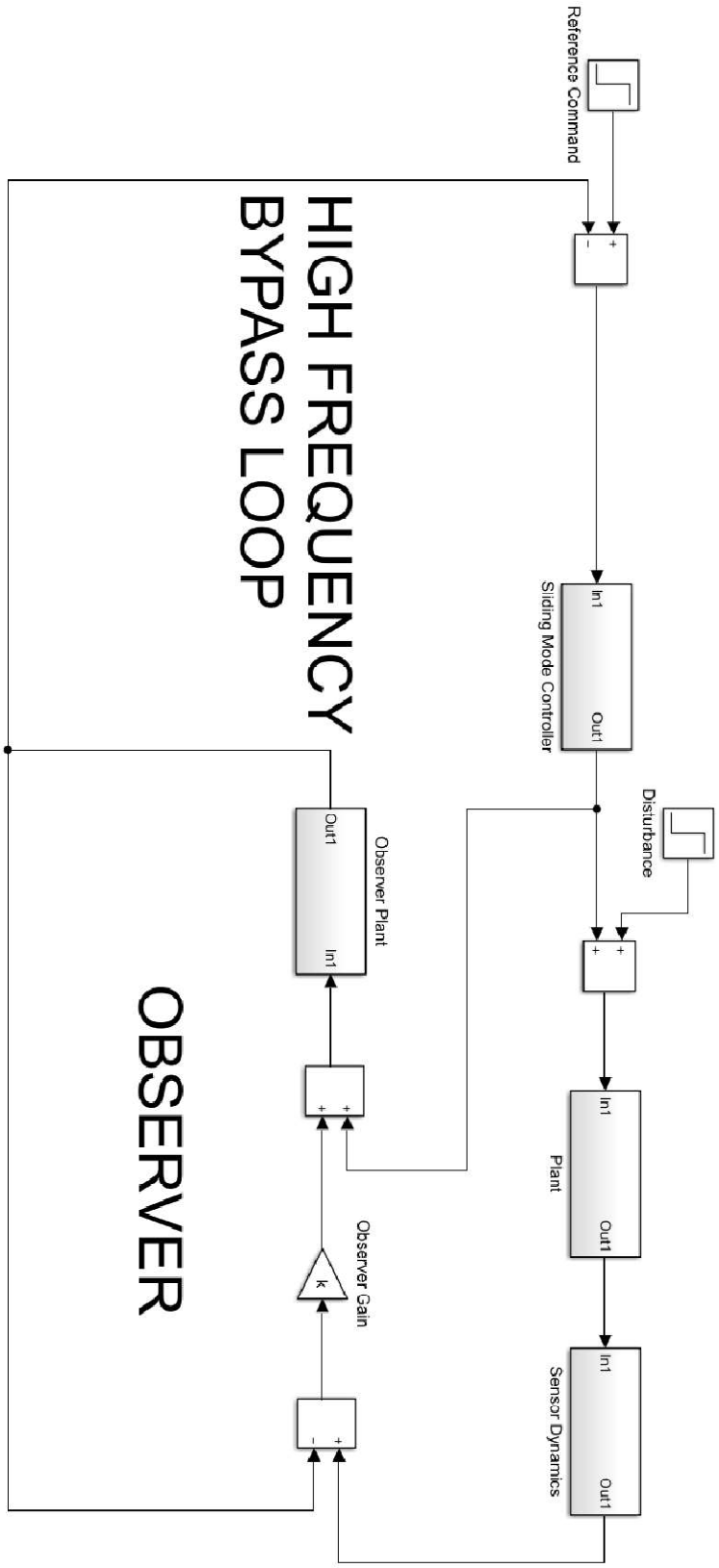

Figure 1.8 Observer-based SMC

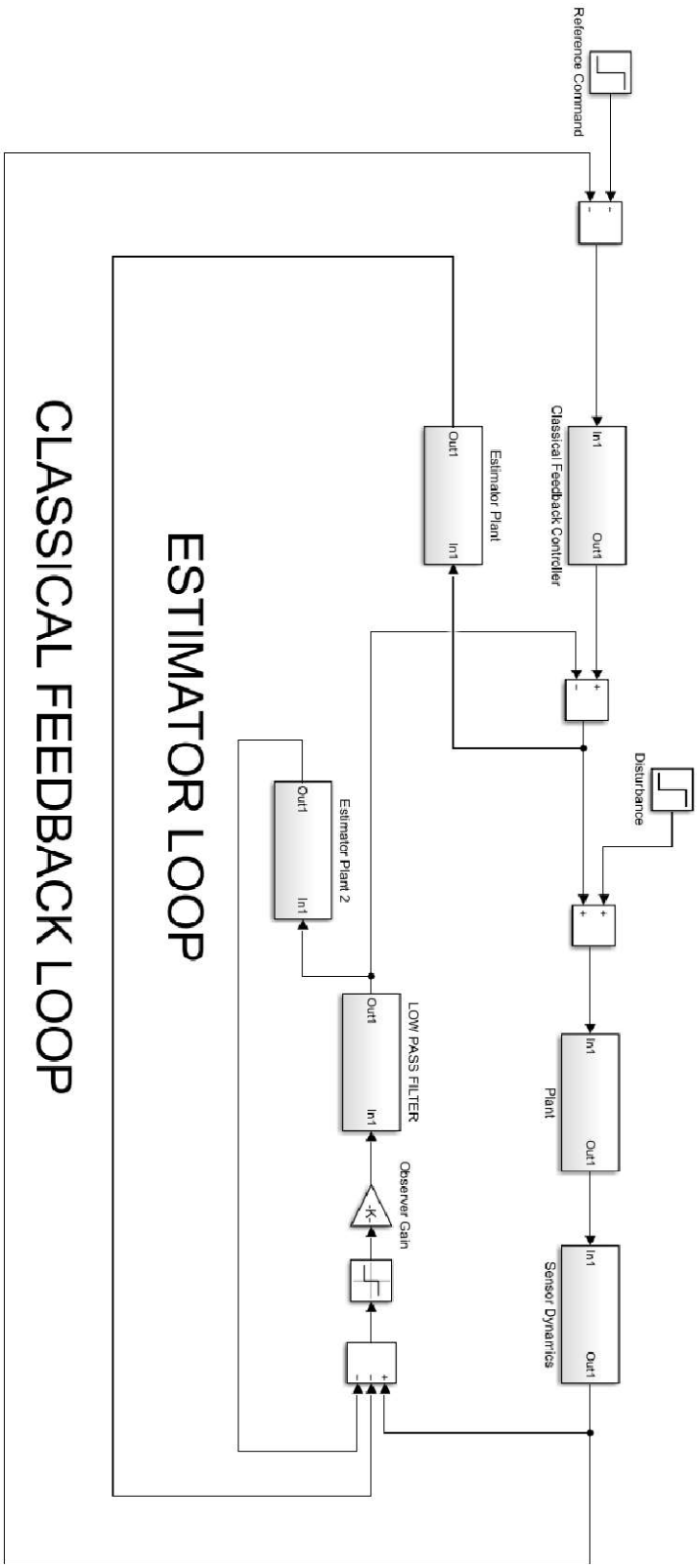

Figure 1.9 Classical feedback loop with sliding mode estimator

1.2.7 AUTOLAND GUIDANCE LAWS

For the outer loop that is responsible for tracking the midline of the runway, the guidance algorithms in the literature must be checked.

During the autoland rollout, the midline is being followed. Line following algorithms are usually named navigation algorithms. Some of these navigation algorithms were examined by Sujit et al. [39]. The first one of these algorithms is the carrot chase algorithm. In this algorithm an imaginary point which is a fixed distance ahead of the aircraft and on the track is followed. Proportional navigation is used for the tracking purpose. The next algorithm that was examined by Sujit et al. [39] is the nonlinear guidance law [40]. In this algorithm again a point on the path a fixed distance away is followed. The difference is the guidance law to track the imaginary point which is a nonlinear guidance law given in Equation 1.1.

$$a_{y_{ref}} = 2\frac{V^2}{L_1}\sin\eta \tag{1.1}$$

Here a_{yref} is the reference lateral acceleration, v is the speed, L_1 is the distance between the target and the plane, and η is the angle of the arc that passes from the target and the plane. Another algorithm that was examined by Sujit et al. [39] is pure pursuit and line-of-sight based algorithm. In this algorithm, there are waypoints on the path. These waypoints are named as W_i and W_{i+1} from the closest to the aircraft to the farthest. While W_i point is followed by the pure pursuit algorithm line-of-sight algorithm works to align the line between W_i and W_{i+1} and the line between the aircraft and W_i. The fourth algorithm that is studied by Sujit et al. [39] is the vector field algorithm. In this algorithm, a vector field that is prearranged before the flight is followed by the aircraft. To correct the angle between the vector field and the aircraft a proportional guidance algorithm is generally used. The important thing is to determine the vector field which dictates the maneuver of the aircraft. Vector fields have two parts. These are called the near field and far field. In the far field, there exists a vector field such that the aircraft travels towards the path with a fixed track angle until it enters the near field. In the near field, track angle is adjusted such that it starts from the far field track angle and finishes parallel to the path. One of the formulae that is used for this adjustment is given in Equation 1.2 [41].

$$\chi^d(y) = -\chi^\infty \frac{2}{\pi}\tan^{-1}(ky) \tag{1.2}$$

Here $\chi^d(y)$ denotes the track angles of the vectors in the near field and χ^∞ denotes the track angle of the far field vectors. The fifth algorithm that is examined by Sujit et al. [39] is the linear quadratic regulator algorithm [42]. Optimal guidance law is given in Equation 1.3.

$$a_{y_{ref}} = \left[\sqrt{\left|\frac{d_b}{d_b - d}\right|}\, d + \sqrt{2\sqrt{\left|\frac{d_b}{d_b - d}\right|} + 1}\, v_d \right] \tag{1.3}$$

Here the distance of the aircraft from the path is denoted as d and the minimum distance is denoted as d_b. The derivative of the d which is the normal velocity to the path is denoted as v_d and reference acceleration is denoted as $a_{y_{ref}}$. After the comparisons Sujit et al. [39] has concluded that the most successful algorithm in terms of tracking the line is the vector field algorithm; however, it requires more control effort compared to the other algorithms.

Literature generally focuses on vector field algorithms. As it is said earlier, the most important thing is how the vector field is generated. Nelson et al. [41] used sliding mode control law for the generation of the vector field. Instead of the sign(x) function sat(x) function is used for the sliding surface formula. Sat(x) is defined as equal to sign(x) when the absolute value of x is bigger than 1 and equal to x when the absolute value of x is smaller than 1. The chattering problem is solved using this sat(x) function. Tiftikçi [43] proposed four different methods for generating the near field. Three of these are suitable for two-dimensional paths and one of them which uses spherical linear interpolation (SLERP) can be used for three-dimensional paths.

1.3 CONTRIBUTION

As can be seen from the literature, most of the autoland system papers focus on in-air part of the landing. A few of them include the on-ground part.

This thesis focuses on the on-ground part of the landing. A 6-DOF aircraft dynamics model with a tricycle landing gear model including strut states and cornering power factor estimation is used and a novel autoland system with sliding mode control was designed and compared with the industry standard PID controller. The system is found to be robust

against crosswinds, brake failures, steering failure, and differences in the cornering power factor of the tires.

The contributions include detailed description of an aircraft landing gear model including validation, trimming, and linear model derivation parts.

1.4 ORGANIZATION OF THE THESIS

This thesis is organized as chapters. Chapter 2 explains the modelling process of the aircraft including the landing gear and tire modelling parts. Chapter 3 explains the validation process of the created model. Chapter 4 focuses on trimming and linear model derivation. Chapter 5 focuses on the dynamics and the mode shapes of the aircraft on the ground. The actual guidance and autopilot design parts are in Chapters 6, 7, and 8 where Chapter 6 explains the outer loop guidance, Chapter 7 explains the design of the inner loop SMC, and Chapter 8 explains the design of the inner loop PID controller. Chapter 9 includes all the important graphs from the simulations and Chapter 10 includes the conclusion.

2. MODEL OF THE AIRCRAFT

Firstly, the coordinate systems must be defined to explain the equations of the model.

2.1 COORDINATE SYSTEMS

The coordinate systems that are used in this thesis are the body coordinate system, north-east-down (NED) coordinate system, wind axis coordinate system and tire coordinate system.

2.1.1 BODY COORDINATE SYSTEM

The body coordinate system is used for Newton and Euler equations of motion. All the forces and moments are shifted and transformed into the body frame for the equations of motion.

The body coordinate system is fixed on the aircraft and rotates with it. It is not an inertial reference frame. In Figure 2.1 it can be seen in more detail.

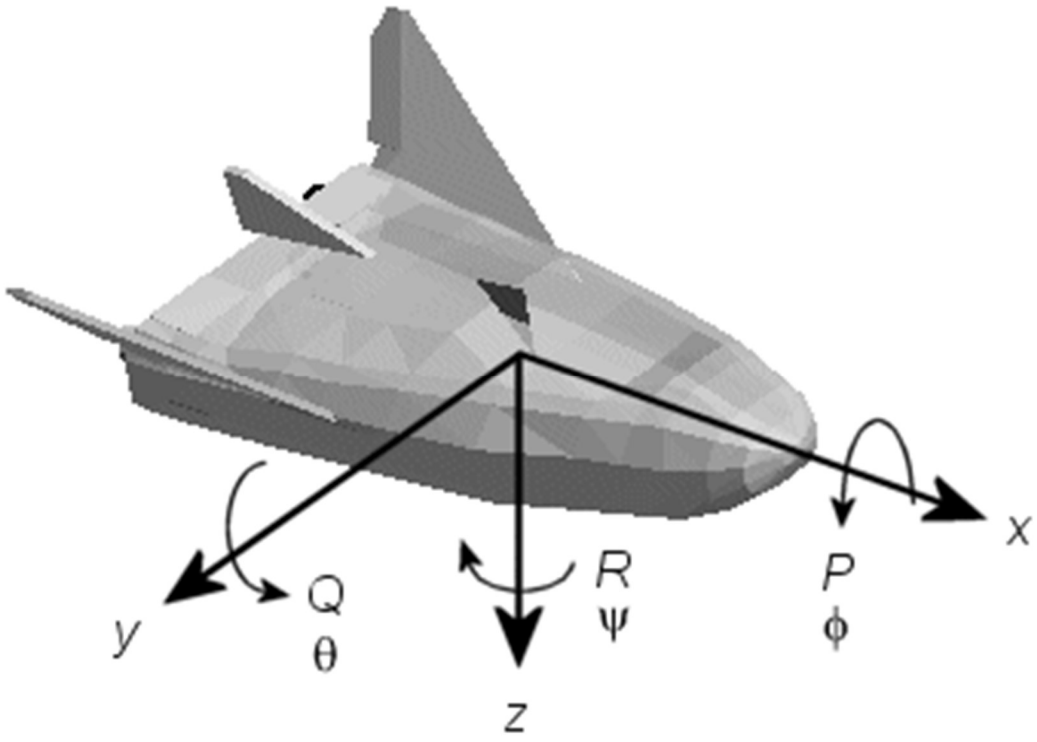

Figure 2.1 Body coordinates of an aircraft [44].

2.1.2 WIND COORDINATE SYSTEM

Wind coordinate is mainly used for calculation of aerodynamics forces. Aerodynamics coefficients are functions of angle of attack and sideslip angles that are defined in wind coordinates. In Figure 2.2 it can be seen in more detail.

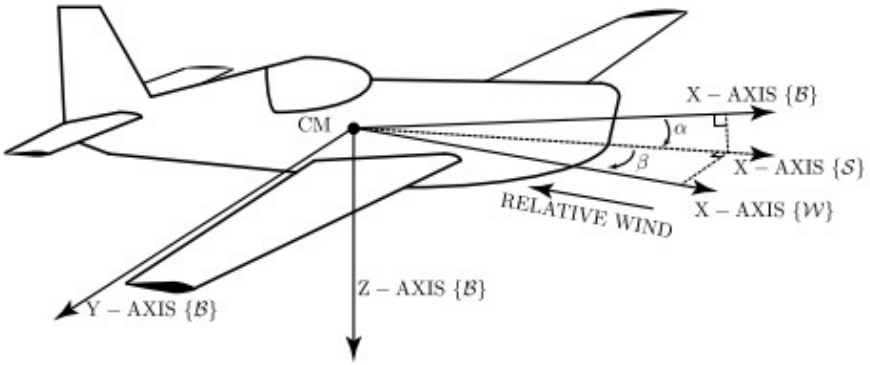

Figure 2.2 Wind axis of an aircraft [45].

2.1.3 NED COORDINATE SYSTEM

North-East-Down (NED) coordinate system is used mainly for the calculation of position and velocity relative to the ground. It can also be used as the inertial reference frame for some aerospace applications where speeds are slow. For this thesis, it is assumed an inertial reference frame. In Figure 2.3 it can be seen in more detail.

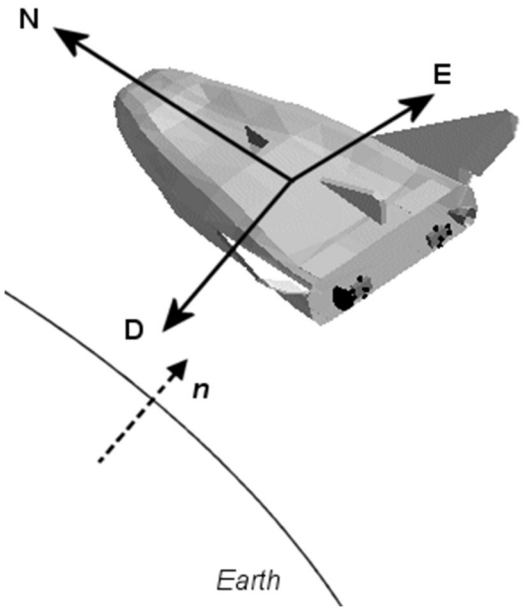

Figure 2.3 NED coordinate system of an aircraft [44].

2.1.4 TIRE COORDINATE SYSTEM

The tire coordinate system is fixed to the individual tires and used for calculation of tire forces. It can be seen in Figure 2.4 in more detail.

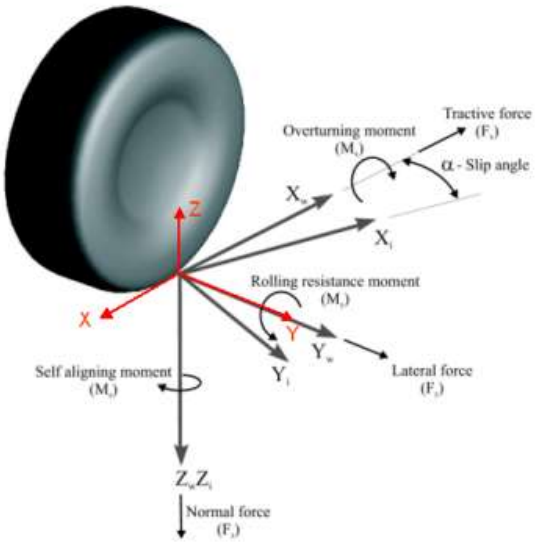

Figure 2.4 Tire coordinate system [46].

2.2 AERODYNAMICS MODEL

Morelli [8] explained the aerodynamics modelling of F-16. This is a polynomial curve fit model that used data of wind tunnels. Details of this aerodynamics model and the related tables and equations are given in Appendix 1.

2.3 PROPULSION MODEL

Gabernet [9] explained the propulsion model of the F-16. The relationship between thrust and throttle and the dynamics of the engine is explained. Thrust values corresponding to throttle settings is shown in Figure 2.5 in more detail.

The dynamics of the propulsion system are model as a first-order transfer function with a period of 1.0 s [9]. The case where power and commanded power are less than 50 percent and the difference between the commanded power and the actual power is 25 percent is used. A Bode plot of the dynamics of the engine for this condition can be seen in Figure 2.6.

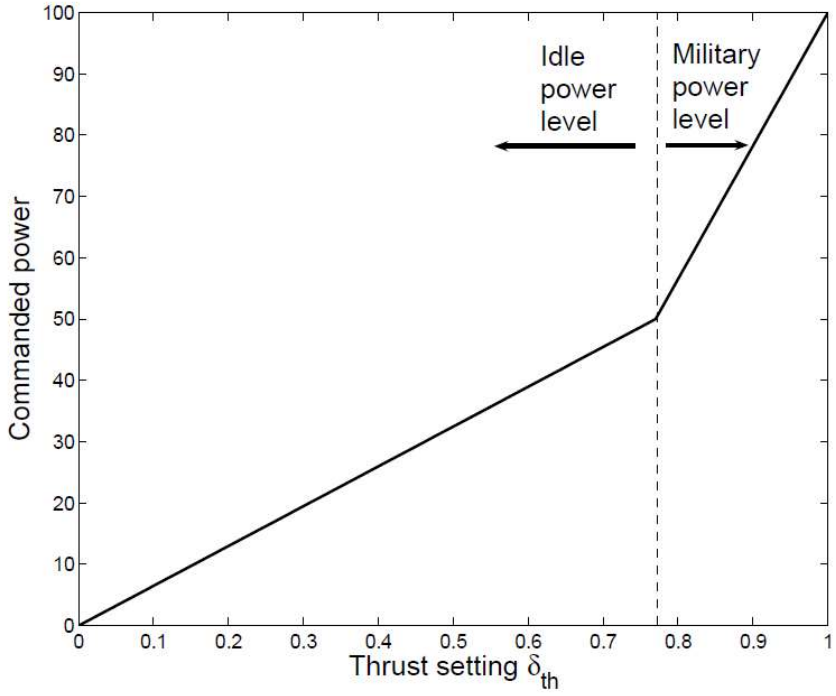

Figure 2.5 Relation between thrust setting and commanded power for F-16 aircraft [9].

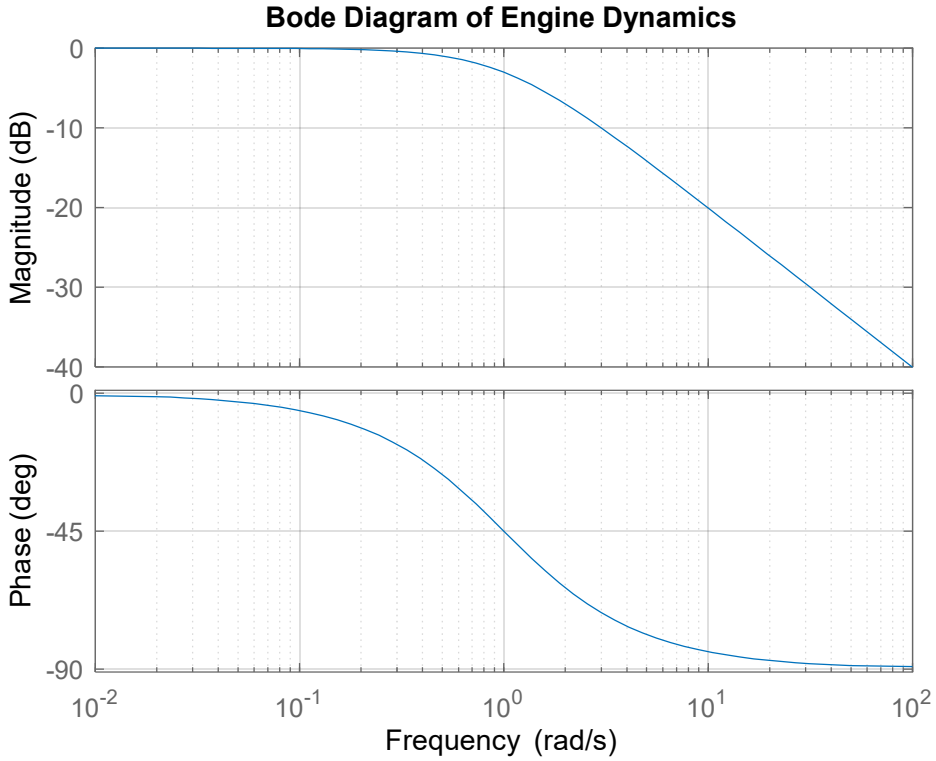

Figure 2.6 Bode Diagram of Engine Dynamics of F-16

2.4 GEOMETRY, MASS, CENTER OF GRAVITY (CG), AND INERTIA

Huo [10] tabulated the geometry, mass, CG, and inertia values of F-16. These values are used for the modeling of the dynamics of the aircraft. In Figure 2.5 Relation between thrust setting and commanded power for F-16 aircraft . Table 2.1 geometry and inertia values can be seen in detail.

Table 2.1 Geometry and inertia values for F-16 aircraft [10].

Symbol	Parameter	Value
W	Vehicle weight (kg)	9000
b	Wing span (m)	9.144
S	Wing area (m^2)	27.87
$\overline{c}$	Mean aerodynamic chord (m)	3.450
I_{xx}	Roll moment of inertia ($kg \cdot m^2$)	12875
I_{yy}	Pitch moment of inertia ($kg \cdot m^2$)	75674
I_{zz}	Yaw moment of inertia ($kg \cdot m^2$)	85552
I_{xz}	Product moment of inertia ($kg \cdot m^2$)	1331
I_{xy}	Product moment of inertia ($kg \cdot m^2$)	0
I_{yz}	Product moment of inertia ($kg \cdot m^2$)	0

2.5 EQUATIONS OF MOTION

Flight mechanics equations are modeled in 6 degrees of freedom. These are 3 Newton's equations for translational and 3 Euler's equations for angular motion calculation. These are given in equations 2.1 to 2.6. Effects of Ixy and Iyz are omitted in these equations. In these equations u, v, w denote body axis translational velocity components; p, q, r denote body axis angular velocity components; X, Y, Z denote body axis force components; and L, M, N denote body axis moment components. Derivation of the equations are explained by Lewis et al. [47] in detail.

$$\dot{u} = r \cdot v - q \cdot w + \frac{X}{m} \tag{2.1}$$

$$\dot{v} = p \cdot w - r \cdot u + \frac{Y}{m} \tag{2.2}$$

$$\dot{w} = q \cdot u - p \cdot v + \frac{Z}{m} \tag{2.3}$$

$$\dot{p} = \frac{I_{xz}\cdot\dot{r} - (I_{zz} - I_{yy})\cdot q\cdot r + I_{xz}\cdot p\cdot q + L}{I_{xx}} \tag{2.4}$$

$$\dot{q} = \frac{-(I_{xx} - I_{zz})\cdot r\cdot p - I_{xz}\cdot(p^2 - r^2) + M}{I_{xx}} \tag{2.5}$$

$$\dot{r} = \frac{I_{xz}\cdot\dot{p} - (I_{yy} - I_{xx})\cdot p\cdot q + I_{xz}\cdot q\cdot r + N}{I_{zz}} \tag{2.6}$$

NED coordinate system is assumed an inertial reference frame.

2.6 ATTITUDE UPDATE METHOD

Attitude is the angular orientation of the body axis of the aircraft with respect to the NED axis that is used as an inertial reference frame. It is necessary to calculate the gravity force components in the body axis and to calculate the NED axis position and velocity components of the aircraft.

Three different attitude update methods can be used. These are simple Euler angles method, quaternion method, and direct integration of direction cosine matrix.

2.6.1 EULER ANGLE METHOD

Euler angles can be used for most of the aircraft flight simulations. It requires 3 states for 3 different Euler angles. It can be used for a large angle space apart from one asymptotic angle where the equations become undefined.

Most of the aircraft simulations use a 3-2-1 Euler angle scheme where 3-2-1 denote yaw, pitch, and roll angles. In equations 2.7 to 2.9 relationship between Euler angle rates and body axis angular velocity components is given for 3-2-1 Euler angle scheme. As can be seen, the equations are undefined when pitch angle is 90 degrees.

$$\dot{\phi} = p + (q\sin\phi + r\cos\phi)\frac{\sin\theta}{\cos} \tag{2.7}$$

$$\dot{\theta} = q\cos\phi - r\sin\phi \tag{2.8}$$

$$\dot{\psi} = \frac{q\sin\phi + r\cos\phi}{\cos\theta} \tag{2.9}$$

Euler angles are used for computing the direction cosine matrix which is then used for calculating the gravity forces and NED components of velocity and position.

2.6.2 QUATERNION METHOD

The quaternion method eliminates the undefined angle problem by increasing the number of attitude states from 3 to 4. Quaternions are used for calculating the direction cosine matrix which is then used for gravity force components calculation and calculation of NED axis position and velocities. Quaternions can also be converted to Euler angles again as outputs which are easier to understand.

2.6.3 DIRECTION COSINE MATRIX INTEGRATION METHOD

In this method, the attitude is defined by the direction cosine matrix itself that is used for coordinate transformation from NED to the body and vice versa. In this method, the direction cosine matrix itself is considered a state which has 9 components. This method is the most accurate.

One disadvantage of this method is the accumulation of the numerical error. The norm of the direction cosine matrix must be checked and equated to 1 in every step. More detail can be seen in [48].

The 3-2-1 Euler angle scheme is used in this thesis since only the landing phase of the flight is modeled. The aircraft comes nowhere close to 90 degrees pitch angle. 3 Euler angle states are sufficient for this purpose.

2.7 GRAVITY FORCE

Gravity force components in the body axis are calculated using Euler angles. These relations are in equations 2.10 to 2.12.

$$X_{grav} = mg \sin\theta \tag{2.10}$$

$$Y_{grav} = mg \cos\theta \sin\phi \tag{2.11}$$

$$Z_{grav} = mg \cos\theta \cos\phi \tag{2.12}$$

2.8 NED VELOCITY AND POSITION

NED velocity components are calculated using body velocity components and Euler angles. Equations 2.13 to 2.15 are used for this purpose.

$$u_{ned} = \cos\theta\cos\psi\, u + (\sin\phi\sin\theta\cos\psi - \cos\phi\sin\psi)v + (\cos\phi\sin\theta\cos\psi + \sin\phi\sin\psi)w \quad (2.13)$$

$$v_{ned} = \cos\theta\sin\psi\, u + (\sin\phi\sin\theta\sin\psi + \cos\phi\cos\psi)v + (\cos\phi\sin\theta\sin\psi - \sin\phi\cos\psi)w \quad (2.14)$$

$$w_{ned} = -\sin\theta\, u + \sin\phi\cos\theta\, v + \cos\phi\cos\theta\, w \quad (2.15)$$

NED position components are calculated by integrating NED velocity components.

2.9 LANDING GEAR FORCES

A tricycle landing gear model with two states for each landing gear is used. Additional 3 inputs of steering angle and left and right brake forces and 3 degrees of freedom for vertical position of the landing gear comes to the model. The states are named as $[s_{ng}, s_{lmg}, s_{rmg}, \dot{s}_{ng}, \dot{s}_{lmg}, \dot{s}_{rmg}]$ and the steering input is named as $[\delta_{steering}]$. Landing gear forces (Equation 2.16) are functions of translational and angular velocity of the aircraft, attitude of the aircraft, position of the aircraft with respect to the runway, steering angle, brake forces, positions and velocities of the landing gear struts. After these forces are calculated, they are shifted to the center of gravity of the aircraft.

$$\vec{F}_{landing\_gear} = f\left(u, v, w, p, q, r, \phi, \theta, \psi, x, y, z, \delta_{steering}, \delta_{left_{brake}}, \delta_{right_{brake}}, s_{ng}, s_{lmg}, s_{rmg}, \dot{s}_{ng}, \dot{s}_{lmg}, \dot{s}_{rmg}\right) \quad (2.16)$$

To find the compression on the tires, position of the tires with respect to the ground must be found. Firstly, the position components of the tires are found in the body axis (Equation 2.17). After that, the position components are transformed to the NED axis. The position components of the tires in NED axis are summed with the position of the aircraft in NED axis to find the position of the tires with respect to the ground (Equation 2.18). After that, runway heights corresponding to the NED positions of the tires are found. Thus, the vertical positions of the tires with respect to the ground are found (Equation 2.19). Axis system and position vectors of the landing gears are shown in Figure 2.7.

$$\vec{p}_{lg} = \vec{p}_{lg0} + \vec{s} \quad (2.17)$$

$$\vec{p}_{lg/eart} = \vec{p}_{aircraft/ear} + \vec{p}_{lg/aircraft} \quad (2.18)$$

$$h_{runway/lg} = f\left(x_{lg}^{ned}, y_{lg}^{ned}\right) \quad (2.19)$$

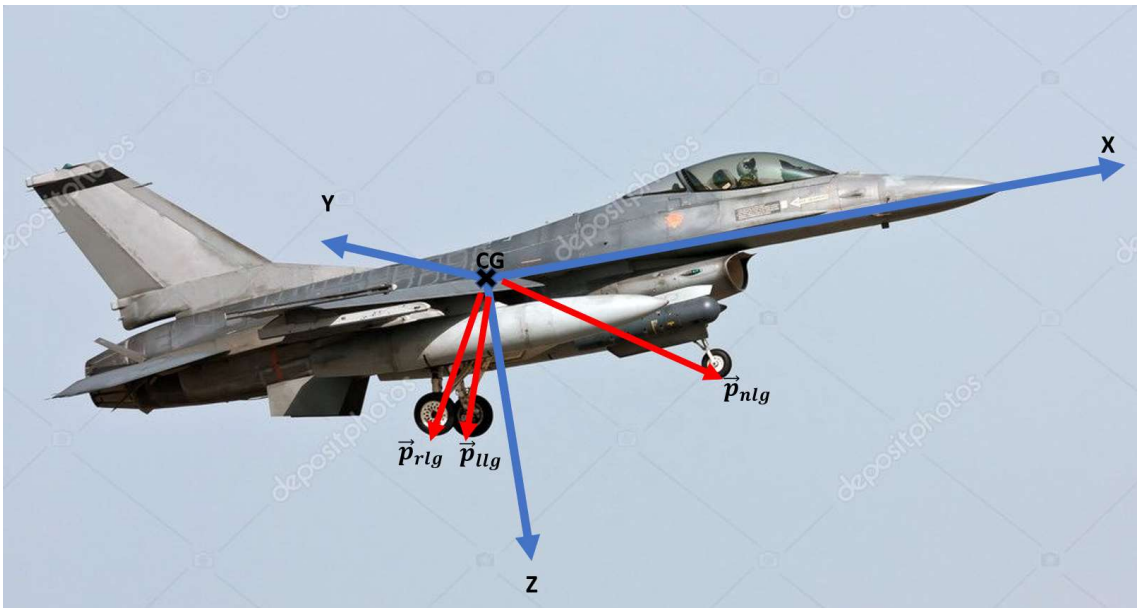

Figure 2.7 Position vectors of F-16 landing gears [49]

Velocity components of the tires with respect to the ground are found by summing, the cross product of the angular velocity of the aircraft with the positions of the tires, the velocity of the aircraft with respect to the ground, the velocity of the tire with respect to the aircraft (Equation 2.20).

$$\vec{v}_{lg} = \vec{v}_{aircraft} + \vec{\omega}_{aircraft} \times \vec{p}_{lg} + \dot{\vec{s}} \tag{2.20}$$

For the strut forces, position, and velocity of the tire with respect to the aircraft are used (Equation 2.21). Stiffness and damping values for the aircraft are shown in Table 2.2.

$$F_{strut} = s \cdot k_{strut} + \dot{s} \cdot c_{strut} \tag{2.21}$$

If the position of the tire with respect to the ground is bigger than zero, the tire is compressed. In this case, stiffness and damping forces for tire compressions are calculated (Equations 2.22 and 2.23).

$$F_{k\_tire} = s_{tire} \cdot k_{tire} \tag{2.22}$$

$$F_{c\_tire} = \dot{s}_{tire} \cdot c_{tire} \tag{2.23}$$

After the calculation of tire and strut forces, acceleration of the tire with respect to the aircraft is found (Equation 2.24). The velocity of the tire with respect to the aircraft is found by integrating the acceleration. Likewise, the position is found by integrating the velocity. Here, an inertial reference frame assumption is made. Forces due to the angular velocity and angular acceleration of the landing gear are neglected. Since these forces are

small compared to the strut forces this assumption can be made with little change in accuracy.

$$\ddot{s} = (F_{tire} - F_{strut})/m_{whee} \tag{2.24}$$

For the longitudinal and lateral tire forces, ground velocities of the tires in the tire axis must be found. The velocity of the aircraft is summed with the cross product of the angular velocity of the aircraft and the position of the tires (Equation 2.25). The lateral slip angle of the tire is found using these ground velocity components of the tires (Equation 2.26).

$$\vec{v}_{tire\_ned} = \vec{v}_{aircraft\_ned} + \vec{\omega}_{aircraft} \times \vec{r}_{tire\_aircraft} \tag{2.25}$$

$$\beta_{tire} = \text{atan}\left(\frac{v_{tire}}{u_{tire}}\right) \tag{2.26}$$

Longitudinal tire force is found using rolling resistance and brake forces (Equation 2.27). The values that are used are in Table 2.2.

$$F_{x\_tire} = F_{z\_tire} \cdot \mu_{roll} + F_{brake} \tag{2.27}$$

By using the vertical force and the slip angle, the lateral force of the tires can be found (Equation 2.28). This part is explained in more detail in the next section.

$$F_{y\_tire} = F_{z\_tire} \cdot \beta_{tire} \cdot C_{y,z} \tag{2.28}$$

Parameters that were used for calculation of the landing gear forces are given in Table 2.2.

2.9.1 LATERAL TIRE FORCE

A necessary addition to the calculation of the lateral force of the tires is the calculation of the cornering power factor. Smiley et al. [16] presented empirical formulae for the calculation of the cornering power factor. In this section, these empirical formulae are explained.

One of the equations that were used by Smiley et al. [16] is Equation 2.29. Here, the gross footprint pressure is found by using the ratio of tire compression to tire pressure. Here p_g denotes gross footprint pressure, p_t denotes tire pressure, p_r denotes rated tire pressure, δ_{tire} denotes tire compression and w_{tire} denotes tire width. C_z is a nondimensional coefficient.

$$\frac{p_g}{p_t+0.08p_r} = \begin{cases} 0.6 + \frac{81}{1600c_z}(\delta_{tire}/w_{tire}), & (\delta_{tire}/w_{tire}) \leq \frac{40}{9} \\ 1.05 - \frac{c_z}{(\delta_{tire}/w_{tire})}, & (\delta_{tire}/w_{tire}) > \frac{40}{9} \end{cases} \quad (2.29)$$

Table 2.2 Parameters used for landing gear model of F-16 aircraft

Main Gear			Nose Gear		
Parameter	Value	Unit	Parameter	Value	Unit
$\vec{p}_{lg0}$	[-0.6 ±1.28 1.86]	m	$\vec{p}_{lg0}$	[2.78 0 1.86]	m
k_{strut}	1e6	N/m	k_{strut}	2e5	N/m
c_{strut}	1e5	Ns/m	c_{strut}	2e4	Ns/m
k_{tire}	2e6	N/m	k_{tire}	8e5	N/m
c_{tire}	2e3	Ns/m	c_{tire}	1e3	Ns/m
m_{wheel}	50	kg	m_{wheel}	20	kg
f_{acc}	10	-	f_{acc}	10	-
μ_{roll}	0.02	-	μ_{roll}	0.02	-
F_{brake}	2e5	N	F_{brake}	-	-

Net footprint pressure is found by dividing the gross footprint pressure by ratio “a” which is the ratio of gross footprint area to net footprint area (Equation 2.30).

$$p_n = \frac{p_g}{a_{tire}} \quad (2.30)$$

Cornering power (C) is found by Equation 2.31. The denominator of the left side is named tire pressure area. Cc and Cz values are given in Table 2.3.

$$\frac{C}{c_c(p_t+0.44p_r){w_{tire}}^2} = \begin{cases} 1.2\frac{\delta_{tire}}{d_{tire}} - 8.8\left(\frac{\delta_{tire}}{d_{tire}}\right)^2, & \frac{\delta_{tire}}{d_{tire}} \leq 0.0875 \\ 0.0674 - 0.34\frac{\delta_{tire}}{d_{tire}}, & \frac{\delta_{tire}}{d_{tire}} > 0.0875 \end{cases} \quad (2.31)$$

The maximum coefficient of friction is a function of bearing pressure and can be approximated by Equation 2.32.

$$\mu_{max} = 0.93 - 0.0011p_n \quad (2.32)$$

The value of C is multiplied by a correction factor to estimate the corrected C value (Equation 2.33). This correction factor is found by industry experience and is between 0.25 and 0.35.

$$C_{corr} = C \cdot f_{corr} \tag{2.33}$$

Table 2.3 Parameters used for tire force calculations

Main Gear			Nose Gear		
Parameter	Value	Unit	Parameter	Value	Unit
p_r	160	psi	p_r	160	psi
c_z	0.03	-	c_z	0.03	-
w_{tire}	0.15	m	w_{tire}	0.10	m
d_{tire}	0.40	m	d_{tire}	0.25	m
a_{tire}	0.75	-	a_{tire}	0.7	-
c_c	1.2	N/(psi·m^2·deg)	c_c	1.2	N/(psi·m^2·deg)
f_{corr}	0.3	-	f_{corr}	0.3	-

2.10 ACTUATORS

Control surface actuators are modeled as second-order transfer functions according to Muir et al. [50]. The transfer function can be seen in Equation 2.44.

$$G_{cs} = \frac{1}{1+0.0191401s+\ .000192367s^2} \tag{2.44}$$

Bode diagrams of the actuators can be seen in Figure 2.8. As can be seen from the figure, cutoff frequency is about 80 Hz.

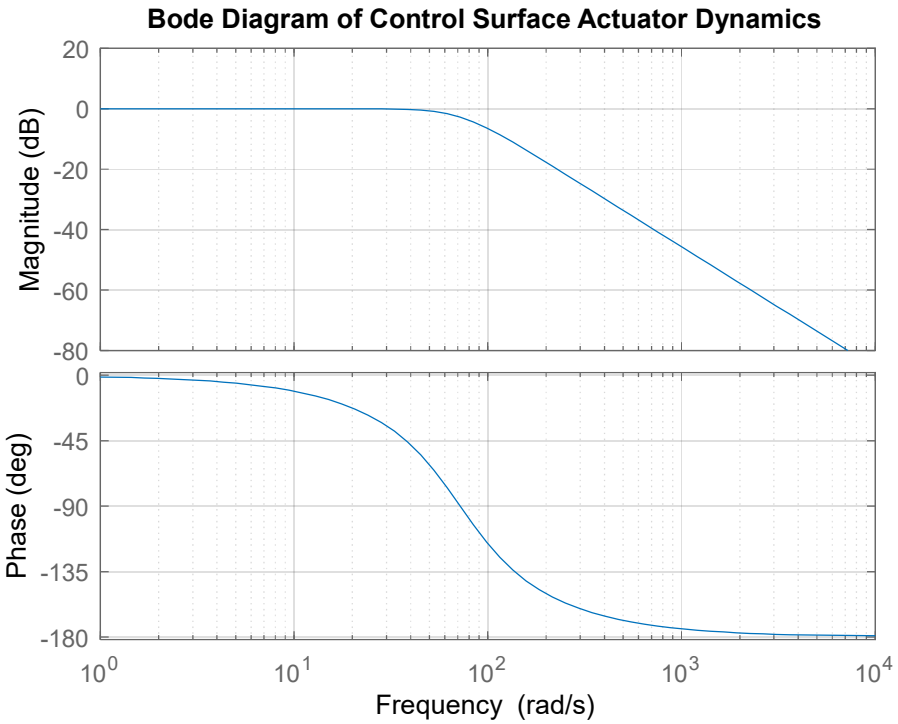

Figure 2.8 Bode Diagram of Actuators of the Aircraft Model

2.11 SENSORS

Sensors are modeled as transfer functions. The transfer function for rates and accelerations are given in Equation 2.45, transfer function of air data is given in Equation 2.46, transfer function for attitudes is given in Equation 2.47 [50].

$$G_{ra} = \frac{1-0.0173s \quad .00019\ ^2}{1+0.0401s+0.00070 \quad ^2} \tag{2.45}$$

$$G_{ad} = \frac{905.92-14.437s+0.116s^2}{908.77+2\ .573s+s^2} \tag{2.46}$$

$$G_{at} = \frac{7161.8-82.317s+0.3417s^2}{7162.3+190.85s+s^2} \tag{2.47}$$

Bode diagrams of the sensor dynamics transfer functions are given in Figure 2.9, Figure 2.10, and Figure 2.11. Cutoff frequencies are about 35-40 Hz.

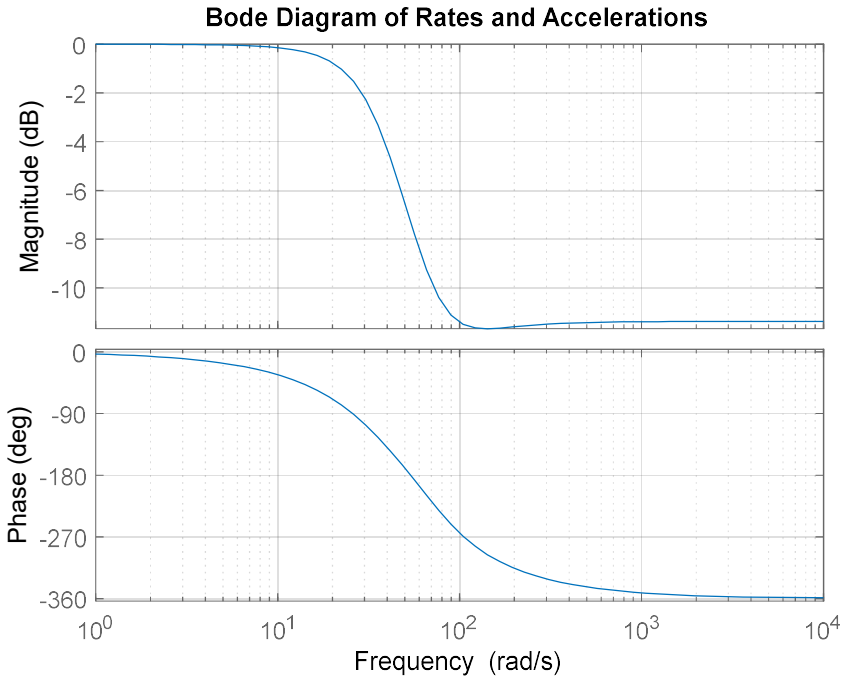

Figure 2.9 Bode Diagram of Rate and Acceleration Sensors

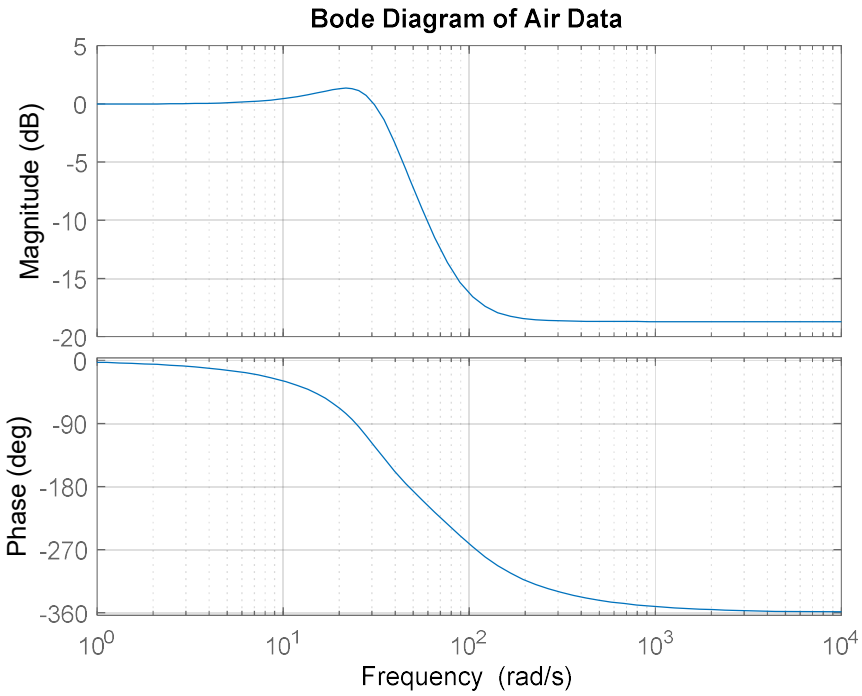

Figure 2.10 Bode Diagram of Air Data Sensors

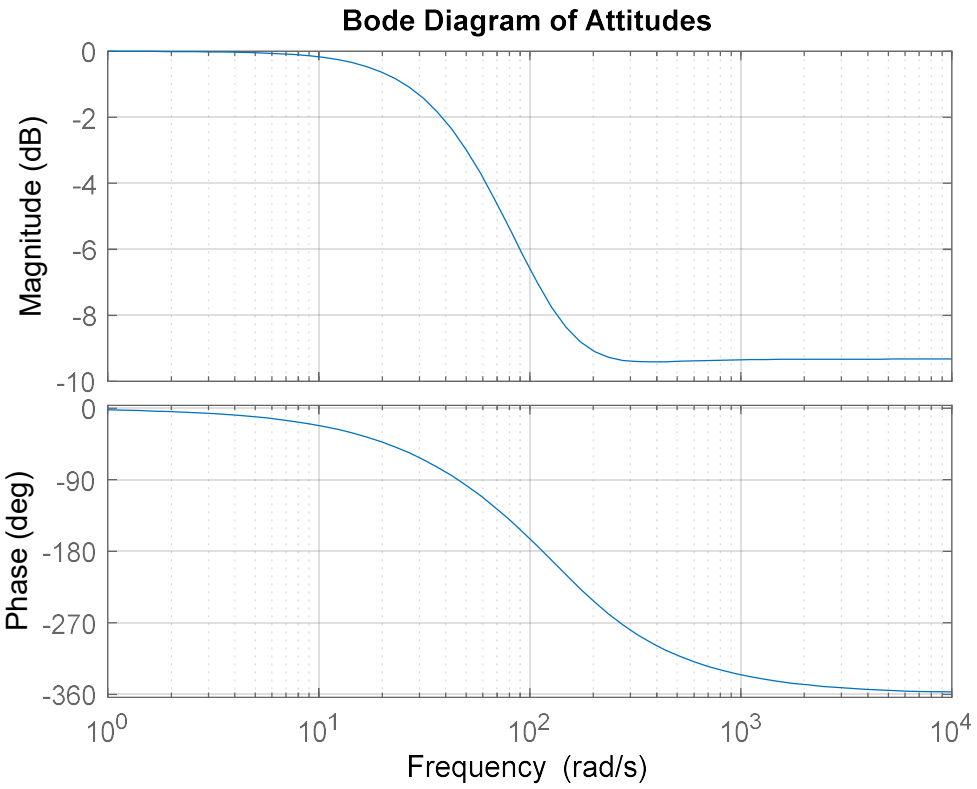

Figure 2.11 Bode Diagram of Attitude Sensors

2.12 WIND MODEL

There are wind models commonly used in industry, most notable one of them is Dryden Wind Turbulence Model [51]. However, in this study, wind is assumed to be uniform for crosswind landing simulations. Turbulence and wind shears are neglected.

2.13 MODEL STRUCTURE

The model is composed of aircraft dynamics block, sensors block, actuators block, autopilot block, wind disturbance and malfunctions block. Aircraft dynamics block is used for the dynamics of the aircraft, trimming and linear model derivation. Actuators block contains the dynamics of the actuators, sensors block contains the dynamics of the sensors and autopilot block includes the guidance and control laws. Wind disturbance block contains wind inputs and malfunctions block contains the malfunctions. The structure is given in Figure 2.12.

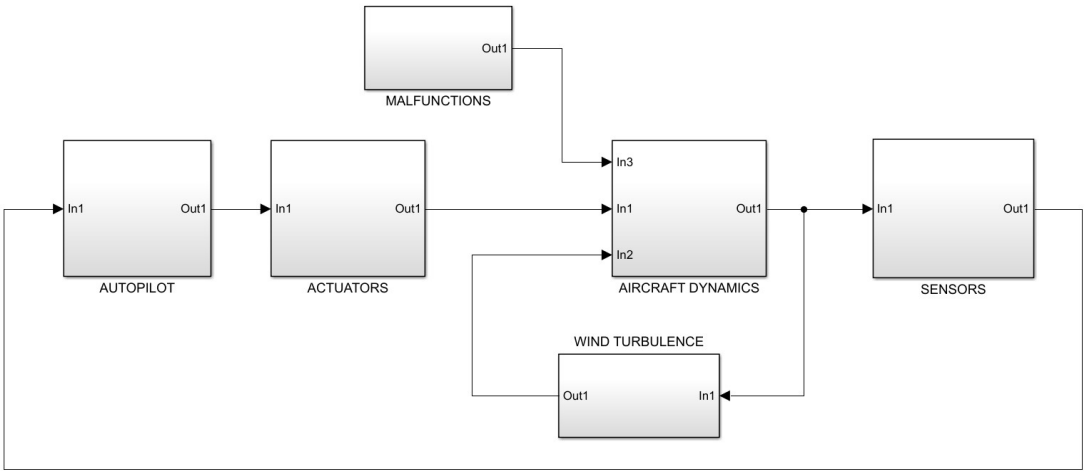

Figure 2.12 Model Structure

2.14 INPUTS, STATES, AND OUTPUTS OF THE AIRCRAFT DYNAMICS BLOCK

Inputs (Table 2.4), states (Table 2.5), and outputs (Table 2.6) of the aircraft dynamics block must be given since they are used for trimming and linear model derivation.

Table 2.4 Inputs of the model

Name of the input	**Symbol**	**Unit**
Throttle	δ_{thr}	%
Elevator	δ_{ele}	Degree
Aileron	δ_{ail}	Degree
Rudder	δ_{rud}	Degree
Steering	$\delta_{steering}$	Degree
Left brake	δ_{left_brake}	%
Right brake	δ_{right_brake}	%

Table 2.5 States of the Model

Name of the state	**Symbol**	**Unit**
Body axis translational velocity components	u, v, w	m/s
Body axis angular velocity components	p, q, r	rad/s
Euler angles	ϕ, θ, ψ	rad
NED axis position components	x, y, z	m
mass	m	kg
Strut displacements	s_{lmg}, s_{rmg}, s_{ng}	m
Strut velocities	$\dot{s}_{lmg}, \dot{s}_{rmg}, \dot{s}_{ng}$	m/s

Table 2.6 Outputs of the model

Name of the output	**Symbol**	**Unit**
True air speed	TAS	m/s
Flight path angle	γ	degree
Sideslip angle	β	degree
Track angle	χ	degree
Lateral acceleration	a_y	m/s^2

3. VERIFICATION OF THE MODEL

Sensors and actuator parts contains only linear transfer functions. Thus, these parts are easy to verify. The hardest part to verify is the aircraft dynamics block. In this block, many different functions compute different parts of the model. The first thing to do is to unit test the functions.

3.1 UNIT TESTS FOR FUNCTIONS

Unit tests are done for every function inside the aircraft dynamics block and the functions are verified. However, it is impossible to test every possible case for every function. Another necessary step for verification is to conduct test simulations for the entire aircraft dynamics block from some specified initial conditions.

3.2 VERIFICATION SIMULATIONS

In this part, simulations are done to verify the combined usage of the functions inside the aircraft dynamics block. These verification simulation steps are given below. Results of the verification simulations are in Appendix 2. Simulation results agree with the expected results.

1. Aerodynamics, propulsion, and gravity forces in the model are neglected. The aircraft simulation starts from zero velocity. The expected result is that the aircraft stays at zero velocity when there is no force and no initial velocity.
2. Aerodynamics, propulsion, and gravity forces in the model are neglected. The simulation starts with a translational velocity component. The expected result is that the aircraft stays at the initial velocity when there is no force or moment.
3. Aerodynamics, propulsion, and gravity forces in the model are neglected. The aircraft starts with an angular velocity component. The expected result is that the aircraft stays at the initial angular velocity when there is no force or moment.
4. Aerodynamics, propulsion, and gravity forces in the model are neglected. The aircraft starts with both translational velocity and angular velocity components. The expected result is that the aircraft stays at the initial angular velocity and it stays at the initial NED axis velocity when there is no force or moment.

5. Aerodynamics and propulsion blocks in the model are neglected. The gravity block is set to work. The aircraft starts from zero velocity. The expected result is that the aircraft accelerates downwards with gravitational acceleration.
6. Aerodynamics and propulsion blocks in the model are neglected. The gravity block is set to work. The aircraft starts with a forward translational velocity parallel to the ground. The expected result is that the aircraft accelerates downwards with gravitational acceleration and the forward NED velocity component stays at the initial value.
7. Aerodynamics and gravity blocks in the model are neglected. Propulsion forces are set working. Propulsive moments are canceled. The aircraft starts with zero initial velocity and a propulsion force. The expected result is that the aircraft accelerates in the forward direction.
8. Propulsion and gravity blocks in the model are neglected. Aerodynamics forces and moments are set working. The aircraft starts with an initial forward velocity. The expected result is that the aircraft slows down due to the drag force.
9. Propulsion and gravity blocks in the model are neglected. Aerodynamics forces and moments are set working. The aircraft starts with a forward velocity parallel to the ground and a high angle of attack. The expected result is that the altitude increases and the angle of attack decreases.
10. Propulsion and gravity blocks in the model are neglected. Aerodynamics forces and moments are set working. The aircraft starts with a forward velocity parallel to the ground and a high angle of sideslip. The expected result is that the heading angle increases, and the sideslip angle decreases.
11. Aerodynamics, propulsion, and gravity blocks are set working. The aircraft simulation starts with a positive roll angle and a positive angle of attack. The expected result is that the heading and track angles increase.
12. Aerodynamics, propulsion, and gravity blocks are set working. The aircraft starts with a forward velocity parallel to the ground. Negative elevator command is given. The expected result is that the pitch angle increases.
13. Aerodynamics, propulsion, and gravity blocks are set working. The aircraft starts with a forward velocity parallel to the ground. Negative aileron command is given. The expected result is that the roll angle increases.

14. Aerodynamics, propulsion, and gravity blocks are set working. The simulation starts with a forward velocity parallel to the ground. Negative rudder command is given. The expected result is that the yaw angle increases.
15. Aerodynamics, propulsion, landing gear, and gravity blocks are set working. The aircraft starts with zero velocity and its landing gears just above the ground. The expected result is that the aircraft falls to the ground, bounces from the ground, and eventually stops.
16. Aerodynamics, propulsion, landing gear, and gravity blocks are set working. The aircraft starts with a forward velocity and its landing gears just above the ground. The expected result is that the aircraft falls to the ground and bounces from the ground. Forward velocity should decrease due to the rolling resistance.
17. Aerodynamics, propulsion, landing gear, and gravity blocks are set working. The aircraft starts with a forward velocity on ground. Brakes are activated. The expected result is that the aircraft slows down and stops due to the brakes.
18. Aerodynamics, propulsion, landing gear, and gravity blocks are set working. The aircraft starts with a forward velocity on the ground. One of the brakes is activated. The expected result is that the aircraft slows down and stops due to the brake and the aircraft maneuvers to the side with a yaw rate and changes its heading and track angle.
19. Aerodynamics, propulsion, landing gear, and gravity blocks are set working. The aircraft starts with a forward velocity on the ground. Steering angle input is given. The expected result is that the aircraft maneuvers to the side with a yaw rate and changes its heading and track angle.
20. Aerodynamics, propulsion, landing gear, and gravity blocks are set working. The aircraft simulation starts with a forward velocity on the ground. Throttle input is given. The expected result is that the aircraft accelerates.

4. TRIMMING AND LINEARIZATION

Trimming is the act of finding the equilibrium points in a dynamics block. Trimming is necessary for starting the simulation from an equilibrium point and derivation of the linear model matrices. Trim points also give an idea about the dynamics envelope of a system. If a system can be trimmed, it can theoretically be controlled at that point. In the case of an aircraft, trim points give an idea about the flight envelope of the aircraft.

There are different versions of trim points. These include but not limited to:

- Forward flight
- Steady climb or descent
- Steady heading steady sideslip
- Pull up
- Coordinated turn
- Barrel roll
- Aileron roll

For this thesis, three different trim point versions are investigated. These are:

- Steady heading and steady sideslip
- Two tires on ground trim
- Three tires on ground trim

Steady heading and steady sideslip trim points are necessary for the start of the simulations. The simulations start just above the ground before the aircraft touches the ground. The aircraft directs itself parallel to the runway flying with a sideslip angle due to the crosswind. However, in the case of F-16 the sideslip angles the aircraft can fly are limited. In the case of crosswinds, the aircraft cannot direct its heading parallel to the runway. Therefore, the aircraft lands with a heading angle not parallel to the runway.

Two tires on the ground trim points are necessary for the portion of the landing roll where only the two main gear tires touch the ground. Three tires on the ground trim points are necessary for the part of the landing rollout phase where all three tires touch the ground. The parameters of these trim points and the algorithm for these trim points are investigated in the next section.

4.1 STEADY HEADING STEADY SIDESLIP TRIM

Steady heading steady sideslip (SHSS) is one of the most used in air trim maneuver conditions. In this trim maneuver, the aircraft has a steady sideslip angle, steady heading, and steady track angle. The floating inputs and states and the fixed state derivatives and outputs are given in Table 4.1.

Table 4.1 Fixed and floating parameters for the steady heading steady sideslip trim maneuver solution.

Inputs	States	State Derivatives	Outputs
$\delta_{thr}, \delta_{ele}, \delta_{ail}, \delta_{rud}$ (Float)	u, v, w (Float)	$\dot{u}, \dot{v}, \dot{w}$ (Fixed)	tas, γ, β, χ (Fixed)
	ϕ, θ, ψ (Float)	$\dot{p}, \dot{q}, \dot{r}$ (Fixed)	

4.2 TWO TIRES ON THE GROUND TRIM

Two tires on the ground trim is necessary for the part where the aircraft travels with two tires on the ground during the landing rollout. Fixed and floating parameters for the two tires on the ground trim maneuver solution is given in Table 4.2.

Table 4.2 Fixed and floating parameters for two tires on the ground trim maneuver solution.

Inputs	States	State Derivatives	Outputs
δ_{rud}(Float)	u, v, w (Float)	$u, \dot{w}$ (Fixed)	tas, γ, β, χ (Fixed)
δ_{ele}(Float)	ϕ, ψ (Float)	$\dot{p}, \dot{q}, \dot{r}$ (Fixed)	
δ_{thr}(Float)	z (Float)	$\ddot{s}_{lmg}, \ddot{s}_{rmg}$ (Fixed)	
	s_{lmg}, s_{rmg} (Float)		

4.3 THREE TIRES ON THE GROUND TRIM

Three tires on the ground trim is necessary for the part where the aircraft travels with all tires including the nose gear on the ground during the landing rollout. Fixed and floating parameters for the three tires on the ground trim maneuver solution is given in Table 4.3.

Table 4.3 Fixed and floating parameters for three tires on the ground trim maneuver solution

Inputs	States	State Derivatives	Outputs
δ_{pedal}(Float)	u,v,w (Float)	u, $\dot{w}$ (Fixed)	$tas, \gamma, \beta, a_y, \chi$ (Fixed)
δ_{thr}(Float)	ϕ, θ, ψ (Float)	$\dot{p}, \dot{q}$ (Fixed)	
	z (Float)	$\ddot{s}_{lmg}, \ddot{s}_{rmg}, \ddot{s}_{ng}$ (Fixed)	
	s_{lmg}, s_{rmg}, s_{ng} (Float)		

4.4 TRIM ALGORITHM

Trimming is the solution of a nonlinear system of equations. Various methods can be used for trimming. These include:

- Direct search algorithms [17]
- Gradient based algorithms [17]
- Trim by simulation

Gradient-based algorithms can also be divided to two categories. These are:

- Single-axis algorithms
- Multi-axis algorithms [18], [20]

For the direct search algorithms, they can be divided to:

- Heuristic algorithms [52]
- Non-heuristic algorithms

The most popular type of algorithms that are used is multi-axis gradient-based algorithms. They are the fastest algorithms that can be used. The only problem of these multi-axis gradient-based algorithms is their proneness to diverge. While this divergence problem can be partly solved using relaxation still this algorithm is most suitable for continuous functions that do not have too much nonlinearity.

The algorithm that is used for this study is a single-axis gradient-based algorithm. While single-axis algorithms are slower, they can be made more robust using some modifications.

4.5 SINGLE AXIS SEQUENTIAL SECANT ALGORITHM

Single axis sequential secant algorithm is based on pairing the float and fixed parameters and solving the equation system by sequential updates of each float parameters in every loop. In every master loop, every fix and float parameter equation is solved sequentially. For the solution of the single unknown fix and float pairs equations, the secant method is used. A description of the secant method is shown in Figure 4.1.

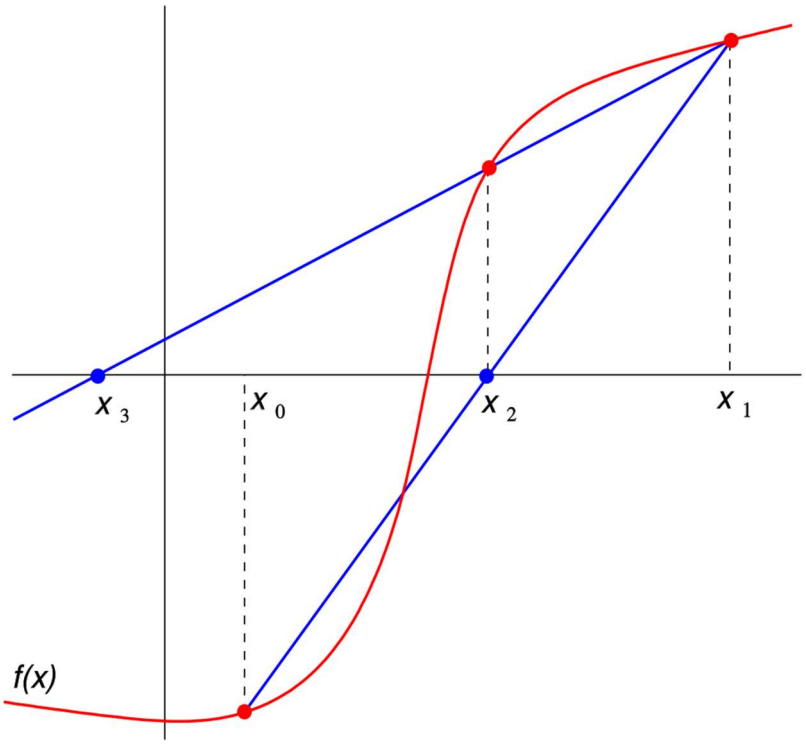

Figure 4.1 Secant algorithm for equations with one unknown [53].

The most important thing about the usage of the algorithm is the pairing. The most relevant parameters must be paired so that the algorithm converges. The other important thing to consider is to update the tolerance of the secant solutions in every master loop so that the algorithm continues converging. To increase the robustness of the algorithm initial guesses of the secant solutions can be reset in every master loop. To increase the speed of the convergence the initial guesses can be taken from the previous master loop. In Table 4.4 Actions for increasing the speed and increasing the robustness the actions for increasing speed or increasing robustness can be seen. In Table 4.5 Fixed and float parameter pairings for trim maneuvers the pairings of the fixed and float parameters can be seen.

Table 4.4 Actions for increasing the speed and increasing the robustness

INCREASE ROBUSTNESS	INCREASE CONVERGENCE SPEED
Decrease secant tolerance slowly.	Decrease secant tolerance fast.
Reset secant initial guesses in each master loop.	Take the initial guesses from the previous master loop.

Table 4.5 Fixed and float parameter pairings for trim maneuvers

IN AIR STEADY HEADING STEADY SIDESLIP		THREE TIRES ON THE GROUND		TWO TIRES ON THE GROUND	
Float parameters	Fixed parameters	Float parameters	Fixed parameters	Float parameters	Fixed parameters
u	TAS	z	$\dot{w}$	z	$\dot{w}$
v	β	u	TAS	u	TAS
w	$\dot{w}$	v	β	v	β
ϕ	$\dot{v}$	w	γ	w	γ
θ	γ	ϕ	$\dot{p}$	ϕ	$\dot{p}$
ψ	χ	θ	$\dot{q}$	ψ	χ
δ_{thr}	$\dot{u}$	ψ	ξ	s_{lmg}	$\ddot{s}_{lmg}$
δ_{ele}	$\dot{q}$	s_{lmg}	$\ddot{s}_{lmg}$	s_{rmg}	$\ddot{s}_{rmg}$
δ_{ail}	$\dot{p}$	s_{rmg}	$\ddot{s}_{rmg}$	δ_{pedal}	$\dot{r}$
δ_{rud}	$\dot{r}$	s_{ng}	$\ddot{s}_{ng}$	δ_{ele}	$\dot{q}$
		δ_{pedal}	a_y		

Tolerance values that are used for each trim maneuver are shown in Table 4.6 Tolerance values used for different trim maneuvers. The number of master iteration is shown by i.

Table 4.6 Tolerance values used for different trim maneuvers

IN AIR STEADY HEADING STEADY SIDESLIP		THREE TIRES ON THE GROUND		TWO TIRES ON THE GROUND	
Fixed parameter	Absolute tolerance	Fixed parameter	Absolute tolerance	Fixed parameter	Absolute tolerance
TAS	$0.001 * 0.5^i$	$\dot{w}$	$1E-6 * 0.9^i$	$\dot{w}$	$1E-6 * 0.9^i$
β	$0.001 * 0.5^i$	TAS	$1E-5 * 0.9^i$	TAS	$1E-5 * 0.9^i$
$\dot{w}$	$0.001 * 0.5^i$	β	$1E-6 * 0.9^i$	β	$1E-6 * 0.9^i$
$\dot{v}$	$0.001 * 0.5^i$	γ	$1E-5 * 0.9^i$	γ	$1E-5 * 0.9^i$
γ	$0.001 * 0.5^i$	$\dot{p}$	$1E-6 * 0.9^i$	$\dot{p}$	$1E-6 * 0.9^i$
χ	$0.001 * 0.5^i$	$\dot{q}$	$1E-6 * 0.9^i$	χ	$1E-6 * 0.9^i$
$\dot{u}$	$0.001 * 0.5^i$	χ	$1E-6 * 0.9^i$	$\ddot{s}_{lmg}$	$1E-6 * 0.9^i$
$\dot{q}$	$0.001 * 0.5^i$	$\ddot{s}_{lmg}$	$1E-6 * 0.9^i$	$\ddot{s}_{rmg}$	$1E-6 * 0.9^i$
$\dot{p}$	$0.001 * 0.5^i$	$\ddot{s}_{rmg}$	$1E-6 * 0.9^i$	$\dot{r}$	$1E-6 * 0.9^i$
$\dot{r}$	$0.001 * 0.5^i$	$\ddot{s}_{ng}$	$1E-6 * 0.9^i$	$\dot{q}$	$1E-6 * 0.9^i$
		a_y	$1E-6 * 0.9^i$		

To show the convergence speed of the trimming algorithm two different trims have been calculated. The trim points are shown in Table 4.7 Two different trim conditions for convergence speed comparison. Convergence speeds are shown in Figure 4.2 Algorithm convergence for air and ground trims. SHSS trim converges faster since it was optimized for faster convergence and the three tires on the ground trim was optimized for robustness.

Table 4.7 Two different trim conditions for convergence speed comparison

Steady Heading Steady Sideslip Trim		Three Tires on the Ground Trim	
m	9000 kg	m	9000 kg
alt	5000 m	TAS	25 m/s
TAS	100 m/s	δ_{ail}	0
γ	0	δ_{ele}	20 deg
β	0	χ	0
		a_y	0
		β	0

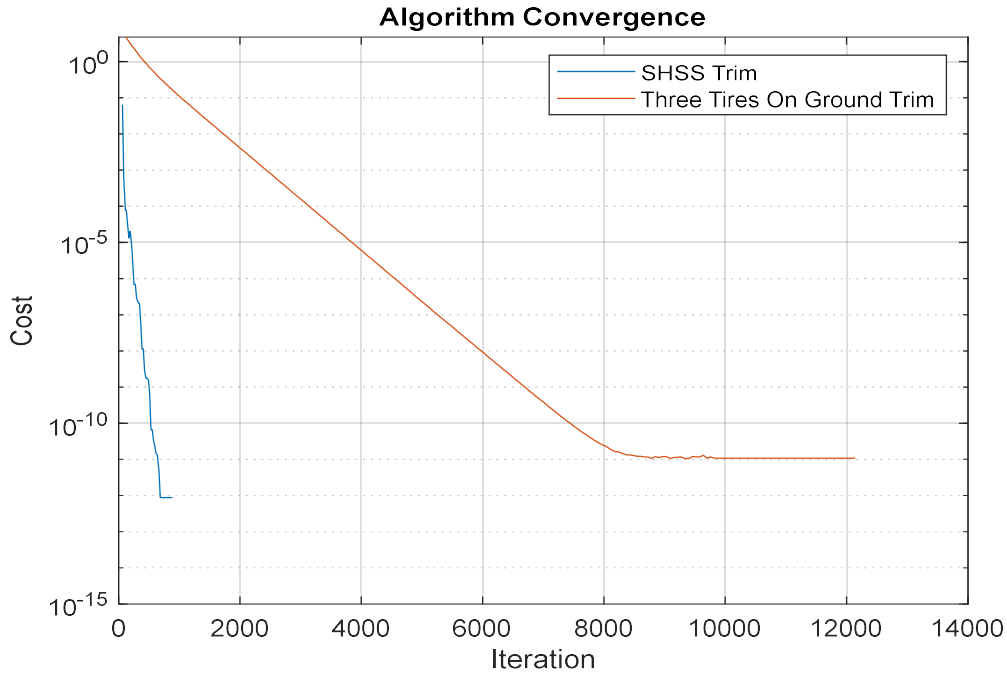

Figure 4.2 Algorithm convergence for air and ground trims

4.6 VERIFICATION OF TRIM POINTS

To verify the trim points the simulation must be started from a trim point. If the states that define the dynamics does not change for a long period, the trim point can be verified. In Figure 4.3 a simulation with 40 seconds duration is shown for the verification of the three tires on the ground trim point.

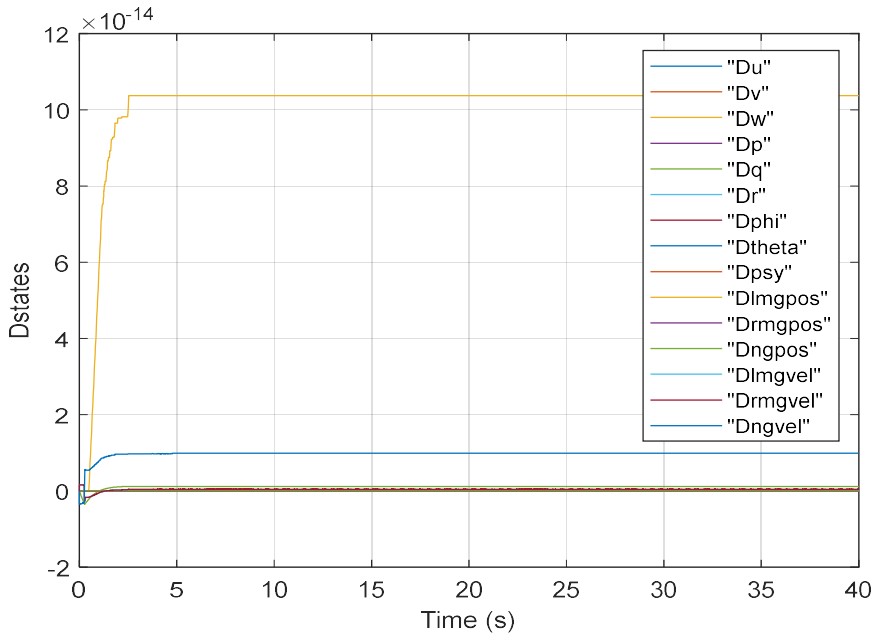

Figure 4.3 Trim point verification simulation

4.7 LINEAR MODELS

Linear models must be calculated to make the autopilot synthesis process more straightforward. Autopilot synthesis can be made systematically using linear models. Most of the control theory is also based on linear time-invariant models.

4.8 PARAMETERS OF LINEAR MODELS

Inputs, states, and outputs of the linear model must be defined so that linear model matrices can be calculated. These parameters can be seen in Table 4.8 Parameters of linear models.

Table 4.8 Parameters of linear models

SHSS TRIM IN AIR		THREE TIRES ON THE GROUND TRIM	
Inputs	$\delta_{thr}, \delta_{ele}, \delta_{ail}, \delta_{rud}$	Inputs	δ_{thr} , δ_{ele} , δ_{ail} , δ_{rud} , $\delta_{leftbrake}$, $\delta_{rightbrake}, \delta_{steer}$
States	u, v, w, p, q, r, ϕ, θ	States	u, v, w, p, q, r, ϕ , θ , s_{lmg}, s_{rmg}, s_{ng}, $\dot{s}_{lmg}, \dot{s}_{rmg}, \dot{s}_{ng}$
Outputs	TAS, β, γ, χ, a_y	Outputs	TAS, β, γ, χ, a_y

4.9 CALCULATION OF LINEAR MODEL MATRICES

For the linear models, the effects of inputs and states on state derivatives and outputs must be calculated. Effects of states on state derivatives are defined in the A matrix, effects of inputs on state derivatives are defined in the B matrix, effects of states on outputs are defined in the C matrix and effects of inputs on outputs are defined in the D matrix. These effects of unit perturbations can also be defined as slopes or gradient.

The two fundamental methods for calculation of the slopes are central difference and forward difference methods. For the forward difference method, an example is where the u state is 100, a calculation is done for the point where u is 100 + du and the slope is calculated using the trim point and one perturbed point. In central difference method, the slope must be calculated using the points u is 100 – du and u is 100 + du. Thus, in the central difference, two extra perturbed points must be calculated.

In the central difference method, the result is expected to be better compared to the forward difference method since the calculation is done using two perturbed points on both sides. In the forward difference method, asymmetrical results may occur; however, the calculation will be faster since one less perturbation is done.

State of the art is the central difference method since it finds better results. Computation time is not too critical for linear model derivation unless the system is too complex. Generally, trimming takes a lot more time compared to linear model derivation.

One important thing to consider during linear model derivation is the unit perturbations. These perturbations are especially important during ground trimming. Perturbations of strut displacements must be small enough, otherwise, the tire will lift from the ground and the calculated dynamics will be wrong. The unit perturbations used in this study are given in Table 4.9.

Table 4.9 Unit Perturbations Used in Linear Model Calculations

Unit Perturbations Used in Linear Model Calculations			
Inputs	Perturbations	States	Perturbations
$\delta_{thr}, \delta_{ele}, \delta_{ail}, \delta_{rud}$	0.01	u, v, w	0.001
$\delta_{leftbrake}, \delta_{rightbrake}, \delta_{steer}$	0.01	p, q, r, ϕ, θ	0.0001
		s_{lmg}, s_{rmg}, s_{ng}, $\dot{s}_{lmg}, \dot{s}_{rmg}, \dot{s}_{ng}$	0.0001

4.10 VERIFICATION OF LINEAR MODELS

For the verification of the linear model, linear and nonlinear models must be compared for the same trim point and with the same inputs [54]. Generally, a doublet input is applied at the trim point and the results are compared. These comparisons must be done for all the inputs available on the aircraft. If the trim point is unstable there may be divergence between nonlinear and linear model simulation results. This is normal. The important point to check is if the initial dynamics responses to the doublet are similar.

In Figure 4.4, Figure 4.5, Figure 4.6, and Figure 4.7 there are example verifications for the three tires on the ground trim point. Linear model is compared with nonlinear model for the ground trim point in Table 4.7 using different inputs.

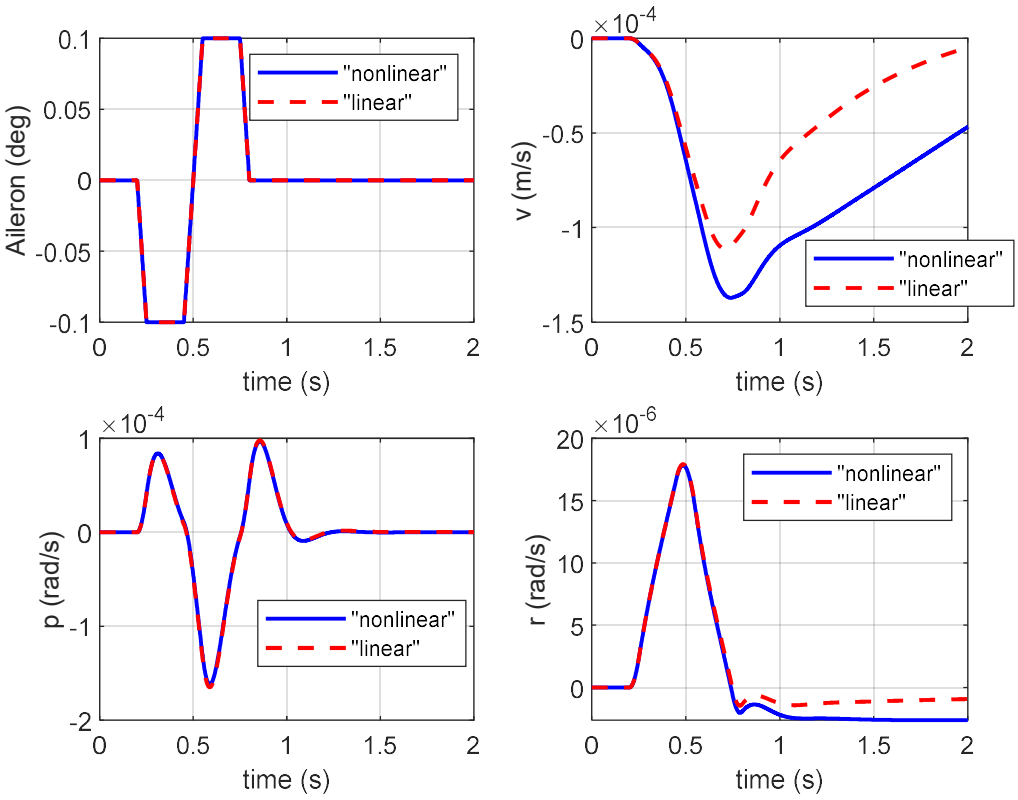

Figure 4.4 Linear model comparison for aileron inputs

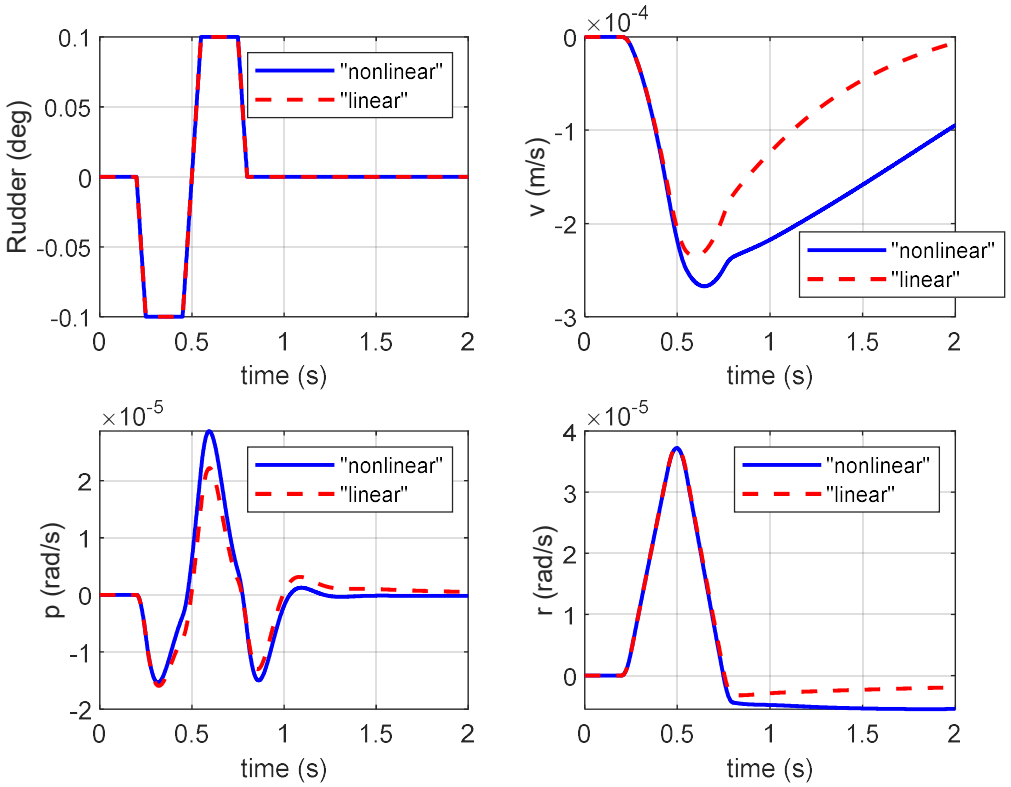

Figure 4.5 Linear model comparison for rudder inputs

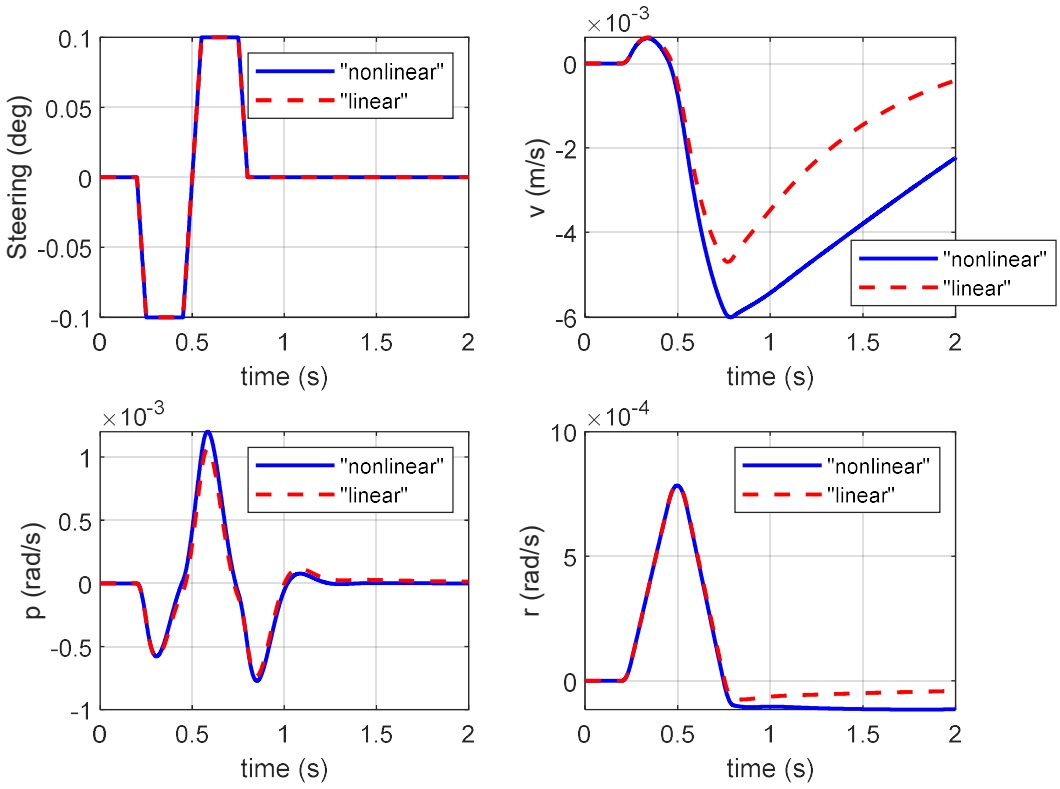

Figure 4.6 Linear model comparison for steering inputs

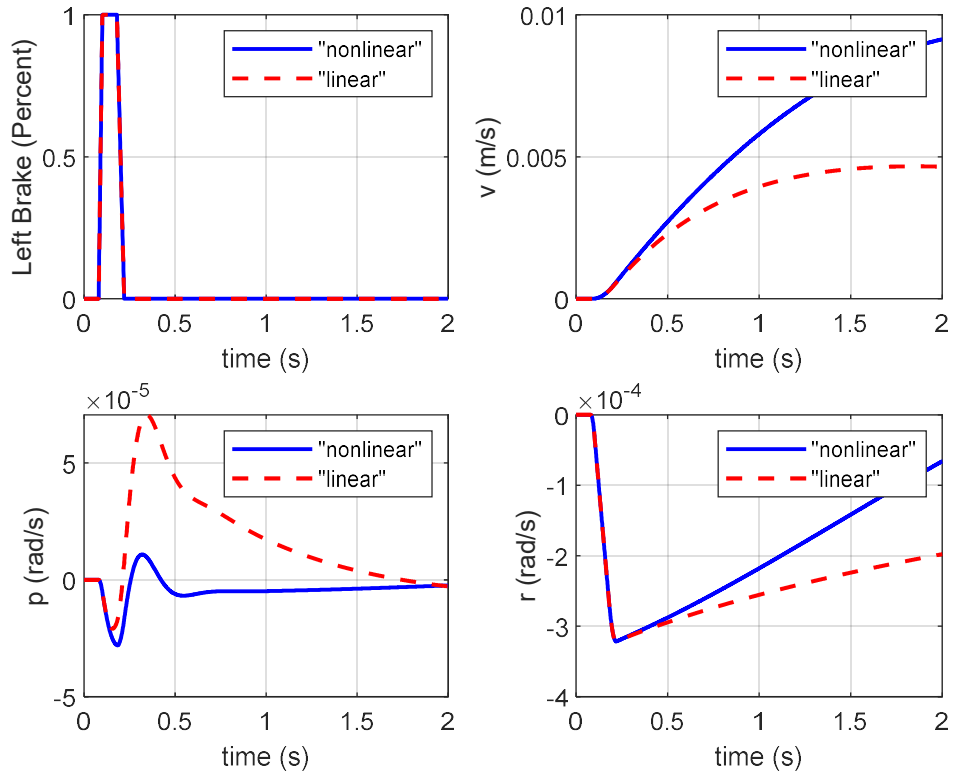

Figure 4.7 Linear model comparison for left brake inputs

5. DYNAMICS AND MODE SHAPES

To design the controller of the aircraft, its dynamics must be learned. The dynamics in air is well known with very well-defined pole names and definitions; however, dynamics on the ground are not very well known.

5.1 ON GROUND MODE SHAPES

Three tires on the ground aircraft have 14 poles and two tires on the ground aircraft have 12 poles that affect the dynamics of the aircraft. The linear models can be defined with standard states in the simulation or an adjustment to the landing gear states can be done. These are shown in Table 5.1. Here, s_{mgavg} is the average of s_{lmg} and s_{rmg}, and s_{mgdiff} is the difference between s_{lmg} and s_{rmg}. By defining the main gear states like this longitudinal and lateral states can be separated easier. Two different trim points are calculated to show the dynamics of the aircraft. These are shown in Table 5.2.

Table 5.1 Linear Model States

	Three Tires On The Ground	Two Tires On The Ground
Standard Linear Model States	u, v, w, p, q, r, ϕ, θ, s_{lmg}, s_{rmg}, s_{ng}, $\dot{s}_{lmg}$, $\dot{s}_{rmg}$, $\dot{s}_{ng}$	u, v, w, p, q, r, ϕ, θ, s_{lmg}, s_{rmg}, $\dot{s}_{lmg}$, $\dot{s}_{rmg}$
Alternative Linear Model States	u, v, w, p, q, r, ϕ, θ, s_{mgavg}, s_{mgdiff}, s_{ng}, $\dot{s}_{mgavg}$, $\dot{s}_{mgdiff}$, $\dot{s}_{ng}$	u, v, w, p, q, r, ϕ, θ, s_{mgavg}, s_{mgdiff}, $\dot{s}_{mgavg}$, $\dot{s}_{mgdiff}$

Table 5.2 On ground trim points for ground dynamics investigation of the aircraft

Two Tires on Ground Trim		Three Tires on Ground Trim	
m	9000 kg	m	9000 kg
TAS	45 m/s	TAS	20 m/s
δ_{ail}	0	δ_{ail}	0
θ	16 deg	δ_{ele}	-25 deg
χ	0	χ	0
β	0	a_y	0
		β	0

5.1.1 LONGITUDINAL POLES OF TWO TIRES ON THE GROUND AIRCRAFT

Eigenvalues and eigenvectors are shown in Table 5.3 and Table 5.4. Explanations are done for the modes that are present. Variations of poles with airspeed are shown in Appendix 7.

Table 5.3 Eigenvalues of longitudinal A matrix for two tires on ground trim point

# 1	-169.46	0	0	0	0	0	0	0
# 2	0	-34.833	0	0	0	0	0	0
# 3	0	0	0.830326	0	0	0	0	0
# 4	0	0	0	-1.2018	0	0	0	0
# 5	0	0	0	0	-0.0103	0	0	0
# 6	0	0	0	0	0	-0.4486	0	0
# 7	0	0	0	0	0	0	-11.27	0
# 8	0	0	0	0	0	0	0	-88.723

Table 5.4 Eigenvector matrix for longitudinal two tires on ground trim point

	# 1	# 2	# 3	# 4	# 5	# 6	# 7	# 8
u	0.0031	0.0824	-0.5398	0.2015	0.9855	-0.2029	0	0
w	-0.0119	-0.3122	0.8403	-0.9792	-0.1699	0.9792	0	0
q	-0.0002	-0.0041	0.0319	0.0176	0	-0.0003	0	0
θ	0	0.0001	0.0385	-0.0147	-0.0027	0.0006	0	0
s_{mgavg}	0.0059	0.0272	0.0013	-0.001	-0.0003	0.0007	0	0
s_{ng}	0	0	0	0	0	0	-0.0884	-0.0113
$\dot{s}_{mgavg}$	-0.9999	-0.946	0.0011	0.0012	0	-0.0003	0	0
$\dot{s}_{ng}$	0	0	0	0	0	0	0.9961	0.9999

1st and 2nd modes (Main gear tire heave modes):

The first two modes are the fast motion of the aircraft tire in between the ground and the aircraft. The dominant state is the velocity of the main gear strut. The aircraft gets affected by the motion in a minimal amount. The motion of the aircraft in these modes can be neglected in controller synthesis.

3rd mode (Unstable pitch mode):

In this mode, the dominant state is w. The aircraft makes a pitching motion while the main gear tires remain on the ground. This mode is unstable.

4th and 6th modes (Stable pitch modes):

In these modes the dominant state is again w. The aircraft makes this time a stable pitching motion around the main landing gear tires.

5th mode (Phugoid on the ground):

This is a very long period mode in which the dominant state is u. It describes the long period effect of u on other states of the aircraft.

7th and 8th modes (Nose gear vibration modes):

In these modes the dominant state is the velocity of the nose landing gear strut. They describe the short period vibration of the nose gear wheel with respect to the aircraft. Since the nose landing gear does not touch the ground, it does not affect the motion of the aircraft.

5.1.2 LATERAL POLES OF TWO TIRES ON THE GROUND AIRCRAFT

Eigenvalues and eigenvectors are shown in Table 5.5 and Table 5.6. Explanations are done for the modes that are present. Variations of poles with airspeed are shown in Appendix 8.

1st and 2nd modes (Main gear tire roll modes):

In these modes, main gear wheels of the aircraft move asymmetrically opposite to each other. These modes have very short periods. The dynamics of the aircraft do not get considerably affected by these modes. The dominant state is the difference between main gear strut velocities.

3rd and 4th modes (Rolling vibration of aircraft on the ground)

In these modes the aircraft makes a rolling vibration with respect to the ground. All the states get affected from these modes in a considerable way. The dominant state is p.

5th and 6th modes (Dutch roll on the ground)

In these modes, the dominant pole is v. The aircraft periodically makes changes to its direction in a vibratory way. It is a stable mode.

Table 5.5 Lateral poles of two tires on ground trim point

# 1	-169.84	0	0	0	0	0
# 2	0	-20.799	0	0	0	0
# 3	0	0	-7.730 +14.74i		0	0
# 4	0	0	0	-7.730 -14.74i	0	0
# 5	0	0	0	0	-0.2933 + 1.002i	0
# 6	0	0	0	0	0	-0.2933 - 1.002i

Table 5.6 Eigenvectors for lateral two tires on ground trim point

	# 1	# 2	# 3	# 4	# 5	# 6
v	0.0006643	0.1868	-0.2053 - 0.3523i	-0.2053 + 0.3524i	0.9997	0.9997
p	-0.01056	-0.3767	0.6442	0.6442	0.0002705 + 0.007857i	0.0002705 - 0.007857i
r	-0.0005821	-0.02058	0.03498 - 0.0003780i	0.03498 + 0.0003780i	-0.001882 - 0.02111i	-0.001882 + 0.02111i
ϕ	6.32E-05	0.0184	-0.01826 - 0.03481i	-0.01826 + 0.03481i	0.001731 - 0.0002384i	0.001731 + 0.0002384i
s_{mgdiff}	0.005887	0.04355	-0.03379 - 0.01883i	-0.03379 + 0.01883i	0.001465 - 0.0002475i	0.001465 + 0.0002475i
$\dot{s}_{mgdiff}$	-0.9999	-0.9058	0.5387 - 0.3525i	0.5387 + 0.3525i	-0.0001818 + 0.001539i	-0.0001818 - 0.001539i

5.1.3 LONGITUDINAL POLES OF THREE TIRES ON THE GROUND AIRCRAFT

Eigenvalues and eigenvectors are shown in Table 5.7 and Table 5.8. Explanations are done for the modes that are present. Variations of poles with airspeed are shown in Appendix 9.

1st and 4th modes (Main gear tire heave modes):

These two modes are the fast motion of the aircraft tire in between the ground and the aircraft. The dominant state is the velocity of the main gear strut.

2nd and 3rd modes (Nose gear pitch vibration modes):

In these modes, the dominant state is the velocity of the nose landing gear strut. These modes describe the very short period vibration of the nose gear with respect to the aircraft. The aircraft moves in a minimal amount.

5th and 6th modes (Pitch vibration of the aircraft):

These modes describe the pitch vibration of the aircraft with respect to the ground. While w is the dominant state of these modes, all the modes get affected by a considerable amount.

7th and 8th modes (Phugoid modes on the ground):

These are long period modes that describe the relation between states u and w. The dominant state of 7th mode is u while the dominant state of 8th mode is w.

Table 5.7 Longitudinal poles of three tires on ground trim point

# 1	-168.3	0	0	0	0	0	0	0
# 2	0	-51.95 +47.42i	0	0	0	0	0	0
# 3	0	0	-51.95 -47.42i	0	0	0	0	0
# 4	0	0	0	-35.48	0	0	0	0
# 5	0	0	0	0	-1.007 + 4.546i	0	0	0
# 6	0	0	0	0	0	-1.007 - 4.546i	0	0
# 7	0	0	0	0	0	0	-0.00509	0
# 8	0	0	0	0	0	0	0	-0.4022

Table 5.8 Longitudinal eigenvectors for three tires on ground trim point

	# 1	# 2	# 3	# 4	# 5	# 6	# 7	# 8
u	-0.00043046	-5.7610e-06 + 0.00057050i	-5.7610e-06 - 0.00057050i	0.010112	-0.016512 - 0.0030870i	-0.016512 + 0.0030870i	-0.99742	-0.040465
w	-0.012982	-0.00076549 + 0.017899i	-0.00076549 - 0.017899i	0.30418	-0.8605	-0.8605	0.071751	0.99918
q	-0.0010242	-0.00026059 - 0.0054511i	-0.00026059 + 0.0054511i	0.026173	-0.06503 - 0.18831i	-0.065026 + 0.18831i	2.37E-06	3.36E-05
θ	6.08E-06	-4.9510e-05 + 5.9736e-05i	-4.9510e-05 - 5.9736e-05i	-0.00073743	-0.036779 + 0.022197i	-0.036779 - 0.022197i	-0.000301	-0.0001035
s_{mgavg}	0.0059406	3.7080e-05 - 6.4475e-06i	3.7100e-05 + 6.4475e-06i	-0.026562	-0.014174 + 0.011441i	-0.014174 - 0.011441i	-8.21E-05	0.000631
s_{ng}	-7.56E-06	-0.010497 - 0.0095818i	-0.010497 + 0.0095818i	0.0036964	0.077670 - 0.057528i	0.077670 + 0.057528i	0.0007285	0.0012372
$\dot{s}_{mgavg}$	-0.9999	-0.0016216 + 0.0020942i	-0.0016216 - 0.0020942i	0.94274	-0.038152 - 0.075369i	-0.038152 + 0.075369i	6.48E-07	-0.0002048
$\dot{s}_{ng}$	0.0012728	0.99972	0.99972	-0.1312	0.18563 + 0.40799i	0.18563 - 0.40799i	-5.75E-06	-0.0004014

5.1.4 LATERAL POLES OF THREE TIRES ON THE GROUND AIRCRAFT

Eigenvalues and eigenvectors are shown in Table 5.9 and Table 5.10. Explanations are done for the modes that are present. Variations of poles with airspeed are shown in Appendix 10.

Table 5.9 Lateral poles of three tires on ground trim point

# 1	-168.74	0	0	0	0	0
# 2	0	-18.948	0	0	0	0
# 3	0	0	-10.269 + 14.412i	0	0	0
# 4	0	0	0	-10.269 - 14.412i	0	0
# 5	0	0	0	0	-1.3325	0
# 6	0	0	0	0	0	-0.33384

Table 5.10 Lateral eigenvectors for three tires on ground trim point

	# 1	# 2	# 3	# 4	# 5	# 6
v	-0.00013809	0.039228	-0.013692 - 0.069388i	-0.013692 + 0.069388i	0.99968	0.99871
p	0.011697	-0.44373	0.55718 + 0.37550i	0.55718 - 0.37550i	-0.015035	-0.0040677
r	0.00012235	-0.004231	0.0058895 + 0.0032306i	0.0058895 - 0.0032306i	0.0003006	-0.048708
ϕ	-6.93E-05	0.023415	-0.00099021 - 0.037951i	-0.00099021 + 0.037951i	0.011286	0.010267
s_{mgdiff}	-0.0059258	0.047168	-0.024105 - 0.033829i	-0.024105 + 0.033829i	0.010071	0.008858
$\dot{s}_{mgdiff}$	0.99991	-0.89374	0.73507	0.73507	-0.013419	-0.0029571

1st and 2nd modes (Main gear tire roll modes):

In these modes, the main gear wheels of the aircraft move asymmetrically opposite to each other. These modes have very short periods. The dynamics of the aircraft do not get affected by these modes in a considerable way. The dominant state is the difference between main gear strut velocities.

3rd and 4th modes (Rolling vibration of aircraft on the ground)

In these modes, the aircraft makes a rolling vibration with respect to the ground. All the states get effected by these modes in a considerable way. The dominant state is p.

5th and 6th modes (Spiral on the ground)

In these modes the dominant state is v. The aircraft periodically makes changes to its direction.

5.2 INITIAL CONDITION OF SIMULATIONS

Initial conditions can be found using steady heading and steady sideslip trim calculation. The initial conditions that are calculated are shown in Table 5.11.

Table 5.11 Initial condition of simulations

Crosswind (m/s)	Y position (m)	Track angle (deg)
0	2	2
7.72	2	2
-7.72	2	2

Simulations start when main landing gears are 0.1 meters above the ground. The descent rate is taken as 150 fpm.

5.3 REFERENCE PITCH ANGLE

During the two tires on the ground phase, the controller tracks 16 degrees pitch angle and during the three tires on the ground phase the aircraft still tries to track the reference pitch angle. At this phase, the less vertical force nose gear has the more stable the aircraft is. Keeping more weight on the main gears is also advantageous for braking performance. Trimmable and untrimmable regions and the reference pitch angle are shown in Figure 5.1.

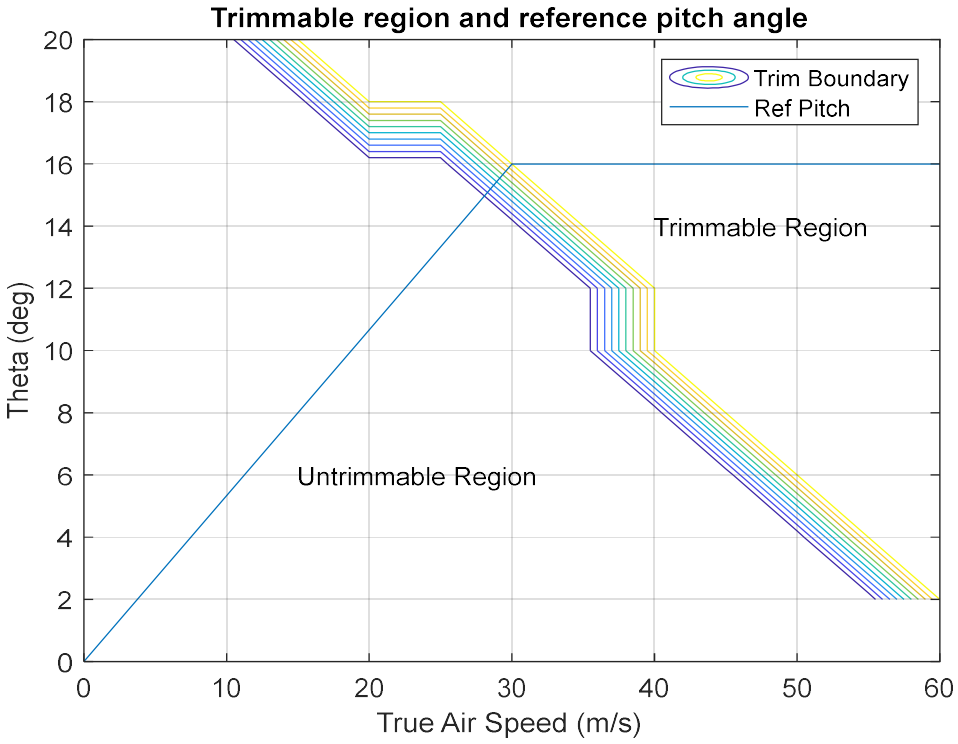

Figure 5.1 Trimmable and untrimmable regions and the reference pitch angle

5.4 CONTROL ALLOCATION OF RUDDER, STEERING AND DIFFERENTIAL BRAKE

B matrices are created for the trim points throughout the landing rollout. Effects of the rudder, steering and differential braking are shown in Table 5.12.

Differential braking is only applied if the other two inputs are not enough. Relationship between percent differential braking and rudder angle is given in Figure 5.2.

For the part where nose gear is on the ground a constant allocation between rudder and steering is given. This allocation constant is 0.5 degrees of steering per 1 degree of the rudder.

Table 5.12 Effectiveness of rudder, steering and differential braking

True airspeed (m/s)	Rudder effectiveness $(deg/s^2)/deg$	Steering effectiveness $(deg/s^2)/deg$	Differential braking effectiveness $(deg/s^2)/percent$
5	-6.12E-05	-0.03277	-0.003002
10	-0.00024	-0.03272	-0.003002
15	-0.00055	-0.03258	-0.003001
20	-0.00098	-0.03225	-0.003001
25	-0.00153	-0.03160	-0.003000
30	-0.00206	0	-0.002796
35	-0.00281	0	-0.002796
40	-0.00367	0	-0.002796
45	-0.00464	0	-0.002796
50	-0.00573	0	-0.002796
55	-0.00693	0	-0.002796
60	-0.00825	0	-0.002796

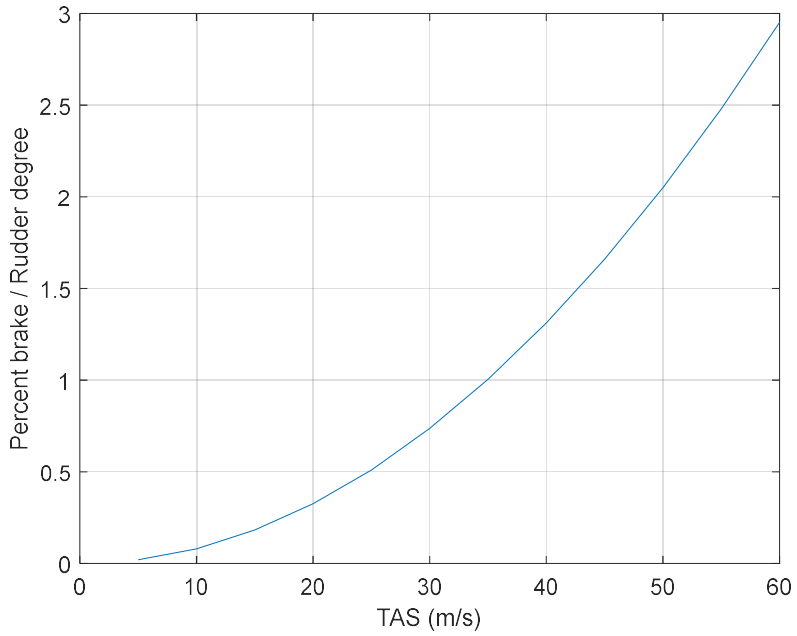

Figure 5.2 Relationship between differential brake and rudder with respect to speed of the aircraft

5.5 ON GROUND LATERAL CONTROL STRATEGY

There are three possible strategies for lateral control on the ground. These are:

- Fix the roll angle at zero and control the lateral acceleration using the yaw angle
- Fix the yaw angle at zero and control the lateral acceleration using the roll angle
- Control the lateral acceleration using both the yaw angle and roll angle

The third strategy is used for maximum control authority.

Lateral acceleration must be limited for safety. The limit is taken as 1 m/s^2.

Yaw reference is produced such that the aircraft tracks the reference lateral acceleration. Roll angle reference is produced such that for 1 m/s^2 lateral acceleration reference 6 degrees of reference roll is also commanded. 6 degrees per 1 m/s^2 is selected based on the calculation of lateral acceleration created by a 1 g lift producing wing. When the lift is equal to weight 6 degrees of roll angle creates approximately 1 m/s^2 lateral acceleration. At high speeds, effect of the roll angle on lateral acceleration is dominant whereas at low speeds where there is no longer aileron authority to control the roll angle, effect of the yaw angle on lateral acceleration is dominant.

6. OUTER LOOP GUIDANCE

An outer loop guidance for tracking the midline of the runway is necessary for the autoland system application. Outer loop guidance creates reference lateral acceleration and inner loop autopilot makes the maneuver with the specified lateral acceleration.

In this chapter, a comparison study for outer loop guidance algorithms is done. Five different algorithms are selected. The first of these algorithms is the carrot chase algorithm which is also studied by Sujit et al. [39]. In the original carrot chase algorithm, an imaginary point Δx ahead of the aircraft is tracked. In this study, this is modified as $\Delta x + V\Delta t$. The reason for this is the variable speed during the landing rollout. Because of the highly variable speed Δx is not sufficient for a successful guidance algorithm in this case. Another algorithm that is studied is the vector field guidance algorithm. For the creation of the near vector field, a simple linear varying equation is used. The third algorithm is the sliding mode guidance algorithm. Here, a nonlinear function that contains sign(x) is used to guarantee the tracking of the sliding surface in finite time. The fourth algorithm is the linear sliding mode guidance algorithm. Here, sat(x) function is used instead of the sign(x) [41]. While this cannot guarantee the tracking of the sliding surface in finite time, the algorithm became linear and there is no chattering phenomenon. The fifth algorithm that is studied is the geometric predictive guidance algorithm. This algorithm uses two minimum radius circles [55] in which one of which is tangent to the velocity of the plane, and the other one is tangent to the midline of the runway. The two circles are also tangent to each other. Using these two tangent circles the route of the aircraft is predicted.

6.1 MODELING THE AIRCRAFT AND INNER LOOP CONTROLLER

The lateral dynamics of the aircraft and the inner controller loop which tracks the lateral acceleration is modeled as a first order transfer function (Figure 6.1). The time constant of this transfer function is assumed as 0.4s. The aircraft is assumed to track the lateral acceleration in accordance with this first-order transfer function.

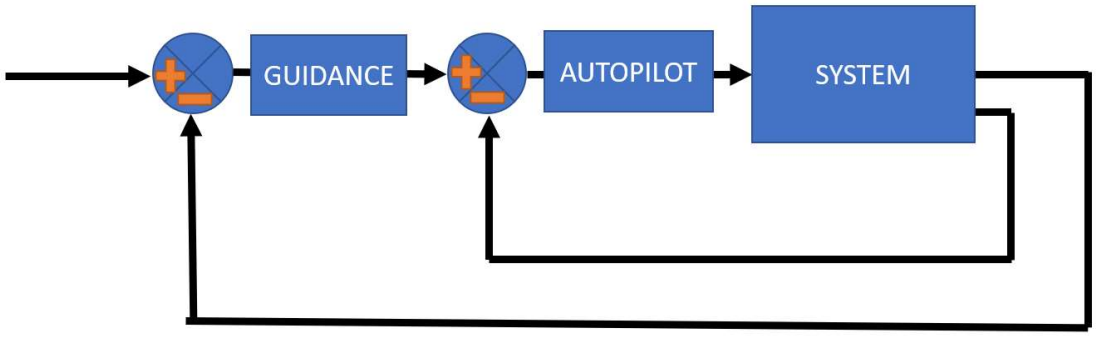

Figure 6.1 Outer loop and inner loop

6.2 GUIDANCE ALGORITHMS

Before the introduction of the guidance algorithms the runway coordinate system which is used for the calculations must be presented.

6.2.1 RUNWAY COORDINATE SYSTEM

The touchdown point is taken as origin. The direction at which the aircraft lands is taken as the x-axis, down direction is taken as the z-axis. When the x-axis is rotated 90 degrees in the direction of the z-axis it becomes the y-axis (Figure 6.2). This coordinate system is the modified NED axis in which the coordinate system is rotated around the z-axis such that the x-axis aligns with the landing direction.

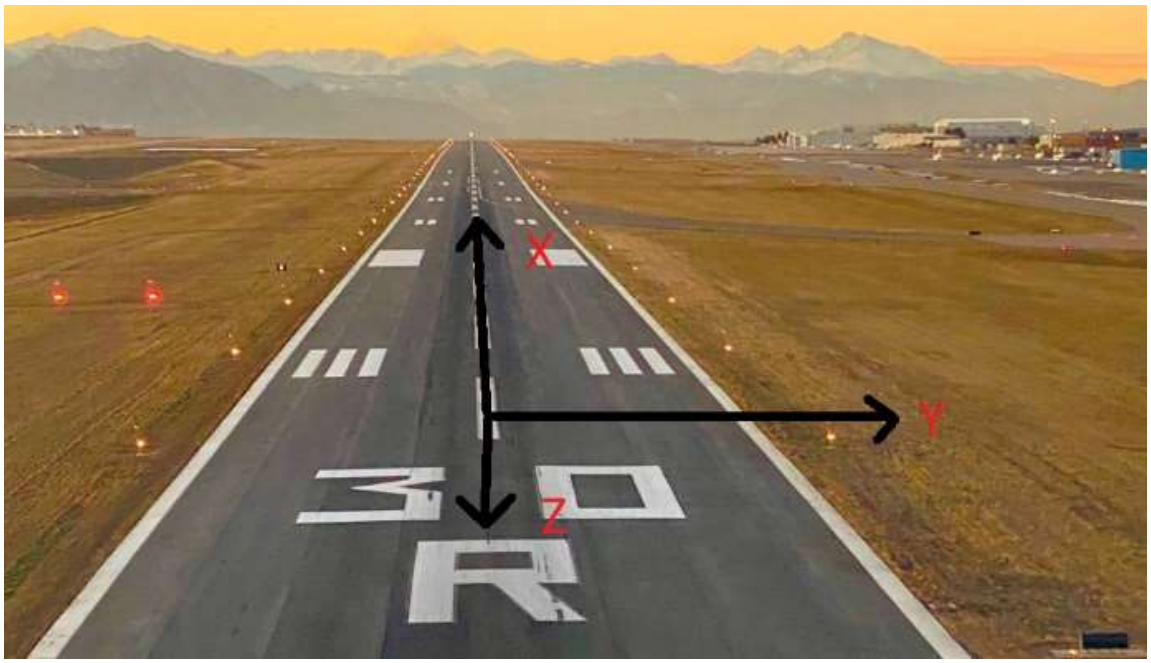

Figure 6.2 Runway coordinate system [56]

6.2.2 SUCCESS CRITERIA FOR THE GUIDANCE ALGORITHMS

Before the selection of the guidance algorithm, success criteria must be decided. The expected behavior of the aircraft during landing rollout is to go straight with minimal lateral maneuver and stay inside the runway. While the aircraft is not required to track the midline strictly, staying close to the runway midline can be considered a bonus. Important point is to land safely.

Reference acceleration commands of the guidance algorithms are limited to 1 m/s^2 in each direction. As a result of this, the aircraft does not make hard maneuvers.

For all the algorithms integral of the midline tracking error and the integral of lateral acceleration are calculated. The results of the integrals are compared. The expected result is that the integrals of both tracking error and lateral acceleration are small.

6.2.3 MODIFIED PROPORTIONAL CARROT CHASE ALGORITHM

In proportional guidance (Equation 6.1) a point is tracked.

$$a_{ref} = N_{PG}\dot{\lambda}\Delta V \tag{6.1}$$

In the equation a_{ref} denotes the acceleration command, N_{PG} is a proportionality constant, $\dot{\lambda}$ denotes the rate of change of line-of-sight angle between the vehicle and the target, ΔV denotes the relative speed between the vehicle and the target.

The task is to specify an imaginary point on the midline. The imaginary point that is proposed in this study is a point that is $\Delta x + V\Delta t$ ahead of the aircraft and on the midline of the runway (Figure 6.3). Here, V is taken as the speed of the aircraft with respect to the ground.

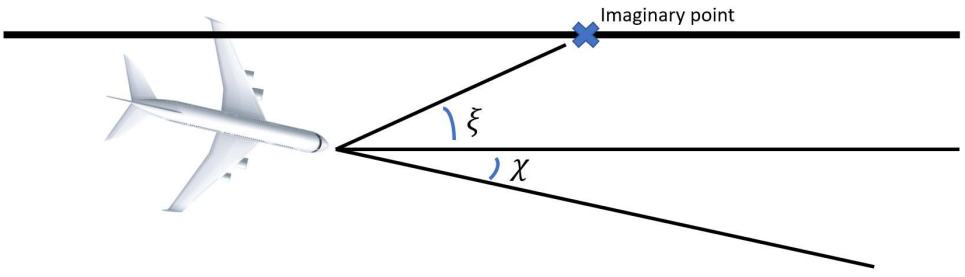

Figure 6.3 Modified proportional carrot chase algorithm

Two angles must be defined. Track angle (χ) is the angle between the velocity vector of the aircraft and the x-axis of the runway. Target angle (ξ) is the angle of the target with respect to the aircraft in runway axis (Figure 6.3). Sum of these two angles shows the angle of the target with respect to the velocity vector of the aircraft.

The relation of χ with x and y is shown in Equations 6.2 and 6.3. Relation of χ with a_y is shown in Equation 6.4.

$$\dot{x} = V\cos\chi \tag{6.2}$$

$$\dot{y} = V\sin\chi \tag{6.3}$$

$$\dot{\chi} = a_y/V \tag{6.4}$$

The relation of ξ with position and velocity is shown in Equations 6.5 and 6.6. Equation 6.5 is differentiated with respect to time to obtain Equation 6.6.

$$\xi = -\tan^{-1}\left(\frac{y}{V\Delta t+\Delta x}\right) \tag{6.5}$$

$$\dot{\xi} = -\left(\frac{1}{1+\left(\frac{y}{V\Delta t+\Delta x}\right)^2}\right)\frac{\dot{y}(V\Delta t+\Delta x)-y\dot{V}\Delta t}{(V\Delta t+\Delta x)^2} \tag{6.6}$$

The relation between a_y and $a_{y_{ref}}$ is given in Equation 6.7. τ_{a_y} is defined as the time constant of the inner loop.

$$\dot{a}_y = (a_{y_{ref}} - a_y)\frac{1}{T_{a_y}} \tag{6.7}$$

Guidance law is given in Equation 6.8.

$$a_{y_{ref}} = N_{PG}(\dot{\xi} - \dot{\chi})V \tag{6.8}$$

The aircraft is assumed to decelerate with 4 m/s^2. States that are used in the simulation are given in Table 6.1 States for simulation of modified proportional carrot chase algorithm.

Table 6.1 States for simulation of modified proportional carrot chase algorithm

State Symbol	State Name
X	X position
Y	Y position
V	Ground speed of the aircraft
χ	Track angle
a_y	Lateral acceleration

6.2.4 VECTOR FIELD GUIDANCE ALGORITHM

In this algorithm, there is a predefined vector field that is tracked by the aircraft. The vector field that is used in this study is given in Figure 6.4 Vector field on the runway. In this vector field, reference track angles are given with respect to the lateral position of the aircraft. This vector field is specified such that the track angle changes proportionally with the lateral position.

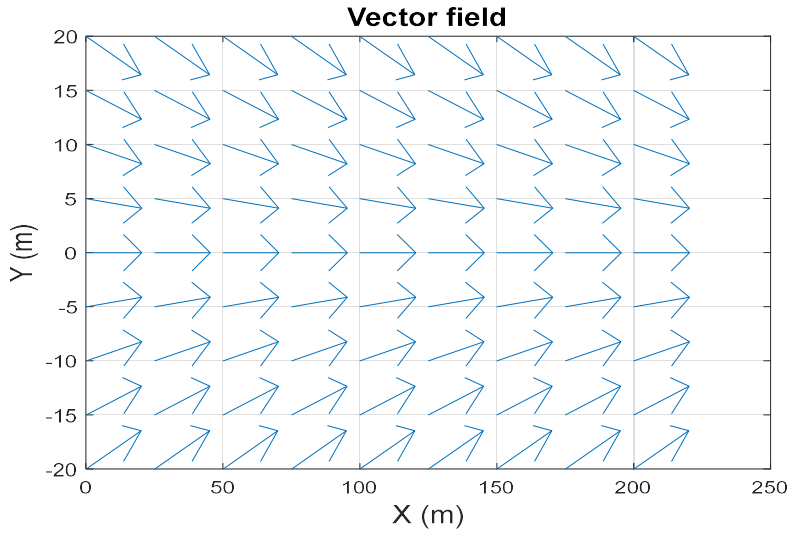

Figure 6.4 Vector field on the runway

Equations 6.2, 6.3, 6.4 and 6.7 hold for this algorithm too. Guidance law is given in Equation 6.9. To track the reference track angle, proportional navigational guidance law is used. To adjust for the change in speed a new parameter V_{ref} is added. Proportional guidance is designed for a specific speed and adjusted for other speeds. Under the speeds of 10 m/s guidance law is calculated as if speed is 10 m/s so that the algorithm works at slow speeds.

$$a_{y_{ref}} = N_{PG}(\chi_{ref} - \chi)\frac{V_{ref}}{\max([V,10])} \tag{6.9}$$

6.2.5 SLIDING MODE GUIDANCE ALGORITHM

In this algorithm, lateral speed and lateral position is required to follow a sliding surface. There are two different commands for two different sides of the sliding surface. The designed manifold and the commands for two sides of it are shown in Equation 6.10.

$$a_{y_{ref}} = \begin{cases} 1, & \dot{y} \leq -0.1 \operatorname{sign} y \, y^2 \\ -1, & \dot{y} > -0.1 \operatorname{sign} y \, y^2 \end{cases} \tag{6.10}$$

Equations 6.2, 6.3, 6.4 and 6.7 hold for the simulation of this algorithm also.

6.2.6 LINEAR SLIDING MODE GUIDANCE ALGORITHM

To make the guidance law linear, the sliding surface must be linear and the transition between the two sides of the sliding surface must be dictated by a linear relation.

The linear sliding surface function is given in Equation 6.11. The time constant of the sliding surface was selected such that it is slower than the time constant of the inner loop.

$$\dot{y} = -0.3y \tag{6.11}$$

The guidance law that dictates the linear transition at the sliding surface is shown in Equation 6.12.

$$a_{y_{ref}} = (\dot{y} - (-0.3y)) * (-3) \tag{6.12}$$

$a_{y_{ref}}$ is bounded between -1 and 1 m/s^2. Inside this bound it changes linearly according to Equation 6.12.

6.2.7 GEOMETRIC PREDICTIVE GUIDANCE

In this algorithm, two minimum radius circles calculated using the maximum allowable lateral acceleration are used to predict the maneuver of the aircraft [54]. These circles and the critical point (CP), midpoint (MP), and line point (LP) that are used in the algorithm are shown in Figure 6.5.

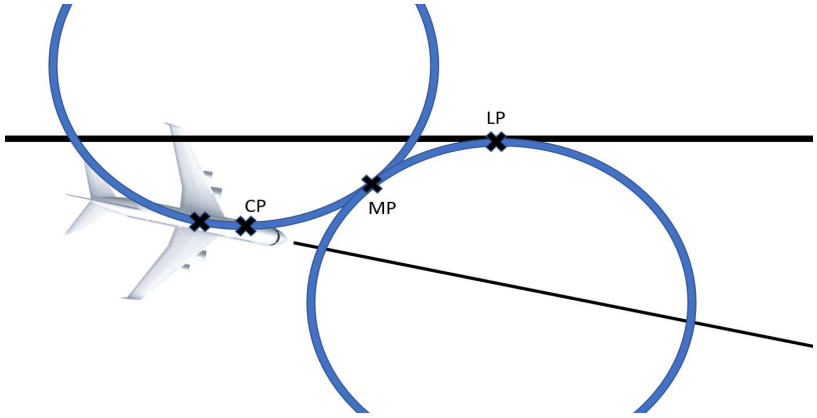

Figure 6.5 Geometric predictive guidance algorithm

To find the coordinates in Figure 6.5 the first thing that must be done is to calculate the radius of the circles (Equation 6.13). In this equation, a_y is taken as 1 m/s^2.

$$r_c = \frac{V^2}{a_y} \tag{6.13}$$

Guidance law is given in Equation 6.14. CP and MP are calculated. If the aircraft hasn't arrived at CP yet, maximum acceleration command towards MP is given. If the aircraft is between CP and MP, again maximum acceleration command towards MP is given. If the aircraft has passed MP maximum acceleration command in the opposite direction is given.

$$
\begin{aligned}
&If\ y \leq 0\{\\
&\quad x_{CP} = x - r\sin\chi\\
&\quad y_{CP} = y - r\sin\chi\sin\chi\\
&\quad y_{MP} = y_{CP}/2\\
&\quad If\ x_{CP} > x\{\\
&\quad\quad a_{y_{ref}} = 1\}\\
&\quad Else\ If\ x_{CP} \leq x\{\\
&\quad\quad If\ \frac{y}{y_{MP}} < 1\{\\
&\quad\quad\quad a_{y_{ref}} = -1\}\\
&\quad\quad Else\ If\ \frac{y}{y_{MP}} \geq 1\{\\
&\quad\quad\quad a_{y_{ref}} = 1\}\}\}\\
&Else\ If\ y > 0\{\\
&\quad x_{CP} = x + r\sin\chi\\
&\quad y_{CP} = y + r\sin\chi\sin\chi\\
&\quad y_{MP} = Y_{CP}/2\\
&\quad If\ x_{CP} > x\{\\
&\quad\quad a_{y_{ref}} = -1\}\\
&\quad Else\ If\ X_{CP} \leq X\{\\
&\quad\quad If\ \frac{y}{y_{MP}} < 1\{\\
&\quad\quad\quad a_{y_{ref}} = 1\}\\
&\quad\quad Else\ If\ \frac{y}{y_{MP}} \geq 1\{\\
&\quad\quad\quad a_{y_{ref}} = -1\}\}\}
\end{aligned}
\tag{6.14}
$$

If a maximum command is given between CP and MP the aircraft will arrive at the midline in minimum time, however; this is not necessary. To soften the response in this interval one can make adjustments to the guidance law. An example adjustment is given in Figure 6.6.

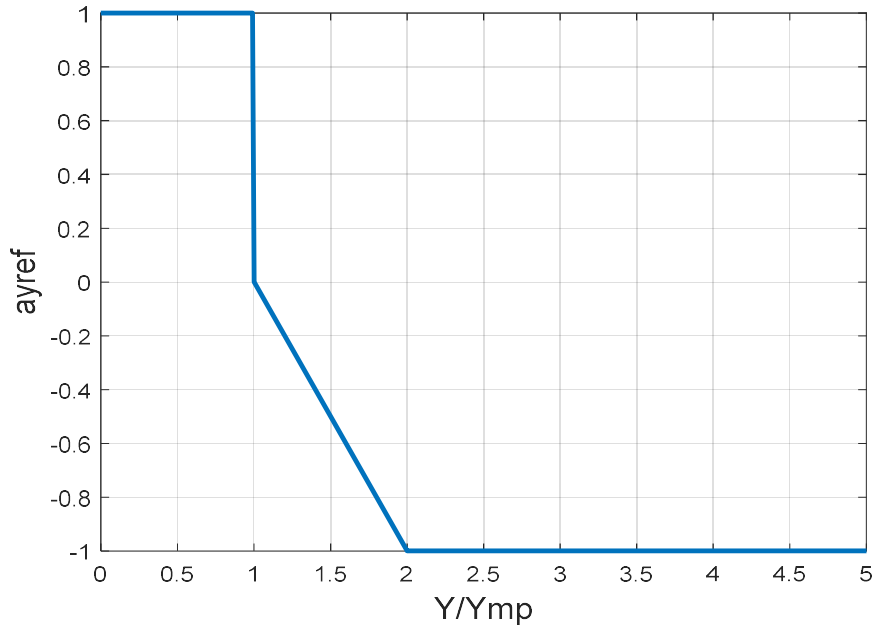

Figure 6.6 Adjustment to reference lateral acceleration command

6.3 RESULTS

Aircraft simulation starts from 80 m/s ground speed, -2 m y position, with $-2°$ and $2°$ track angles. Results are shown in Figures Figure 6.7 to Figure 6.16.

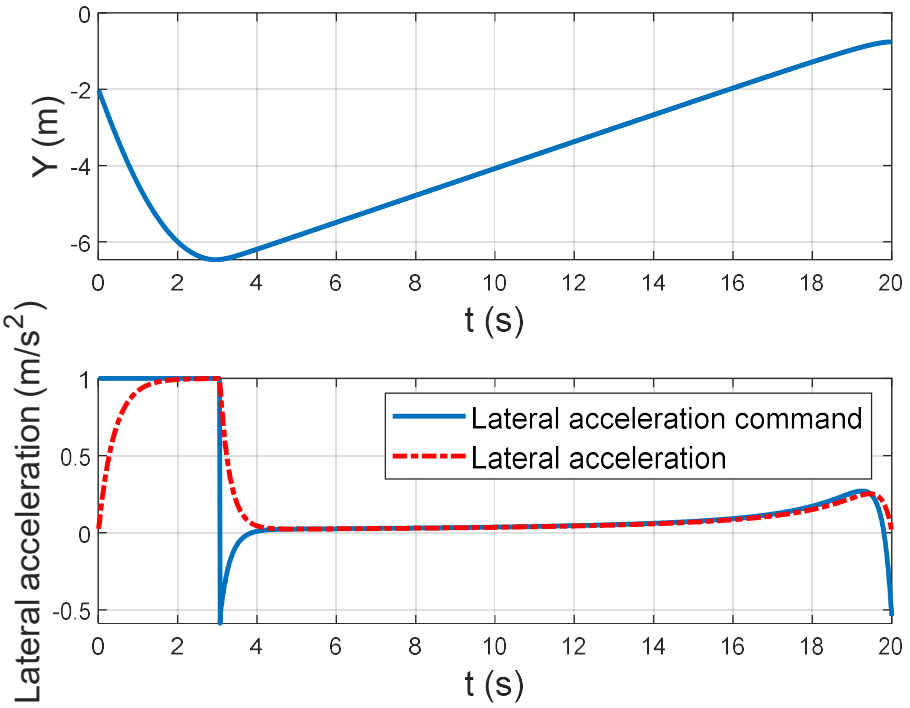

Figure 6.7 Performance of modified proportional carrot chase algorithm with -2 degrees track angle and -2 m lateral position initial condition

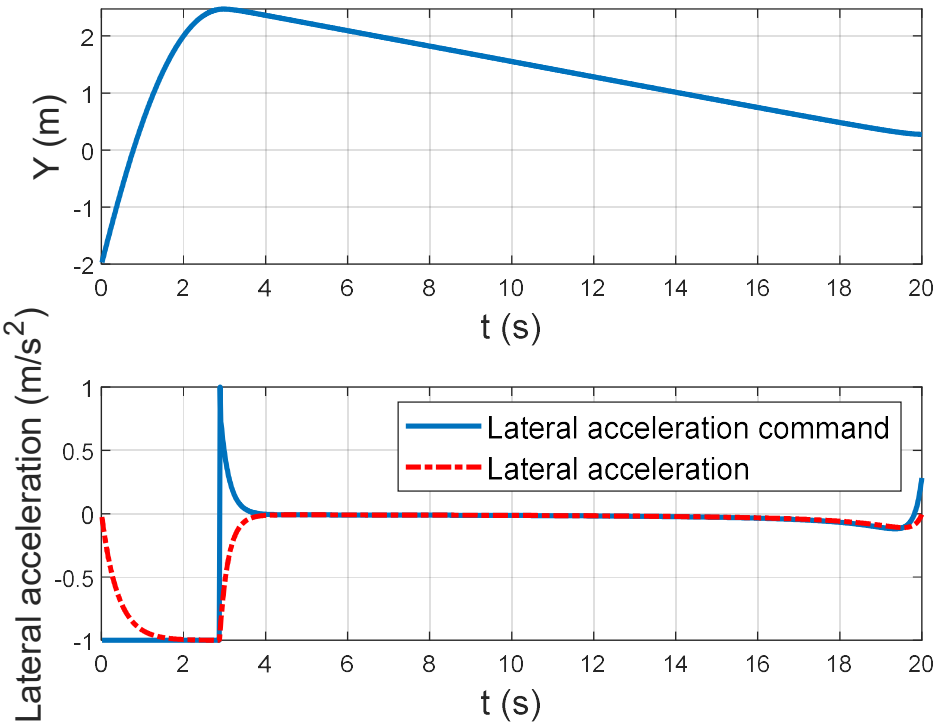

Figure 6.8 Performance of modified proportional carrot chase algorithm with 2 degrees track angle and -2 m lateral position initial condition

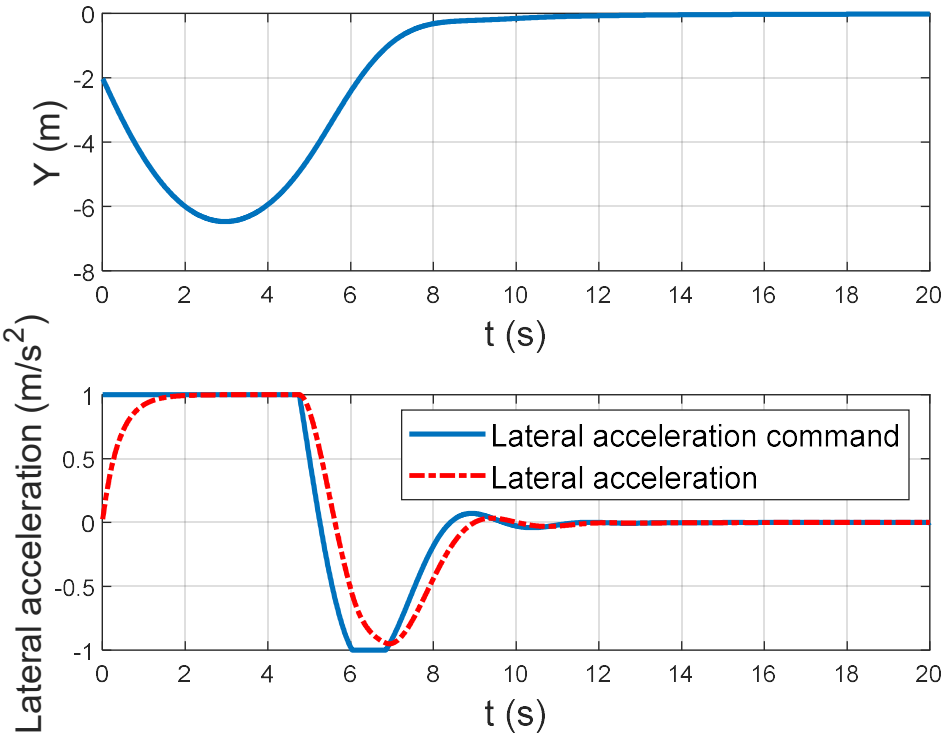

Figure 6.9 Performance of vector field guidance algorithm with -2 degrees track angle and -2 m lateral position initial condition

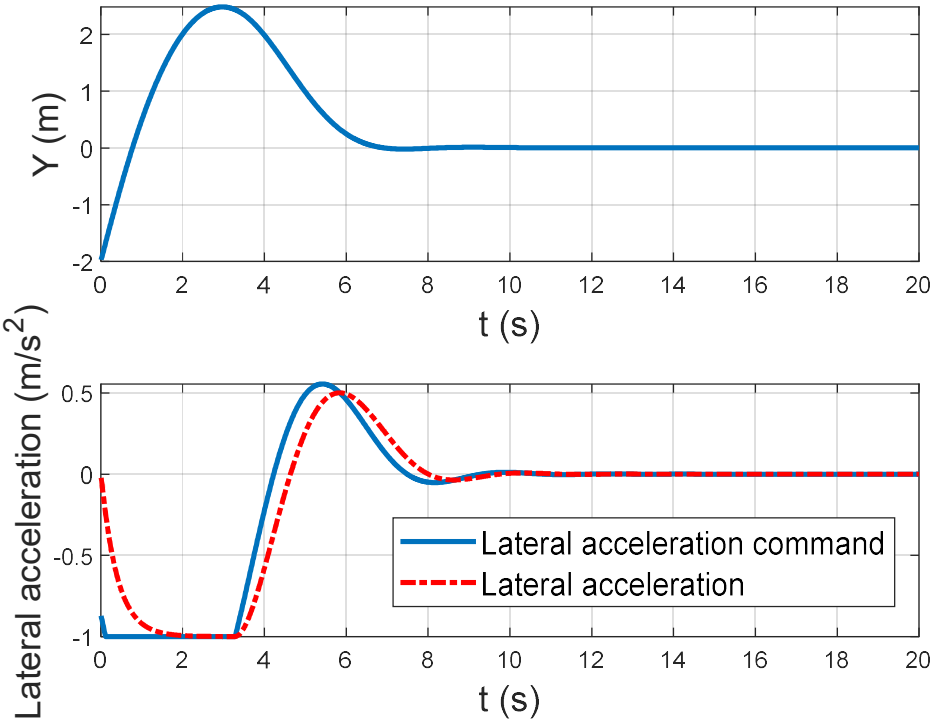

Figure 6.10 Performance of vector field guidance algorithm with 2 degrees track angle and -2 m lateral position initial condition

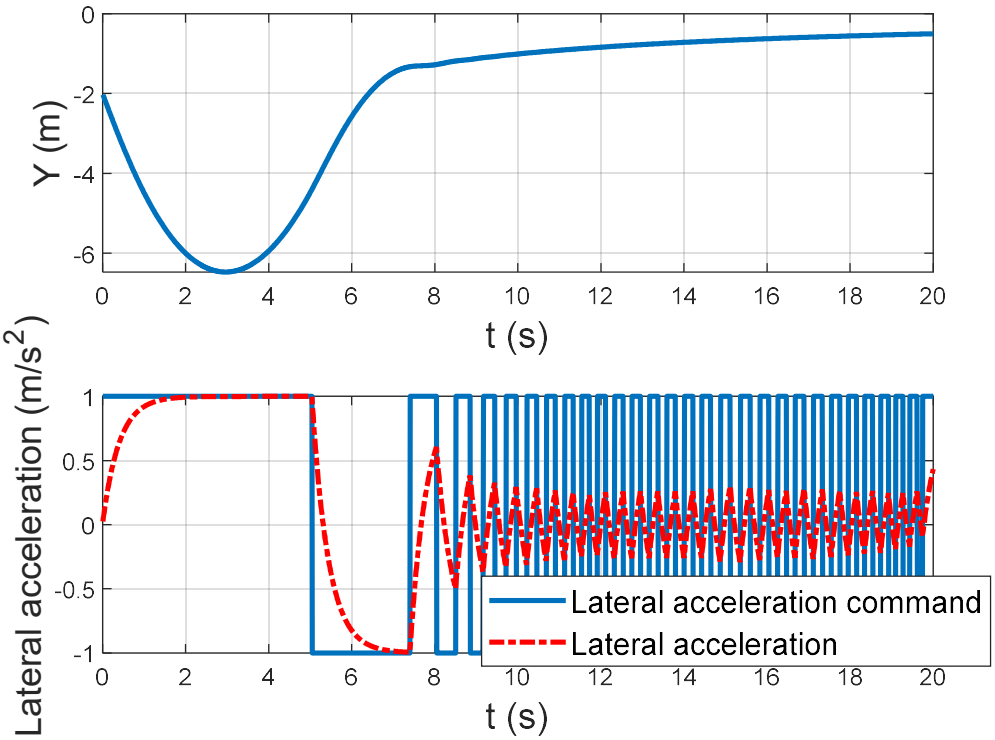

Figure 6.11 Performance of sliding mode guidance algorithm with -2 degrees track angle and -2 m lateral position initial condition

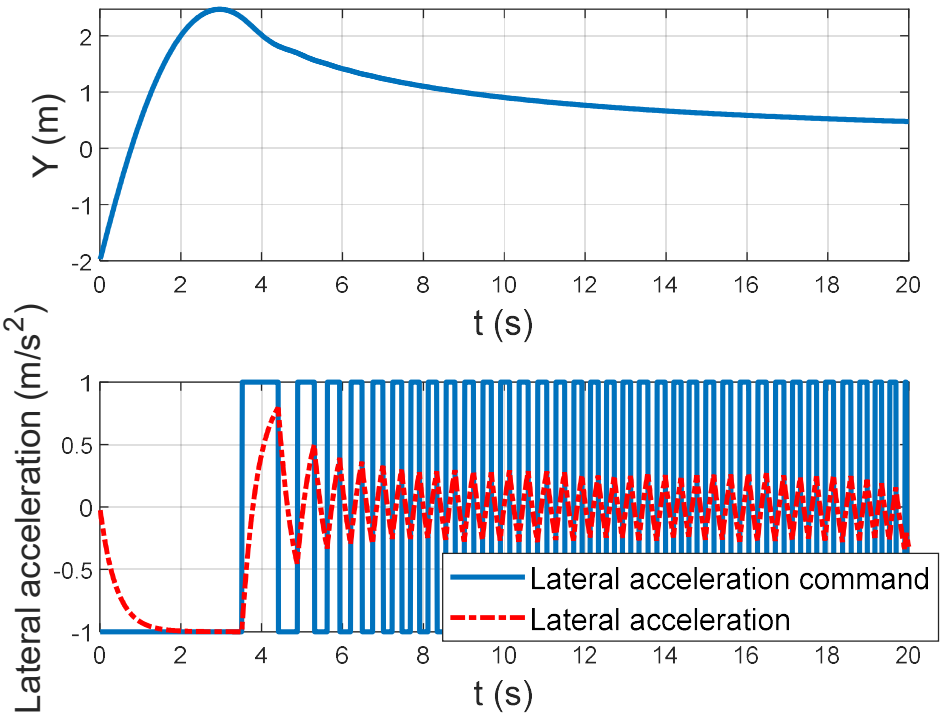

Figure 6.12 Performance of sliding mode guidance algorithm with 2 degrees track angle and -2 m lateral position initial condition

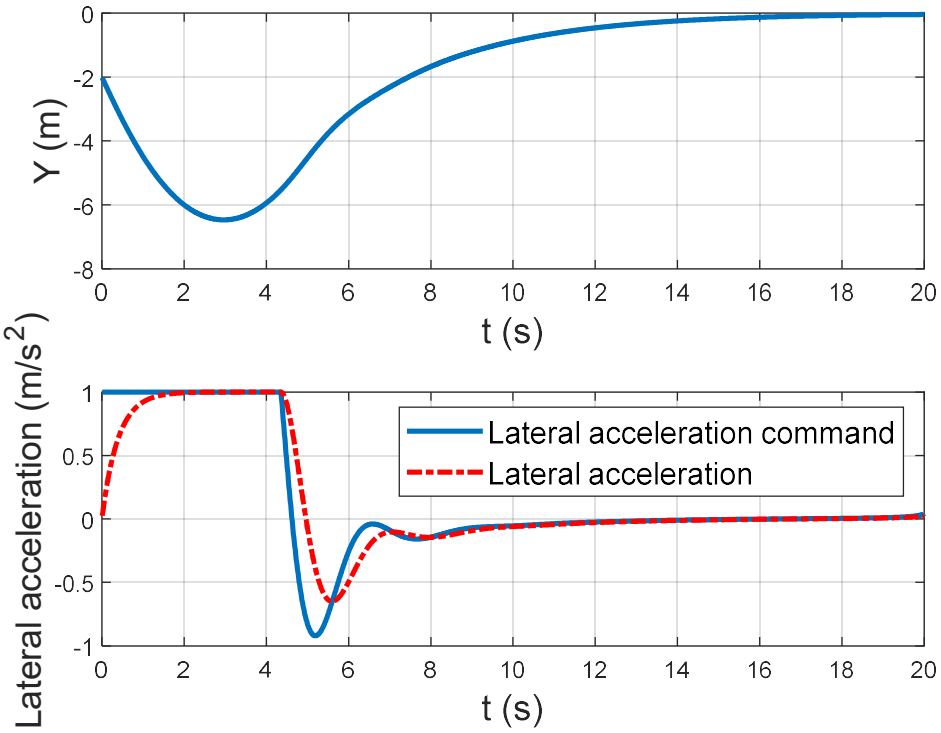

Figure 6.13 Performance of linear sliding mode guidance algorithm with -2 degrees track angle and -2 m lateral position initial condition

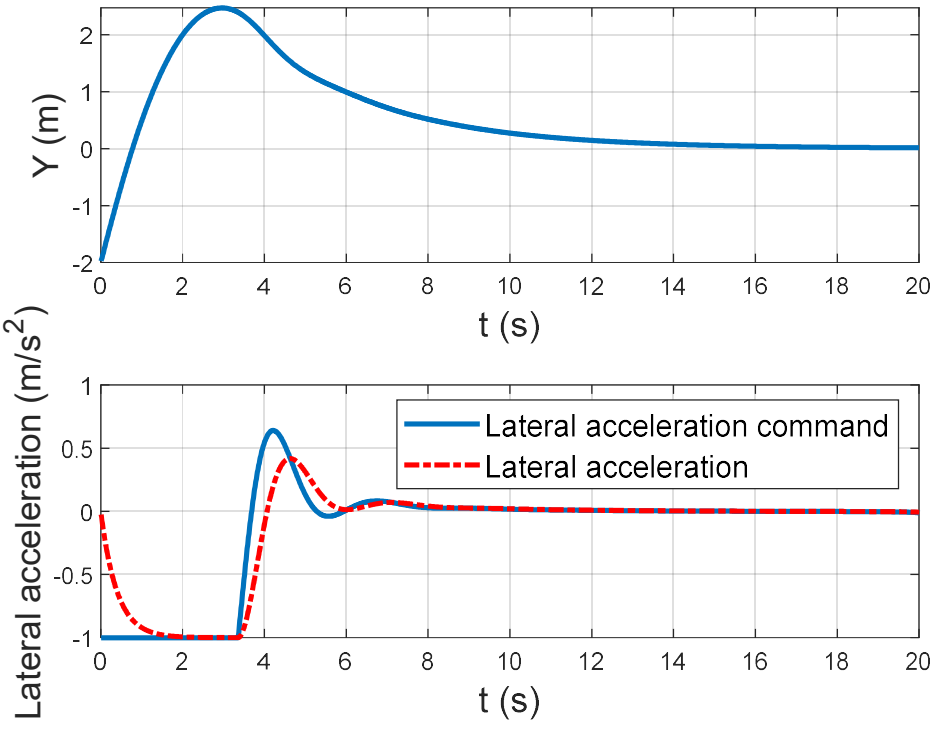

Figure 6.14 Performance of linear sliding mode guidance algorithm with 2 degrees track angle and -2 m lateral position initial condition

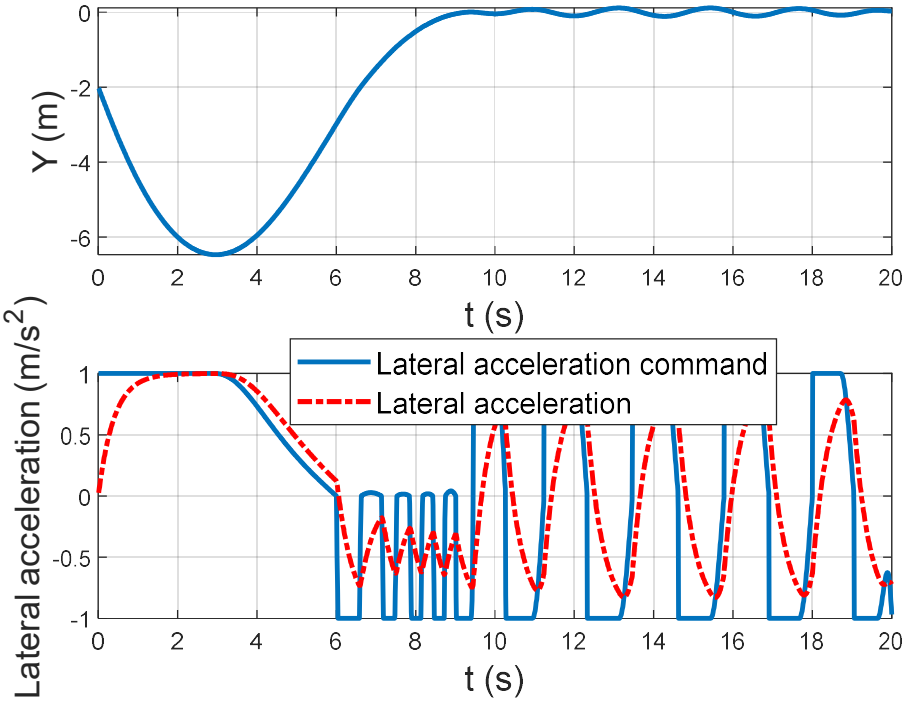

Figure 6.15 Performance of geometric predictive guidance algorithm with -2 degrees track angle and -2 m lateral position initial condition

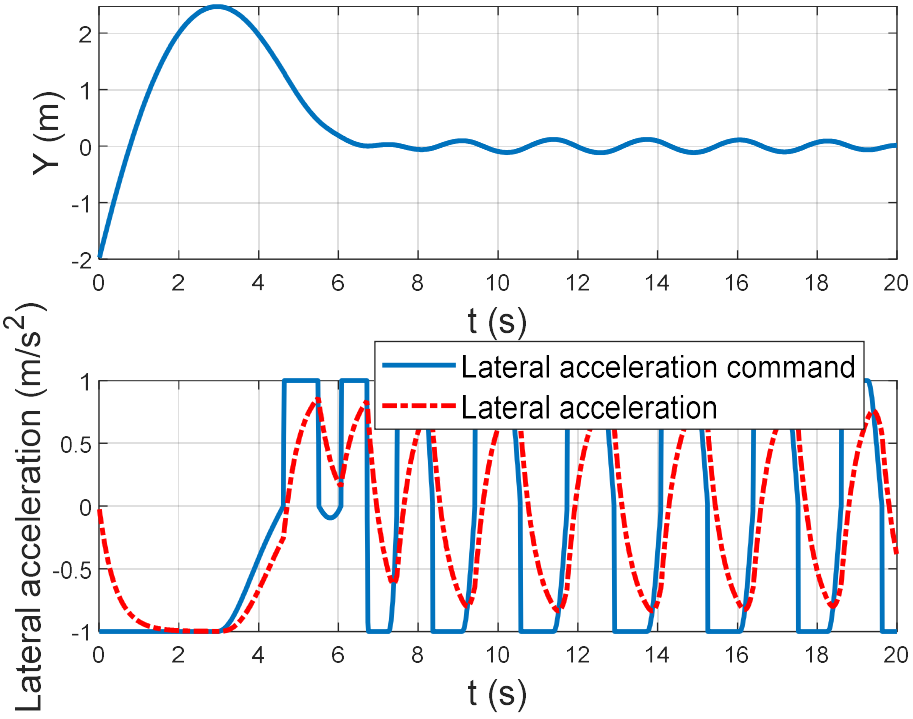

Figure 6.16 Performance of geometric predictive guidance algorithm with 2 degrees track angle and -2 m lateral position initial condition

For two different initial conditions, error and control effort values are in Table 6.2. In parallel to the findings in the literature vector guidance algorithm has the least tracking error while the modified proportional carrot chase algorithm has the least control effort value and the linear sliding mode guidance law performs in between these two algorithms for both criteria. For the remaining two algorithms control effort values are too high to be considered a viable option for the aircraft landing rollout application.

In this study, linear sliding mode guidance is chosen as the outer loop guidance method.

Table 6.2 Comparisons of different guidance algorithms in terms of midline tracking and control effort

Algorithm	Position tracking error (Midline tracking)		Integral of lateral acceleration (Control effort)	
Initial track angle (degree)	-2	2	-2	2
Modified proportional carrot chase algorithm	75.48	27.46	4.03	3.14
Vector field guidance algorithm	33.07	8.98	6.80	4.68
Sliding mode guidance algorithm	42.55	20.99	42.98	21.31
Linear sliding mode guidance algorithm	40.15	12.57	5.56	4.00
Geometric predictive guidance algorithm	34.45	9.52	11.55	11.73

7. INNER LOOP SLIDING MODE CONTROLLER SYNTHESIS

In this part, the synthesis of the inner loop sliding mode controller is done. Tracking performance, stability, and disturbance rejection characteristics are proven. There are three different controllers to be designed. One of them is the pitch angle controller which is needed to keep the pitch angle of the aircraft in the desired position. The reference pitch angle is a function of the ground speed of the aircraft. The second controller is the lateral acceleration controller. Reference lateral acceleration comes from the outer loop guidance. The third controller that is designed is the roll angle controller. Here, the reference roll angle again comes from the outer loop guidance. 6 degrees roll angle command per 1 m/s^2 lateral acceleration command is given.

Before the synthesis of the controller, the theory of sliding mode control and the structure of the controller must be explained, and the requirements of the controller must be defined.

7.1 THEORY OF SLIDING MODE CONTROL

In this section, the theory of sliding mode control is explained based on the first chapter of Shtessel et al. [57]. For an illustration of the theory a simple system of one-dimensional motion of a unit mass is defined. Here, x_1 denotes position, x_2 denotes velocity, u_1 denotes the control input force and f denotes the disturbance. The equation of motion of the system is shown in Equation 7.1.

$$\begin{cases} \dot{x}_1 = x_2 \\ \dot{x}_2 = u_1 + f(x_1, x_2, t) \end{cases} \tag{7.1}$$

7.1.1 MAIN CONCEPTS OF SLIDING MODE CONTROL

The first job is to determine a desired compensated dynamics for the system in Equation 7.1. A good candidate is the homogeneous linear time-invariant differential equation shown in Equation 7.2.

$$\dot{x}_1 + cx_1 = 0,\ c > 0 \tag{7.2}$$

A general solution to Equation 7.2 is shown in Equation 7.3.

$$\begin{cases} x_1(t) = x_1(0)e^{-ct} \\ x_2(t) = -cx_1(0)e^{-c} \end{cases} \tag{7.3}$$

This is the ideal dynamics of the system that should be achieved by sliding mode controller in presence of disturbances. To this end, another variable denoted σ must be introduced in Equation 7.4.

$$\sigma = x_2 + cx_1,\ c > 0 \tag{7.4}$$

To achieve asymptotic convergence, the sliding variable σ must be driven to zero in finite time by the control input u. This task can be achieved by Lyapunov function techniques. For the dynamics of σ (Equation 7.5) a Lyapunov function can be the one in Equation 7.6.

$$\dot{\sigma} = \dot{x}_2 + cx_2 = cx_2 + u_1 + f(x_1, x_2, t) \tag{7.5}$$

$$V = \frac{1}{2}\sigma^2 \tag{7.6}$$

To guarantee asymptotic stability for σ, the following conditions must hold.

i. $\dot{V}_L < 0$ for $\sigma \neq 0$

ii. $\lim_{|\sigma|\to\infty} V_L = \infty$

Condition ii is already satisfied. Condition i can be modified to be as in Equation 7.7.

$$\dot{V}_L \leq -\alpha {V_L}^{1/2},\ \alpha > 0 \tag{7.7}$$

By separation of variables and integration, one can obtain Equation 7.8.

$${V_L}^{1/2}(t) \leq -\frac{1}{2}\alpha t + {V_L}^{1/2}(0) \tag{7.8}$$

From Equation 7.8 it can be concluded that $V(t)$ reaches zero in finite time t_r which is bounded by the relation in Equation 7.9.

$$t_r \leq \frac{2{V_L}^{1/2}(0)}{\alpha} \tag{7.9}$$

From further calculations, a control law that drives σ to zero in finite time can be calculated as in Equation 7.10. The control gain ρ has a component for sliding mode and a component for disturbance rejection. The component for disturbance rejection must be bigger than the maximum value of the disturbance input signal.

$$u_1 = -cx_2 - \rho\, sign(\sigma),\ \rho > 0 \tag{7.10}$$

Remark 7.1 $\dot{\sigma}$ must be a function of u in to be able to design a controller.

Definition 7.1 σ is called the sliding variable.

Definition 7.2 Equation 7.4 is called a sliding surface.

Definition 7.3 Equation 7.10 is called a sliding mode controller.

Due to the discontinuous nature of Equation 7.10, a phenomenon called chattering occurs. To remedy this problem, following procedures may be implemented.

7.1.2 CHATTERING AVOIDANCE

In practical control systems, chattering is an unwanted phenomenon that must be solved using continuous control signals while also keeping the robust nature of the sliding mode controller. Here, two of the solutions to this problem are explained. These are:

- Quasi sliding mode
- Asymptotic sliding mode

7.1.2.1 QUASI SLIDING MODE

One way to make the control input signal continuous is to make the discontinuous sign function continuous using a sigmoid function (Equation 7.11) or sat function [41].

$$sign(\sigma) \approx \frac{\sigma}{|\sigma|+\varepsilon} \tag{7.11}$$

Equation 7.11 becomes equivalent to sign function if ε is infinitesimally small.

The problem with this approach is the decreased robustness since the sliding variable does not approach zero in finite time and the disturbances are not completely rejected.

7.1.2.2 ASYMPTOTIC SLIDING MODE

Another approach is to control the system with the derivative of the control input variable which is $\dot{u}_1$ in our example system. In this case, $\dot{u}_1$ is discontinuous, however; the integral of $\dot{u}_1$ which is u_1 becomes continuous.

In this case the system is redefined as in Equation 7.12.

$$\begin{cases} \dot{x}_1 = x_2 \\ \dot{x}_2 = u_1 + f(x_1, x_2, t) \\ \dot{u}_1 = v_1 \end{cases} \tag{7.12}$$

Here, the disturbance is assumed to be bounded and continuous with a bounded time derivative.

To design a new sliding mode controller based on the newly defined control input v_1, one must define another auxiliary sliding variable (Equation 7.13).

$$s_1 = \dot{\sigma} + c_1\sigma \tag{7.13}$$

By guaranteeing a finite time convergence of the auxiliary sliding variable s, one can obtain a system with asymptotic convergence for the real sliding variable σ. The control law for this condition can be obtained as Equation 7.14.

$$v_1 = -cc_1x_2 - (c + c_1)u_1 - \rho\, sign(s_1) \tag{7.14}$$

This approach in theory rejects the disturbance and guarantees asymptotic convergence for the states of the system. However, the problem is the differentiation that is done for the real sliding variable in Equation 7.13. Numerical differentiation of an already noisy signal may not work in real life. Nevertheless, there are some solutions to this problem. These are sliding mode observers and differentiators that are discussed in the coming sections.

7.1.3 CONCEPT OF EQUIVALENT CONTROL

An equivalent control function can be estimated for the time after the sliding surface has been reached. In this region, the derivative of the sliding surface is zero (Equation 7.5). Equivalent control input is calculated as Equation 7.15.

$$u_{eq} = -cx_2 - f(x_1, x_2, t) \tag{7.15}$$

Definition 7.4 The control input that is needed to keep the system at sliding mode after it has been reached is called the equivalent control.

The equivalent control can be estimated using a low pass filter (LPF) as it is shown in Equation 7.16. In this equation $\hat{u}_{eq}$ denotes the estimated equivalent control input and t_r denotes the reaching time for the sliding mode.

$$\hat{u}_{eq} = -cx_2 - \rho\, LPF\big(sign(\sigma)\big), \quad t > t_r \tag{7.16}$$

The disturbance term can also be easily estimated (Equation 7.17) by combining Equations 7.15 and 7.16.

$$\hat{f}(x_1, x_2, t) = \rho\, LPF\big(sign(\sigma)\big), \quad t > t_r \tag{7.17}$$

7.1.4 SLIDING MODE EQUATIONS

The dynamics of the system with sliding mode controller have two phases. These are named as reaching phase and sliding phase. Reaching phase is the finite time it takes for the sliding variable to become zero. The sliding phase is the phase after the reaching phase when the sliding variable has reached zero.

During the sliding phase sliding variable is zero. Equation 7.4 can be modified for the dynamics in this phase (Equation 7.18).

$$x_2 = \dot{x}_1 = -cx_1 \tag{7.18}$$

A solution to this equation is shown in Equation 7.19. Here t_r denotes the reaching time.

$$\begin{cases} x_1(t) = x_1(t_r)e^{-c(t-t_r)} \\ x_2(t) = -cx_1(t_r)e^{-c(t-t_r)} \end{cases} \tag{7.19}$$

Parameter c can be selected such that the convergence of the system is of a desired rate.

Design of the sliding mode controller has two steps. The first step is to decide on the sliding surface based on the required dynamics behavior of the system while sliding. The second step is to design the control input such that the system reaches the sliding surface in desired time, and it stays on the sliding surface after it has reached it.

7.1.5 SLIDING MODE OBSERVER/DIFFERENTIATOR

If velocity is not measured but needs to be estimated, one must design a sliding mode observer for it. The following algorithm is proposed for this purpose (Equation 7.20). Here v_1 is the observer input term.

$$\dot{\hat{x}}_1 = v_1 \tag{7.20}$$

An auxiliary sliding variable z_1 denotes the estimation error (7.21).

$$z_1 = \hat{x}_1 - x_1 \tag{7.21}$$

By differentiating Equation 7.21 one can get Equation 7.22.

$$\dot{z}_1 = -x_2 + v_1 \tag{7.22}$$

A sliding mode controller that drives z_1 to zero in finite time is designed as in Equation 7.23.

$$v_1 = -\rho\, sign(z_1) \tag{7.23}$$

After t_r, z_1 and $\dot{z}_1$ becomes zero. Using the concept of equivalent control one can estimate x_2 as in Equation 7.24.

$$\hat{x}_2 = v_{eq} = LPF\big(-\rho\, sign(z_1)\big) \tag{7.24}$$

7.1.6 OUTPUT TRACKING USING SMC

Consider a system where a specific reference output is tracked. This task can be done with a sliding mode controller by different methods.

7.1.6.1 CONVENTIONAL SLIDING MODE CONTROLLER DESIGN

A sliding mode output tracking controller can be designed using the conventional method explained in Section 7.1.1. Here, the sliding variable is slightly changed as in Equation 7.25. e denotes error between position reference and position output and $\dot{e}$ denotes the error between velocity reference and velocity output.

$$\sigma = \dot{e} + ce, \quad c > 0 \tag{7.25}$$

The control law can be derived as in Equation 7.26.

$$u_1 = \rho\, sign(\sigma) \tag{7.26}$$

7.1.6.2 INTEGRAL SLIDING MODE CONTROLLER DESIGN

Another method for output tracking is the integral SMC method. Here, two different input variables named w_1 and w_2 are designed (Equation 7.27).

$$u_1 = w_1 + w_2 \tag{7.27}$$

While w_1 is designed to compensate for the disturbance, w_2 is designed to drive the sliding variable to zero. Here, the sliding variable is the same as in the conventional output tracking SMC (Equation 7.25). Other auxiliary sliding variables are defined (Equation 7.28).

$$\begin{cases} s_1 = \sigma - z_1 \\ \dot{z}_1 = -w_2 \end{cases} \tag{7.28}$$

By calculations, u_1 and u_2 can be found as in Equation 7.29.

$$\begin{cases} w_1 = \rho_1 \, sign(s_1) \\ w_2 = k\sigma \end{cases} \tag{7.29}$$

The overall control law can be found to be as in Equation 7.30.

$$u_1 = \rho_1 \, sign(\sigma + \int k\sigma \, dt) + k\sigma \tag{7.30}$$

7.2 CONTROLLER STRUCTURE

In this section, structure of the controller is explained. The aim is to design one sliding surface for all the controllers, however; if one sliding surface is not enough different sliding surfaces for different trim points can be designed. Stability and disturbance rejection characteristics are functions of the inner loop. For tracking characteristics, if the requirements are not met prefilters can be added to improve transient characteristics.

Controller structure consists of guidance, pitch hold, lateral controller, and control allocation & feedforward blocks.

Guidance block calculates the necessary lateral acceleration of the aircraft by using precise ground position and ground velocity components provided by DGPS.

Pitch-hold block controls the pitch angle of the aircraft. Pitch angle reference is a function of the true airspeed of the aircraft.

Lateral controller block calculates the necessary aileron and rudder commands necessary for tracking the reference lateral acceleration.

Control allocation and feedforward block calculates the necessary rudder and steering commands, and it also contains feedforward gains directly coming from the guidance block.

The structure of the controller is shown in Figure 7.1.

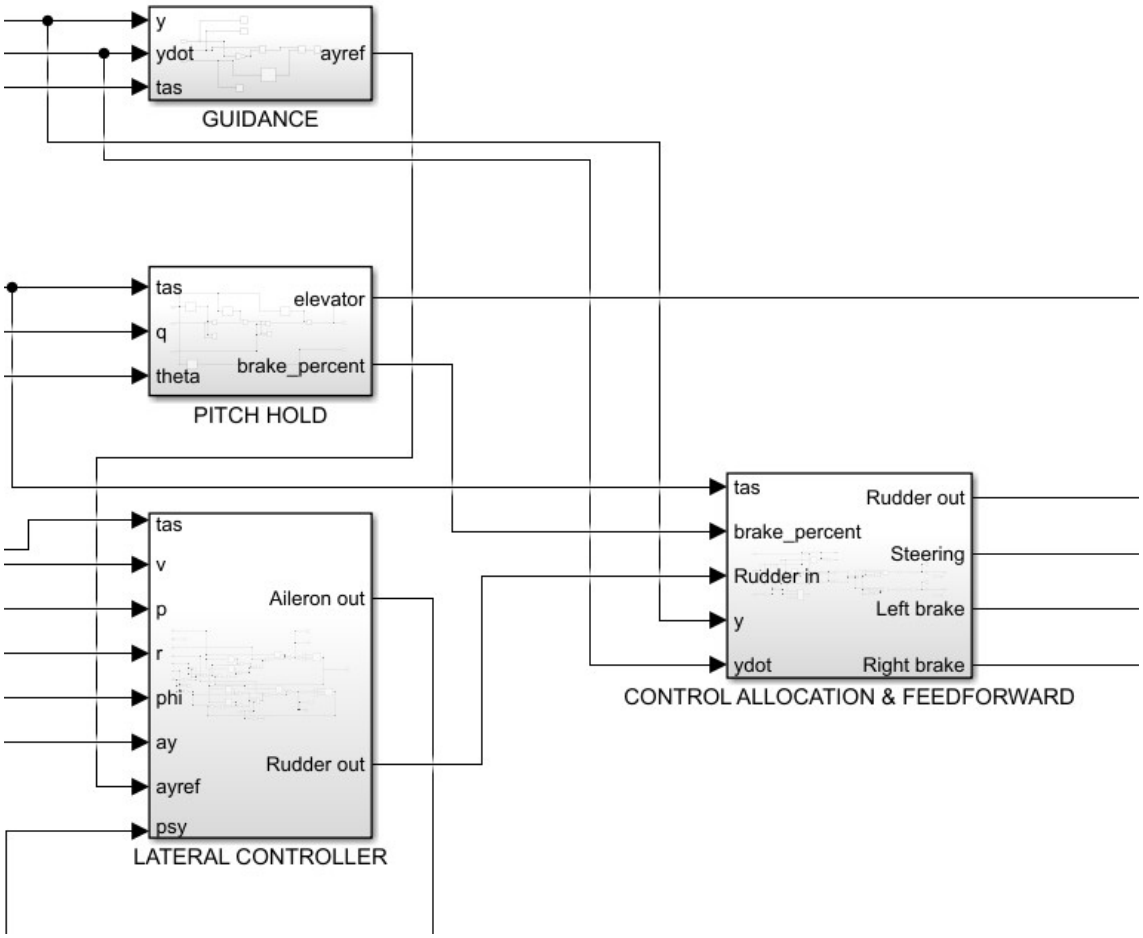

Figure 7.1 Structure of the sliding mode controller

7.3 PERFORMANCE REQUIREMENTS

Performance requirements are decided based on industry experience. For the pitch angle controller rise time is decided to be 0.7 since the pitch angle must be controlled faster than the natural frequency of the aircraft tipping over forwards or backward with its two tires on the ground. The rise time of the lateral acceleration controller is decided based on industry experience. The roll angle controller is an assistant to the lateral acceleration controller. Its rise time is decided such that it is faster than the lateral acceleration controller. A 10 percent overshoot requirement is set for all three controllers. Another factor to decided on is the maximum steady-state error. Since pitch and roll controllers cannot always track the reference input, a steady state error requirement is not set for them. For the lateral acceleration controller, the steady state error must be zero. An

integral sliding mode controller is necessary to guarantee zero steady-state error. Performance requirements for the controllers are shown in Table 7.1.

Table 7.1 Performance requirements for the sliding mode controllers

	Pitch angle controller	Lateral acceleration controller	Roll angle controller
10% to 90% rise time (s)	0.7	2.0	1.0
Overshoot (%)	10	10	10
Maximum Steady State Error	-	0	-

7.4 STABILITY REQUIREMENTS

According to MIL-F 8785 document [58], an aircraft control system must meet the following criteria. The necessary gain and phase margins can be shown with a hexagon shape placed in a Nichols chart [54]. To satisfy these margins, the Nichols plot should not pass inside the hexagon for all the signals used by the controller. These signals include sensor signals and actuator signals. The hexagon shape is shown in Figure 7.2.

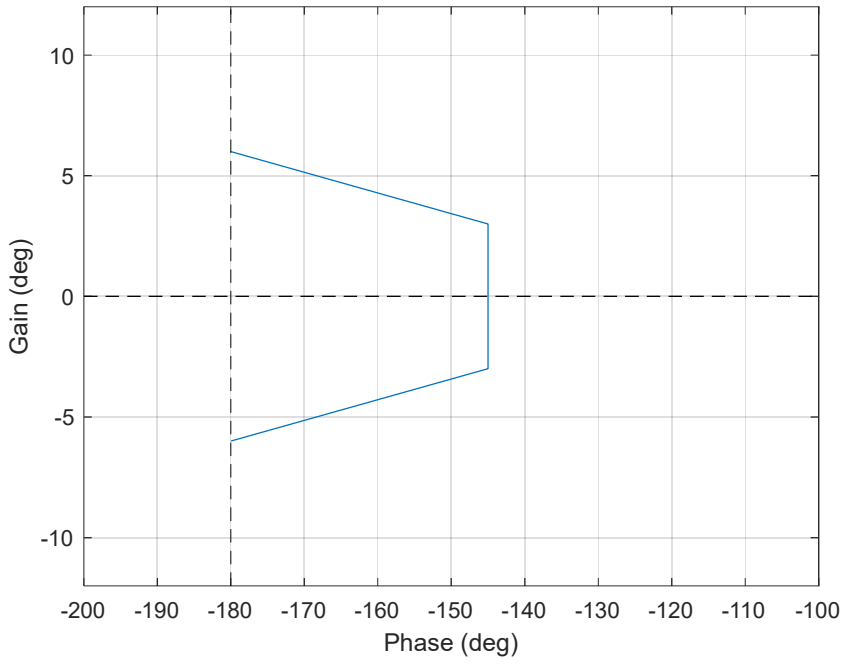

Figure 7.2 Hexagon shape inside Nichols chart used for checking stability requirements

7.5 PITCH ANGLE CONTROLLER

An important part of the controller is the pitch angle controller that tracks the reference pitch angle for the aircraft. In this section, synthesis, proof of performance and stability are explained.

7.5.1 SYNTHESIS

For an ideal sliding mode controller there should be a relation between q and θ such that $q = c\theta$ where c is a constant. This equation would be the sliding surface. If $q < c\theta$, maximum elevator command in the direction of increasing q is given, else maximum elevator command in the direction of decreasing q is given. This will define an ideal sliding mode controller where sliding surface is reached within finite time, disturbances are rejected in finite time and there is no steady-state tracking error. However, in practice this creates oscillations due to instability in the system. Dynamics and delays in sensor and actuator signals limit the gains of the sliding mode controller, infinite gains are not possible in a physical system.

Here, a gain-scheduling classical output tracking sliding mode controller is designed for the pitch controller. Sat(x) function is used for continuous input signal [41]. Sat(x) function is shown in Equation 7.31.

$$sat(x) = \begin{cases} x, & |x| < 1 \\ 1, & |x| \geq 1 \end{cases} \tag{7.31}$$

Structure of the gain scheduling SMC pitch hold controller is shown in Figure 7.3.

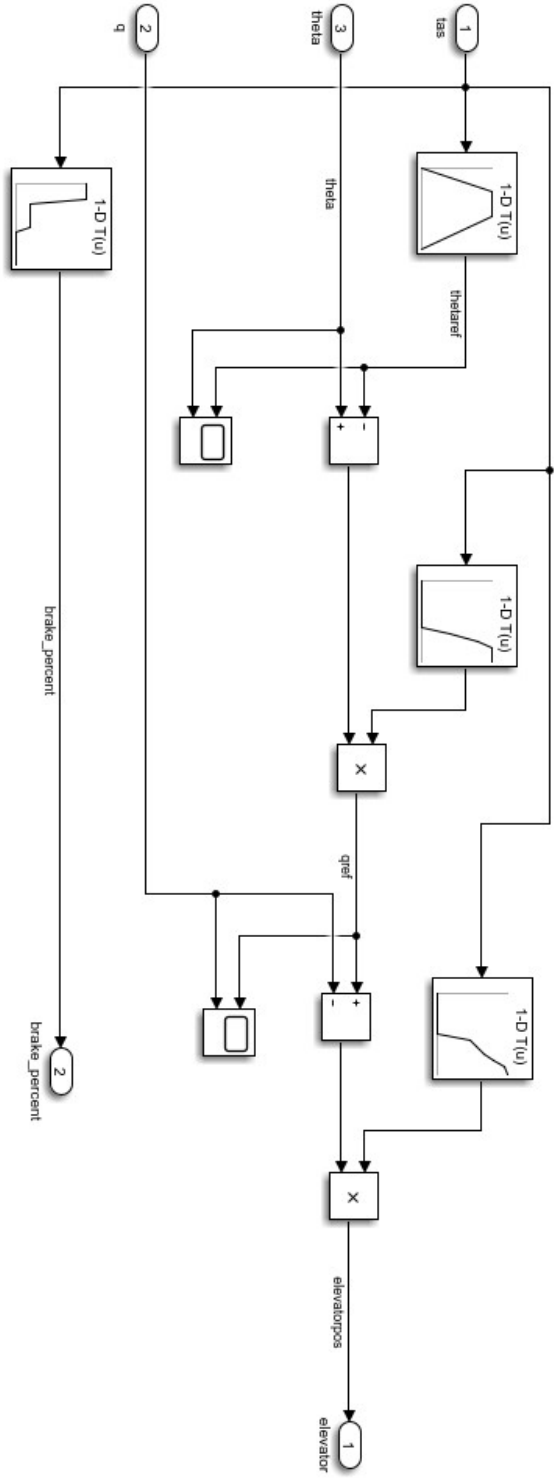

Figure 7.3 Structure of the gain scheduling SMC pitch hold controller

The solution to the synthesis problem is to find the maximum gains that satisfy the stability requirements. The gains that are found are shown in Table 7.2.

Table 7.2 Gains, rise times, and overshoots for the pitch SMC

Pitch SMC				
TAS (m/s)	Gain 1	Gain 2	Rise Time (s)	Overshoot (%)
60	-2.3	-170	0.55	1.4
55	-2.3	-190	0.54	4.6
50	-2.3	-240	0.51	7.2
45	-2.4	-285	0.46	9.8
40	-2.6	-330	0.42	15.6
35	-2.8	-360	0.42	27.4
30	-2.8	-520	0.41	30.7
25	-2.8	-520	-	-
20	-2.8	-520	-	-
15	-2.8	-520	-	-
10	-2.8	-520	-	-
5	-2.8	-520	-	-
0	-2.8	-520	-	-

To decrease the overshoot a first-order filter is added to the reference command. Performance results of the controller with prefilter are shown in Table 7.3.

Table 7.3 Gains, rise times, and overshoots for the pitch SMC with prefilter

Pitch SMC with filter				
TAS (m/s)	Gain 1	Gain 2	Rise Time (s)	Overshoot (%)
60	-2.3	-170	0.74	1.4
55	-2.3	-190	0.7	4.6
50	-2.3	-240	0.67	7.2
45	-2.4	-285	0.61	9.8
40	-2.6	-330	0.55	13.6
35	-2.8	-360	0.52	23.8
30	-2.8	-520	0.52	27
25	-2.8	-520	-	-
20	-2.8	-520	-	-
15	-2.8	-520	-	-
10	-2.8	-520	-	-
5	-2.8	-520	-	-
0	-2.8	-520	-	-

Adding the filter decrease the overshoot for some trim points however it increases rise time for all trim points. For the problem at hand, the controller without filter seems a better choice.

7.5.2 PROOF OF PERFORMANCE AND STABILITY

Performance is shown by the step response in Figure 7.4. Elevator usage is also shown in Figure 7.5. It can be shown from the figures that the input is continuous and because of it there is a steady state error. This can be corrected using an integral sliding mode controller. However, integral SMC is not used for pitch SMC for simplicity purposes.

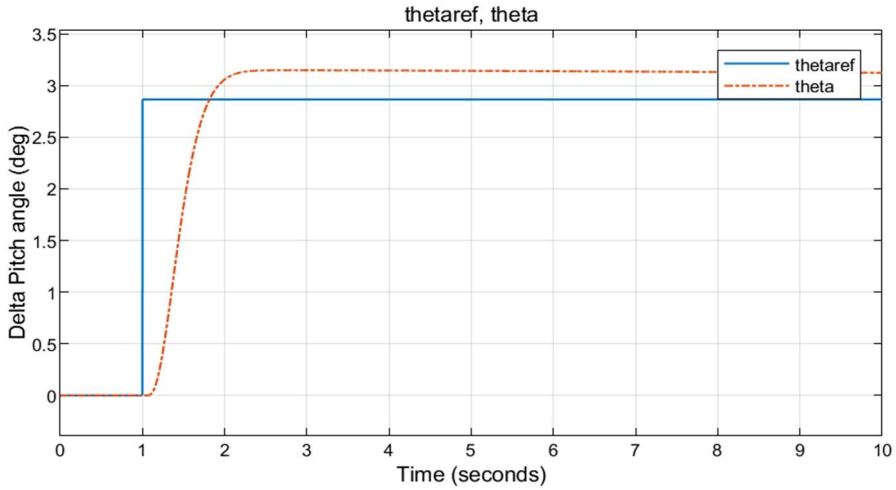

Figure 7.4 Step response of pitch SMC controller at 45 m/s true air speed

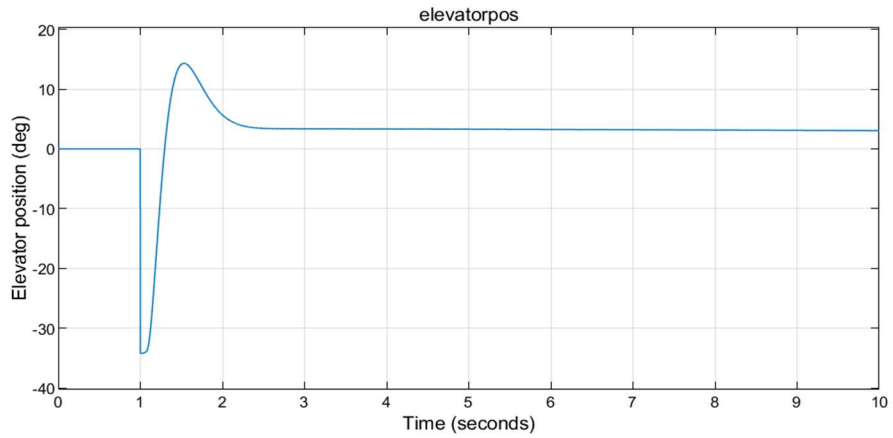

Figure 7.5 Elevator usage at 45 m/s true airspeed

For stability, Nichols charts must be checked. Loop-breaks in sensor and actuator signals are checked. For all the Nichols charts drawn, graphs remained outside of the hexagon. Details and graphs are in Appendix 3.

7.6 LATERAL CONTROLLER

The lateral controller consists of two parts named lateral acceleration controller and roll angle controller. Since they affect each other, these two controllers must be designed simultaneously. In this part, integral SMC method is used for both controllers. The sliding variable have an integral component that drives the steady-state error to zero.

7.6.1 SYNTHESIS

For the roll controller, the states that are controlled are p and ϕ. Sliding variable is same as in Equation 7.25. The control law is designed as in Equation 7.32.

$$\delta_{ail} = k\ sat(k1\ \sigma + \int k2\sigma\ dt) \tag{7.32}$$

For the lateral acceleration controller, the controlled states and outputs are r and a_y. Control law is the same as in Equation 7.32 except the control input is a control allocation function of the rudder, differential brake, and steering. The controller structure can be seen in Figure 7.6. Gains (Table 7.4) are again found such that the stability requirements are met.

Table 7.4 Gains, rise times, and overshoots for lateral integral SMC

Integral SMC									
TAS (m/s)	phiref gain	kp rref	ki rref	kp pref	ki pref	aileron	rudder	Rise Time (s)	Overshoot (%)
60	0.1047	0.0510	0.0850	1.5	0.5	-75	-300	1.6	7.8
55	0.1047	0.0459	0.0765	1.5	0.5	-90	-350	1.2	10.4
50	0.1047	0.0408	0.0680	1.5	0.5	-110	-400	1.2	9.6
45	0.1047	0.0357	0.0595	1.5	0.5	-135	-480	1.3	7.4
40	0.1047	0.0306	0.0510	1.5	0.5	-175	-620	1.5	3.9
35	0.1047	0.0306	0.0510	1.5	0.5	-225	-800	1.5	2.6
30	0.1047	0.0306	0.0510	1.5	0.5	-310	-1100	1.5	0.2
25	0.1047	0.0306	0.0510	1.5	0.5	-450	-300	1.4	15.4
20	0.1047	0.0306	0.0510	1.5	0.5	-700	-350	1.7	8.3
15	0.1047	0.0306	0.0510	1.5	0.5	-1000	-360	2.3	3.9
10	0.1047	0.0306	0.0510	1.5	0.5	-1500	-370	4.3	2.5
5	0.1047	0.0357	0.0595	1.5	0.5	-1500	-450	8.9	0.5
0	0.1047	0.0357	0.0595	1.5	0.5	-1500	-450	8.9	0.5

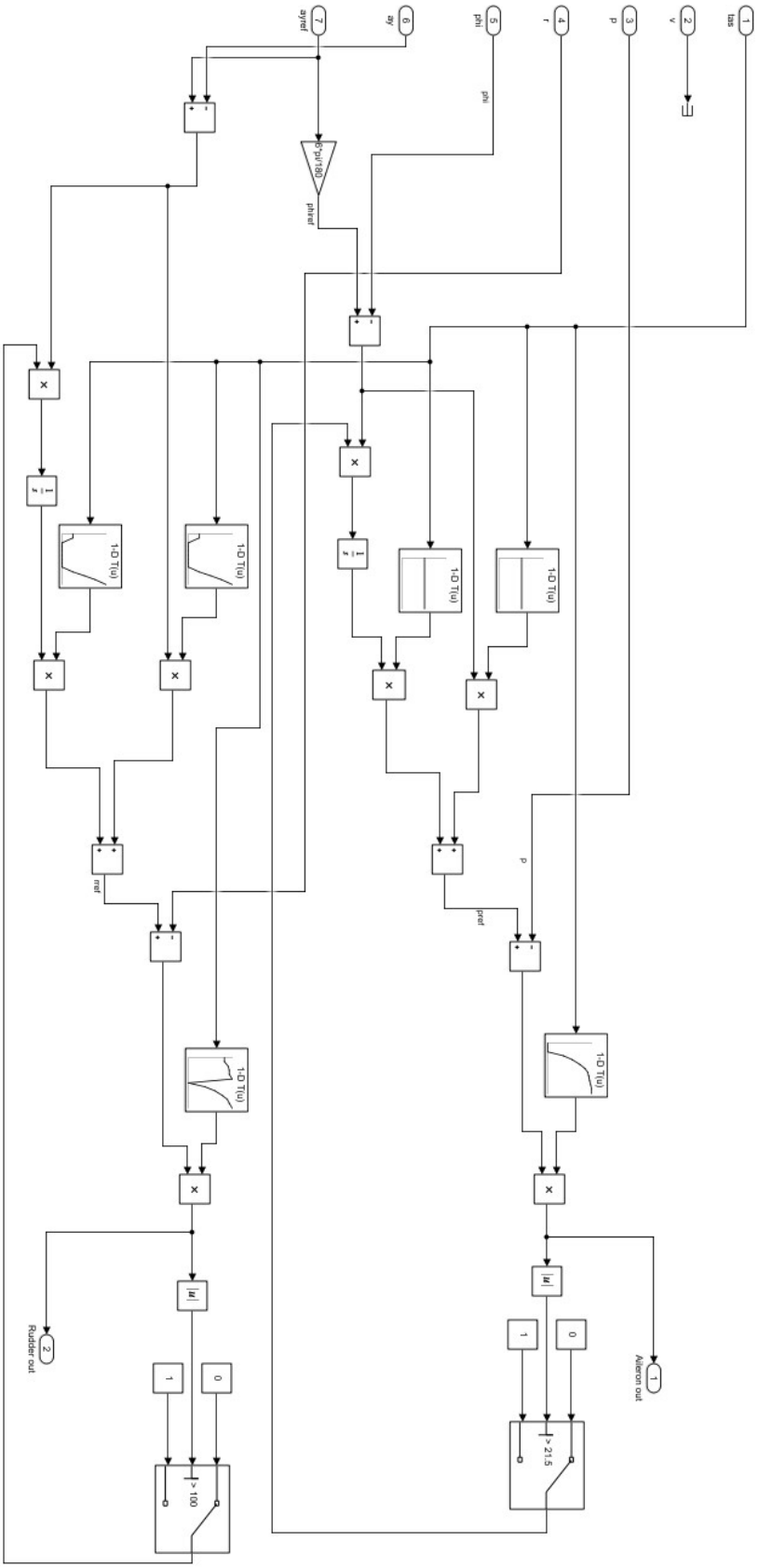

Figure 7.6 Lateral SMC Controller Structure

7.6.2 PROOF OF PERFORMANCE AND STABILITY

The performance of the lateral controller can be shown by the step response. In Figure 7.7, the step response of lateral acceleration can be seen. The system exhibits a non-minimum phase behavior. The initial response of the rudder is a lateral force to the opposite direction that the aircraft tries to turn to. The step response of roll angle also can be seen in Figure 7.8. Aileron force tries to roll the aircraft to the reference roll angle. However, the rolling moment is not enough to counter the rolling moment created by the landing gear struts. Thus, the roll angle is limited. The roll angle controller helps with the lateral acceleration, nonetheless. The way it does this is by changing the vertical forces on the main gear tires. Aileron and rudder usages can also be seen in Figures Figure 7.9, and Figure 7.10. Nichols charts for the proof of stability can be found in Appendix 4.

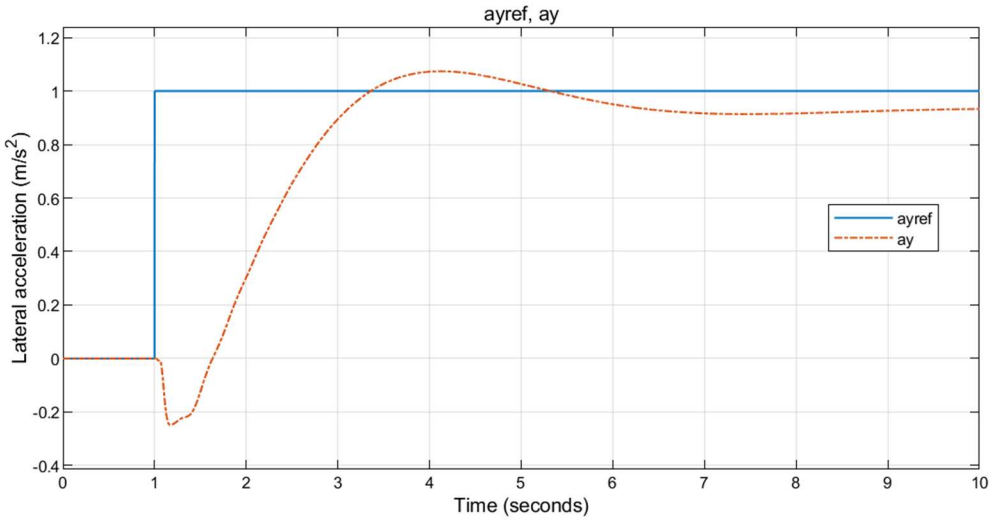

Figure 7.7 Step response of lateral SMC controller at 45 m/s true air speed

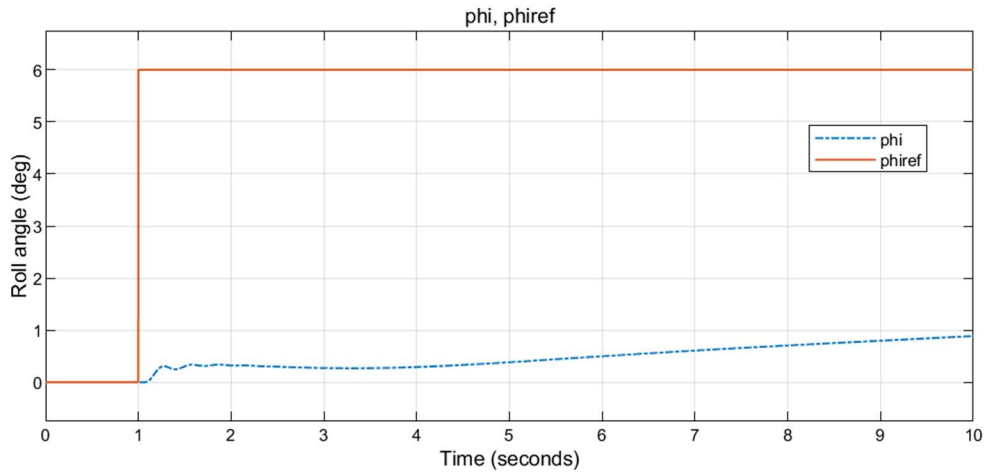

Figure 7.8 Step response of lateral SMC controller at 45 m/s true air speed

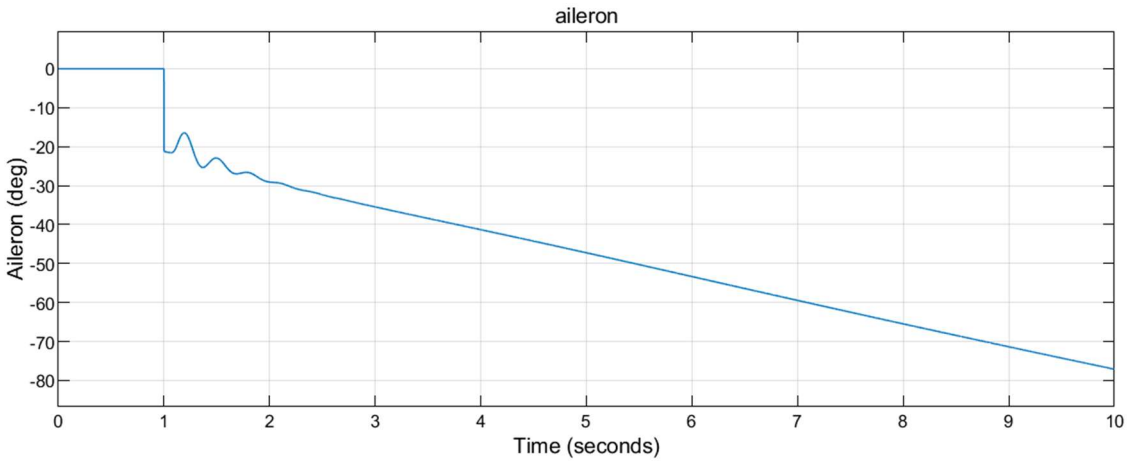

Figure 7.9 Aileron usage at 45 m/s true air speed

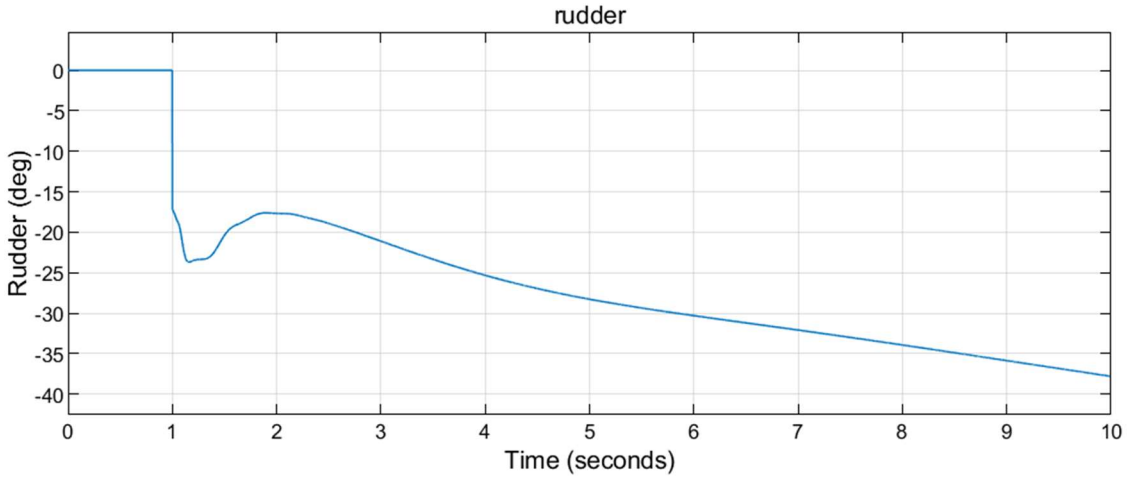

Figure 7.10 Rudder usage at 45 m/s true air speed

7.7 OTHER CONSIDERATIONS

In this part, other key points of the combined guidance and autopilot synthesis are explained.

7.7.1 DELAYS

Delays of the sensors and actuators are modeled inside their respective transfer functions. However, a 10-millisecond communication delay is added to the sensor signal and a 10-millisecond communication delay is again added to the actuator signal. For the position signals, the DGPS position sensor is approximated by a 20-millisecond delay. For the steering actuator, the same transfer function for control surfaces are used and a 10-millisecond delay is added as an extra.

For the modelling of delays, 2nd order Pade approximation [59], [60] is used.

7.7.2 GUIDANCE LAW

Outer loop guidance is chosen as linear sliding mode guidance as in Chapter 6. However, after the simulations, it is found that the natural frequency of the sliding mode of the guidance must be made smaller for low speeds. At low speeds, the natural frequency of the aircraft and the inner loop tends to slow down.

The new guidance equation is decided as in Equation 7.33.

$$\dot{y} = -0.1\, y \tag{7.33}$$

7.7.3 FEEDFORWARD LOOP

To have a fast response mechanism, a feedforward loop is used. Differential braking is used for this purpose since it is the only always-available directional input throughout the landing rollout phase. As long as the aircraft moves along the sliding surface of the guidance (Equation 7.33), no feedforward input is given. Outside of the sliding surface, differential braking input is given such that the aircraft is turned towards the sliding surface. Structure of this feedforward gains can be seen in Figure 7.11. Gains that multiply y and $\dot{y}$ are feedforward gains. These gains are decided based on the simulations.

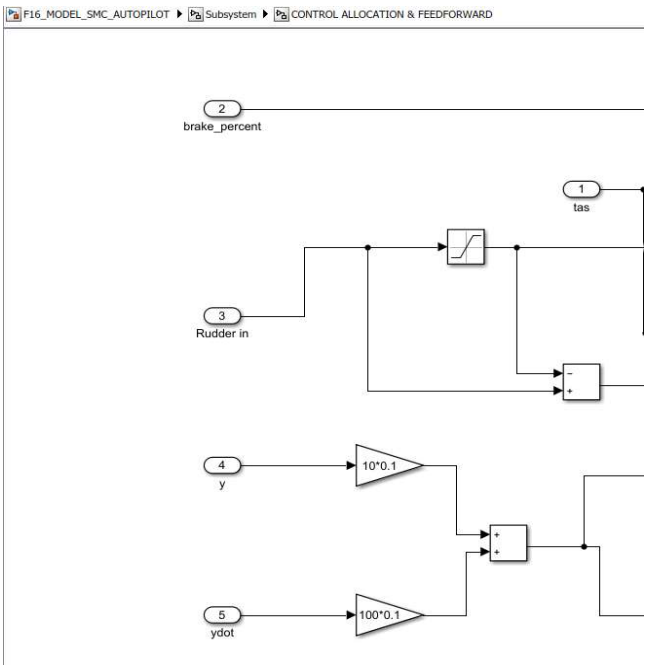

Figure 7.11 Feedforward gains of SMC controller

7.7.4 ANTI-WINDUP

Having an integrator in a controller has one problem. After the control inputs are saturated, the integrator keeps integrating. This results in the loss of all controlling authority of the controller since the saturated integral has driven the input signal out of the useful area of the input saturation bounds. Solution to this problem is anti-windup. Anti-windup is used for the integrators that can saturate the controller. There are two methods of anti-windup used in industry. These are called clamping and back-calculation [61].

Clamping is the method in which the integrator stops integrating if the input is out of bounds and the integrator pushes the input away from the bounds to infinity. If the input is inside the bounds or the integrator pushes the input towards zero, the integrator keeps working.

In the back-calculation method, outside of saturation limits, another integrator is added to the system which drives the input towards zero.

In our case, anti-windup is needed for the integral sliding mode controllers. A partial clamping algorithm is used in which outside of the saturation integrator stops. Although this is not the total of the clamping algorithm it has been found sufficient for this controller application. The structure of the anti-windup scheme is shown in Figure 7.12. Here, when the aileron input is saturated, the switch gives zero as the flag signal. This flag signal is then multiplied with the signal that is integrated.

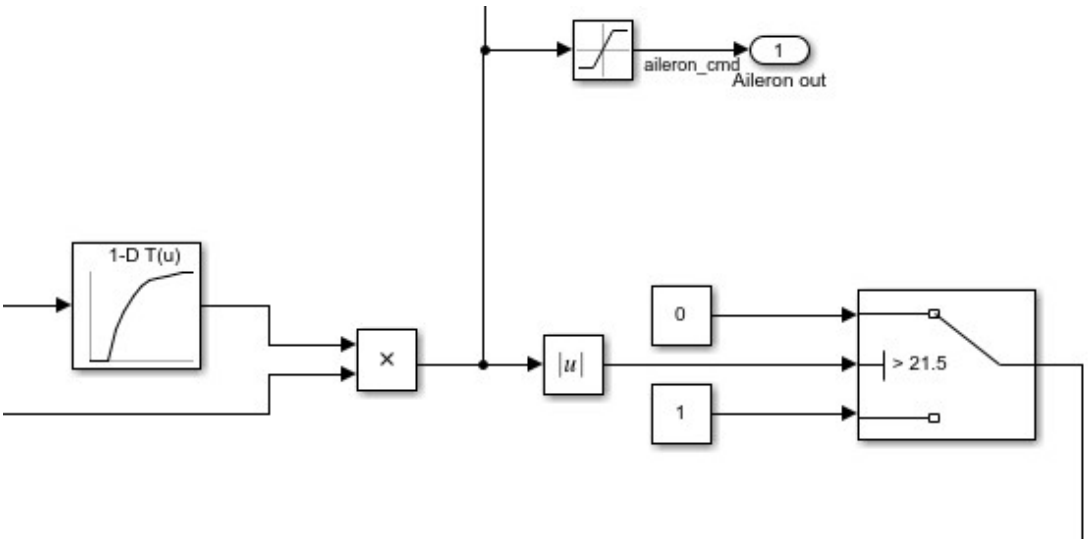

Figure 7.12 Anti-windup for aileron input

7.7.5 YAW ANGLE CORRECTION

A small proportional gain to decrease the yaw angle relative to the runway is added. Differential braking input is used for this purpose.

7.7.6 ZERO ORDER HOLD

The simulations are run in 1000 Hz sampling frequency, however; the autopilot frequency of the aircraft is assumed as 100 Hz. To account for this difference, delay due to zero order hold must be modeled.

The general transfer function of zero order hold is given in Equation 7.34 [62].

$$T_{ZOH} = \frac{1-e^{-s}}{sT} \tag{7.34}$$

The exponential term in Equation 7.34 can than be modeled as a first-order Pade approximation as in Equation 7.35.

$$e^{-Ts} = \frac{-\frac{T}{2}s+1}{\frac{T}{2}s+1} \tag{7.35}$$

By combining Equations 7.34 and 7.35, one can get Equation 7.36 for the transfer function of zero order hold.

$$T_{ZOH} \cong \frac{1}{\frac{T}{2}s+1} \tag{7.36}$$

8. INNER LOOP PID CONTROLLER SYNTHESIS

In this chapter, a PID controller is designed to compare the performance of the SMC with the state of the art. Other than the design of the PID, the other parts of feedforward loops, guidance law and yaw angle correction remain the same.

8.1 PITCH CONTROLLER

For the pitch controller, q and θ states are used. q is used as the derivative signal and error of θ and its integral are used as proportional and integral signals. Structure of the controller can be seen in Figure 8.1.

8.1.1 SYNTHESIS

The biggest gains that do not compromise the stability requirements are found. These gains and the corresponding performance metrics are shown in Table 8.1. A PID controller with prefilter is also designed. The corresponding gains and performance metrics are shown in Table 8.2.

Table 8.1 Gains, rise times and overshoots for pitch PID controller

Pitch PID					
TAS (m/s)	Kp	Kd	Ki	Rise Time (s)	Overshoot (%)
60	400	160	25	0.48	5
55	450	180	27	0.47	9
50	520	200	30	0.45	14.8
45	630	250	36	0.45	16.6
40	780	300	40	0.44	21.6
35	930	350	50	0.44	30.6
30	1170	450	60	0.46	40.2
25	1170	450	60	-	-
20	1170	450	60	-	-
15	1170	450	60	-	-
10	1170	450	60	-	-
5	1170	450	60	-	-
0	1170	450	60	-	-

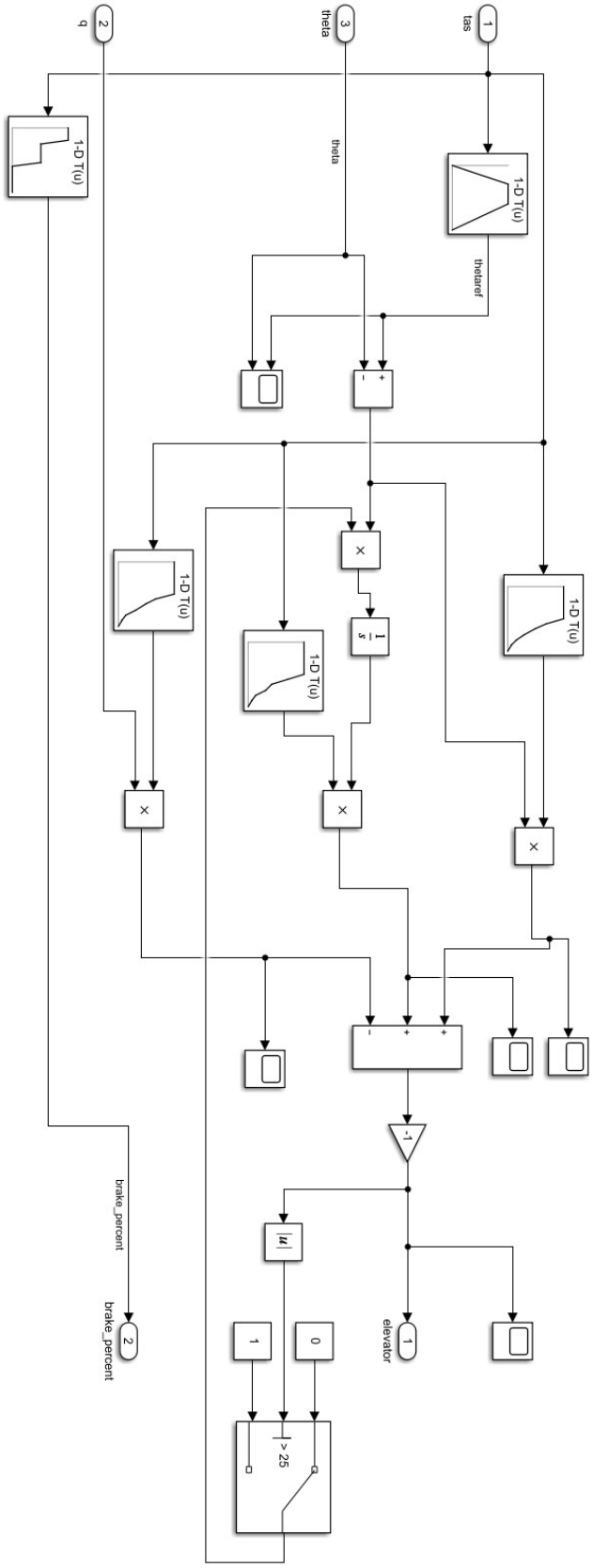

Figure 8.1 Pitch PID Controller Structure

Table 8.2 Gains, rise times, and overshoots for pitch PID with prefilter

Pitch PID with filter					
TAS (m/s)	Kp	Kd	Ki	Rise Time (s)	Overshoot (%)
60	400	160	25	0.63	4.2
55	450	180	27	0.61	7.4
50	520	200	30	0.57	12.2
45	630	250	36	0.58	14.6
40	780	300	40	0.54	19
35	930	350	50	0.54	27.6
30	1170	450	60	0.55	37.4
25	1170	450	60	-	-
20	1170	450	60	-	-
15	1170	450	60	-	-
10	1170	450	60	-	-
5	1170	450	60	-	-
0	1170	450	60	-	-

8.1.2 PROOF OF PERFORMANCE AND STABILITY

Step response and elevator usage can be seen in Figures Figure 8.2, and Figure 8.3. Pitch angle converges to the step input and there is no steady state error. Nichols Charts for the proof of stability of pitch PID controller are included in Appendix 5.

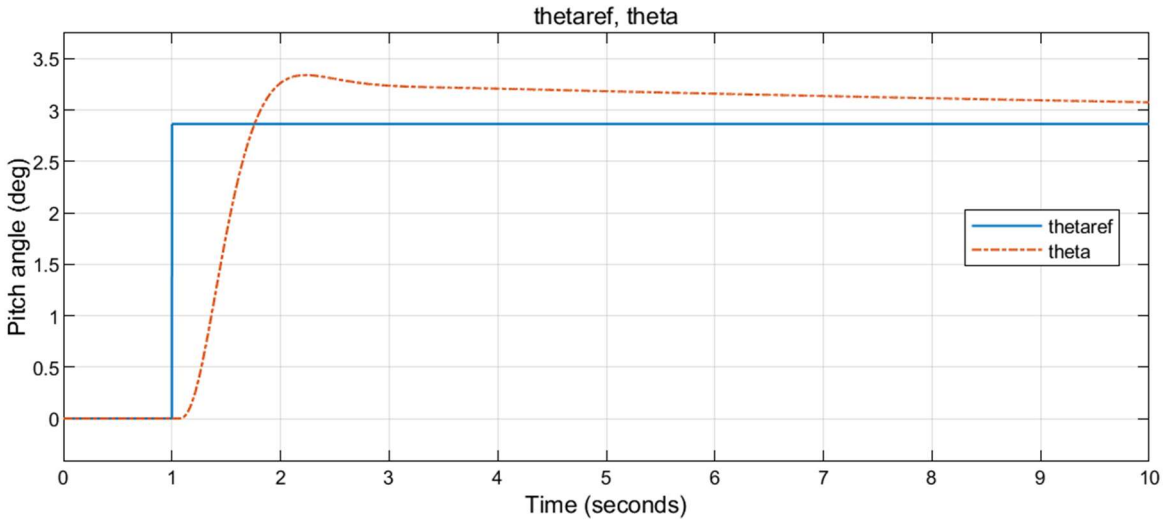

Figure 8.2 Step response of pitch PID controller at 45 m/s true airspeed

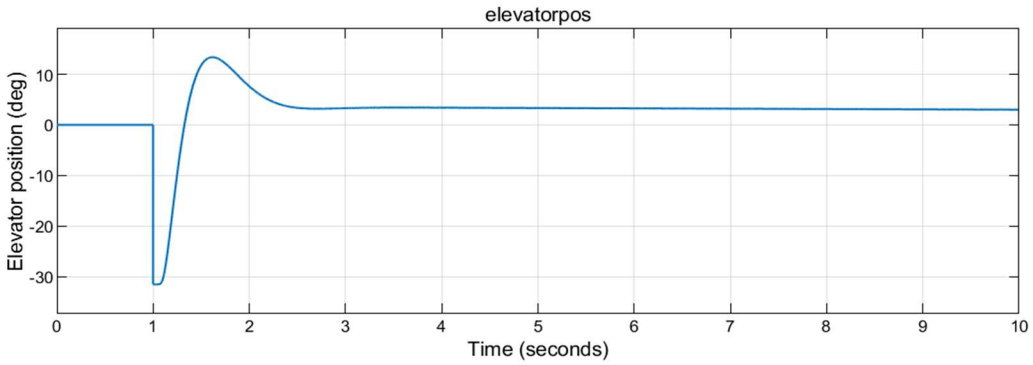

Figure 8.3 Elevator usage at 45 m/s true airspeed

8.2 LATERAL CONTROLLER

As in lateral SMC, the lateral PID controller consists of lateral acceleration and roll angle controllers. Angular velocity signals of r and p are used as derivative signals of the respective PID controllers.

8.2.1 SYNTHESIS

Like the pitch PID controller, gains of the lateral controller are found such that they are the biggest possible gains that do not compromise the stability requirement. The gains that are found can be seen in Table 8.3. The structure of the controller can be seen in Figure 8.4.

Table 8.3 Gains, rise times, and overshoots of lateral PID controller

PID									
TAS (m/s)	phiref gain	kp roll	ki roll	kd roll	kp yaw	ki yaw	kd yaw	Rise Time (s)	Overshoot (%)
60	0.1047	65	13	65	15	10	150	8.2	-
55	0.1047	70	14	70	14	9	150	7.6	-
50	0.1047	80	16	80	14	9	150	7.5	-
45	0.1047	100	20	100	14	9	150	8.3	-
40	0.1047	120	24	120	14	9	150	10	-
35	0.1047	160	32	160	16	11	170	10.2	-
30	0.1047	250	50	250	18	13	170	40.6	-
25	0.1047	300	60	300	12	8	120	1.1	13.3
20	0.1047	400	80	400	12	8	120	1.3	6.4
15	0.1047	500	100	500	12	8	120	1.6	2
10	0.1047	600	120	600	12	8	120	4.6	1.1
5	0.1047	600	120	600	15	11	150	9.5	-
0	0.1047	600	120	600	15	11	150	9.5	-

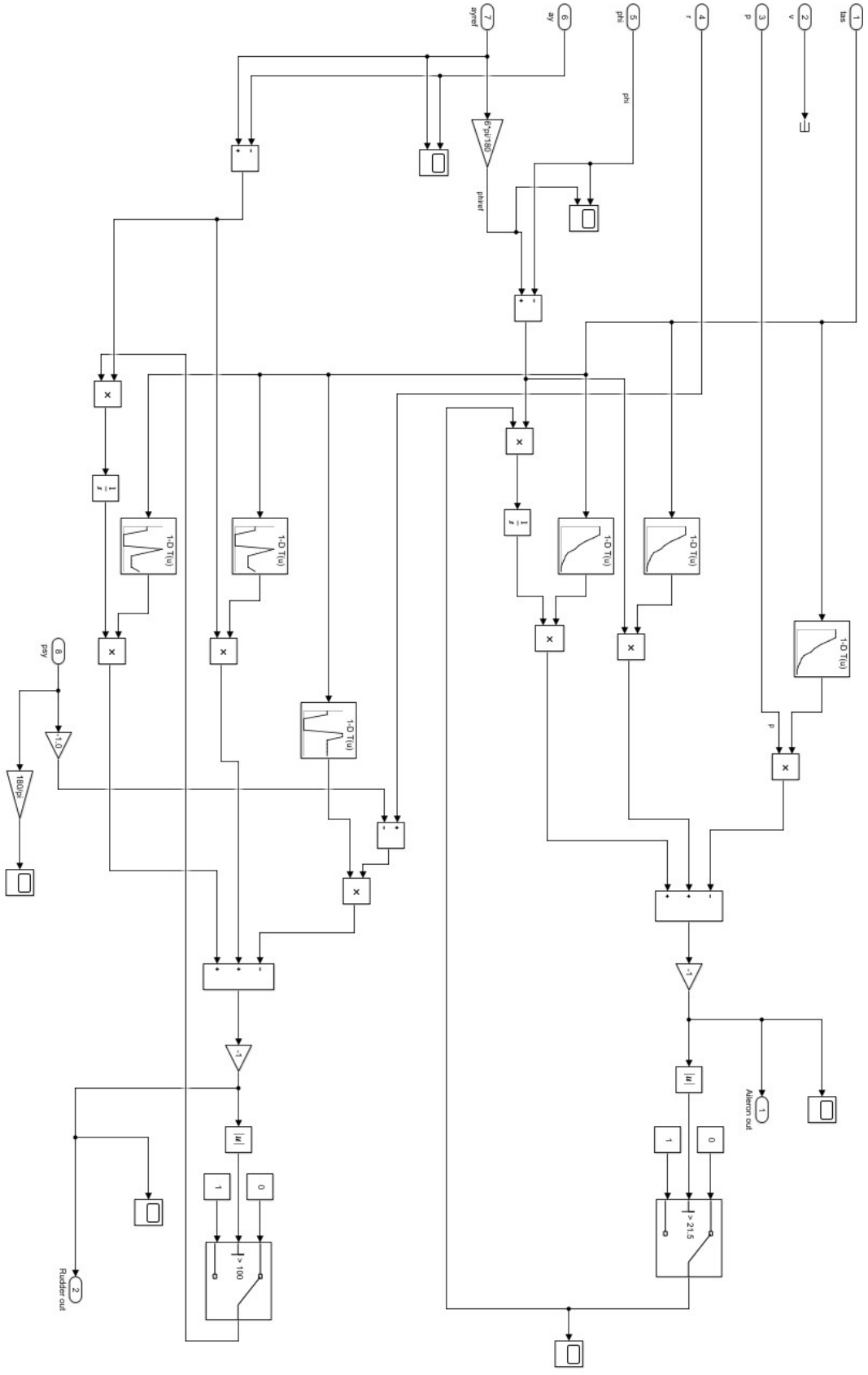

Figure 8.4 Lateral PID controller structure

8.2.2 PROOF OF PERFORMACE AND STABILITY

Step responses for lateral acceleration and roll angle can be seen in Figures Figure 8.5, and Figure 8.6. Rudder and aileron usages can be seen in Figures Figure 8.7, and Figure 8.8. Nichols charts for proof of stability are in Appendix 6.

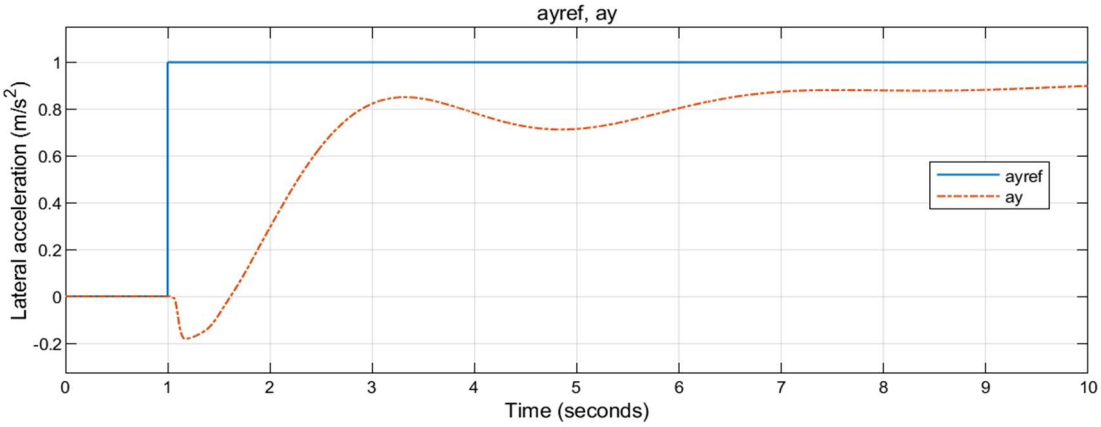

Figure 8.5 Step response of lateral PID controller at 45 m/s true airspeed

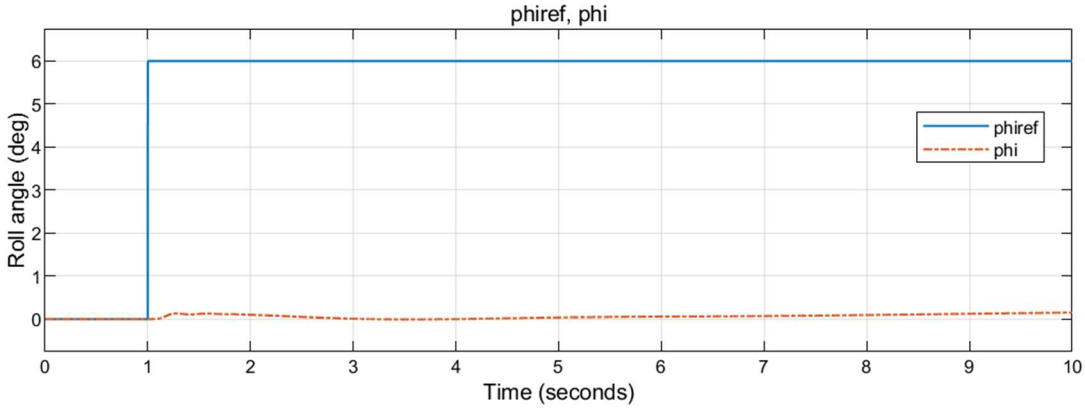

Figure 8.6 Step response of lateral PID controller at 45 m/s true airspeed

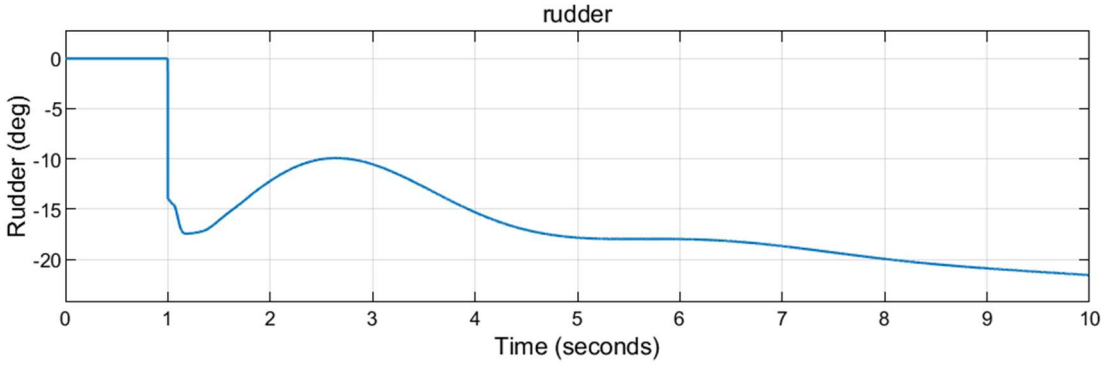

Figure 8.7 Rudder usage at 45 m/s true airspeed

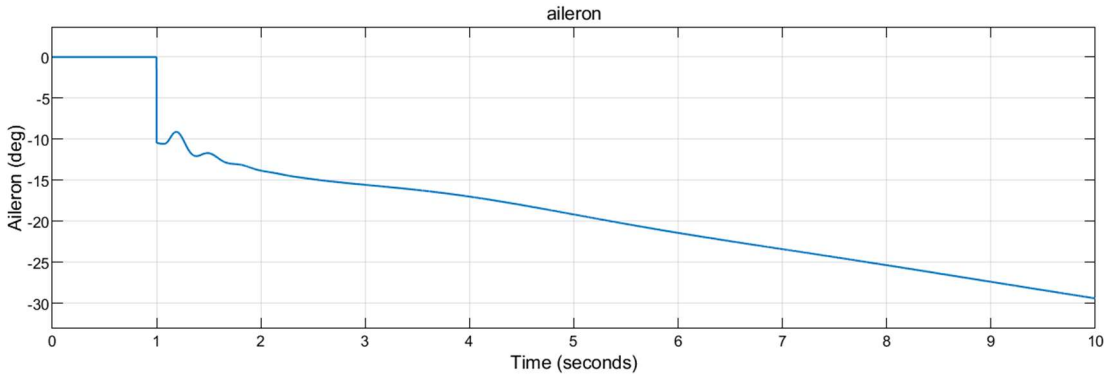

Figure 8.8 Aileron usage at 45 m/s true airspeed

9. SIMULATIONS

Simulations for sliding mode and PID controllers are done for different conditions.

9.1 STANDARD SIMULATIONS WITH LATERAL POSITION AND TRACK ANGLE INITIAL CONDITIONS

In this first simulation condition, a lateral position of 2 m and a track angle of 2 degrees are given. Results are given in Figures Figure 9.1 to Figure 9.18.

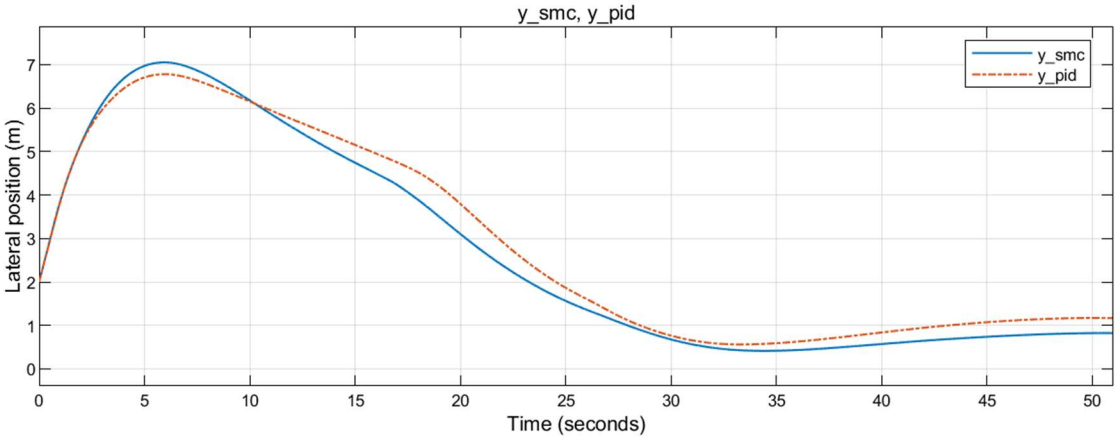

Figure 9.1 Lateral position for the first simulation condition

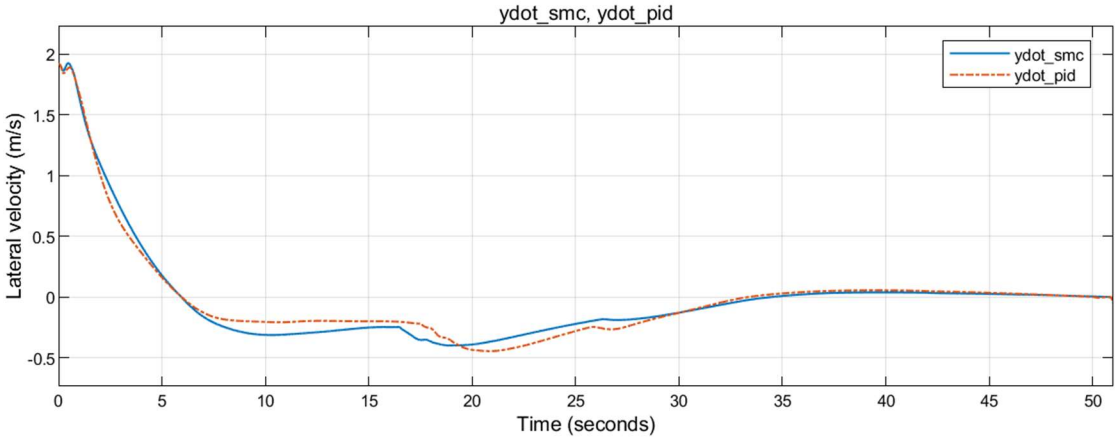

Figure 9.2 Lateral velocity with respect to runway for the first simulation condition

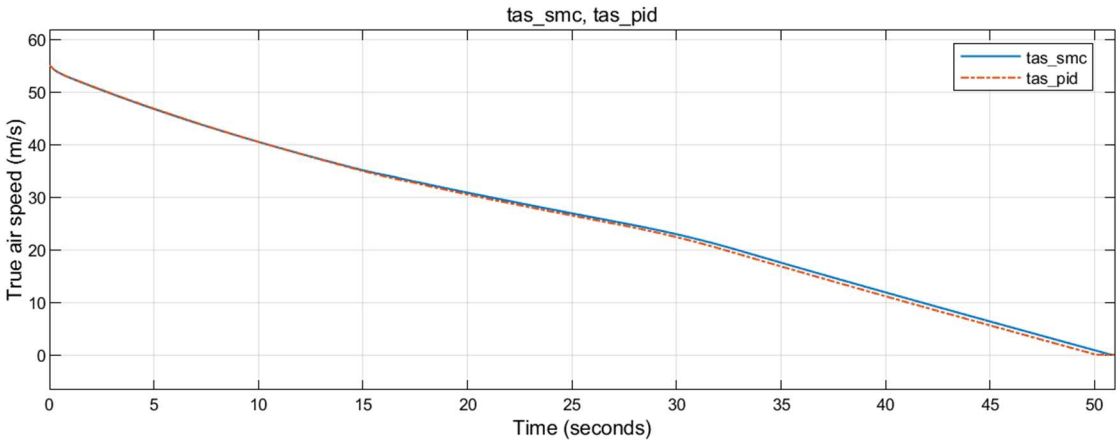

Figure 9.3 True airspeed for the first simulation condition

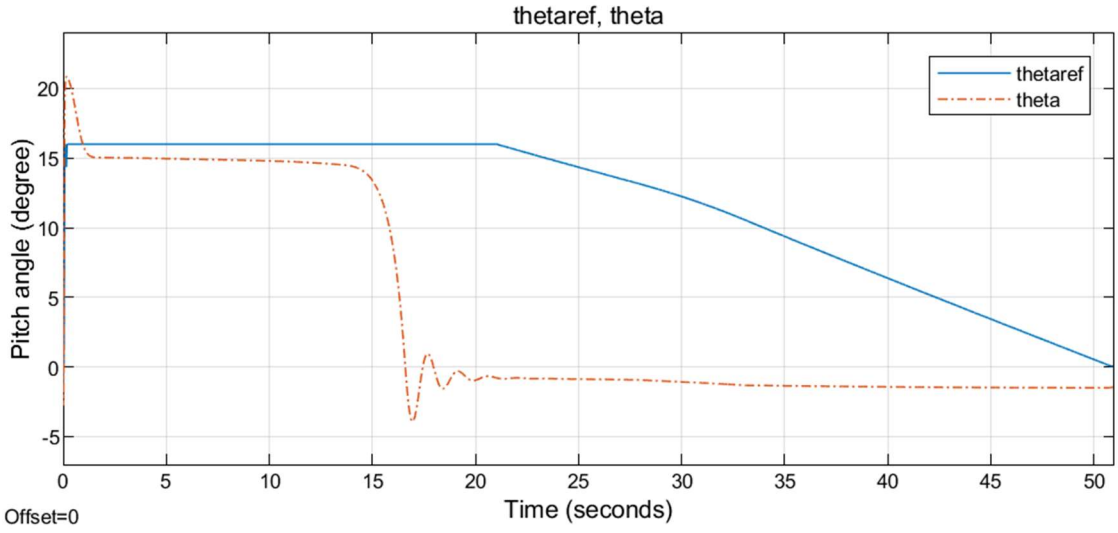

Figure 9.4 Pitch angle for the first simulation condition with SMC

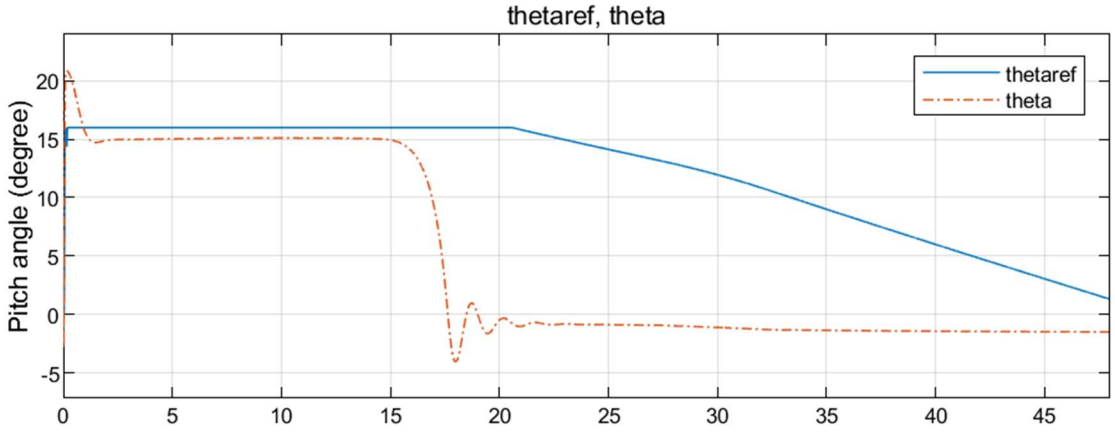

Figure 9.5 Pitch angle for the first simulation condition with PID

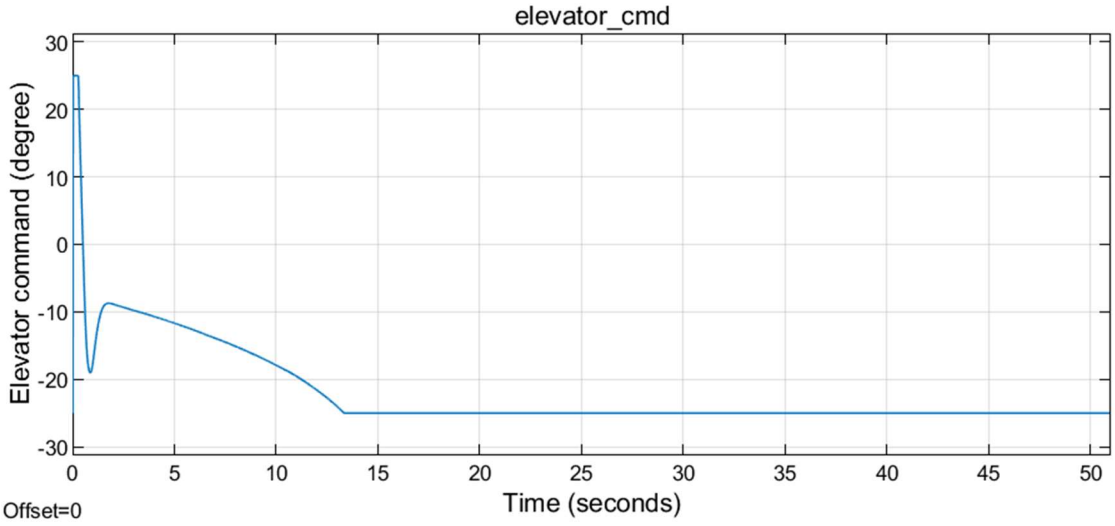

Figure 9.6 Elevator command for the first simulation condition with SMC

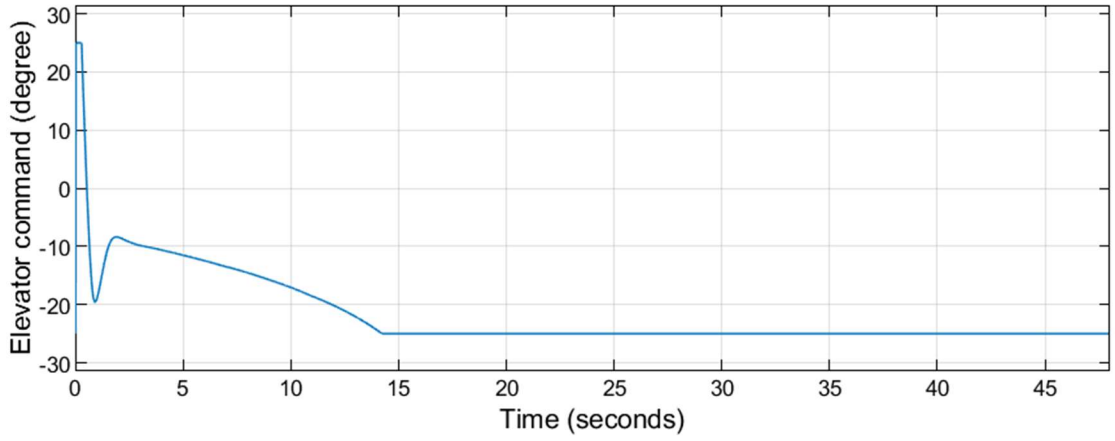

Figure 9.7 Elevator command for the first simulation condition with PID

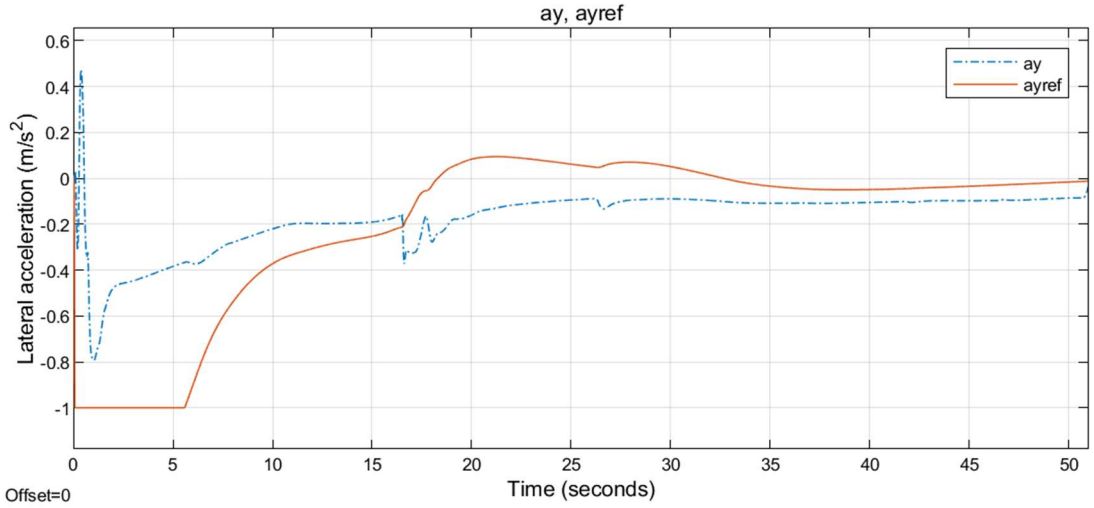

Figure 9.8 Lateral acceleration for the first simulation condition with SMC

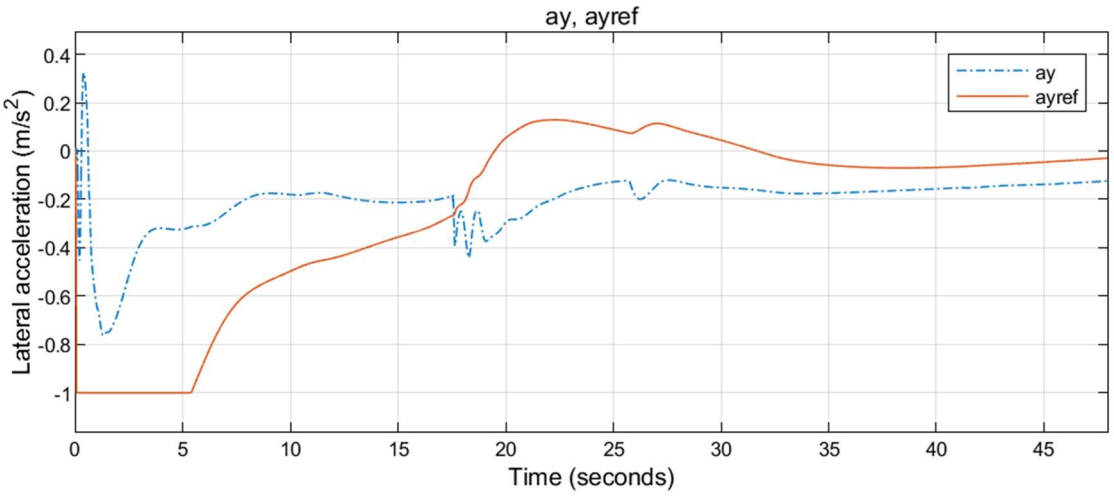

Figure 9.9 Lateral acceleration for the first simulation condition with PID

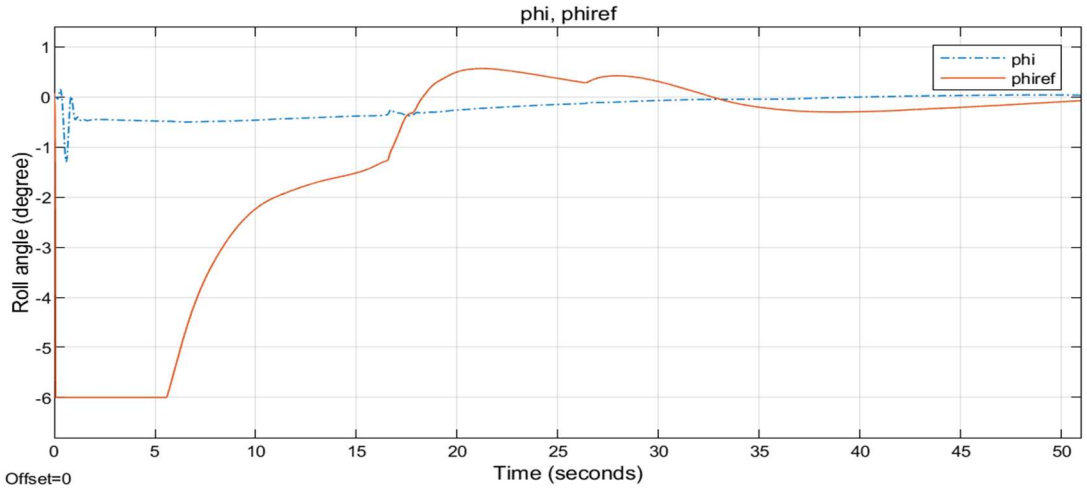

Figure 9.10 Roll angle for the first simulation condition with SMC

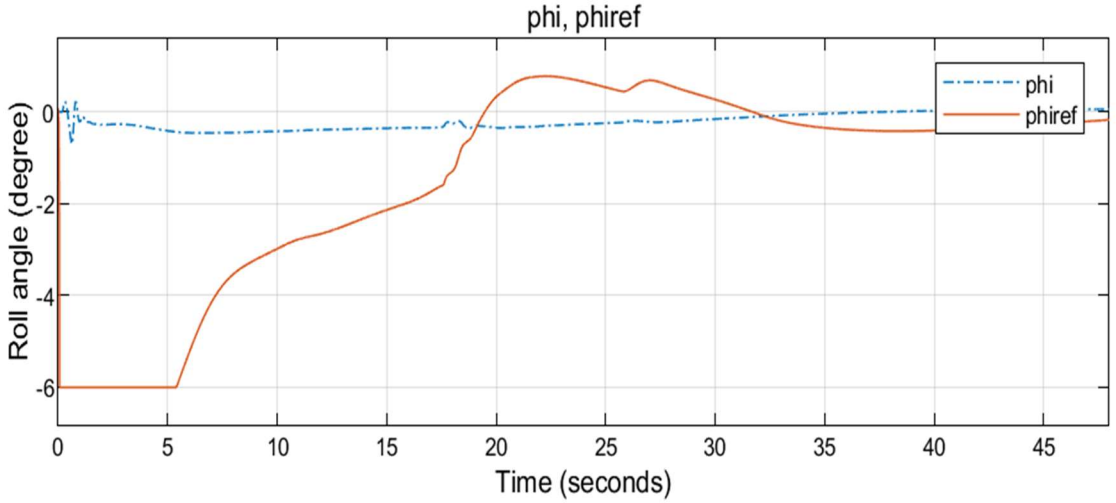

Figure 9.11 Roll angle for the first simulation condition with PID

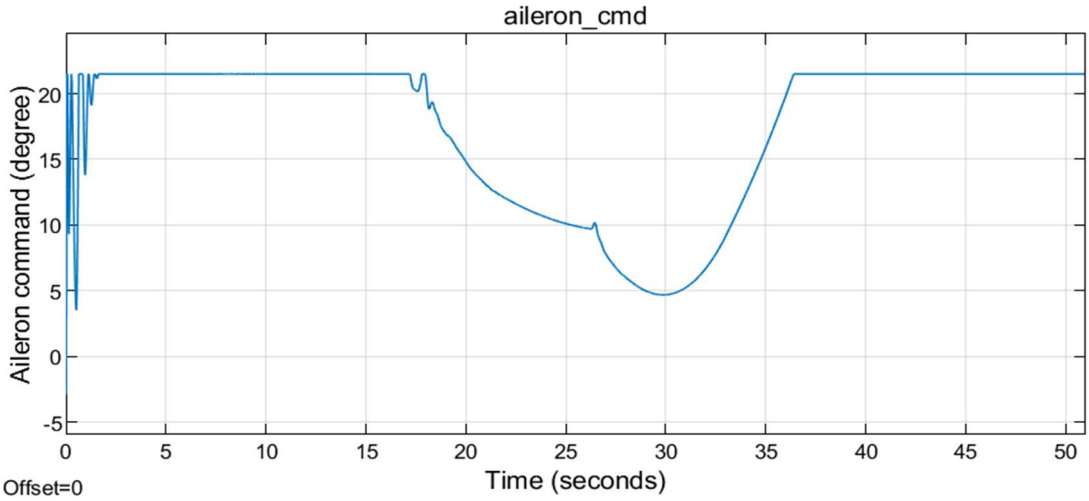

Figure 9.12 Aileron command for the first simulation condition with SMC

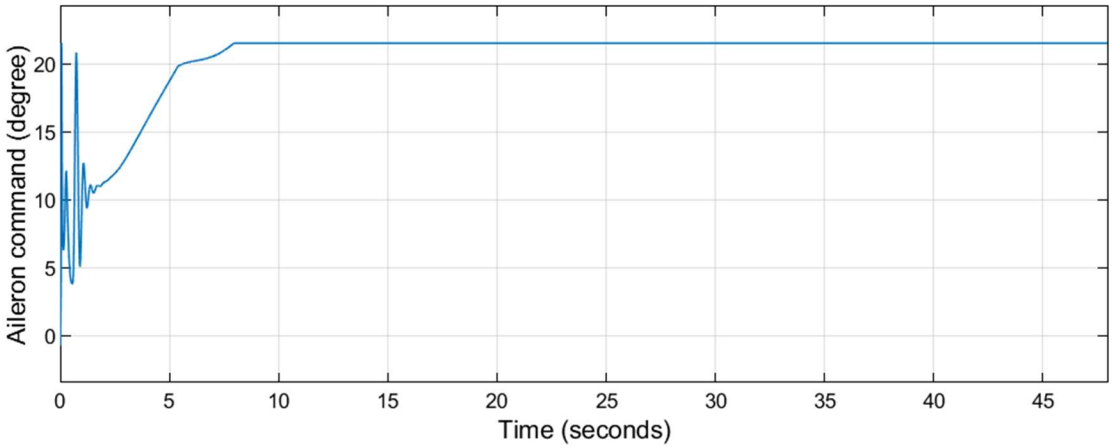

Figure 9.13 Aileron command for the first simulation condition with PID

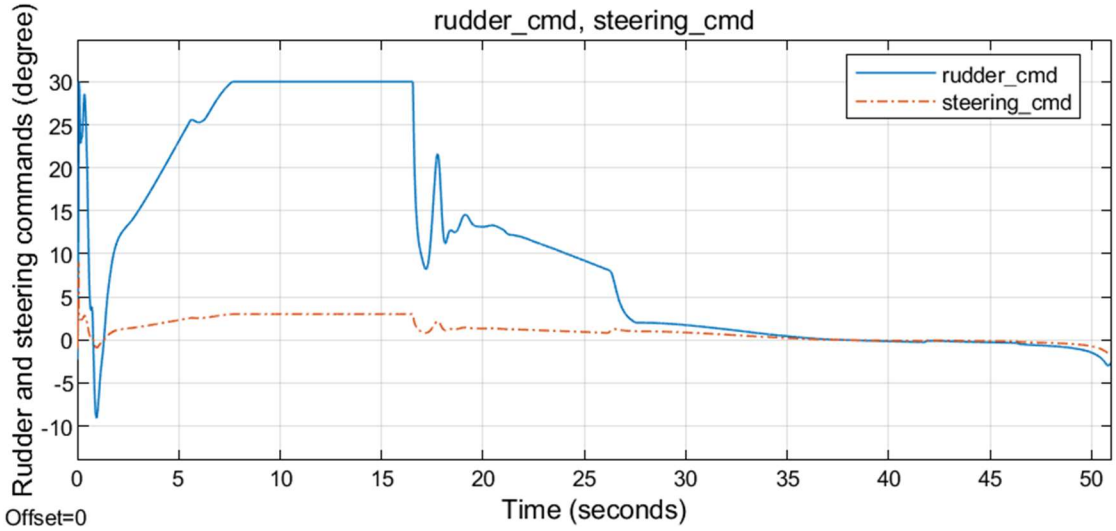

Figure 9.14 Rudder and steering commands for the first simulation condition with SMC

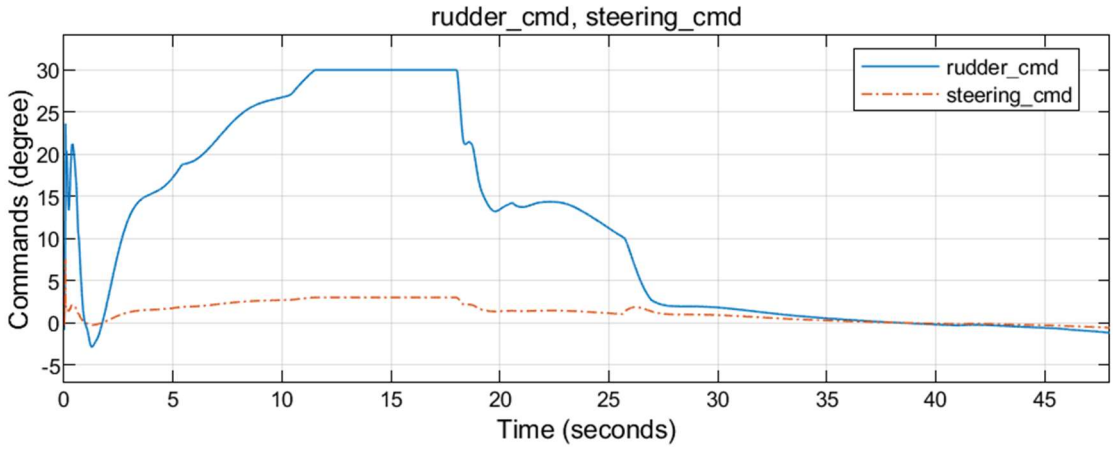

Figure 9.15 Rudder and steering commands for the first simulation condition with PID

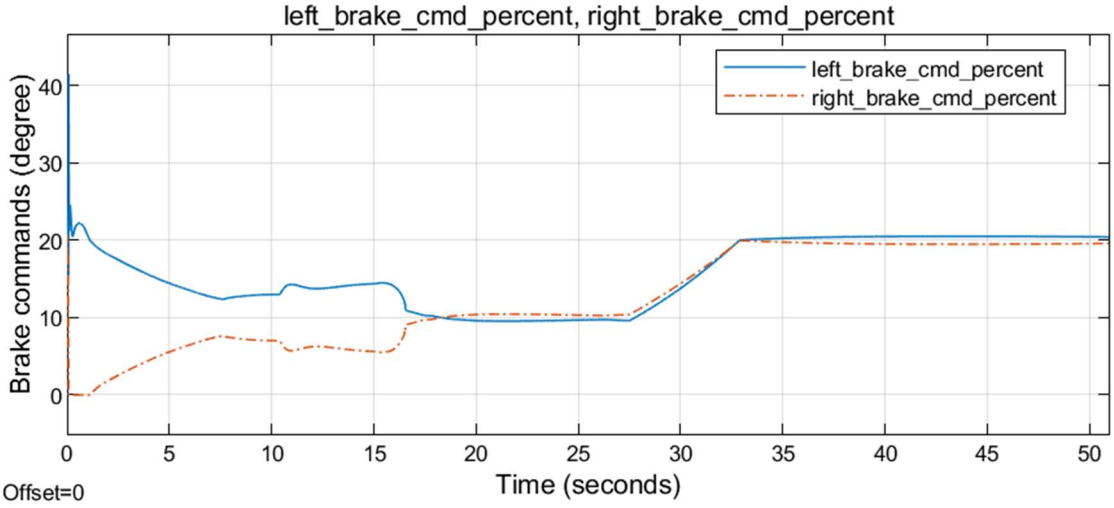

Figure 9.16 Left and right brake commands for the first simulation condition with SMC

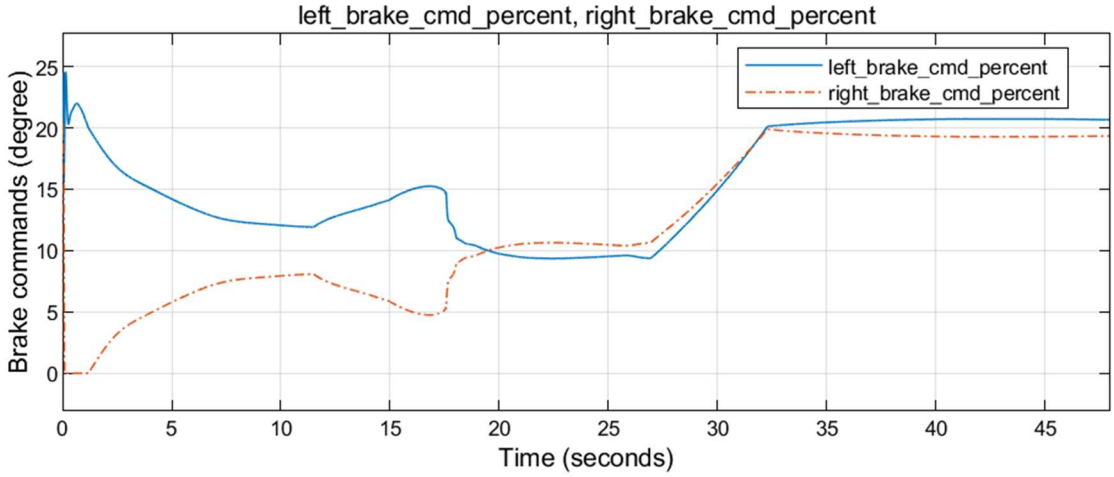

Figure 9.17 Left and right brake commands for the first simulation condition with PID

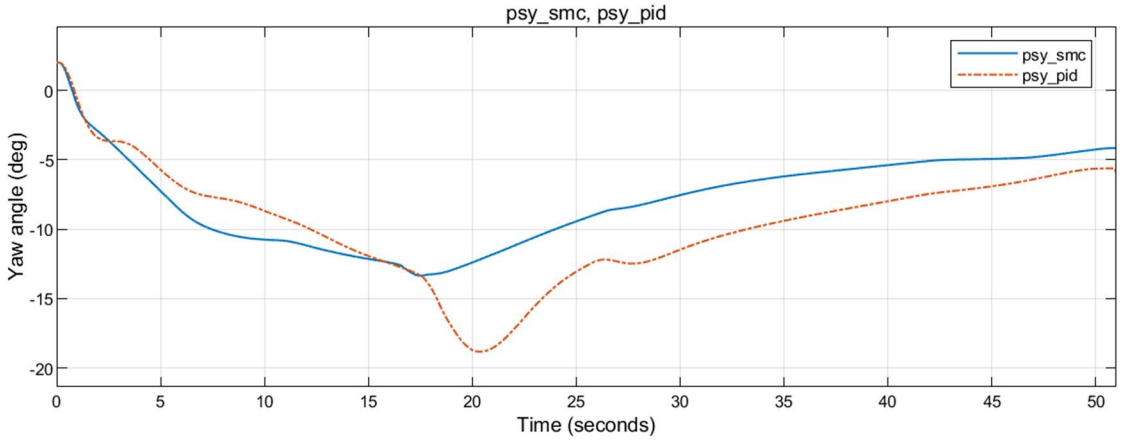

Figure 9.18 Yaw angle for the first simulation condition

9.2 CROSSWIND FROM THE RIGHT SIDE

In this second simulation condition, the same lateral position of 2 m and track angle of 2 degrees initial conditions are given. On top of that there is a constant wind of 15 knots from the east. Results are given in Figures Figure 9.19 to Figure 9.36.

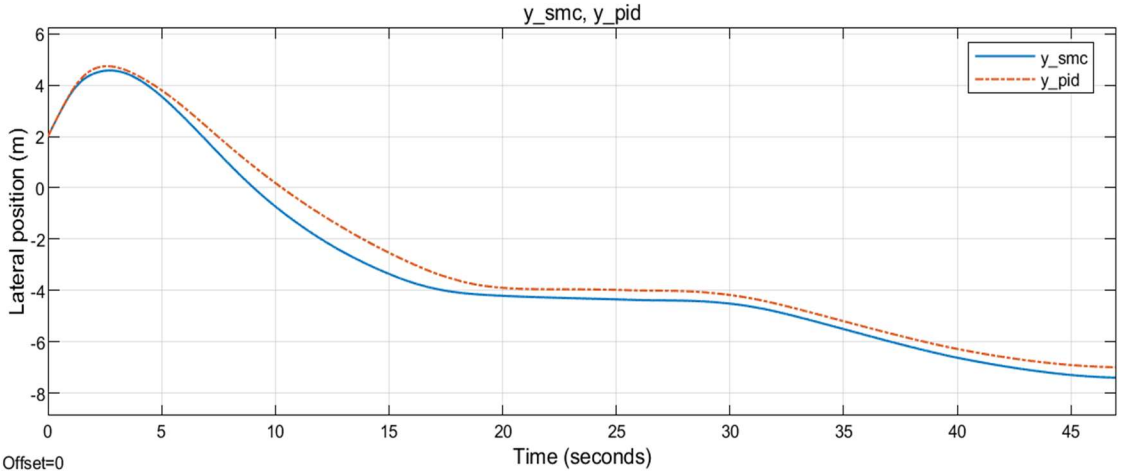

Figure 9.19 Lateral position for the second simulation condition

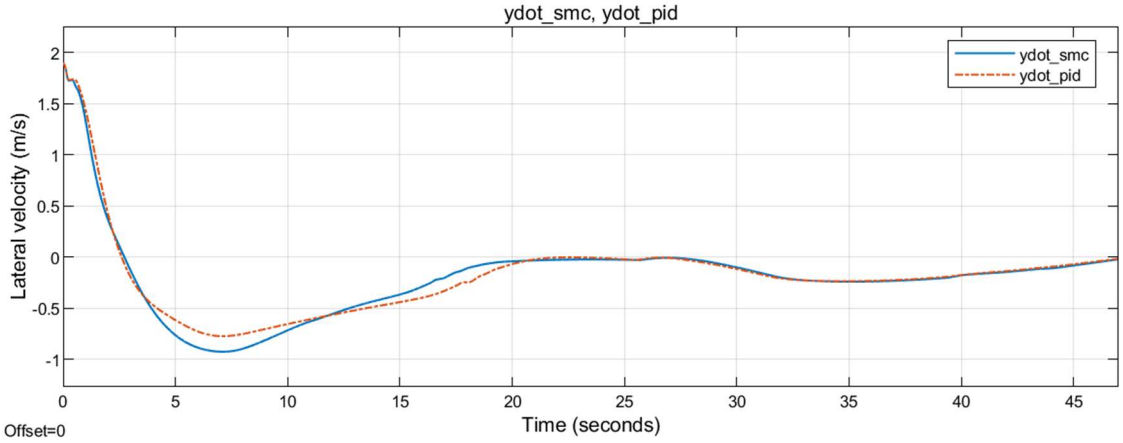

Figure 9.20 Lateral velocity with respect to runway midline for the second simulation condition

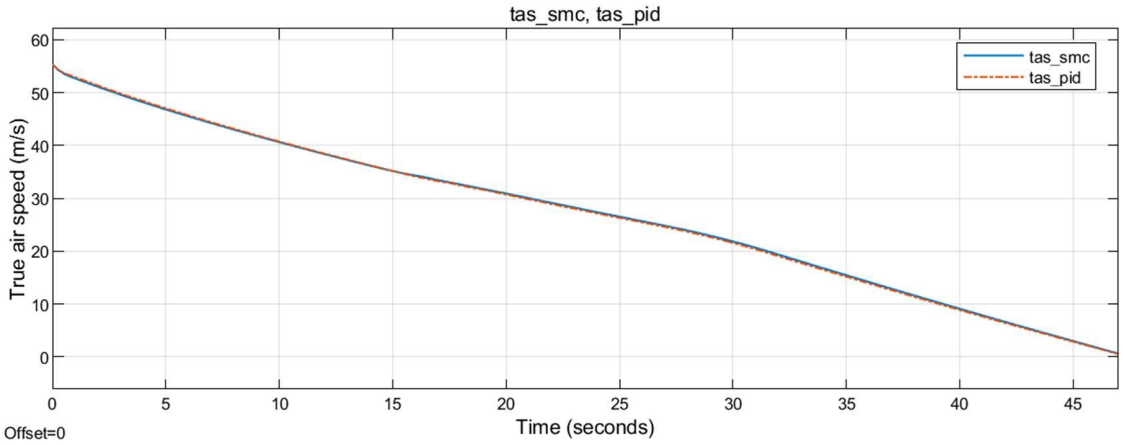

Figure 9.21 True airspeed for the second simulation condition with SMC

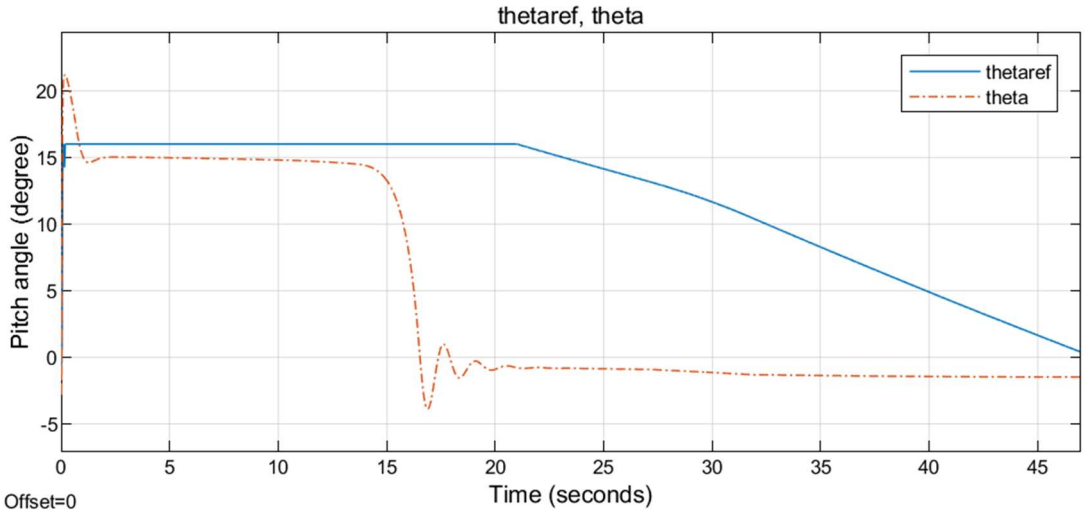

Figure 9.22 Pitch angle for the second simulation condition with SMC

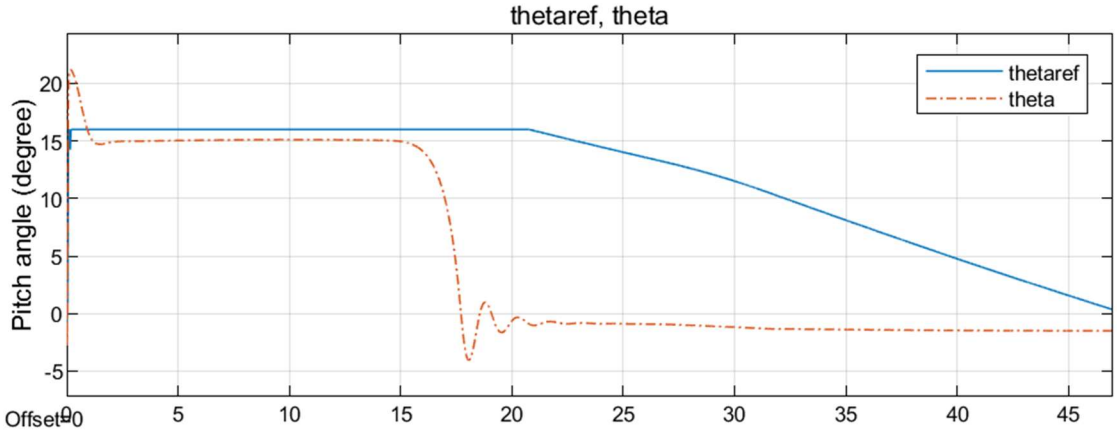

Figure 9.23 Pitch angle for the second simulation condition with PID

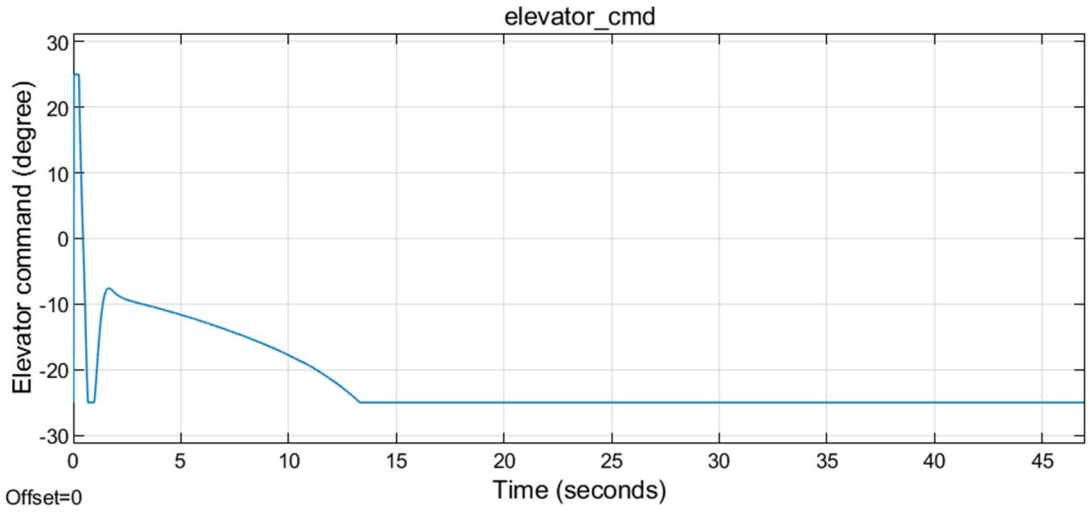

Figure 9.24 Elevator command for the second simulation condition with SMC

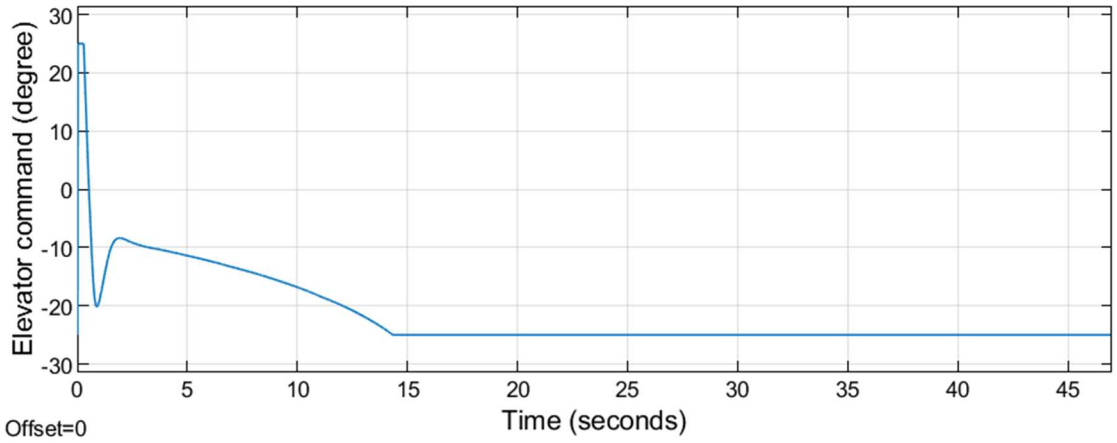

Figure 9.25 Elevator command for the second simulation condition with PID

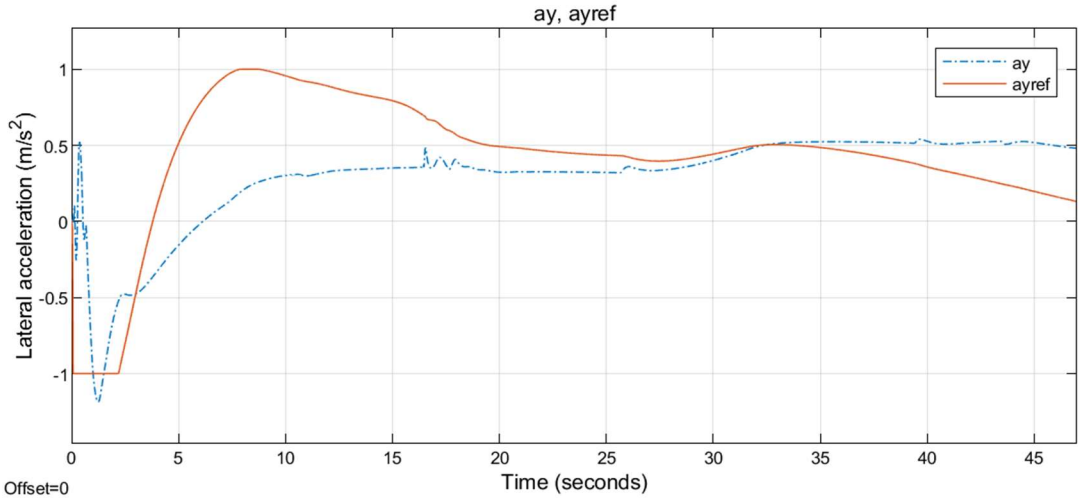

Figure 9.26 Lateral acceleration for the second simulation condition with SMC

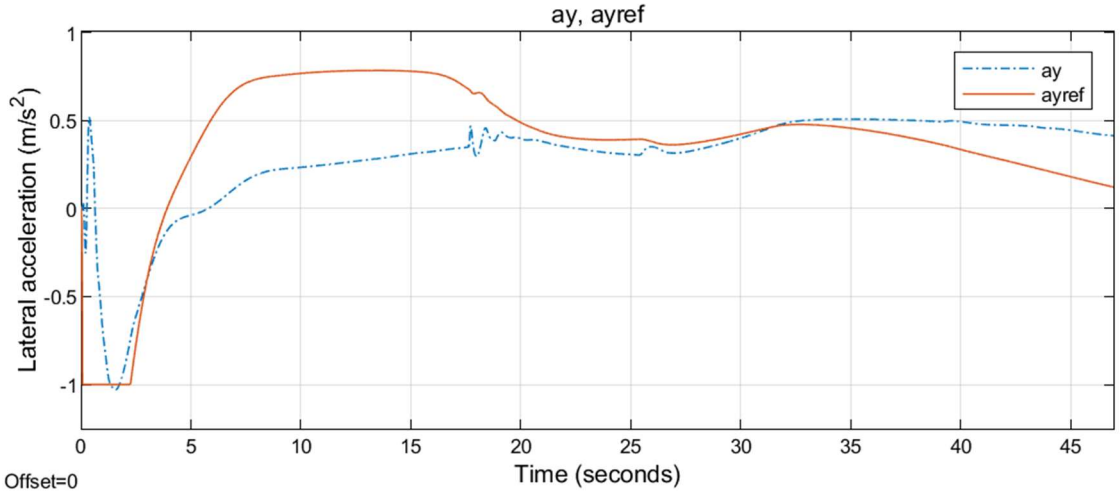

Figure 9.27 Lateral acceleration for the second simulation with PID

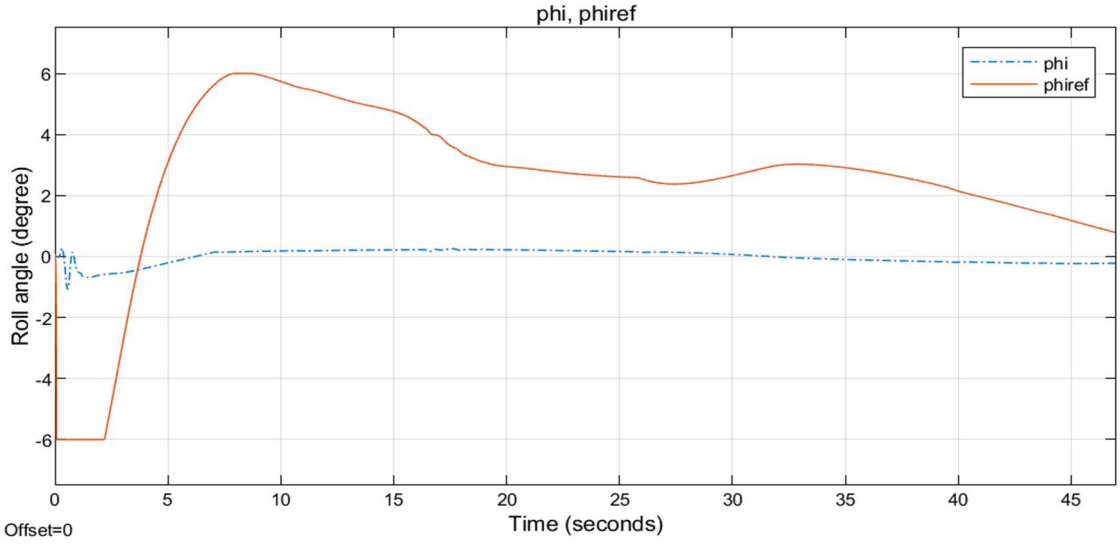

Figure 9.28 Roll angle for the second simulation condition with SMC

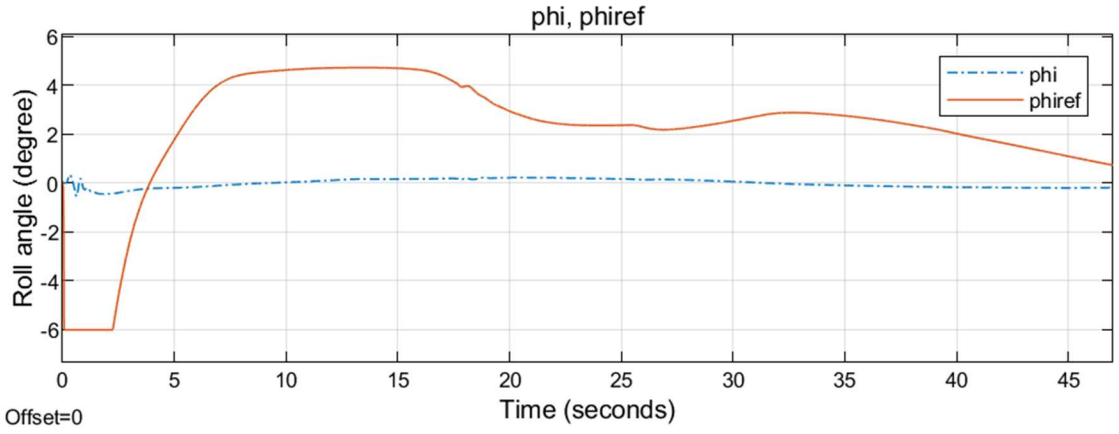

Figure 9.29 Roll angle for the second simulation condition with PID

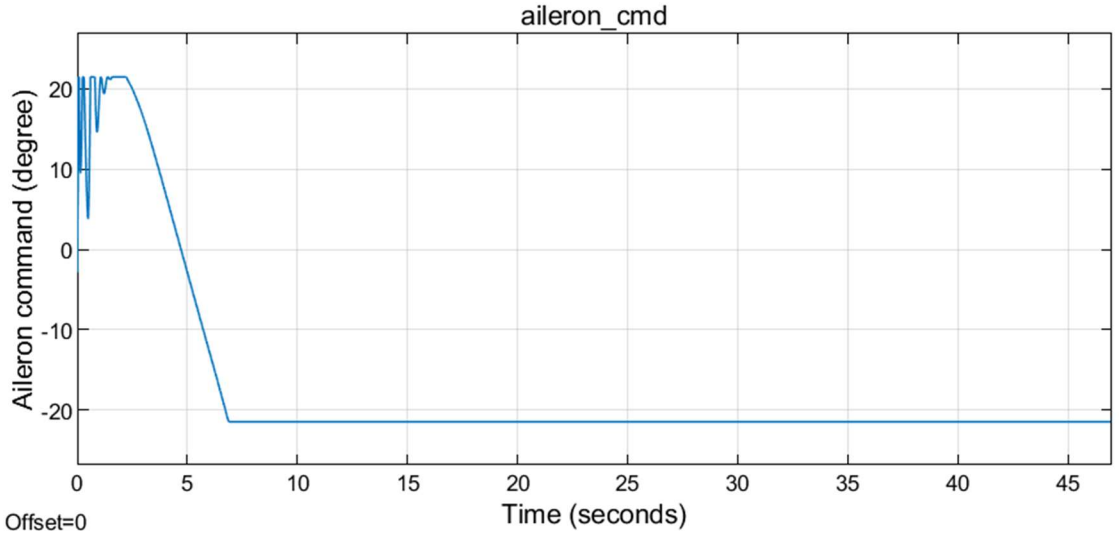

Figure 9.30 Aileron command for the second simulation condition with SMC

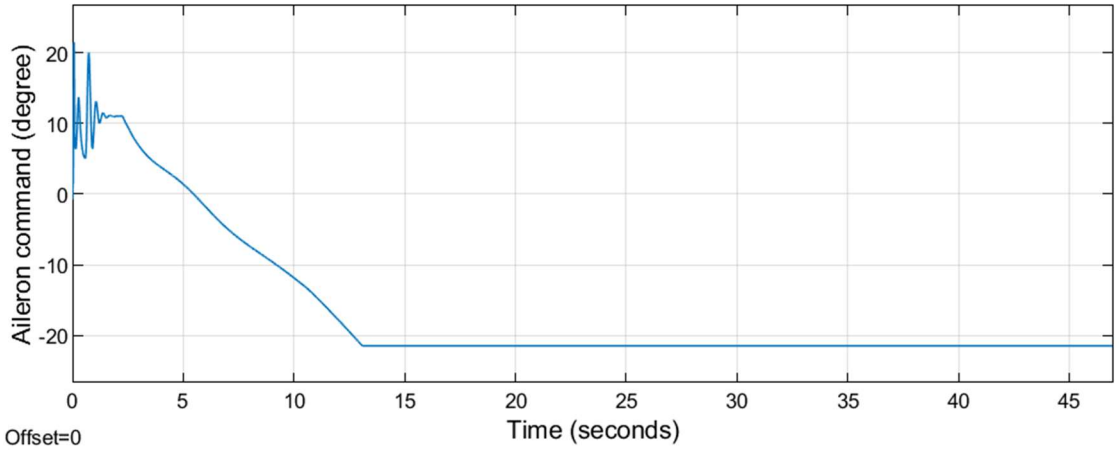

Figure 9.31 Aileron command for the second simulation condition with PID

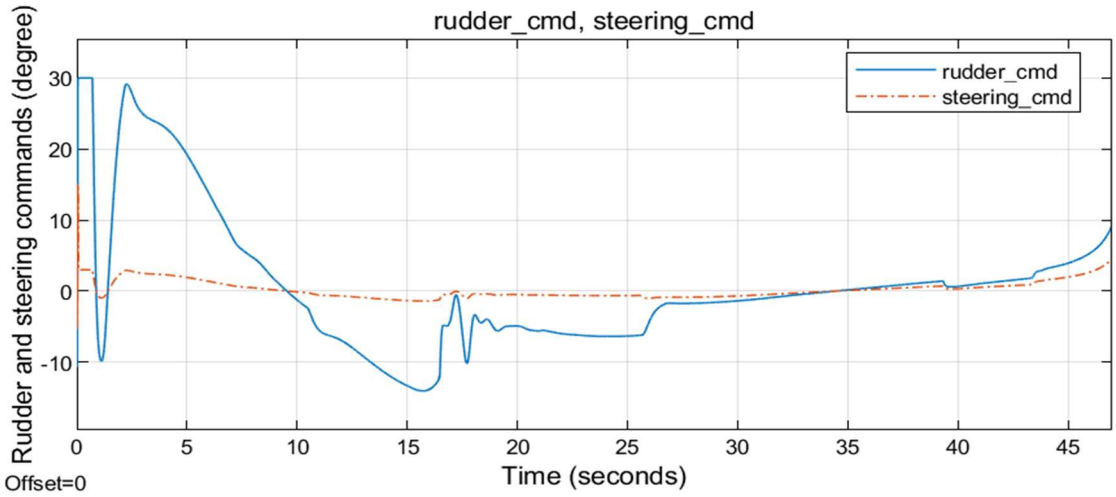

Figure 9.32 Rudder and steering commands for the second simulation condition with SMC

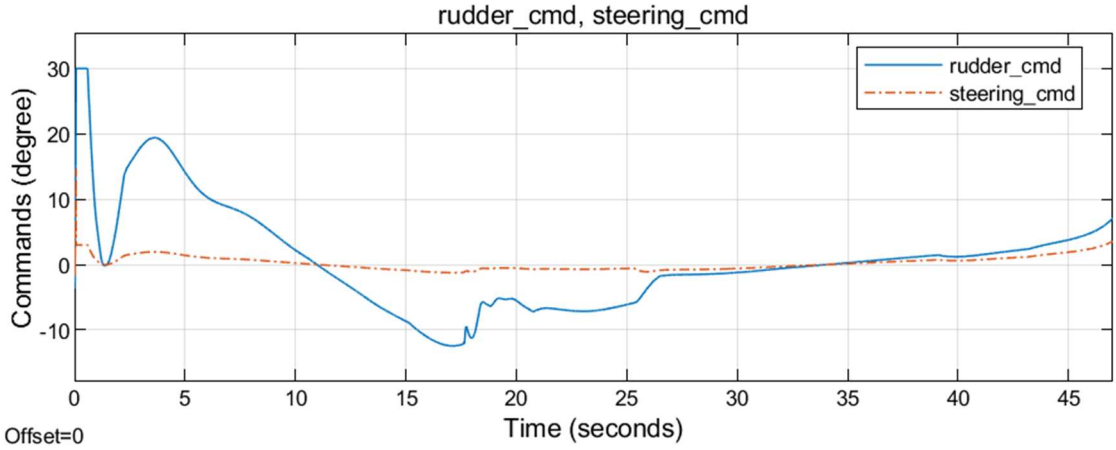

Figure 9.33 Rudder and steering command for the second simulation condition with PID

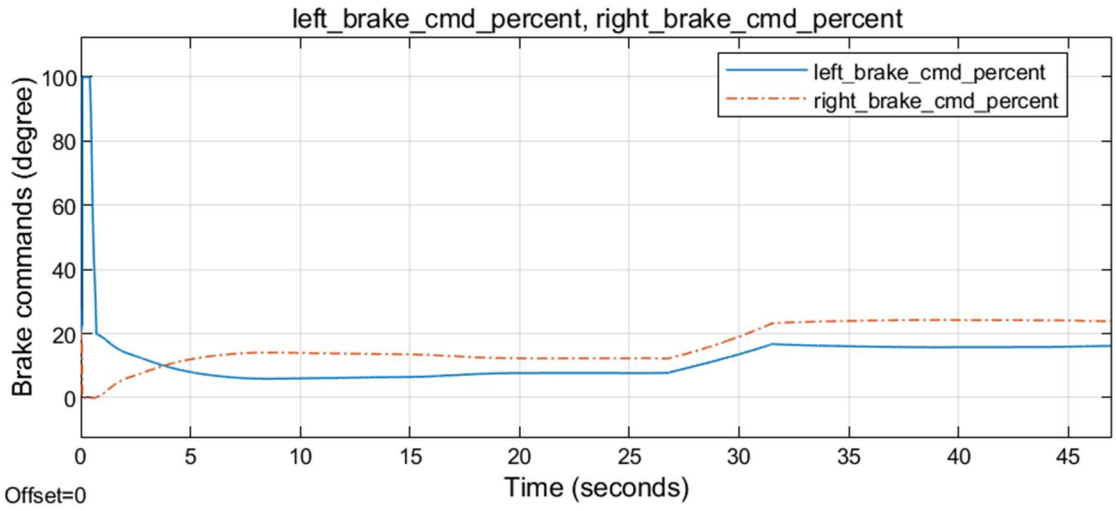

Figure 9.34 Left and right brake commands for the second simulation condition with SMC

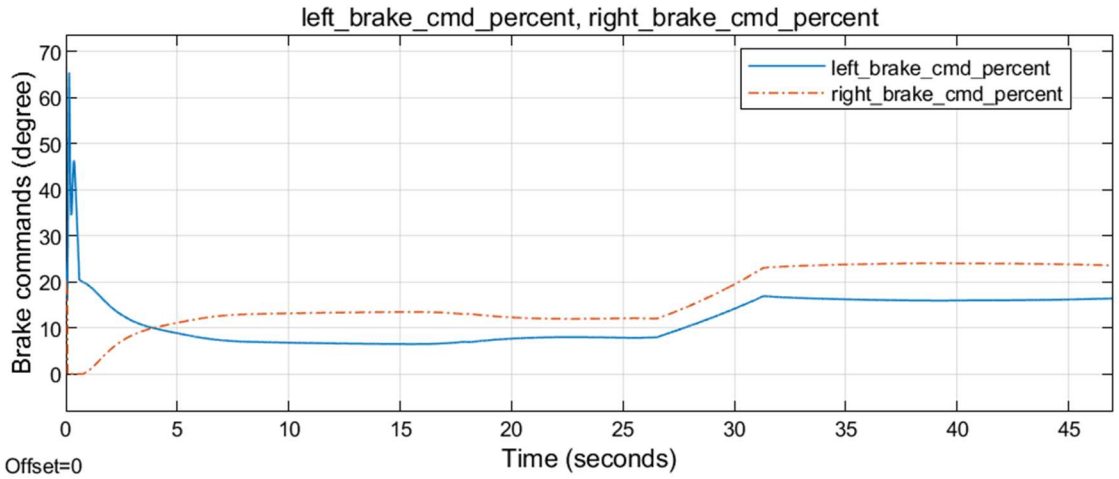

Figure 9.35 Left and right brake command for the second simulation condition with PID

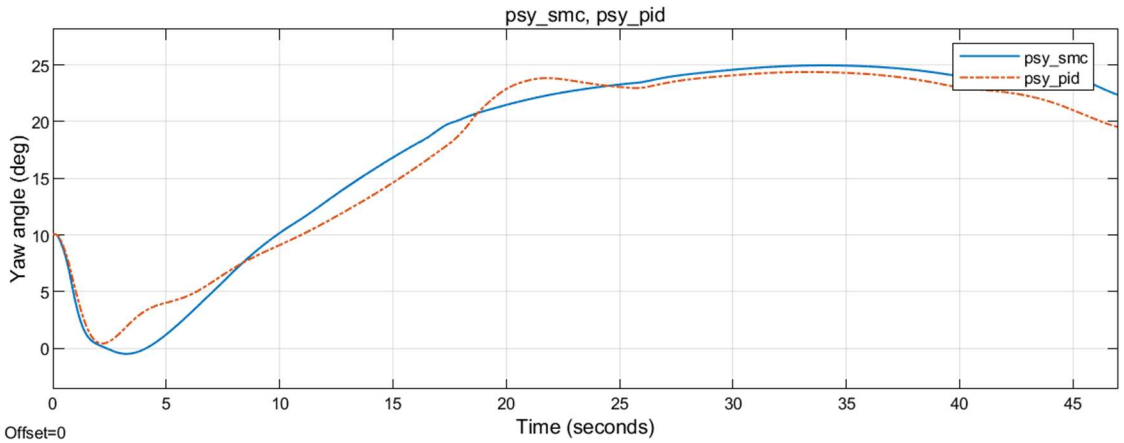

Figure 9.36 Yaw angle for the second simulation condition

9.3 CROSSWIND FROM THE LEFT SIDE

In this third simulation condition, the same lateral position of 2 m and track angle of 2 degrees initial conditions are given. On top of that, there is a constant wind of 15 knots from the west. Results are given in Figures Figure 9.37 to Figure 9.54.

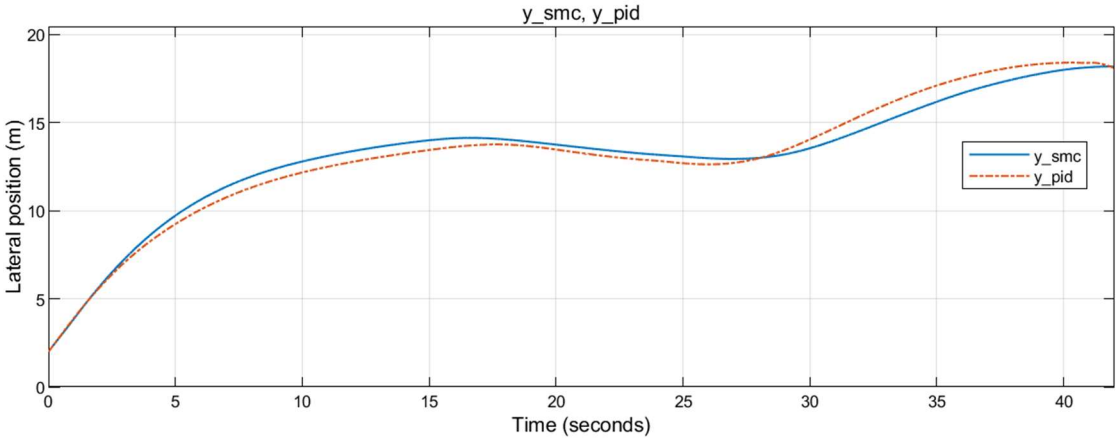

Figure 9.37 Lateral position for the third simulation condition

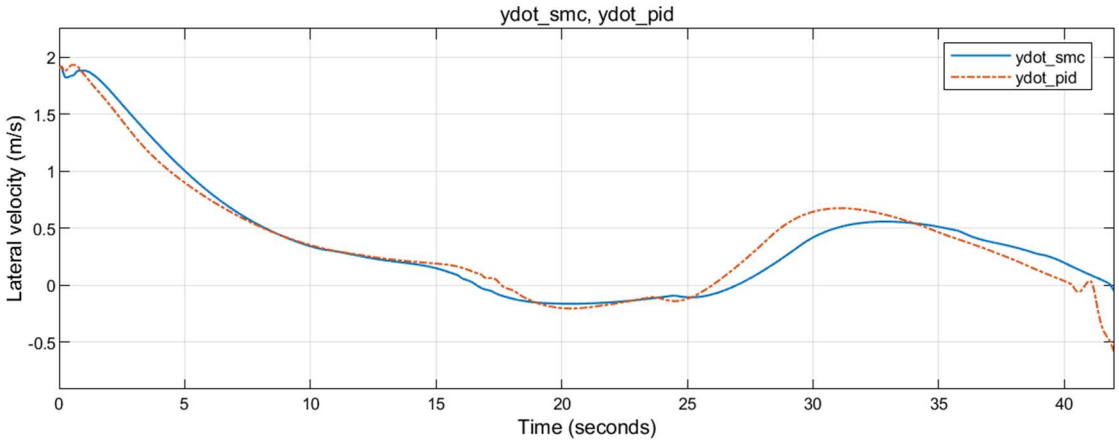

Figure 9.38 Lateral velocity with respect to runway midline for the third simulation condition

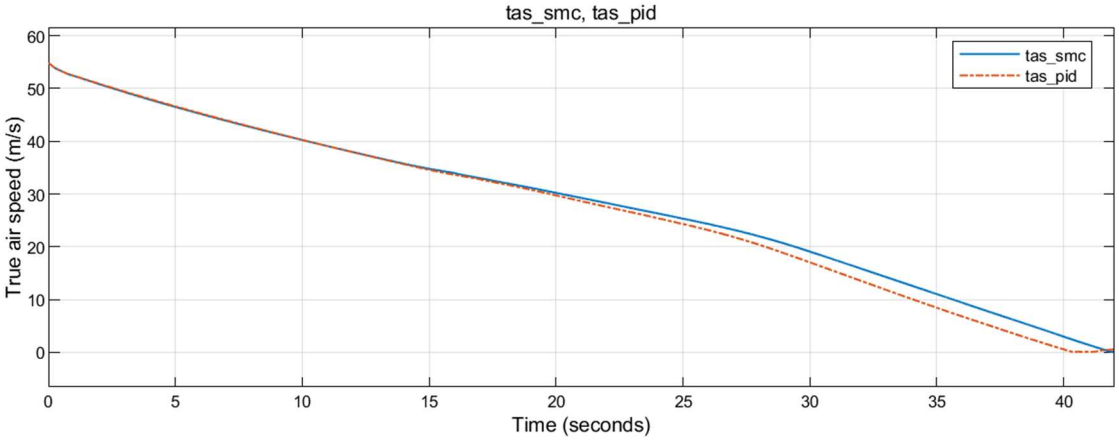

Figure 9.39 True airspeed for the third simulation condition

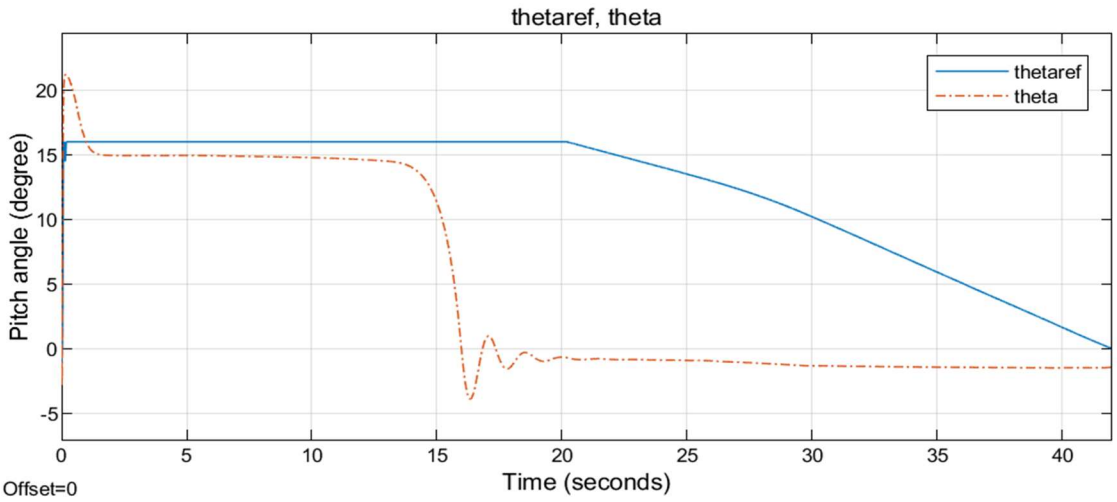

Figure 9.40 Pitch angle for the third simulation condition with SMC

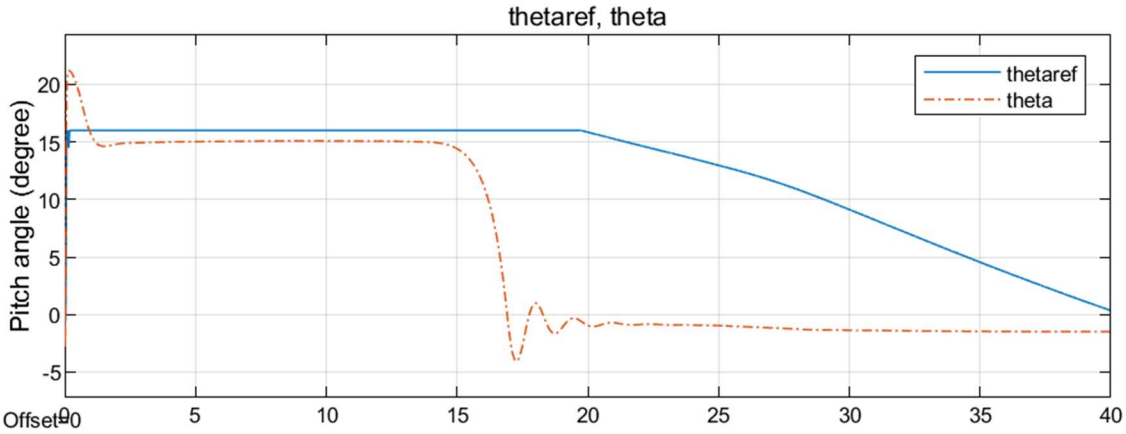

Figure 9.41 Pitch angle for the third simulation condition with PID

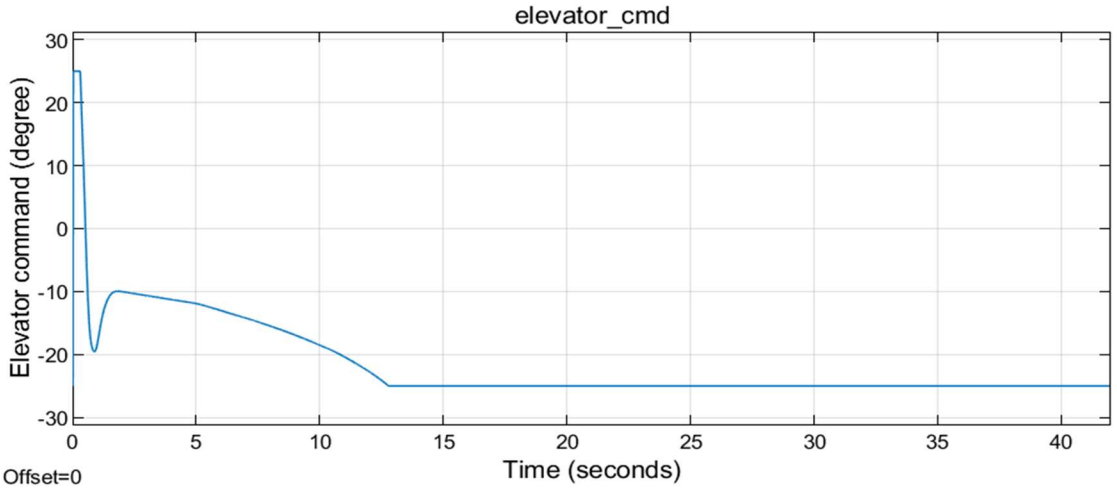

Figure 9.42 Elevator command for the third simulation condition with SMC

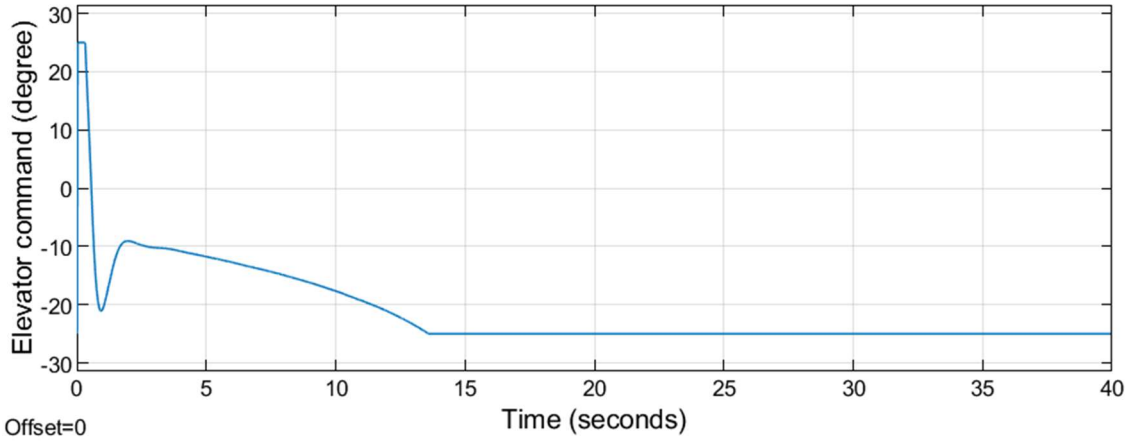

Figure 9.43 Elevator command for the third simulation condition with PID

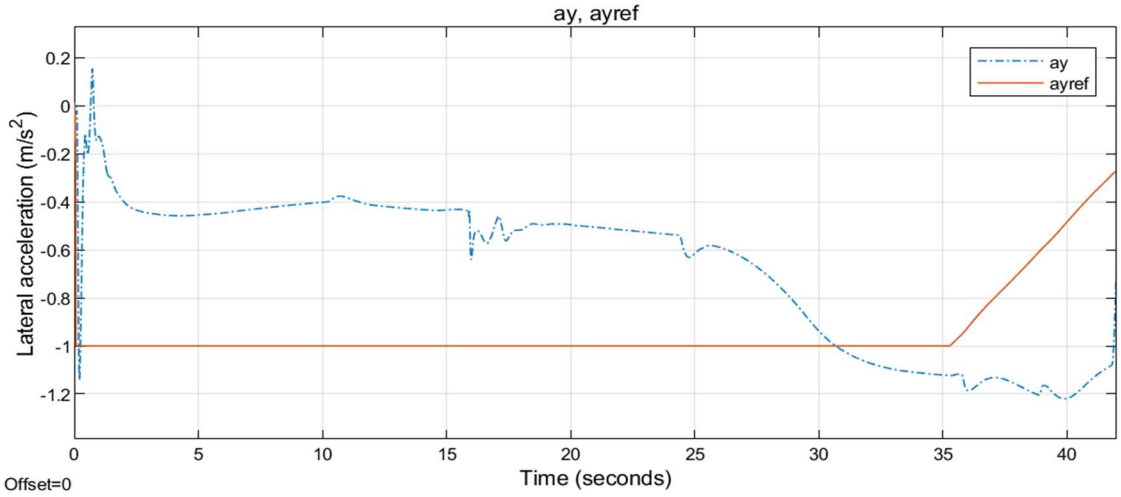

Figure 9.44 Lateral acceleration for the third simulation condition with SMC

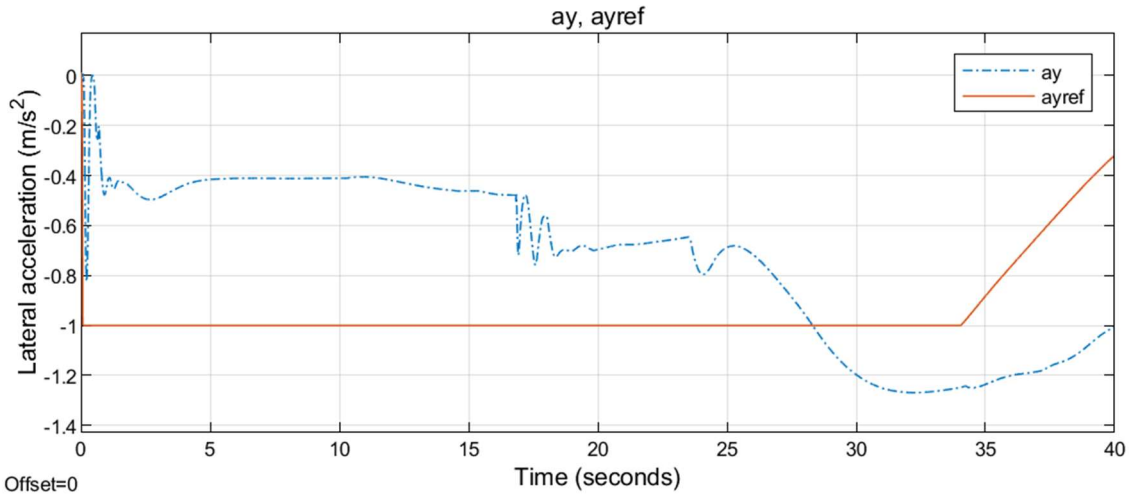

Figure 9.45 Lateral acceleration for the third simulation condition with PID

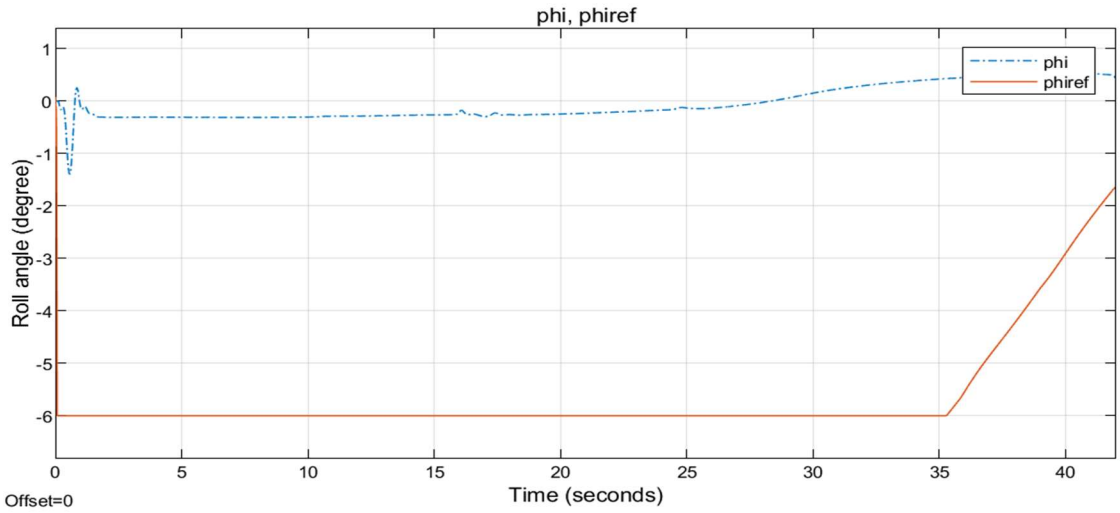

Figure 9.46 Roll angle for the third simulation condition with SMC

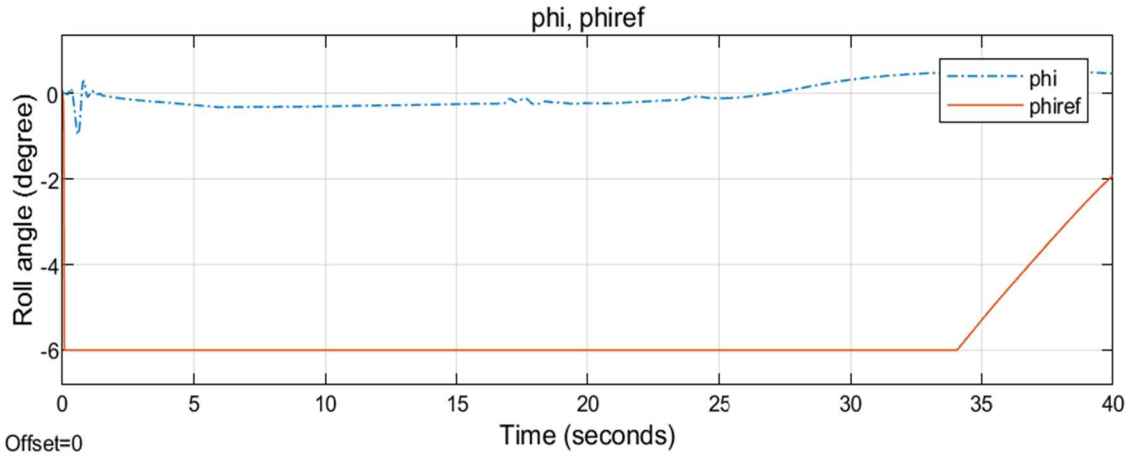

Figure 9.47 Roll angle for the third simulation condition with PID

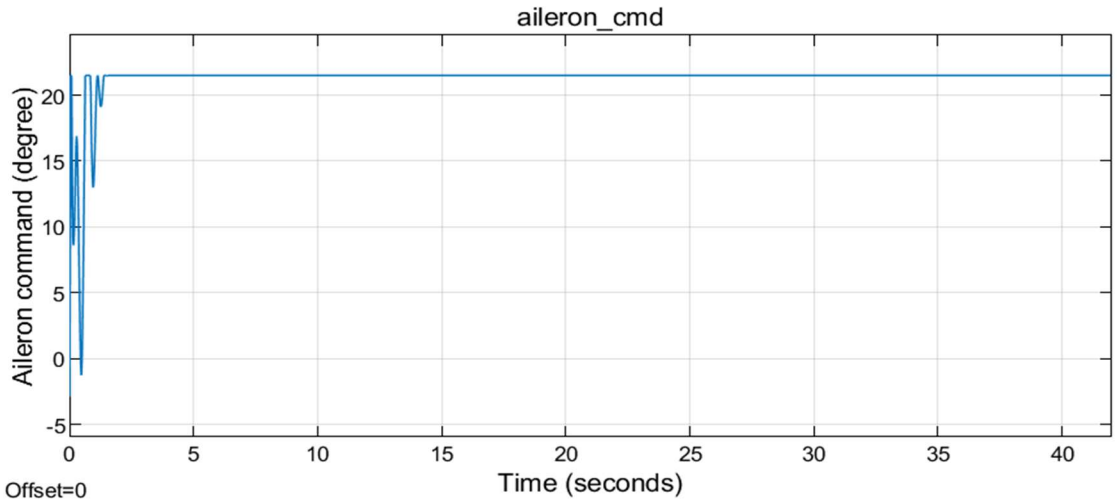

Figure 9.48 Aileron command for the third simulation condition with SMC

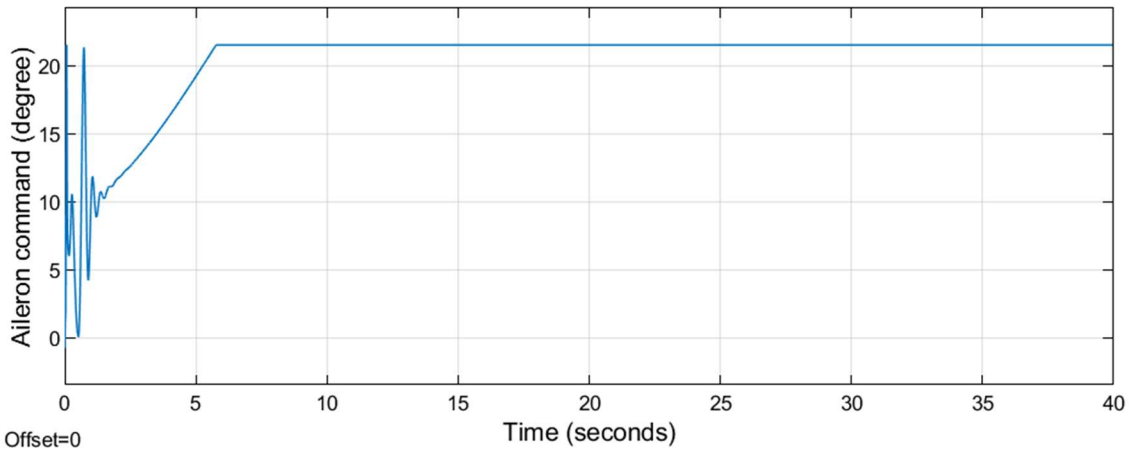

Figure 9.49 Aileron command for the third simulation condition with PID

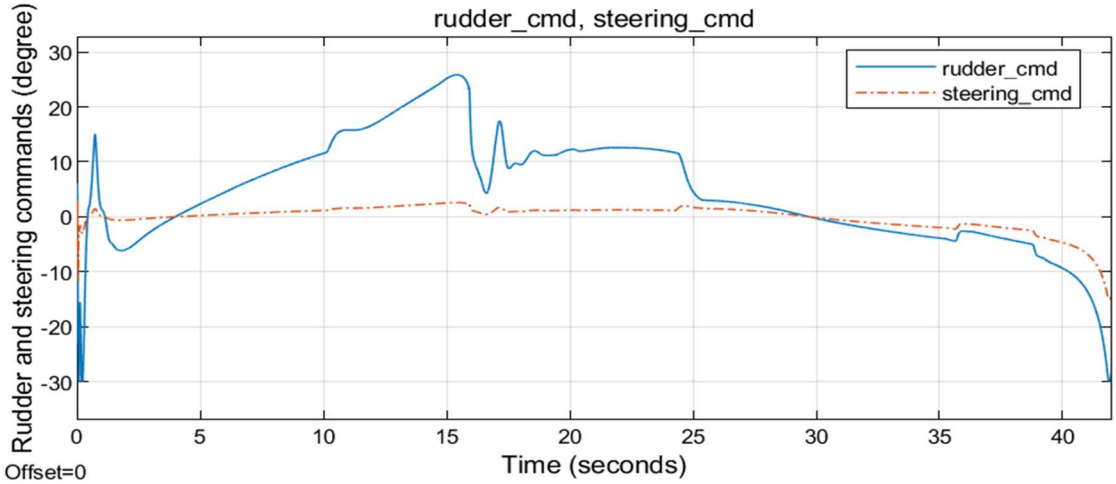

Figure 9.50 Rudder and steering commands for the third simulation condition with SMC

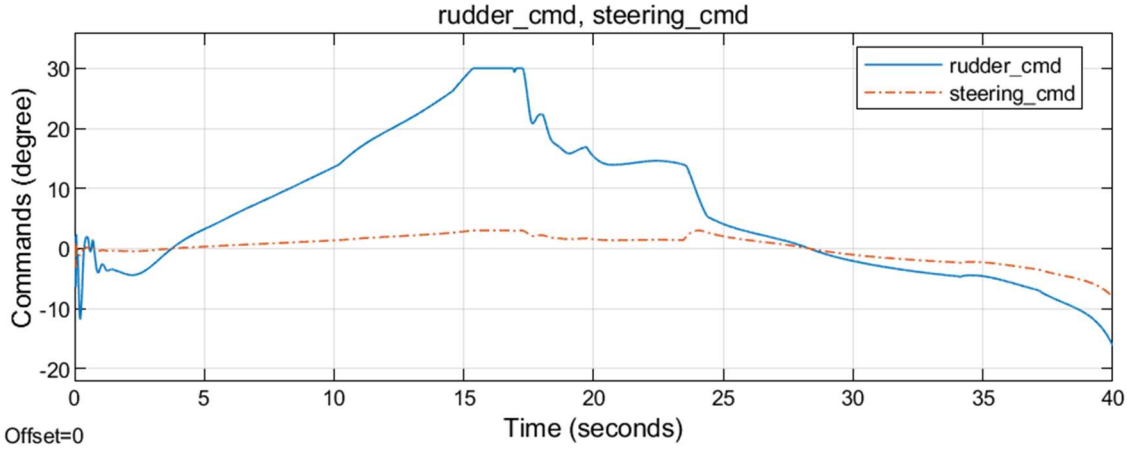

Figure 9.51 Rudder and steering commands for the third simulation condition with PID

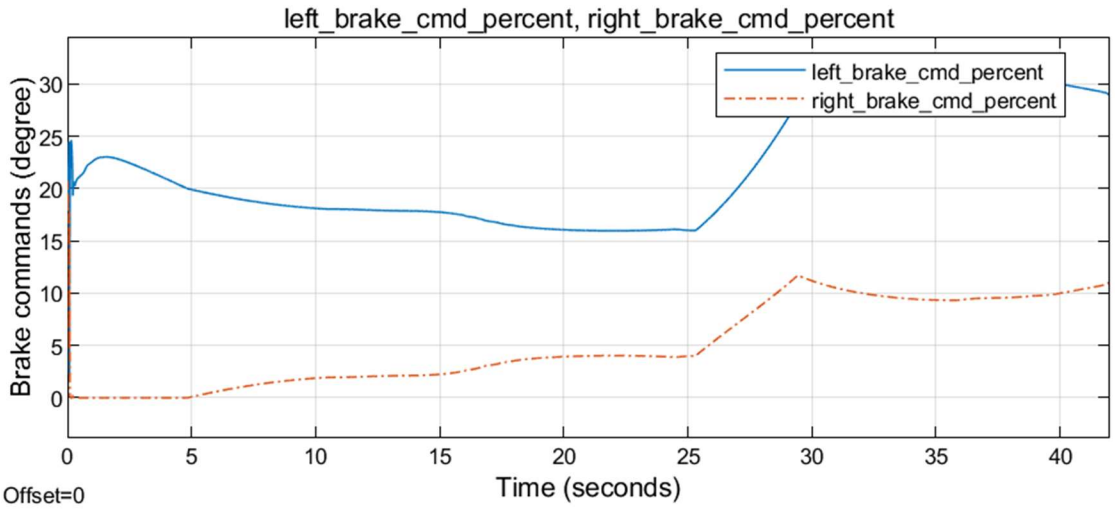

Figure 9.52 Left and right brake commands for the third simulation condition with SMC

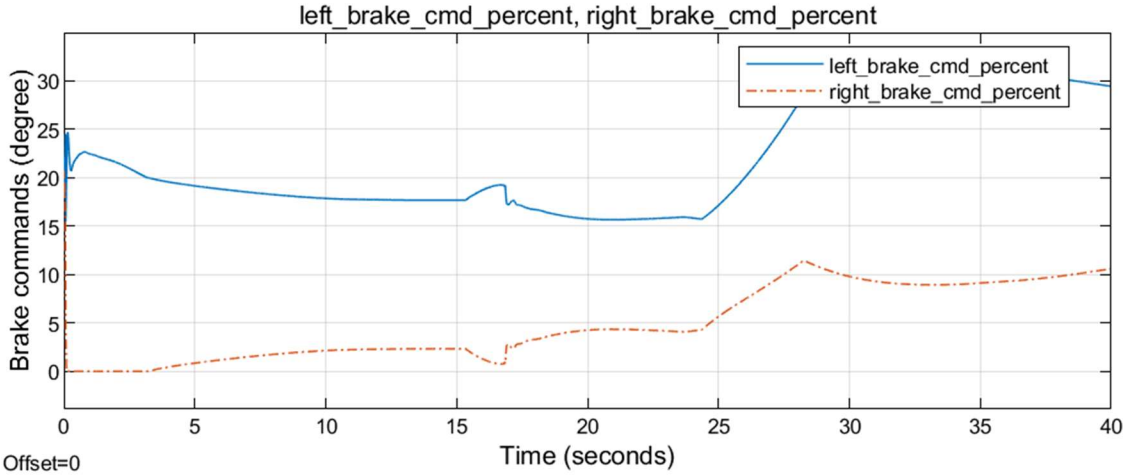

Figure 9.53 Left and right brake command for the third simulation condition with PID

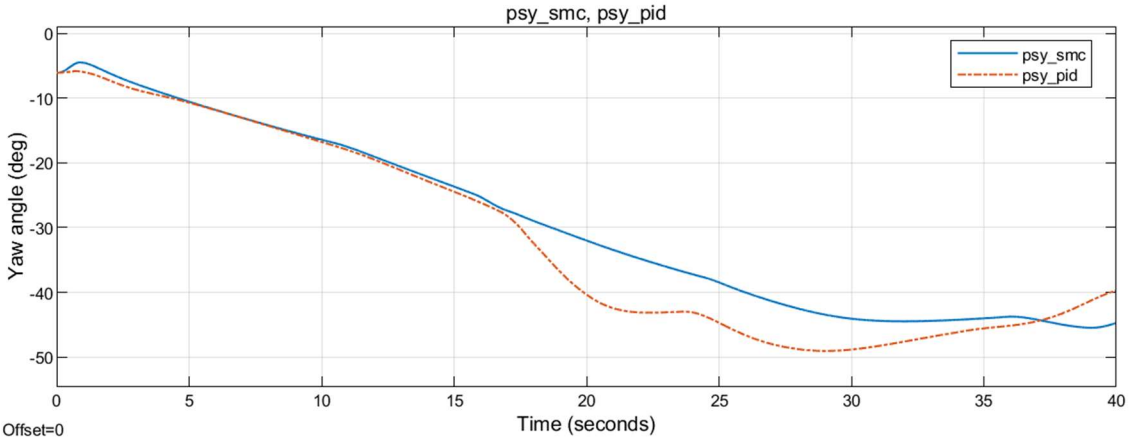

Figure 9.54 Yaw angle for the third simulation condition

9.4 RIGHT BRAKE STUCK

In the fourth simulation condition, the same lateral position of 2 m and track angle of 2 degrees initial conditions are given. On top of that, there is a right brake stuck malfunction. Results are given in Figures Figure 9.55 to Figure 9.72.

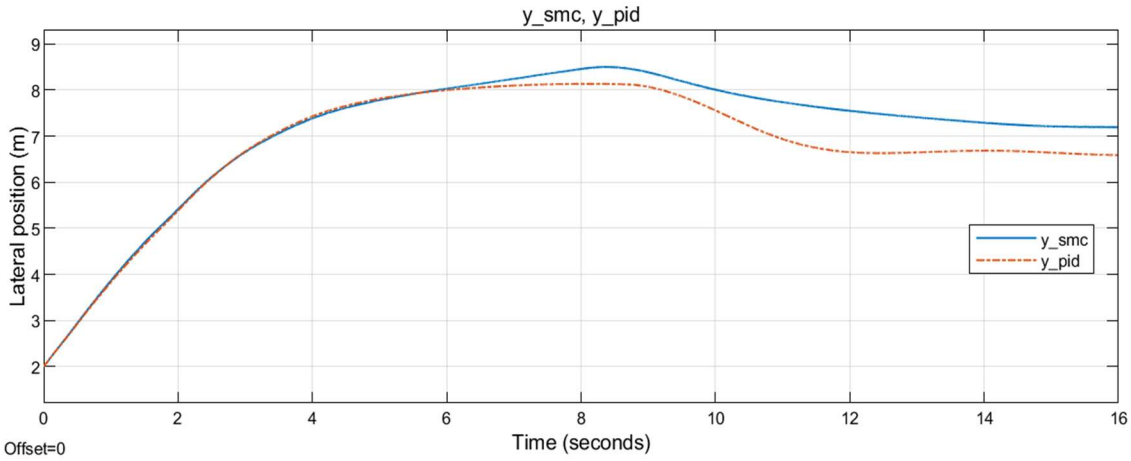

Figure 9.55 Lateral position for the fourth simulation condition

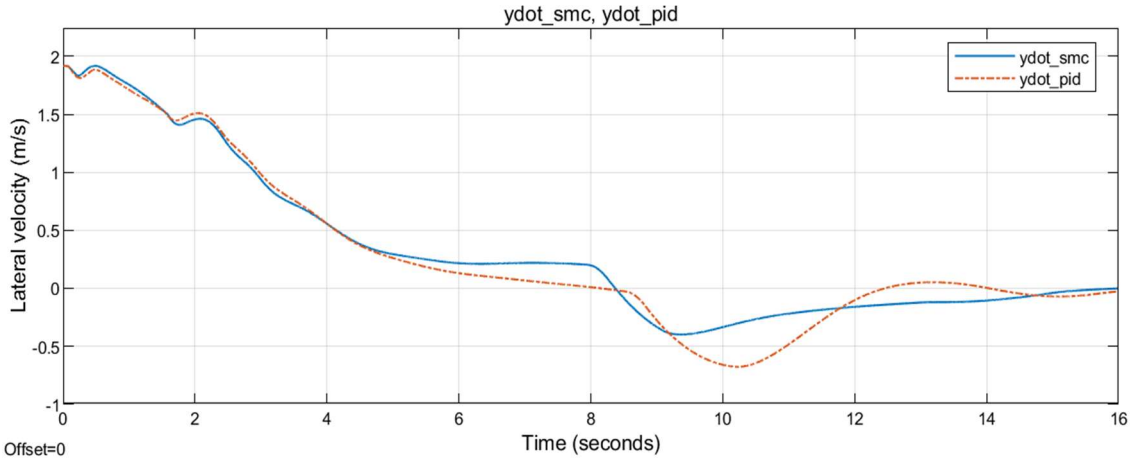

Figure 9.56 Lateral velocity with respect to runway midline for the fourth simulation condition

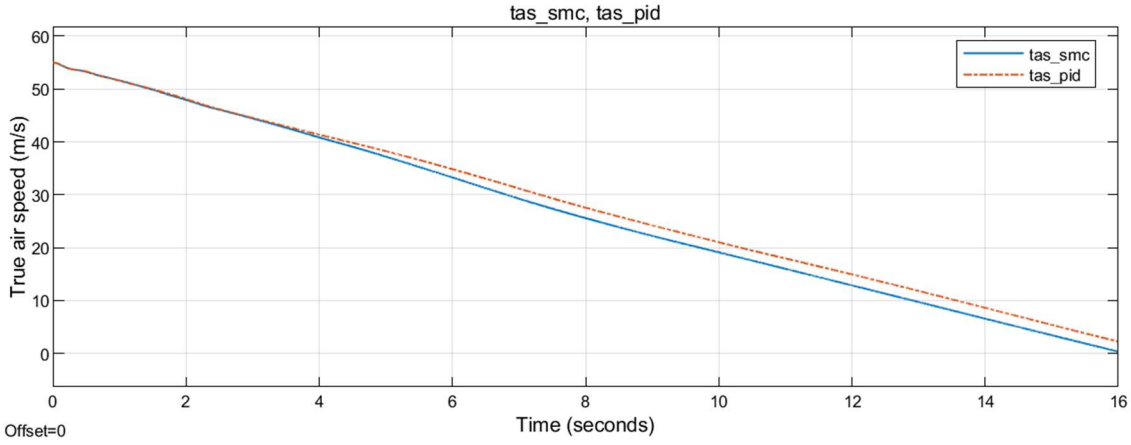

Figure 9.57 True airspeed for the fourth simulation condition

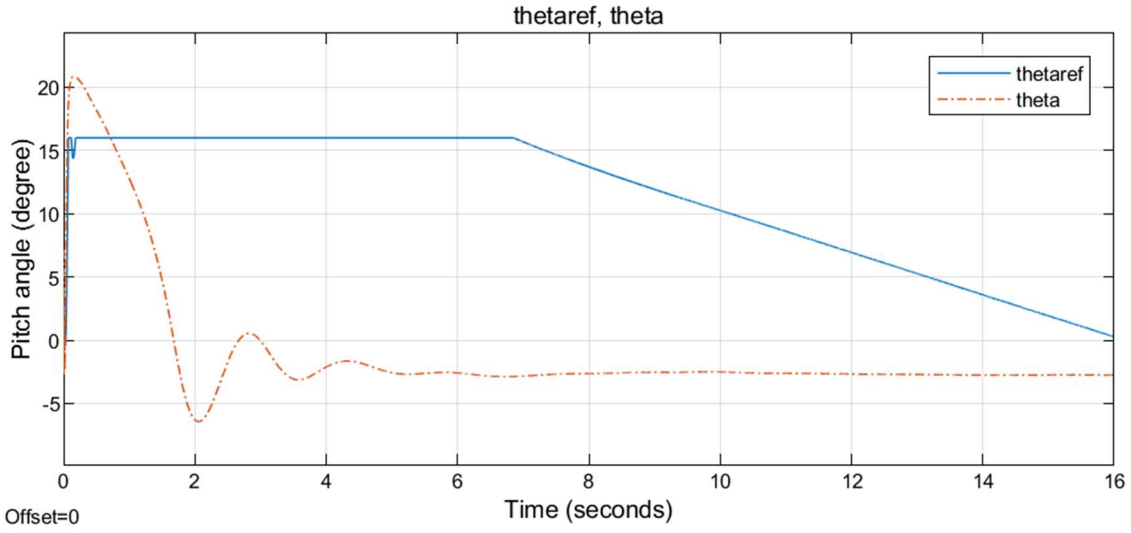

Figure 9.58 Pitch angle for the fourth simulation condition with SMC

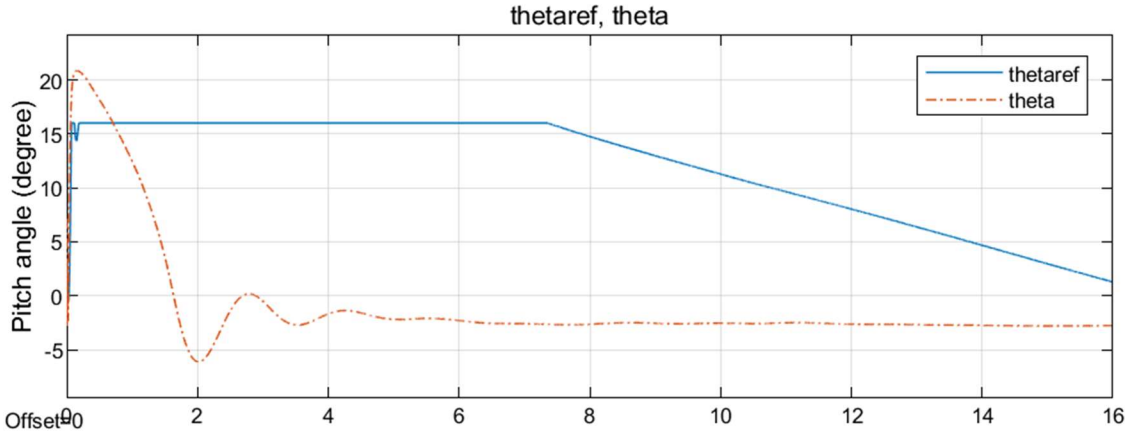

Figure 9.59 Pitch angle for the fourth simulation condition with PID

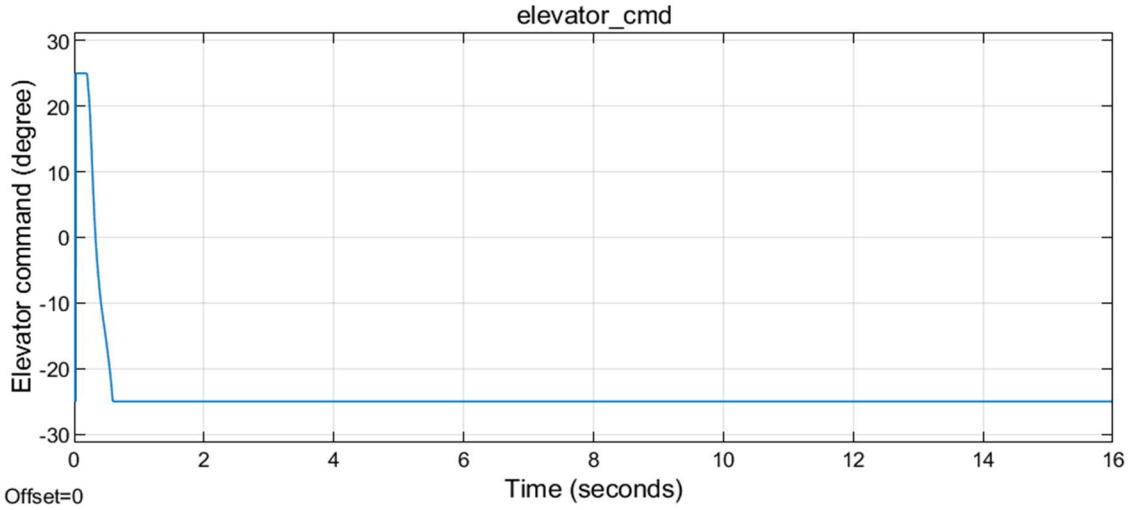

Figure 9.60 Elevator command for the fourth simulation condition with SMC

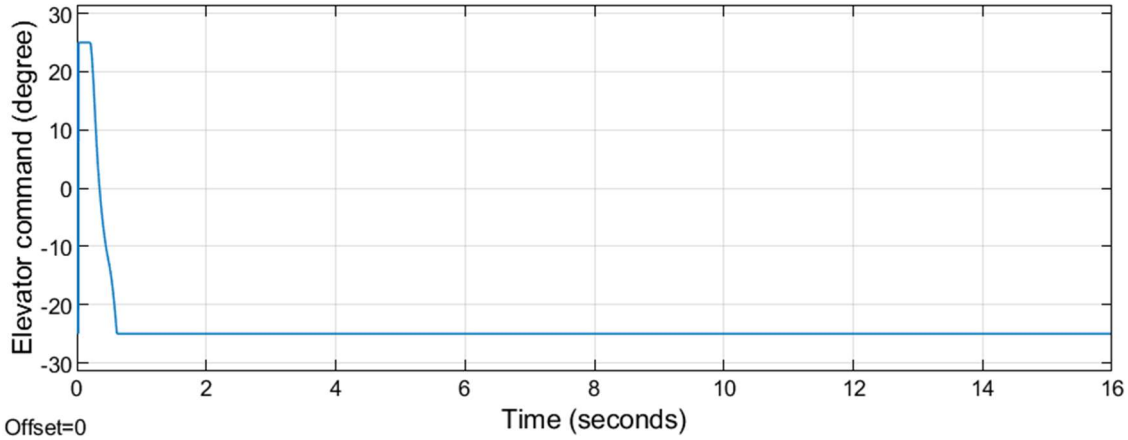

Figure 9.61 Elevator command for the fourth simulation condition with PID

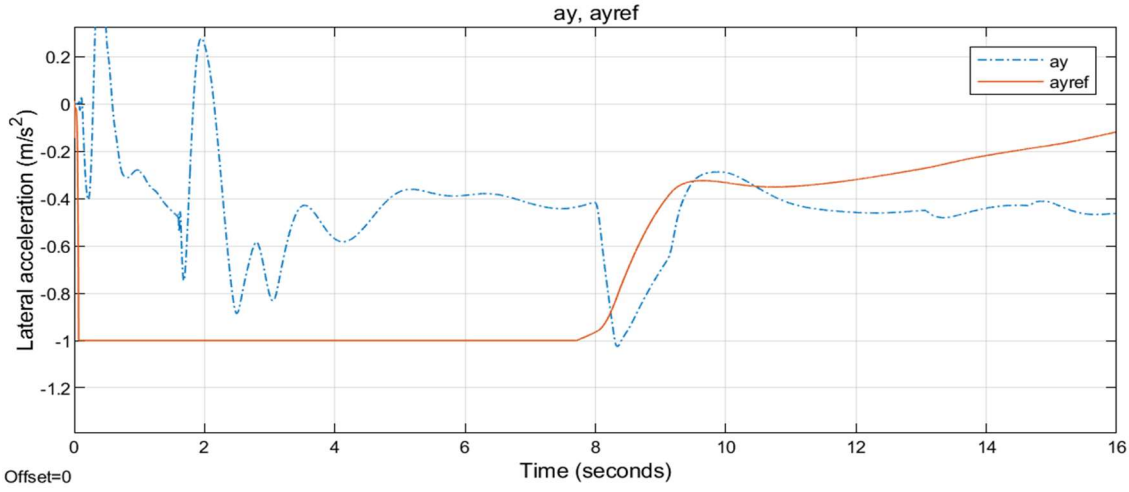

Figure 9.62 Lateral acceleration for the fourth simulation condition with SMC

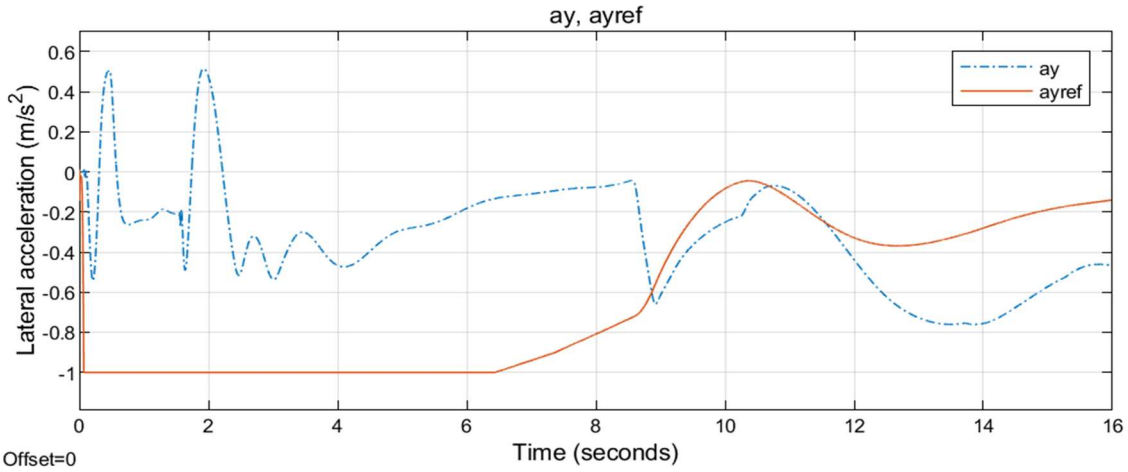

Figure 9.63 Lateral acceleration for the fourth simulation condition with PID

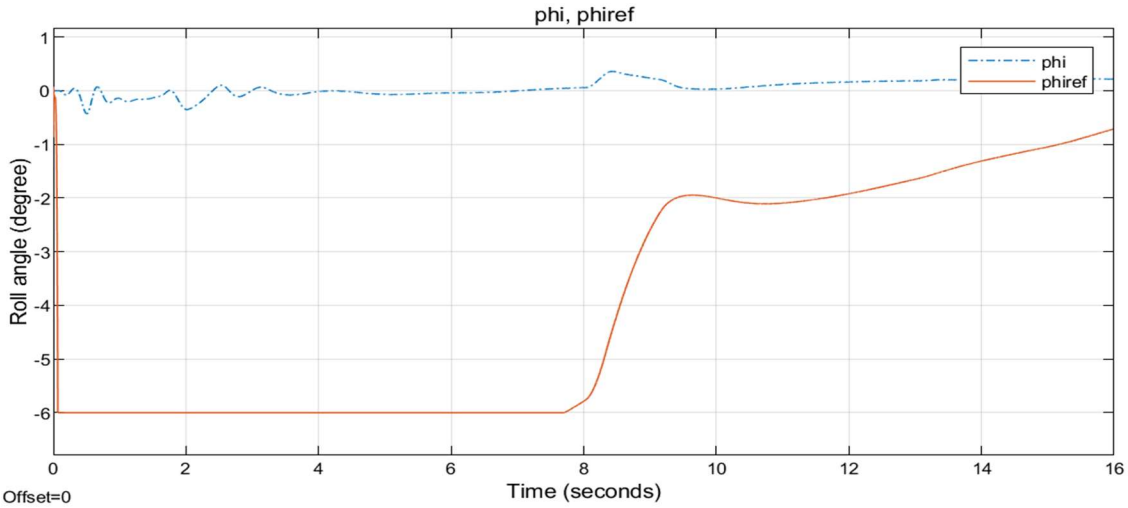

Figure 9.64 Roll angle for the fourth simulation condition with SMC

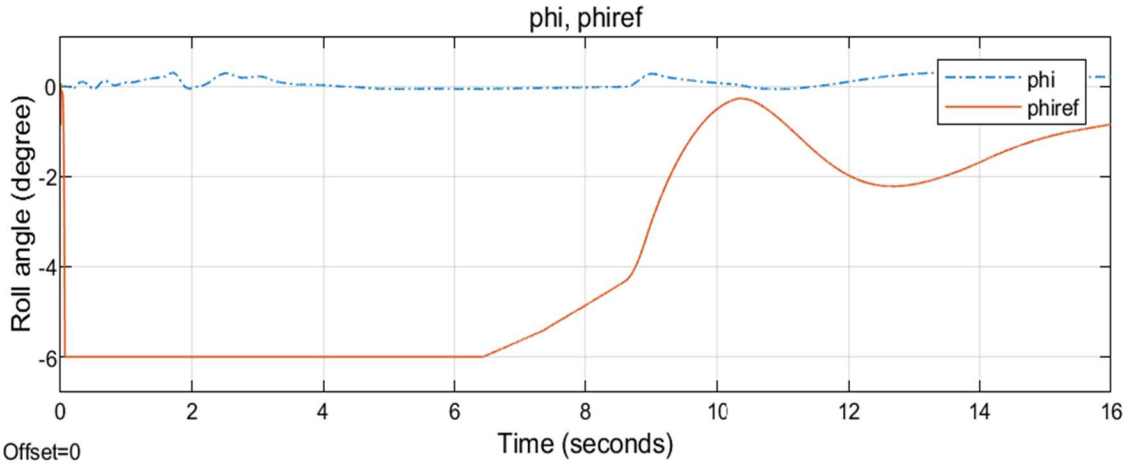

Figure 9.65 Roll angle for the fourth simulation condition with PID

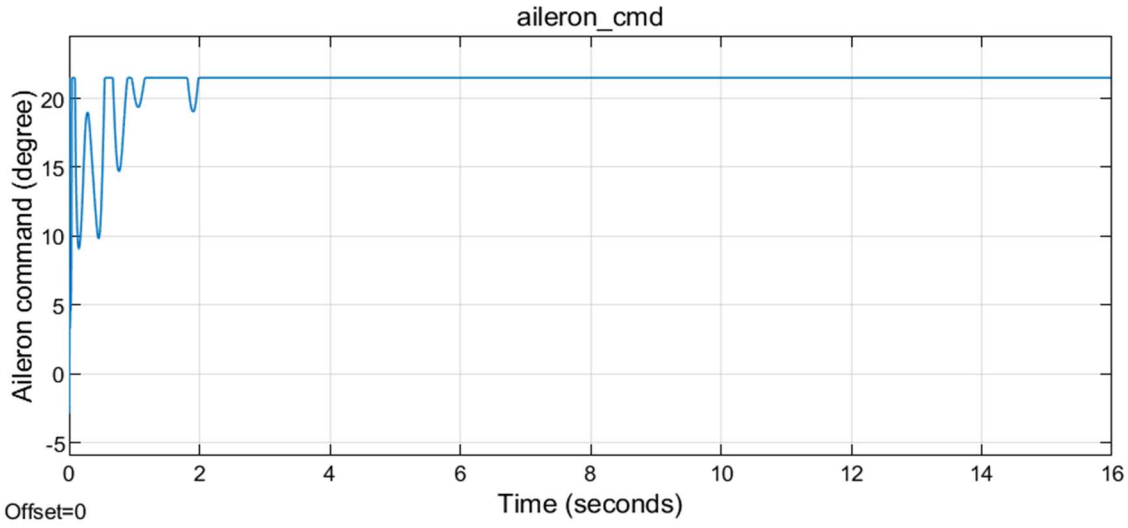

Figure 9.66 Aileron command for the fourth simulation condition with SMC

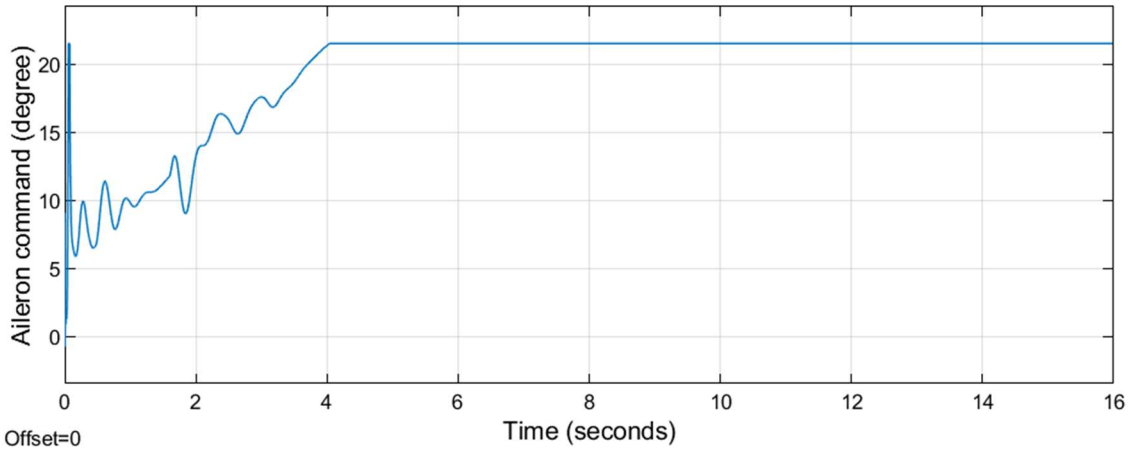

Figure 9.67 Aileron command for the fourth simulation condition with PID

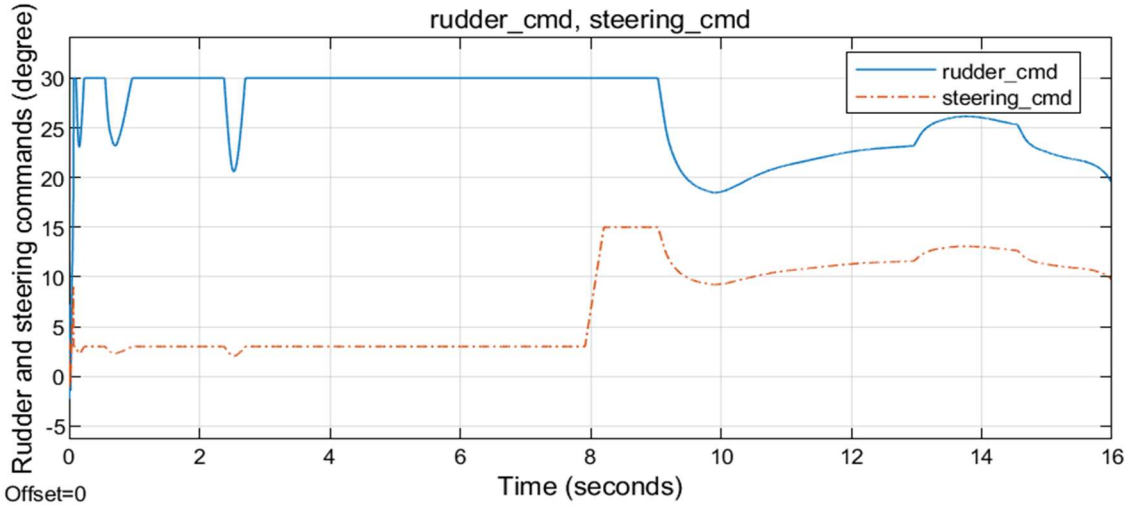

Figure 9.68 Rudder and steering commands for the fourth simulation condition with SMC

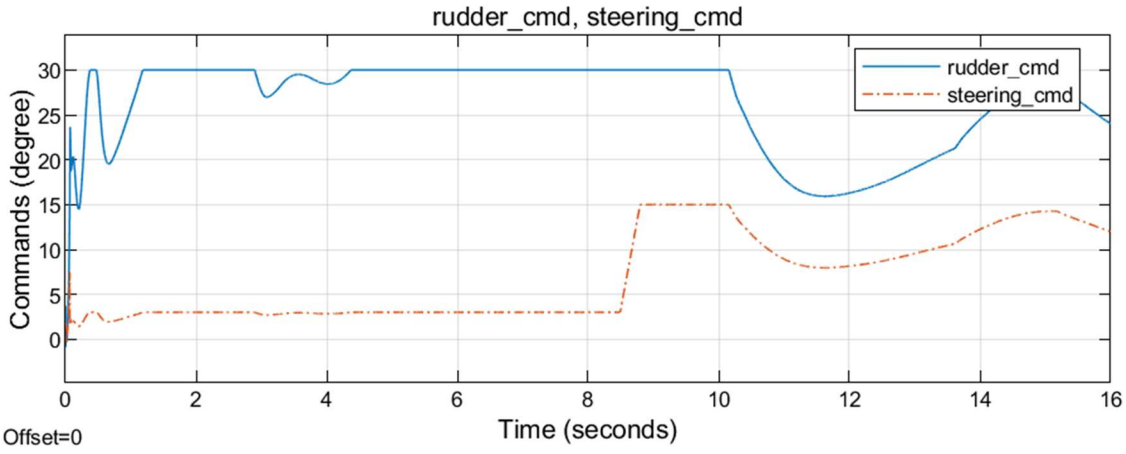

Figure 9.69 Rudder and steering command for the fourth simulation condition with PID

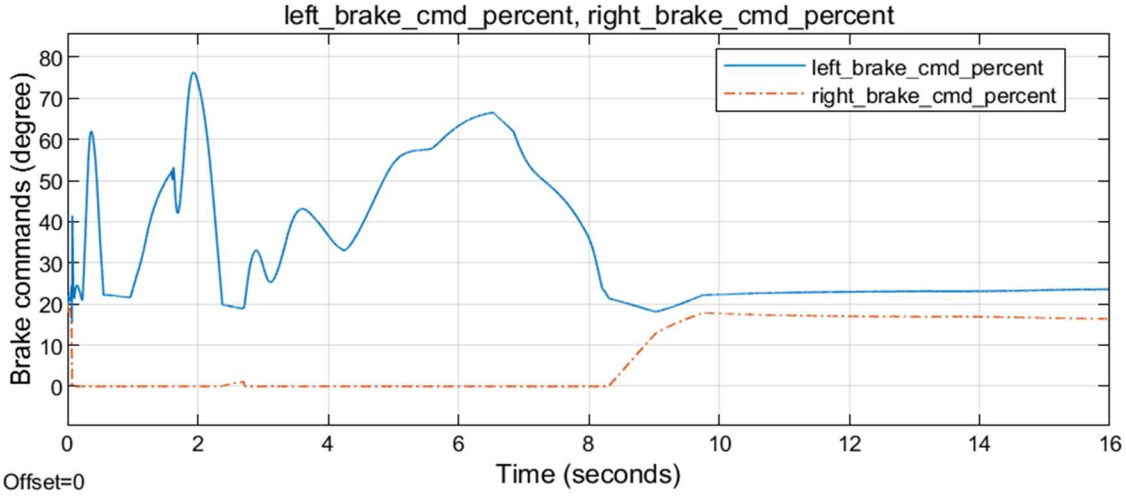

Figure 9.70 Left and right brake commands for the fourth simulation condition with SMC

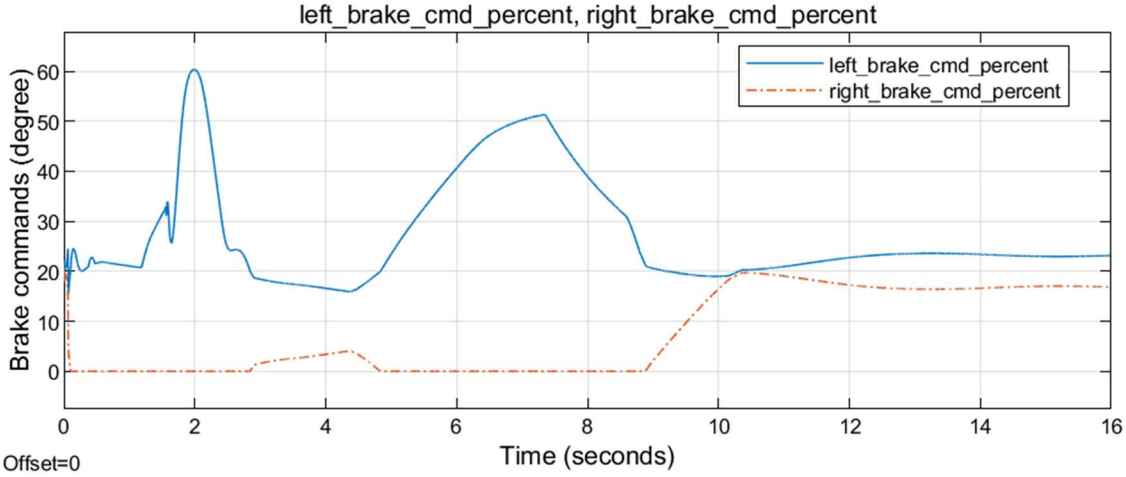

Figure 9.71 Left and right brake commands for the fourth simulation condition with PID

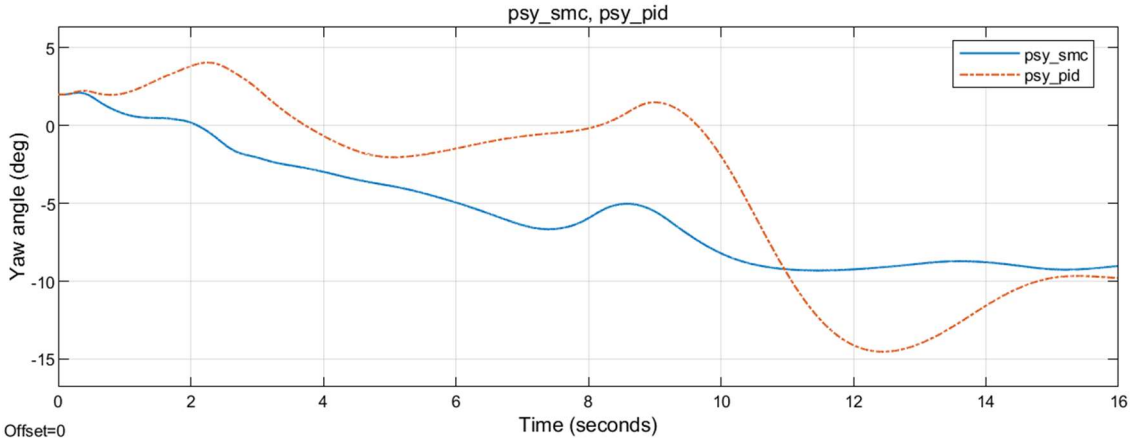

Figure 9.72 Yaw angle for the fourth simulation condition

9.5 LEFT BRAKE STUCK

In the fifth simulation condition, the same lateral position of 2 m and track angle of 2 degrees initial conditions are given. On top of that, there is a left brake stuck malfunction. Results are given in Figures Figure 9.73 to Figure 9.90.

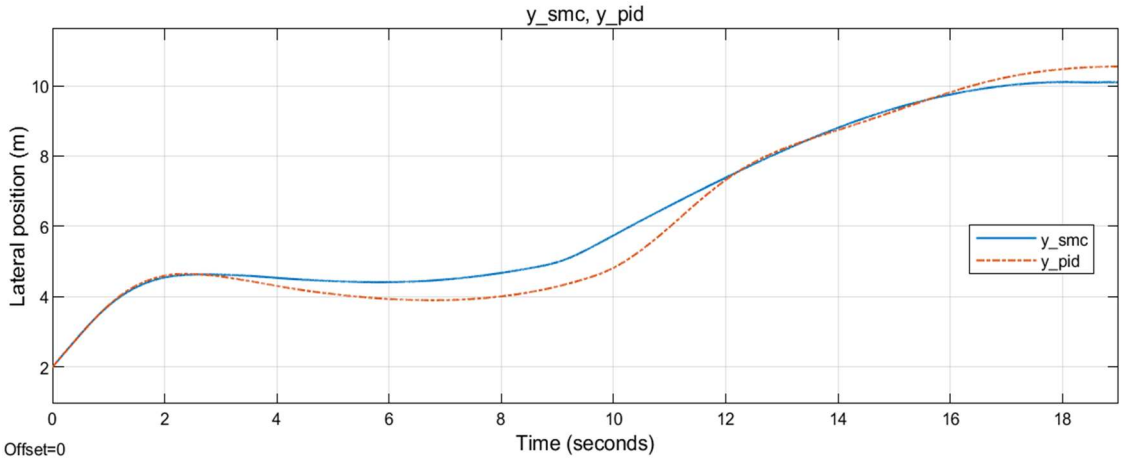

Figure 9.73 Lateral position for the fifth simulation condition

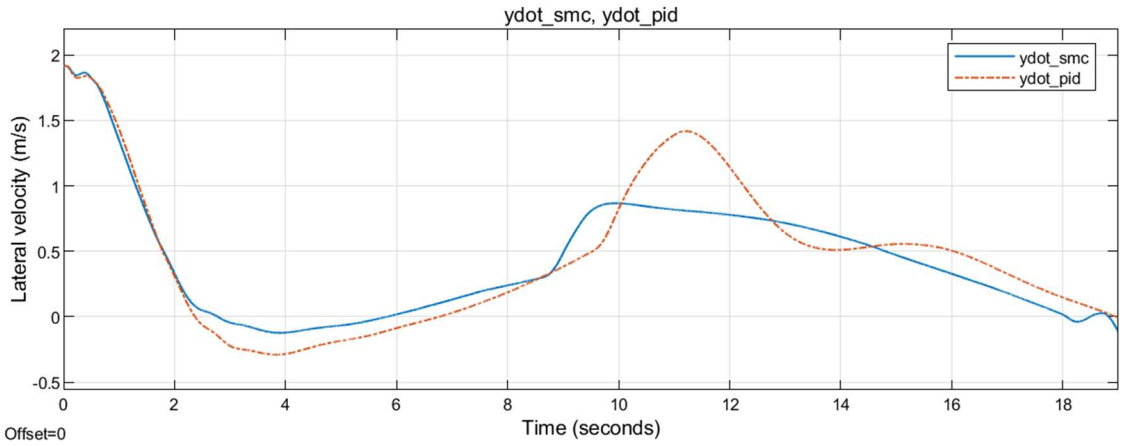

Figure 9.74 Lateral velocity for the fifth simulation condition

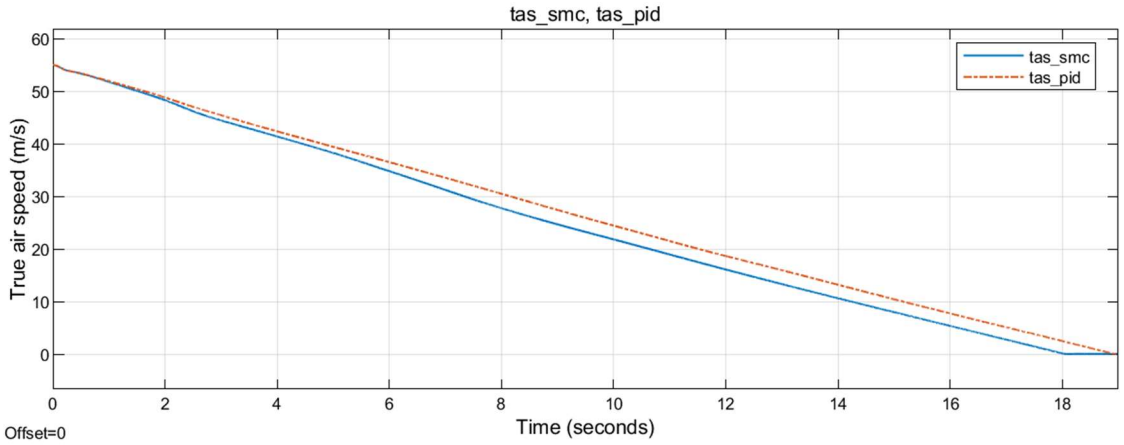

Figure 9.75 True airspeed for the fifth simulation condition

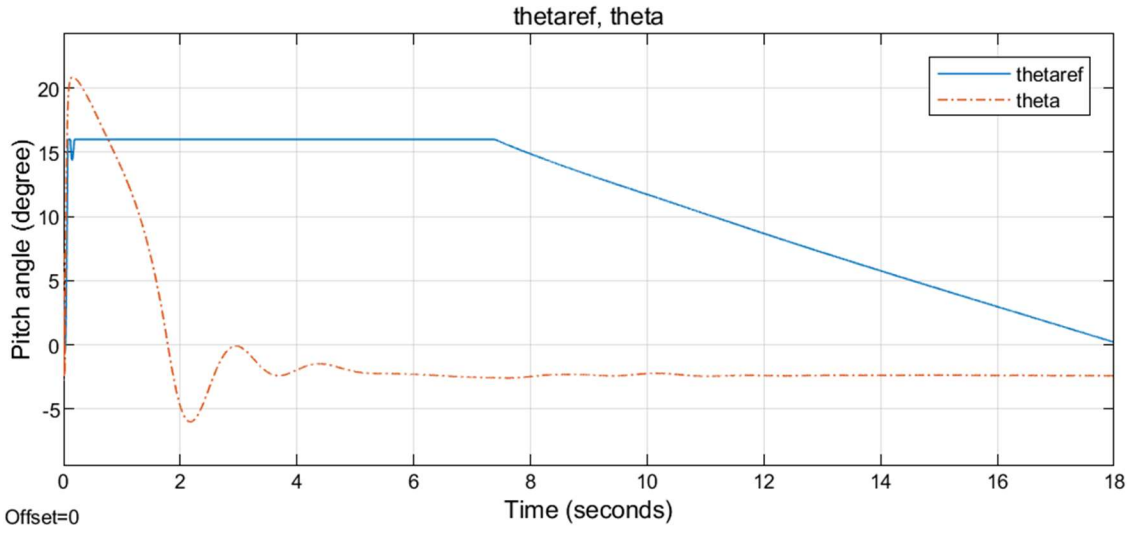

Figure 9.76 Pitch angle for the fifth simulation condition with SMC

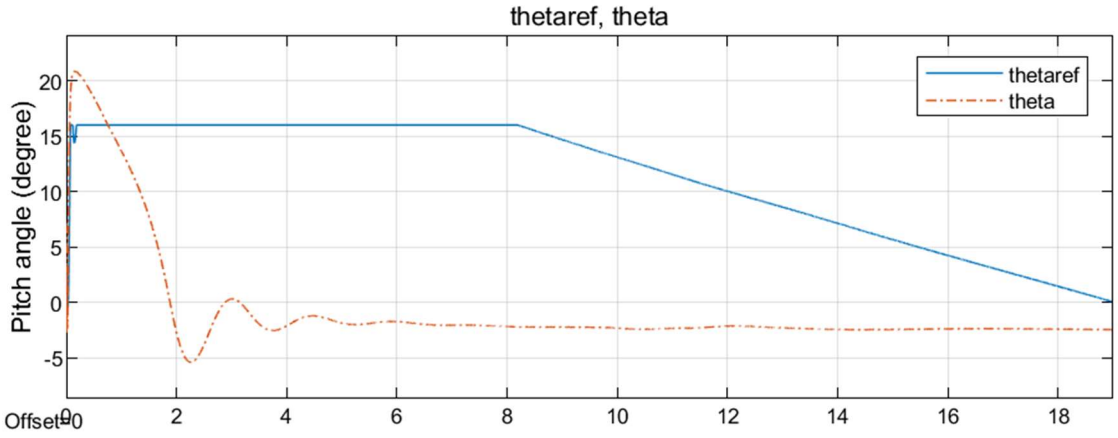

Figure 9.77 Pitch angle for the fifth simulation condition with PID

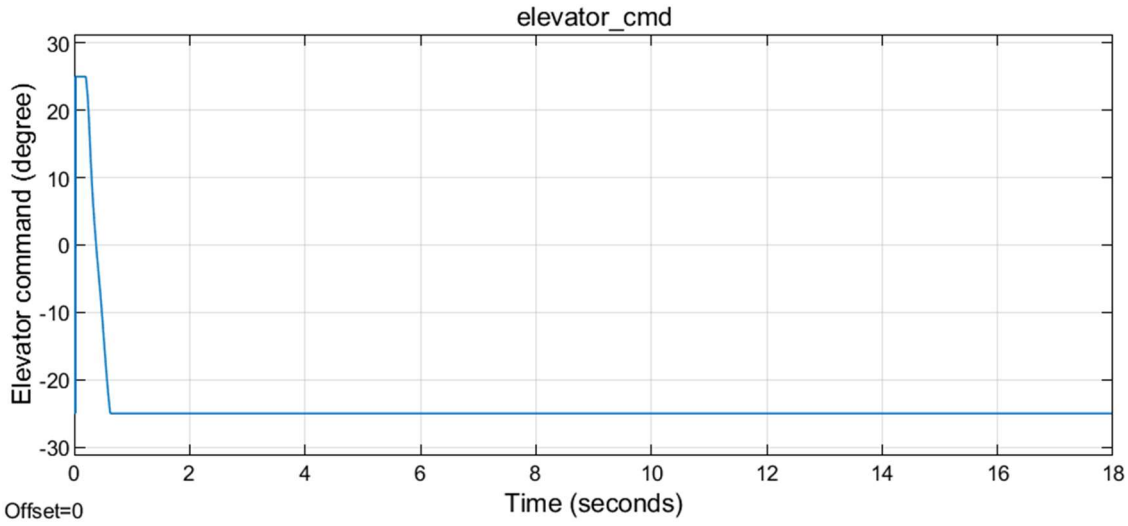

Figure 9.78 Elevator command for the fifth simulation condition with SMC

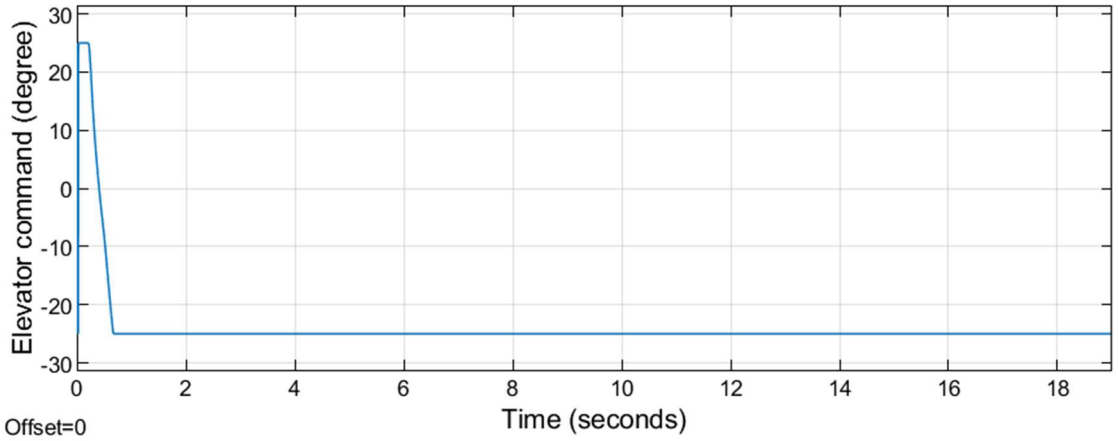

Figure 9.79 Elevator command for the fifth simulation condition with PID

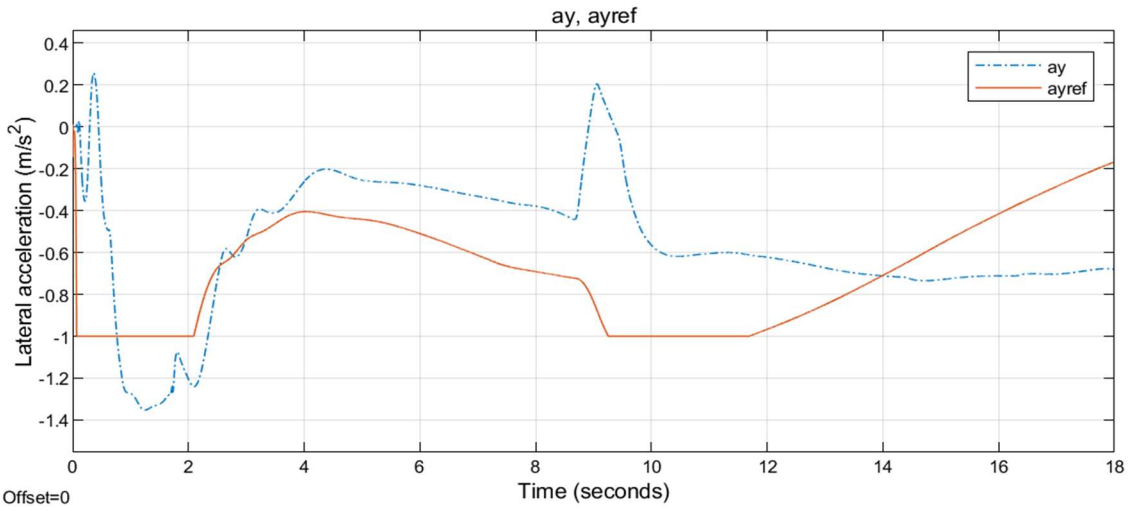

Figure 9.80 Lateral acceleration for the fifth simulation condition with SMC

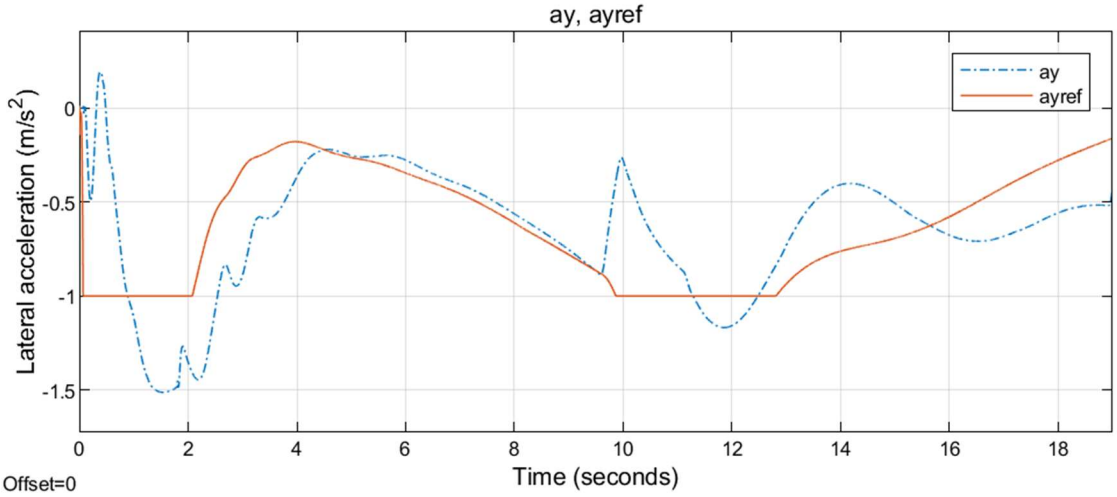

Figure 9.81 Lateral acceleration for the fifth simulation condition with PID

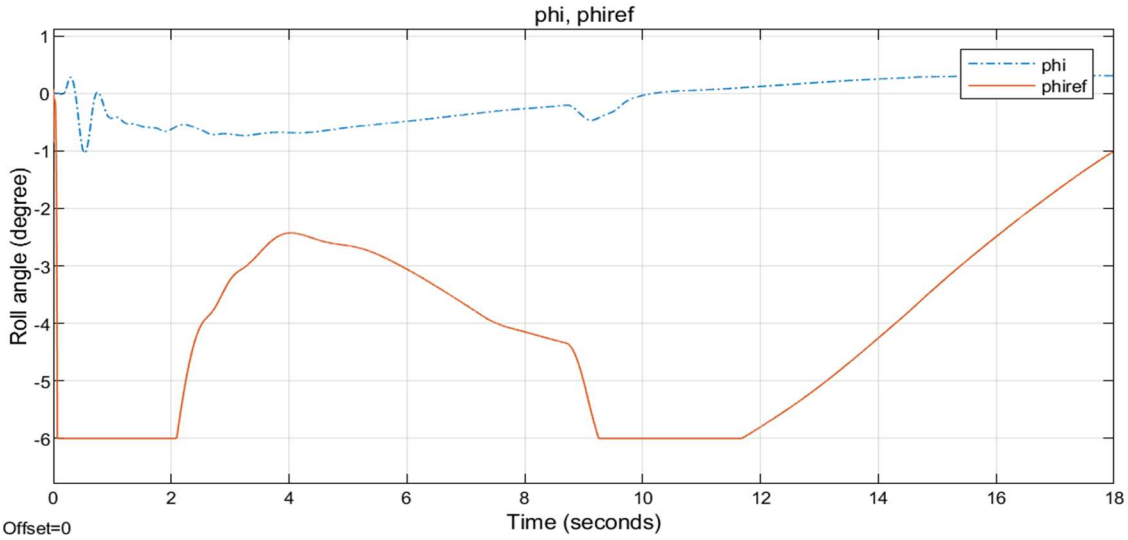

Figure 9.82 Roll angle for the fifth simulation condition with SMC

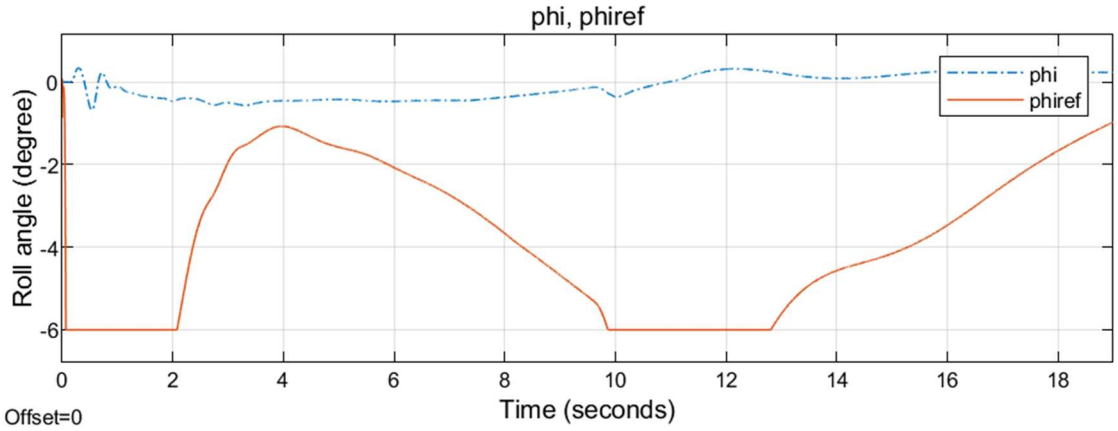

Figure 9.83 Roll angle for the fifth simulation condition with PID

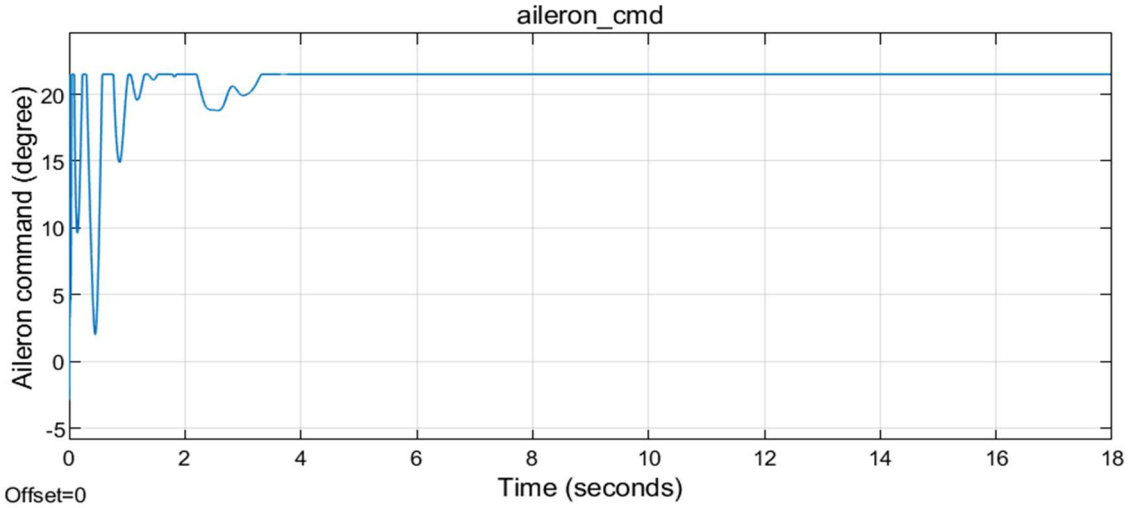

Figure 9.84 Aileron command for the fifth simulation condition with SMC

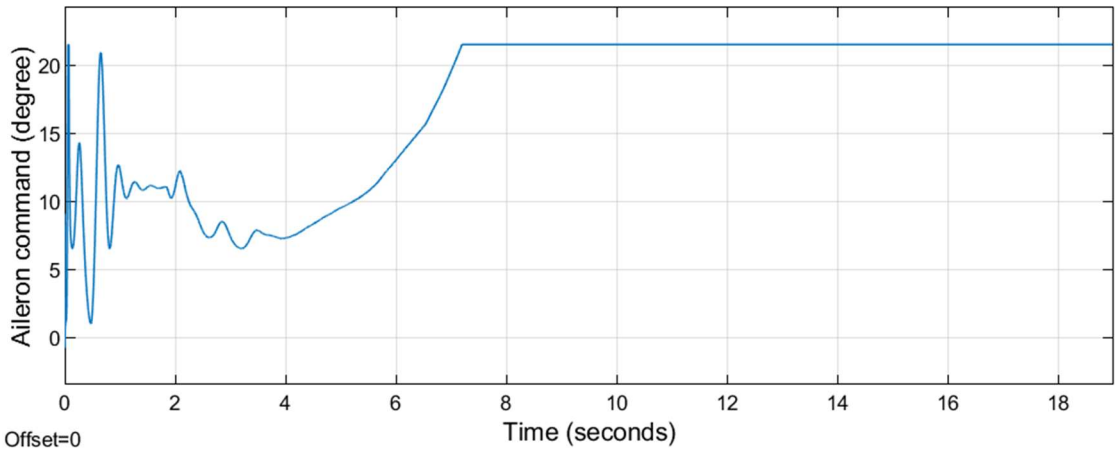

Figure 9.85 Aileron command for the fifth simulation condition with PID

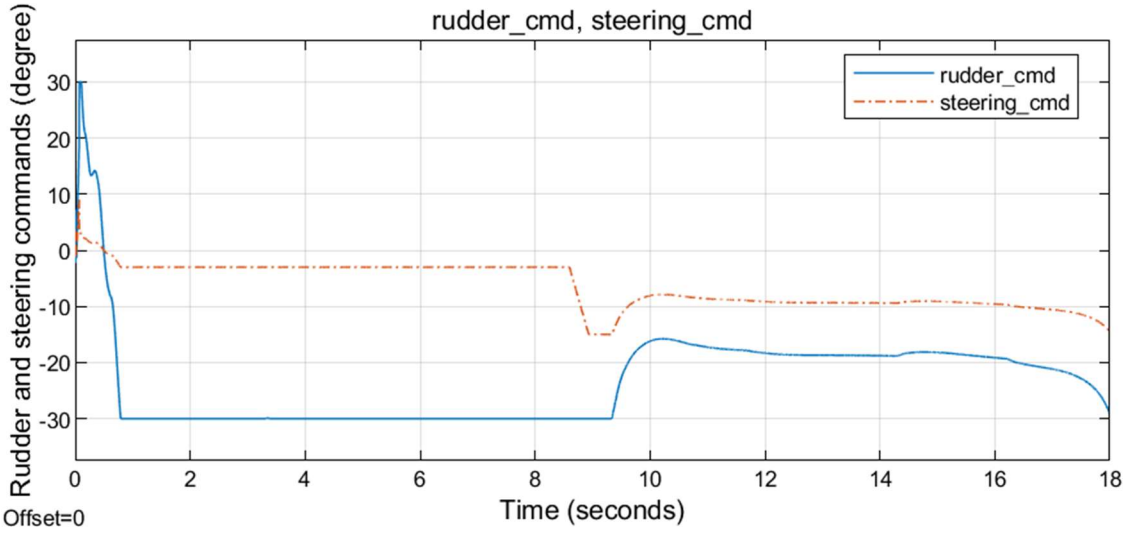

Figure 9.86 Rudder and steering commands for the fifth simulation condition with SMC

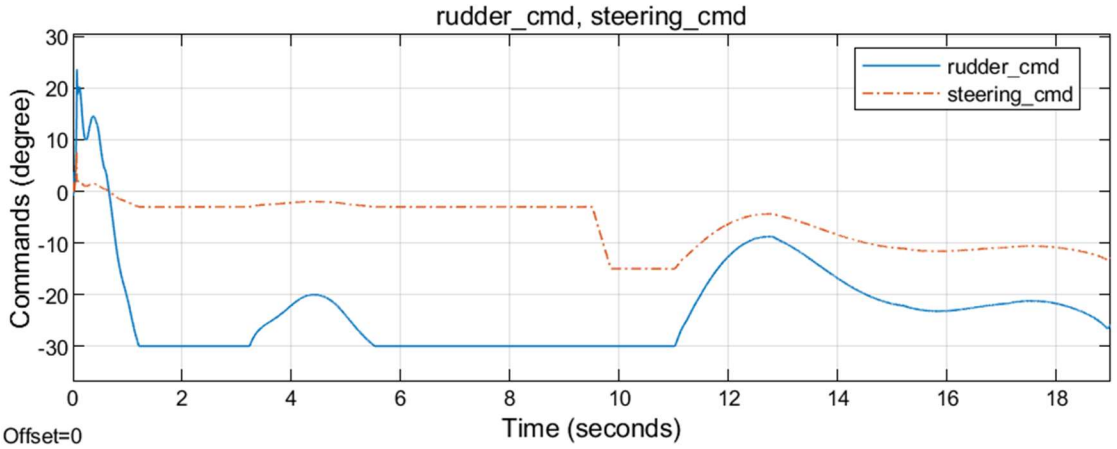

Figure 9.87 Rudder and steering command for the fifth simulation condition with PID

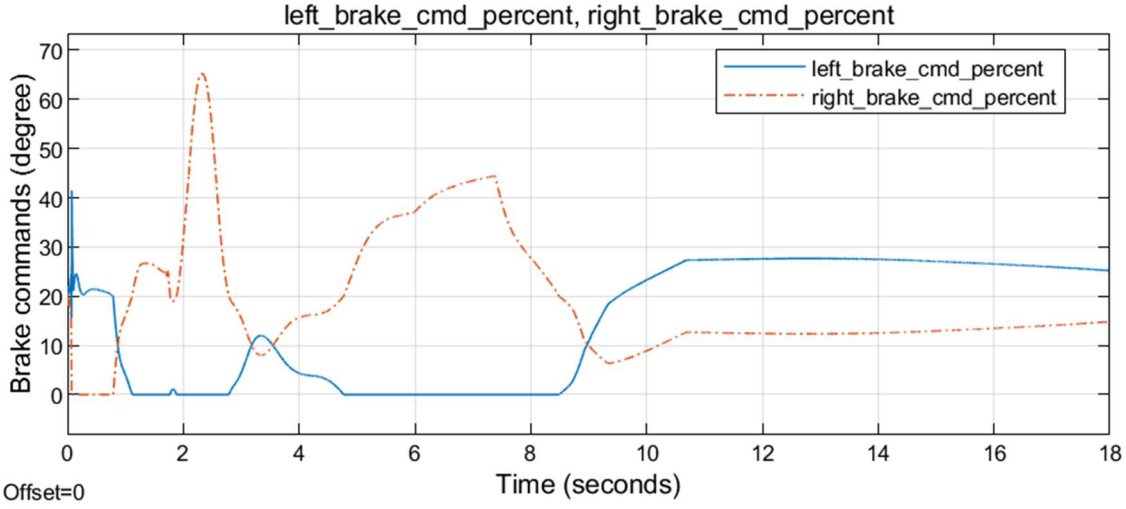

Figure 9.88 Left and right brake commands for the fifth simulation condition with SMC

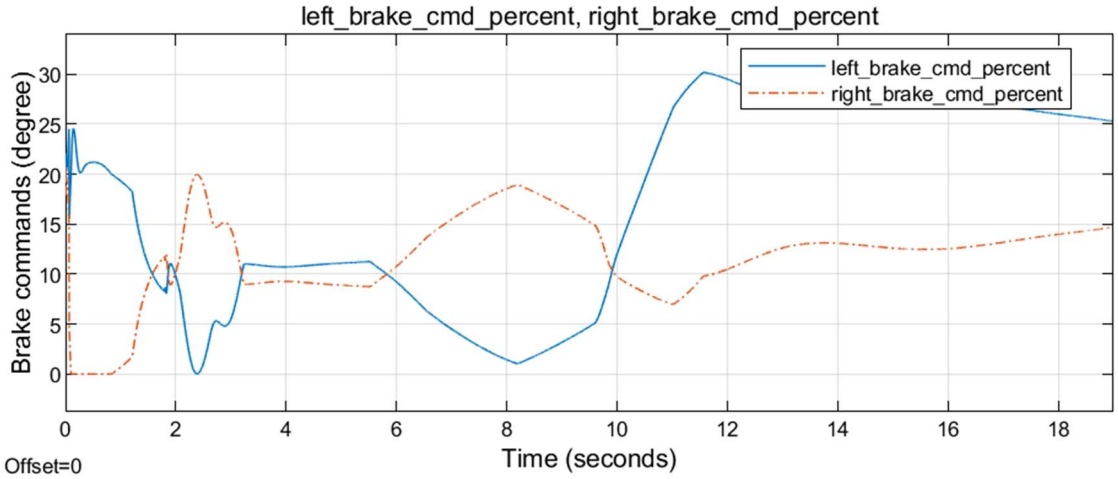

Figure 9.89 Left and right brake commands for the fifth simulation condition with PID

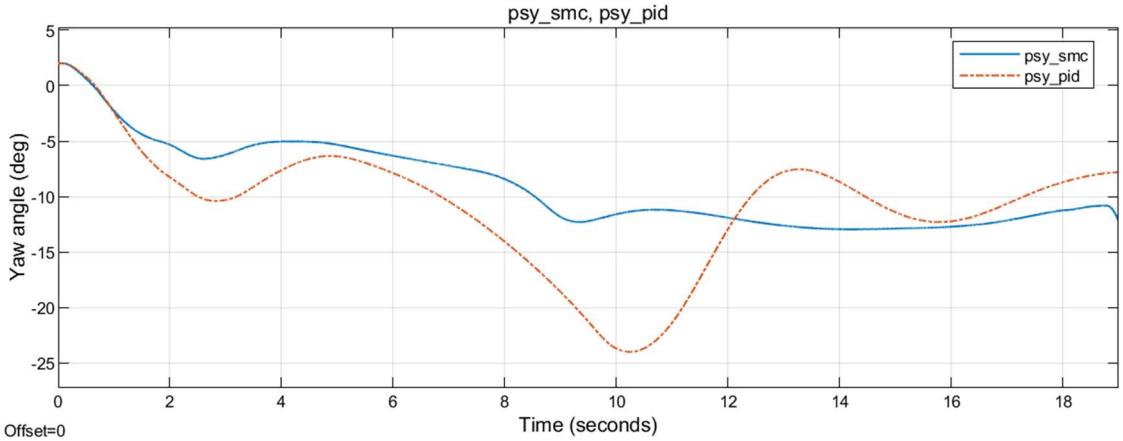

Figure 9.90 Yaw angle for the fifth simulation condition with SMC

9.6 RIGHT BRAKE NOT WORKING

In the sixth simulation condition, the same lateral position of 2 m and track angle of 2 degrees initial conditions are given. On top of that, there is a right brake not working malfunction. Results are given in Figures Figure 9.91 to Figure 9.108.

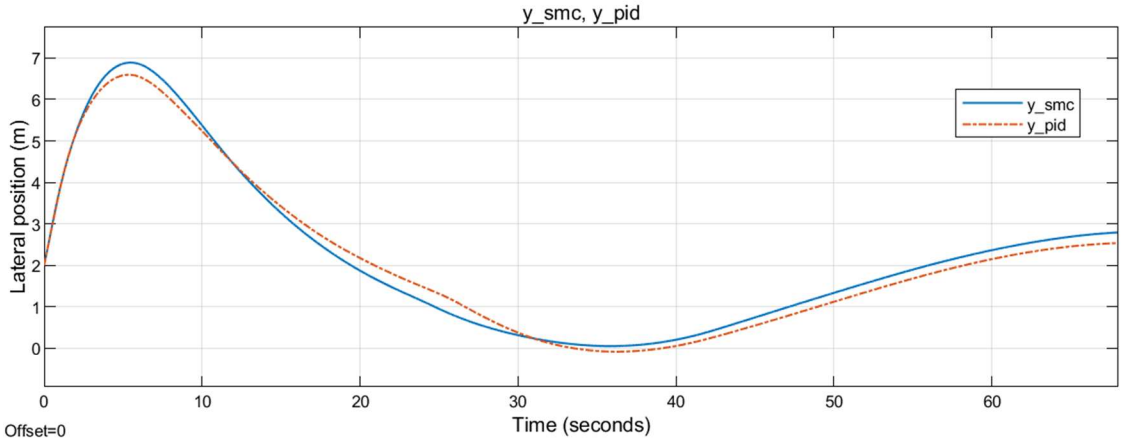

Figure 9.91 Lateral position for the sixth simulation condition

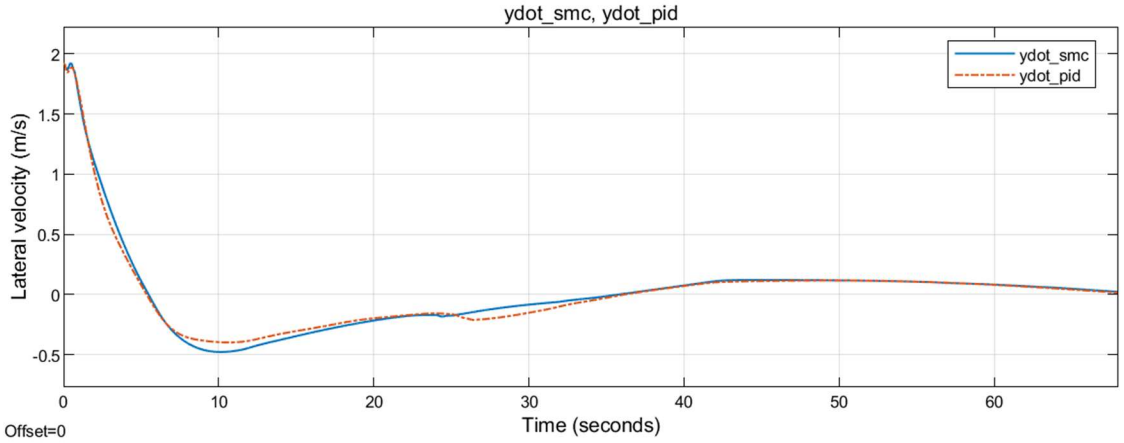

Figure 9.92 Lateral velocity with respect to runway midline for the sixth simulation condition

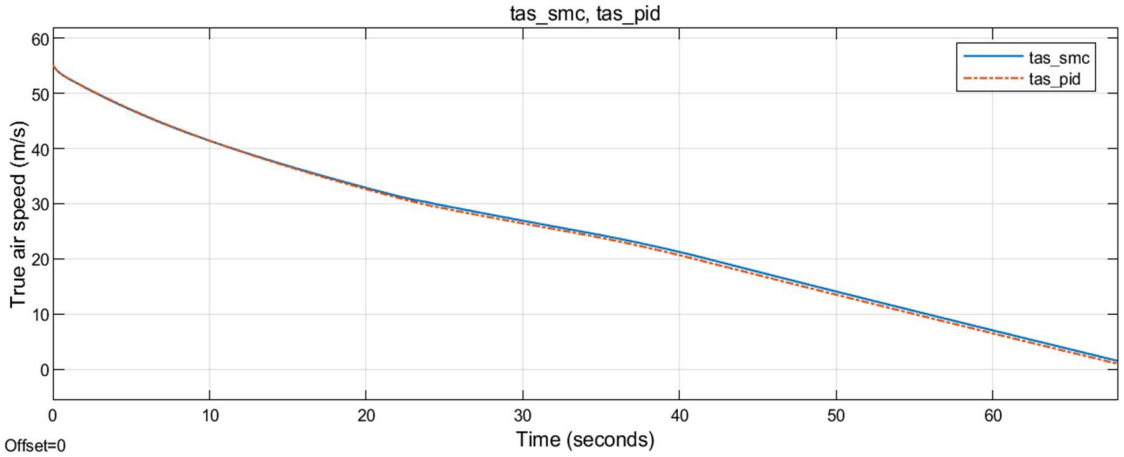

Figure 9.93 True airspeed for the sixth simulation condition

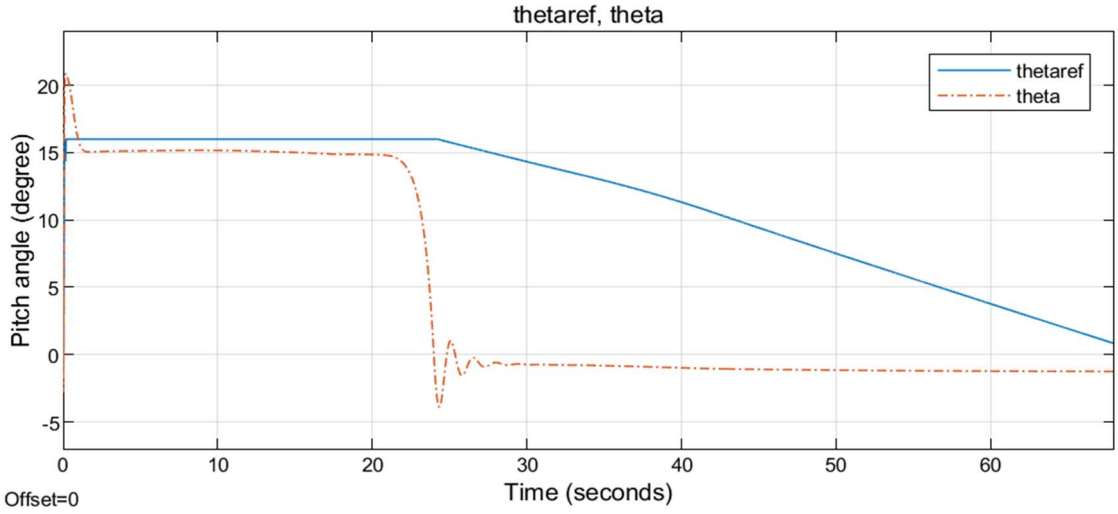

Figure 9.94 Pitch angle for the sixth simulation condition with SMC

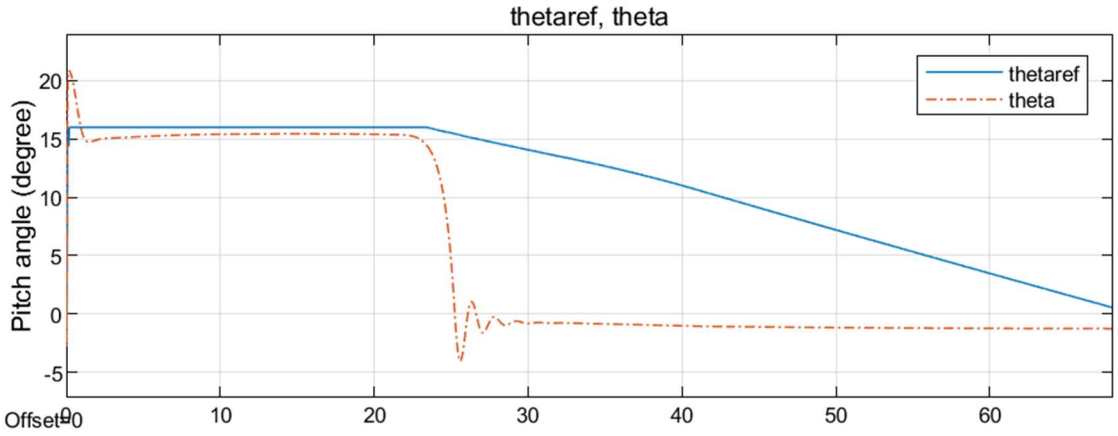

Figure 9.95 Pitch angle for the sixth simulation condition with PID

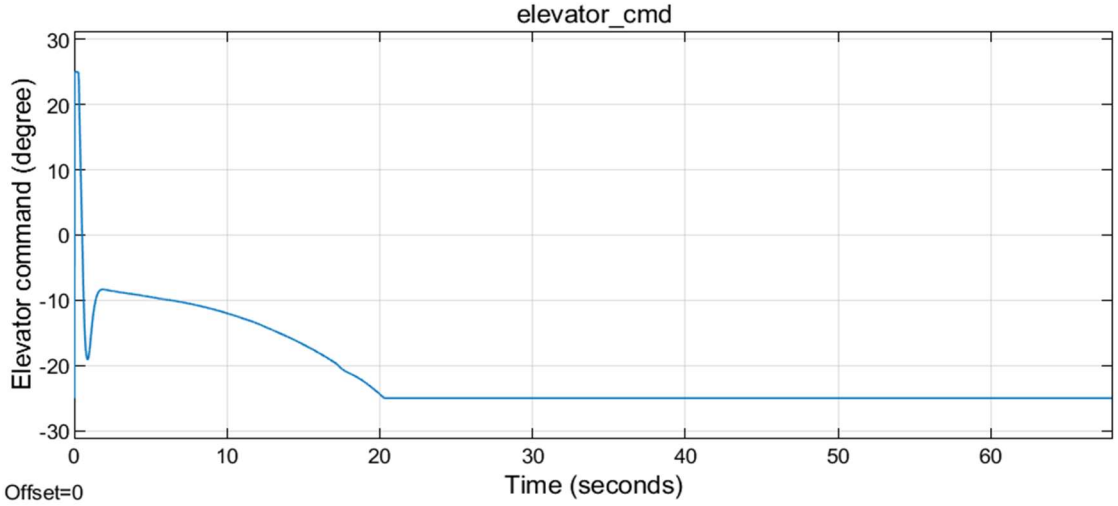

Figure 9.96 Elevator command for the sixth simulation condition with SMC

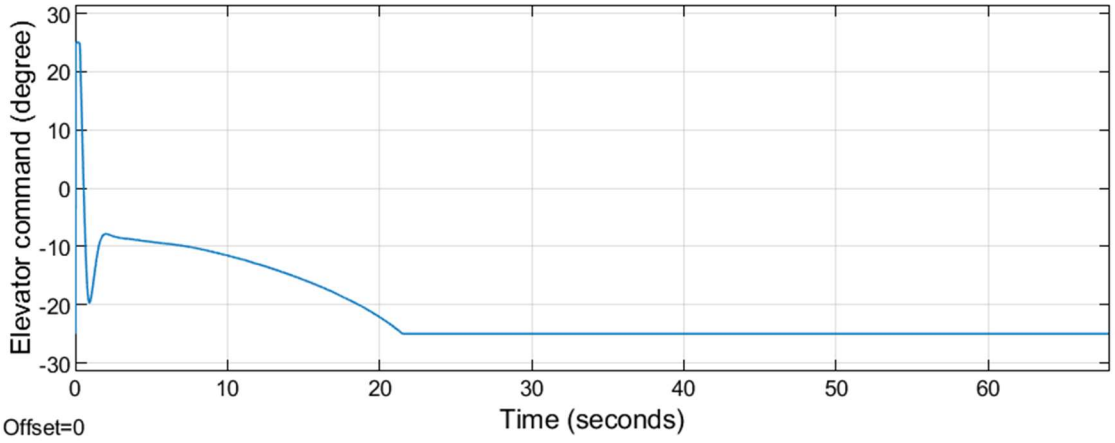

Figure 9.97 Elevator command for the sixth simulation condition with PID

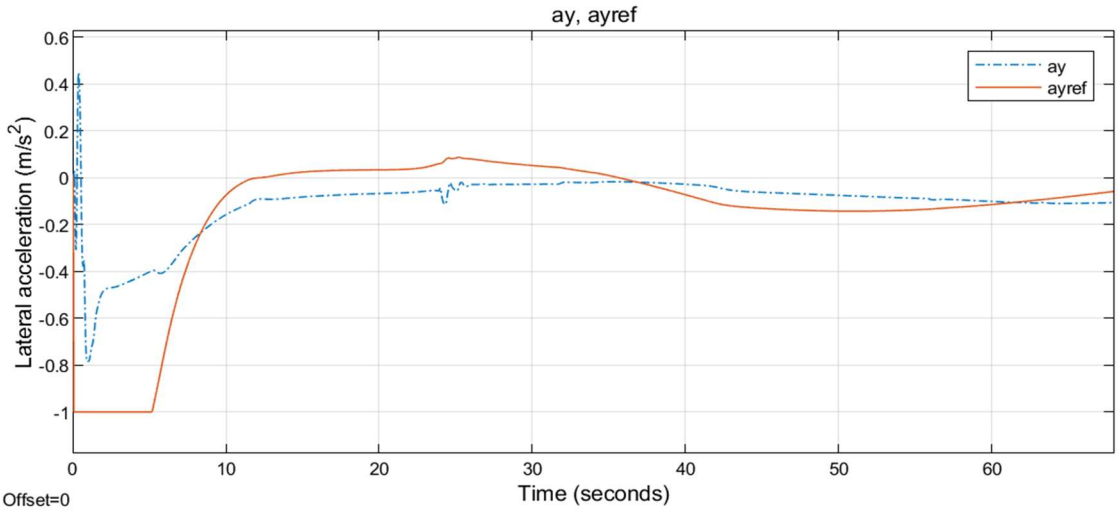

Figure 9.98 Lateral acceleration for the sixth simulation condition with SMC

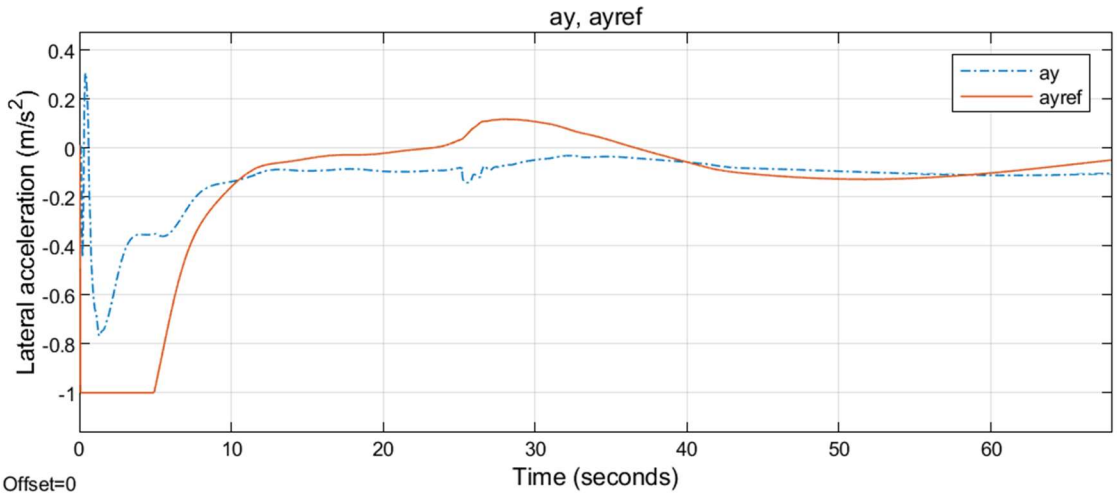

Figure 9.99 Lateral acceleration for the sixth simulation condition with PID

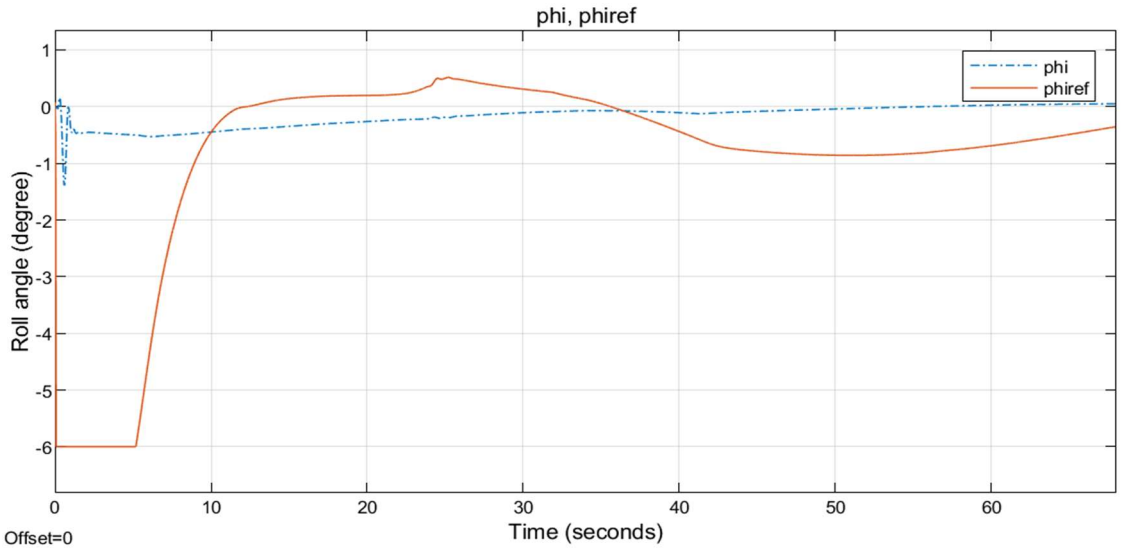

Figure 9.100 Roll angle for the sixth simulation condition with SMC

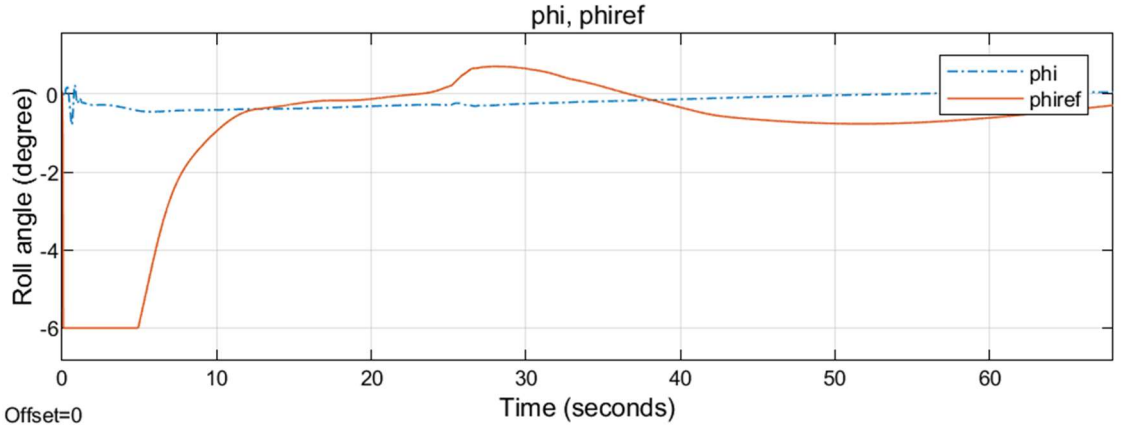

Figure 9.101 Roll angle for the sixth simulation condition with PID

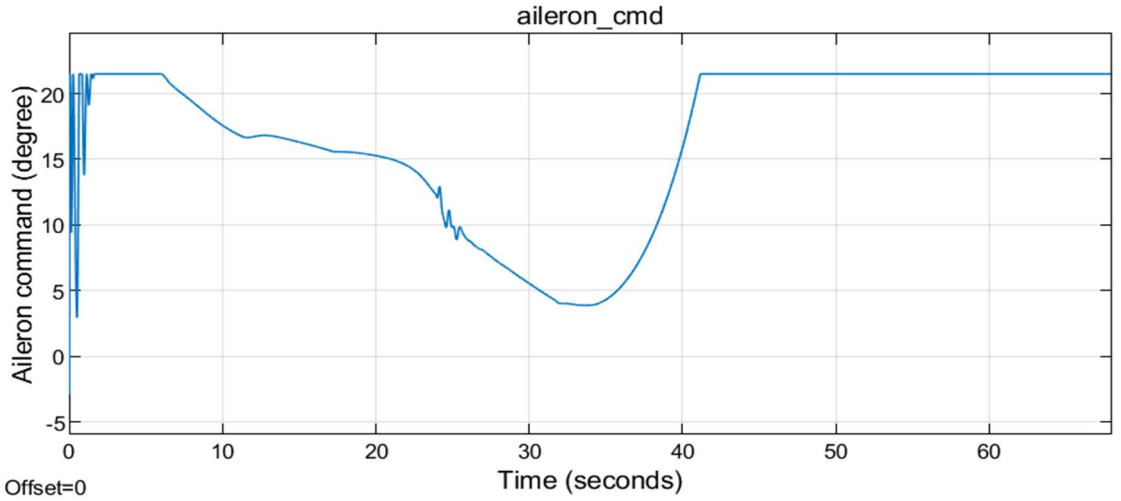

Figure 9.102 Aileron command for the sixth simulation condition with SMC

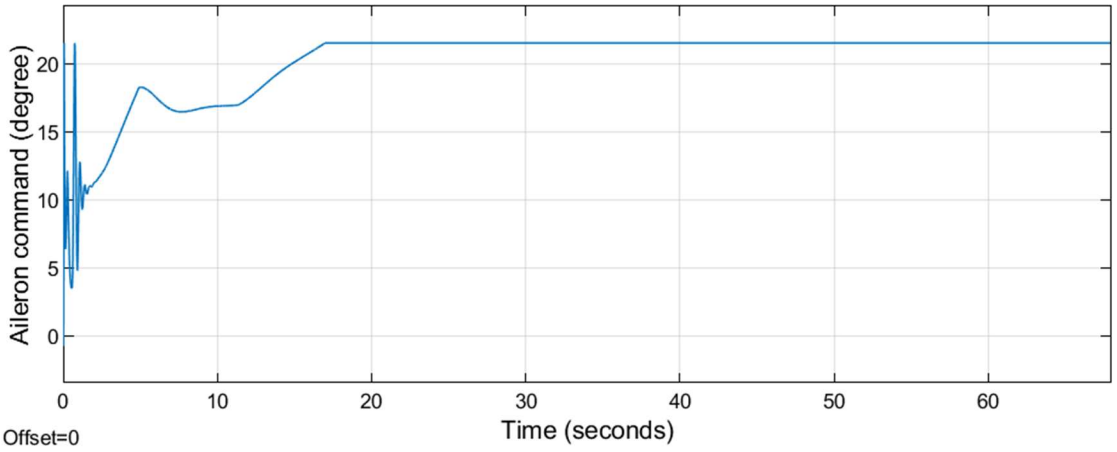

Figure 9.103 Aileron command for the sixth simulation condition with PID

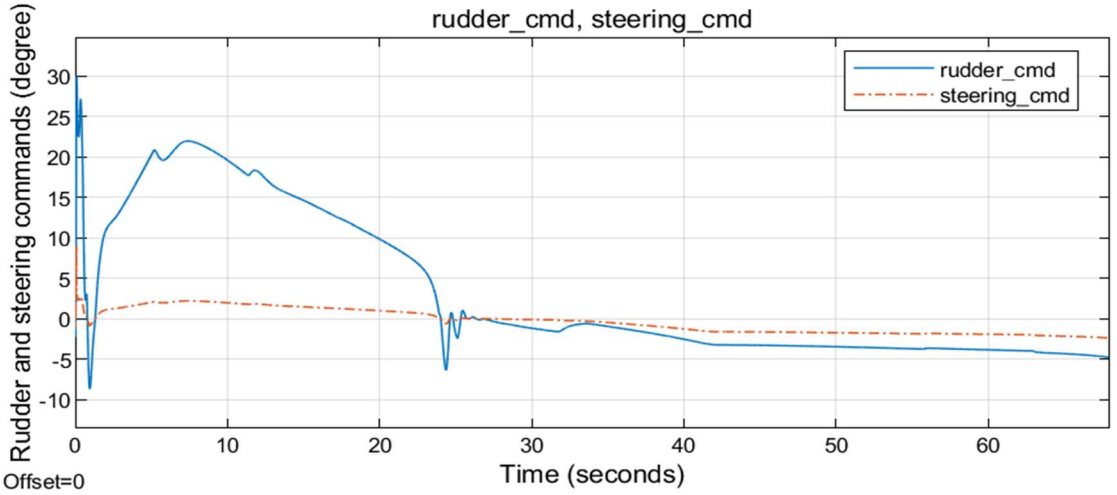

Figure 9.104 Rudder and steering commands for the simulation condition with SMC

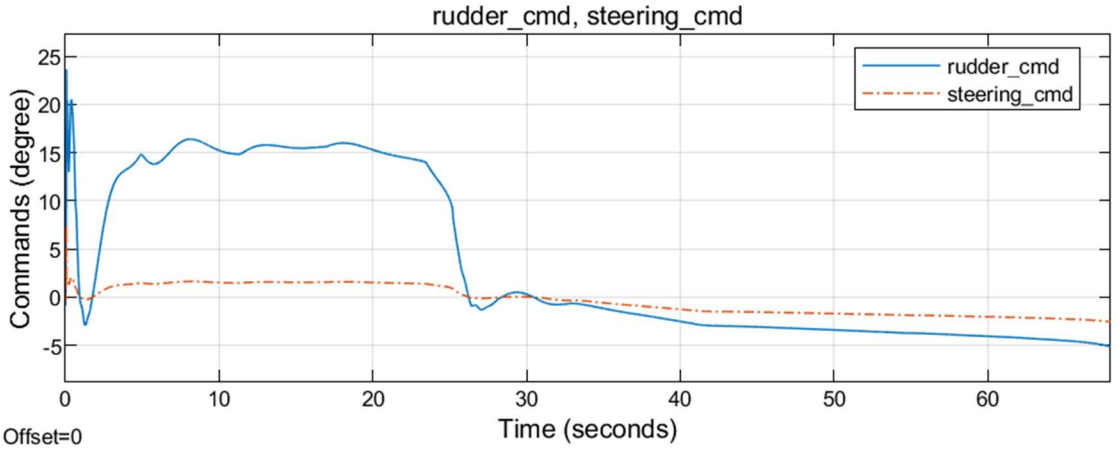

Figure 9.105 Rudder and steering commands for the sixth simulation condition with PID

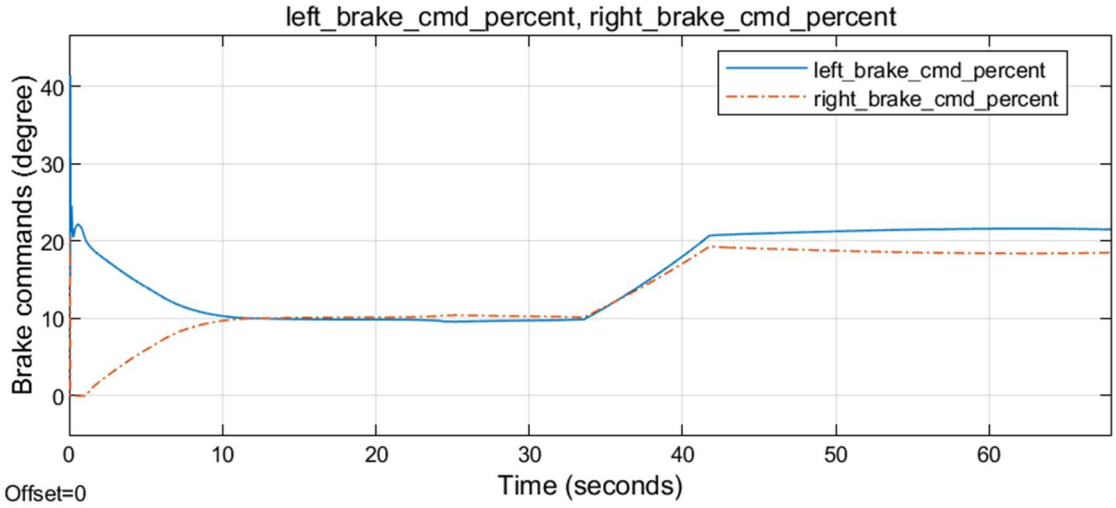

Figure 9.106 Left and right brake commands for the sixth simulation condition with SMC

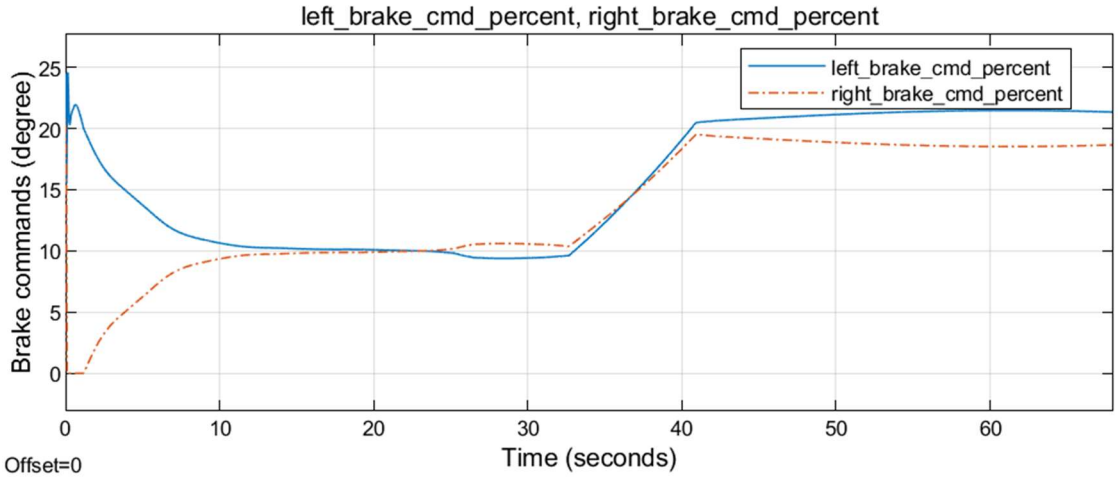

Figure 9.107 Left and right brake commands for the sixth simulation condition with PID

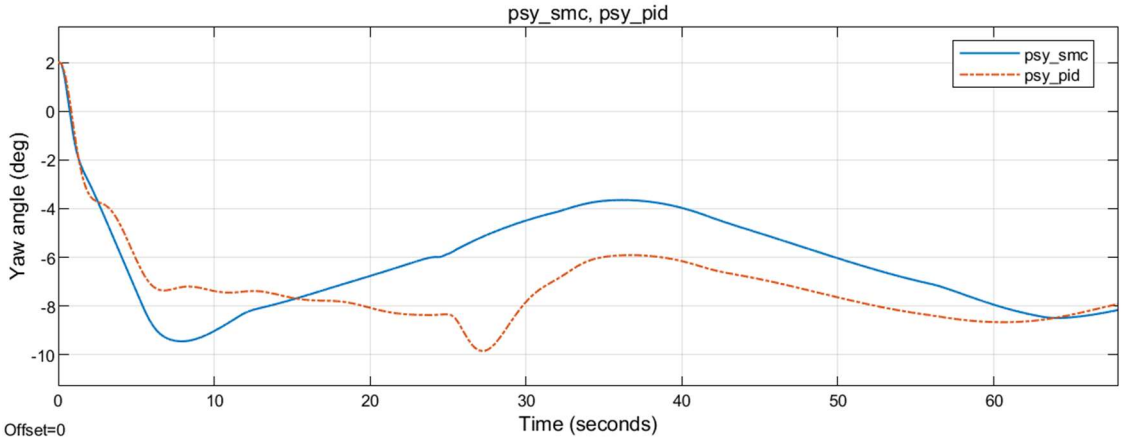

Figure 9.108 Yaw angle for the sixth simulation condition

9.7 LEFT BRAKE NOT WORKING

In the seventh simulation condition, the same lateral position of 2 m and track angle of 2 degrees initial conditions are given. On top of that, there is a left brake not working malfunction. Results are given in Figures Figure 9.109 to Figure 9.126.

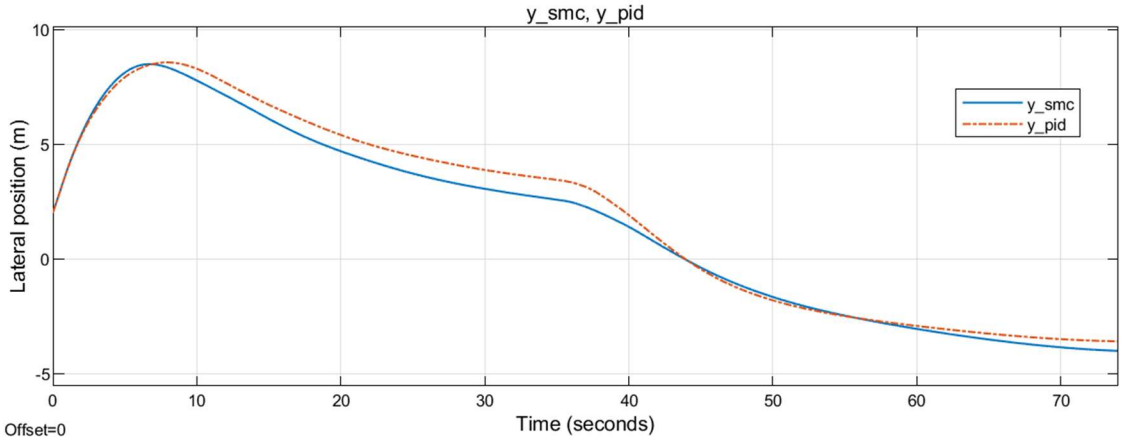

Figure 9.109 Lateral position for the seventh simulation condition

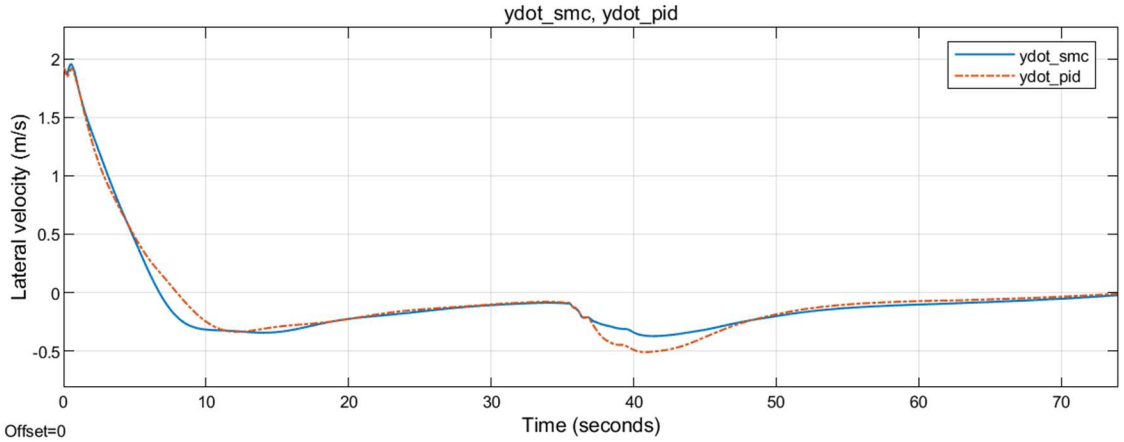

Figure 9.110 Lateral velocity with respect to runway midline for the seventh simulation condition

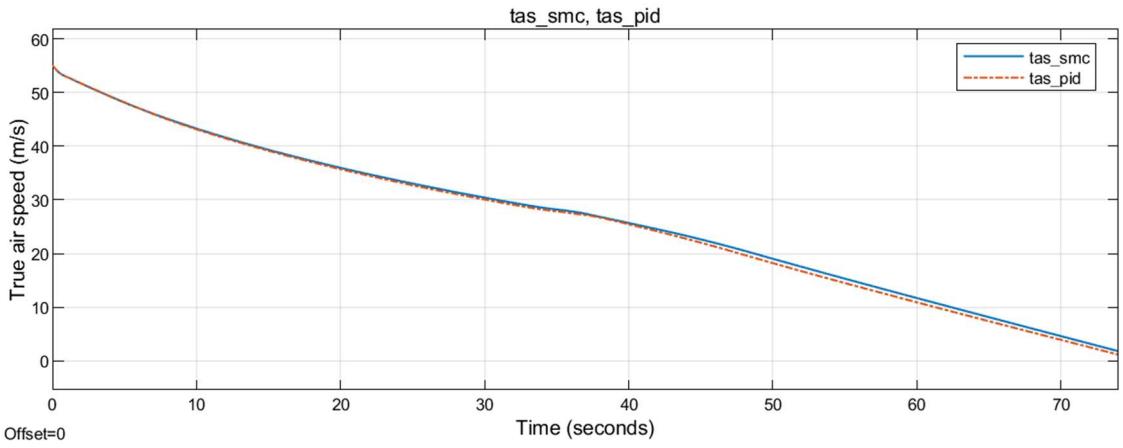

Figure 9.111 True airspeed for the seventh simulation condition

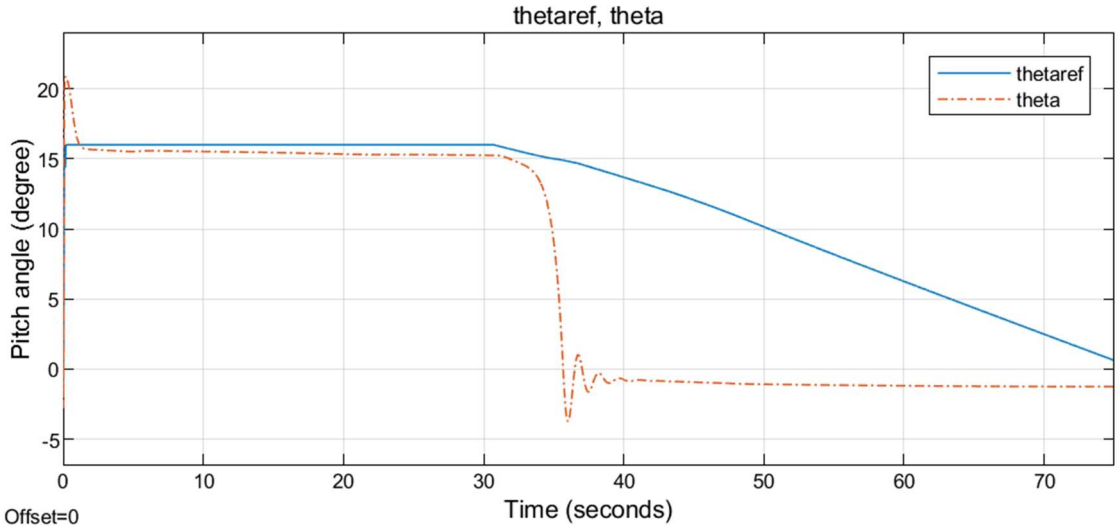

Figure 9.112 Pitch angle for the seventh simulation condition with SMC

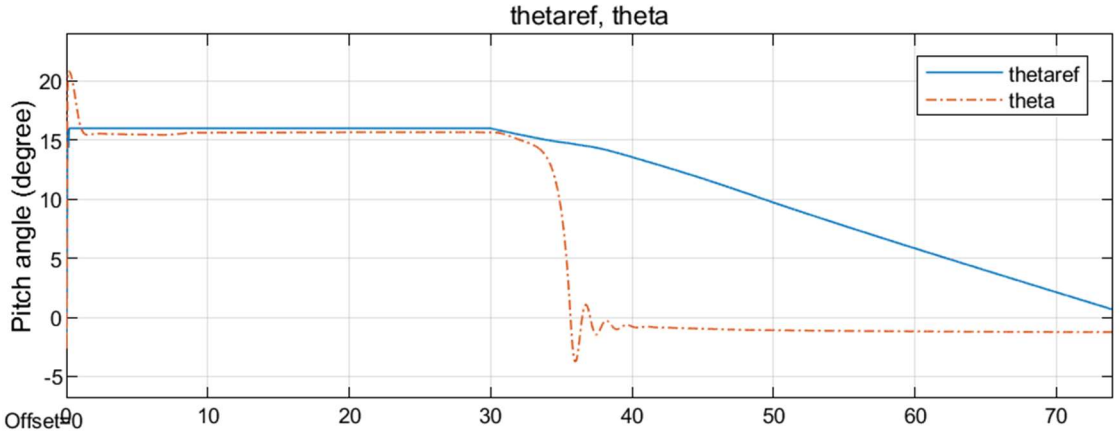

Figure 9.113 Pitch angle for the seventh simulation condition with PID

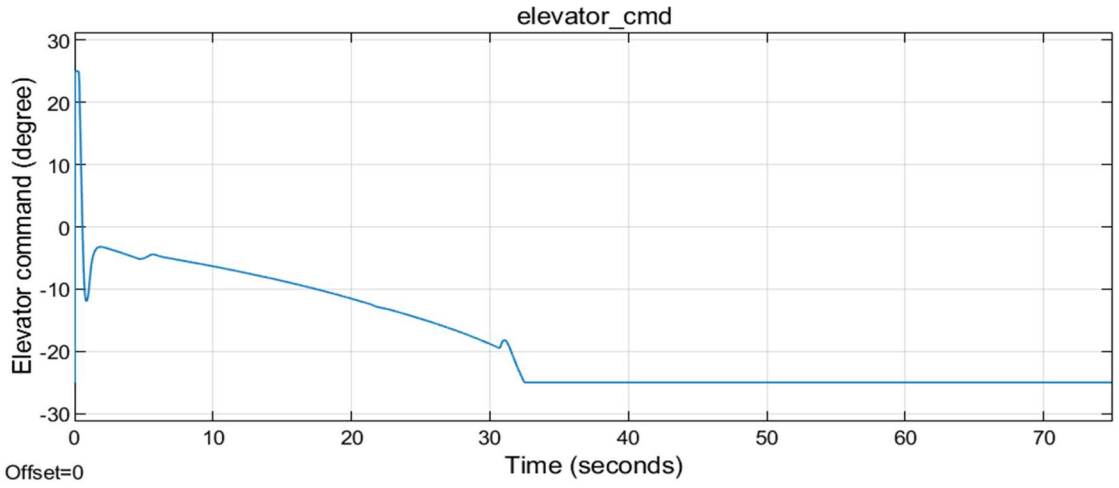

Figure 9.114 Elevator command for the seventh simulation condition with SMC

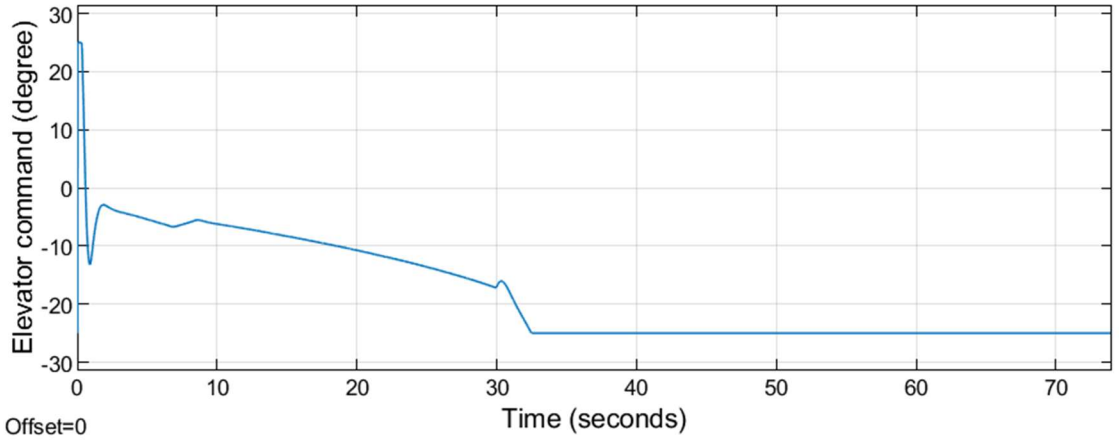

Figure 9.115 Elevator command for the seventh simulation condition with PID

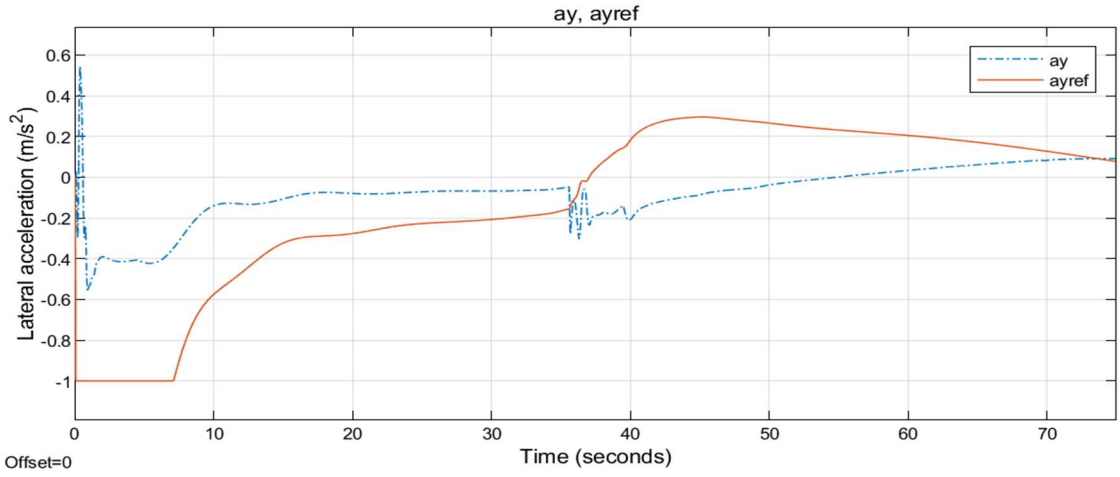

Figure 9.116 Lateral acceleration for the seventh simulation condition with SMC

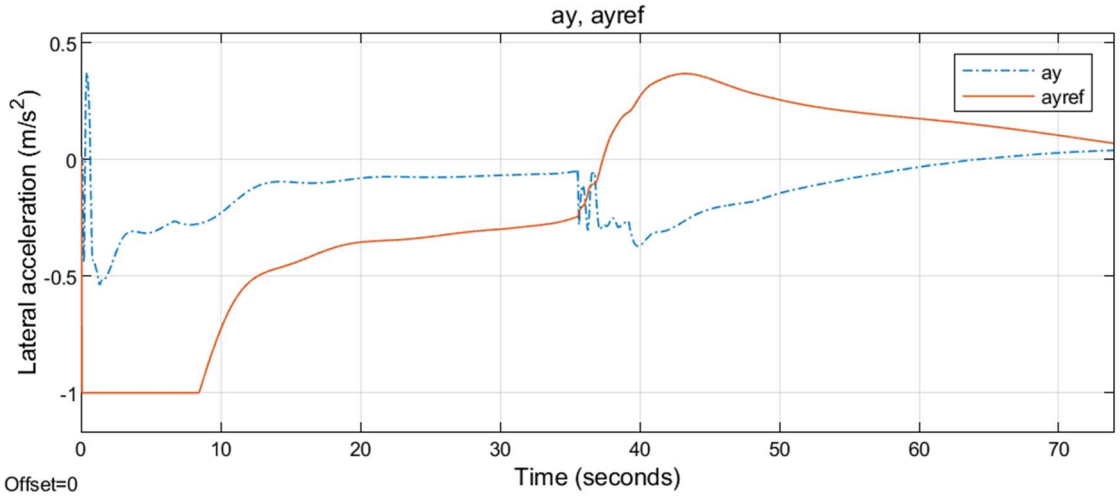

Figure 9.117 Lateral acceleration for the seventh simulation condition with PID

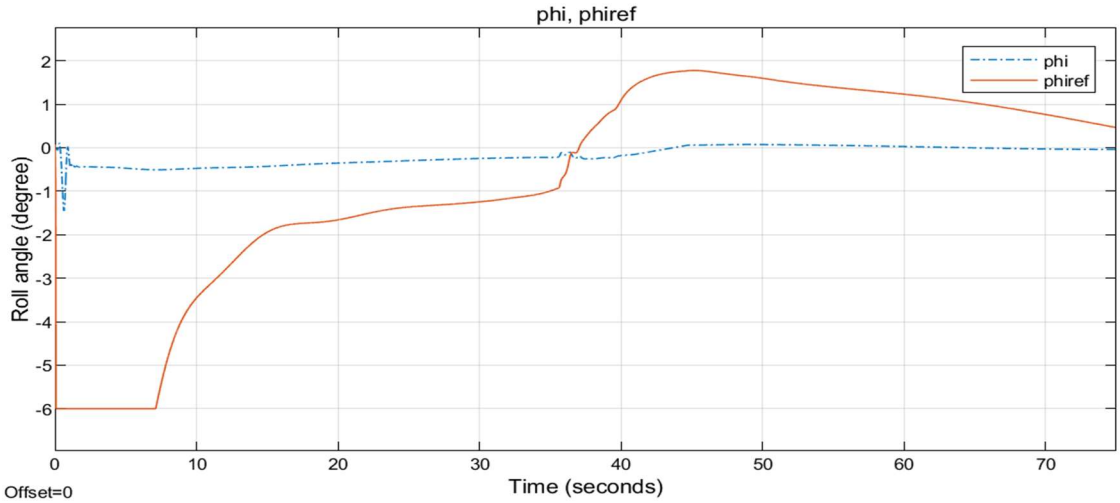

Figure 9.118 Roll angle for the seventh simulation condition with SMC

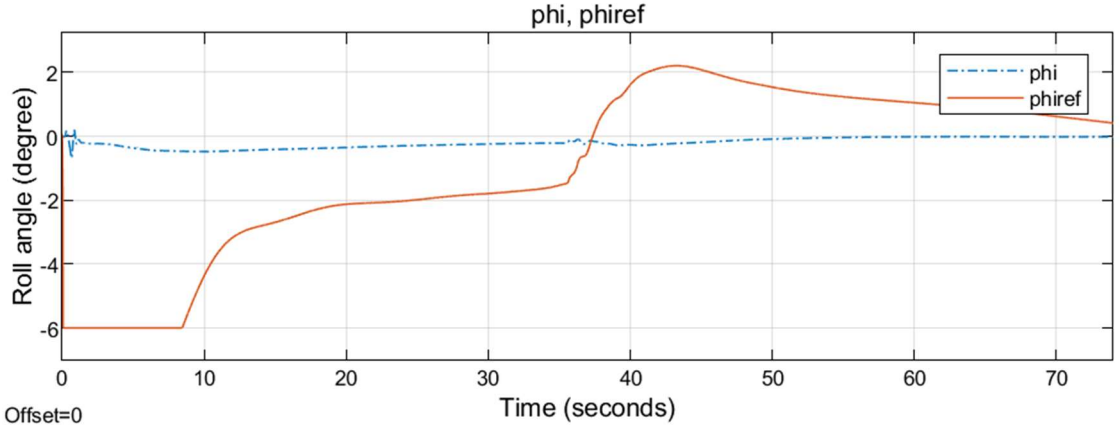

Figure 9.119 Roll angle for the seventh simulation condition with PID

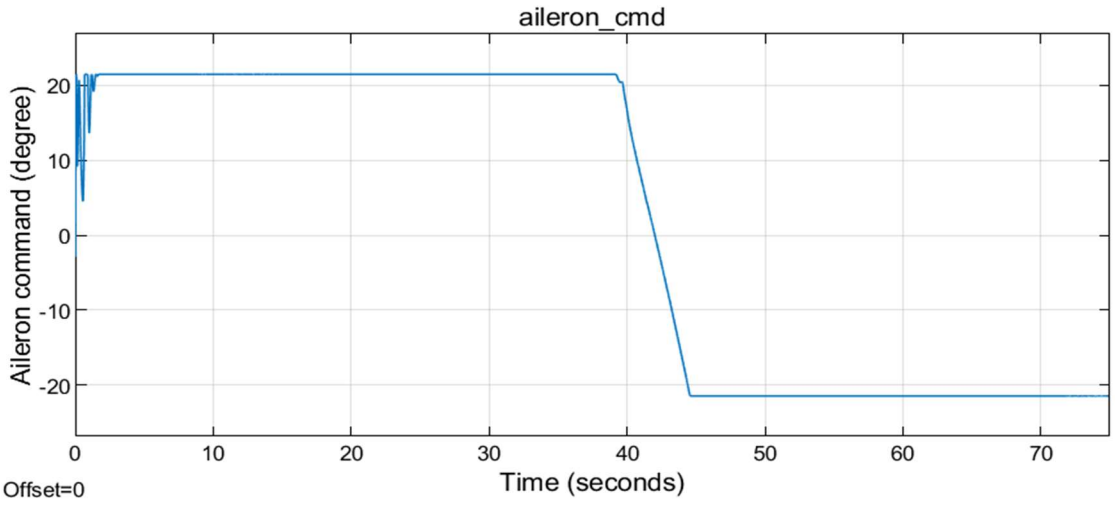

Figure 9.120 Aileron command for the seventh simulation condition with SMC

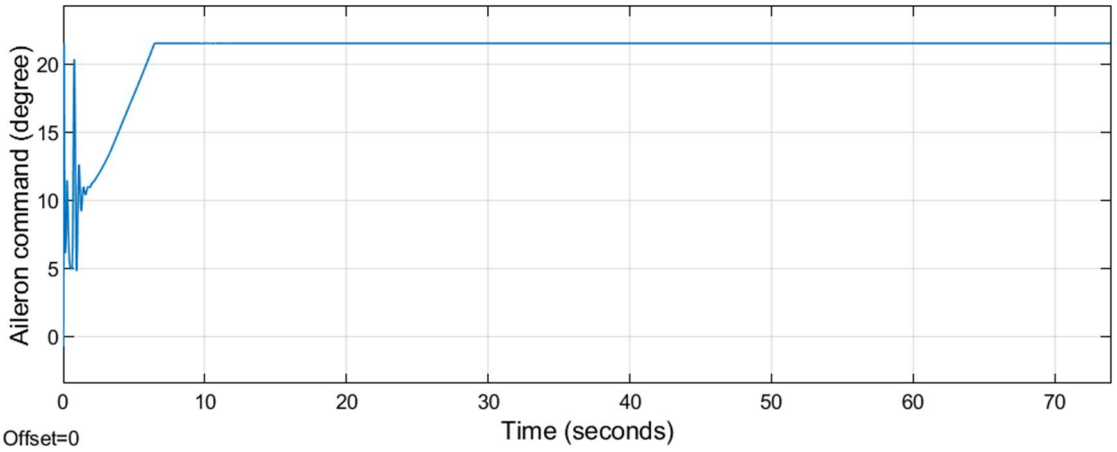

Figure 9.121 Aileron command for the seventh simulation condition with PID

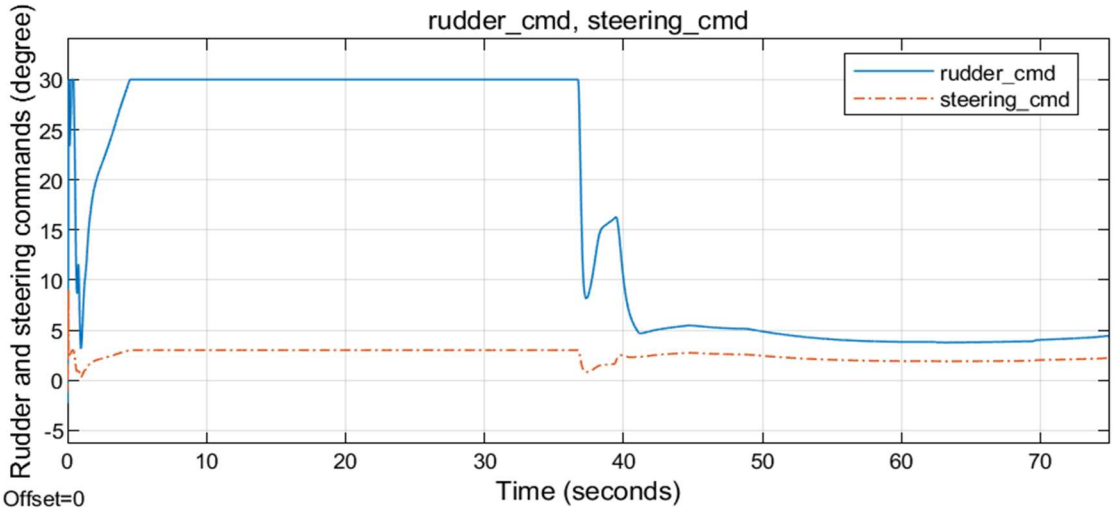

Figure 9.122 Rudder and steering commands for the seventh simulation condition with SMC

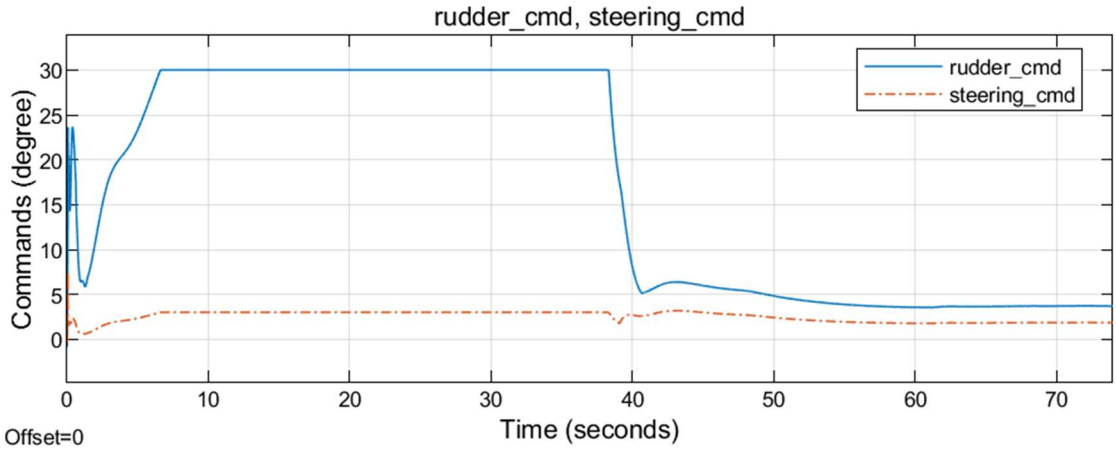

Figure 9.123 Rudder and steering commands for the seventh simulation condition with PID

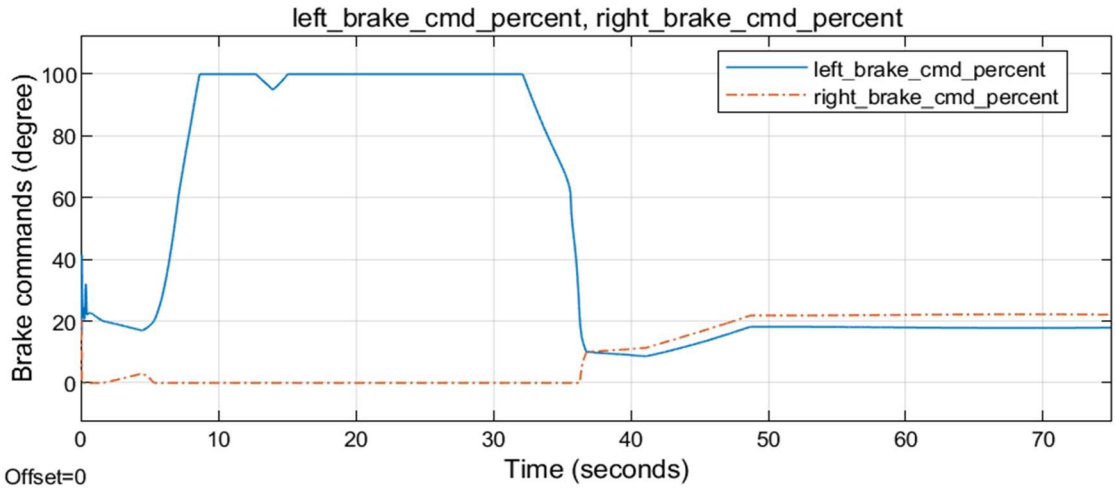

Figure 9.124 Left and right brake commands for the seventh simulation condition with SMC

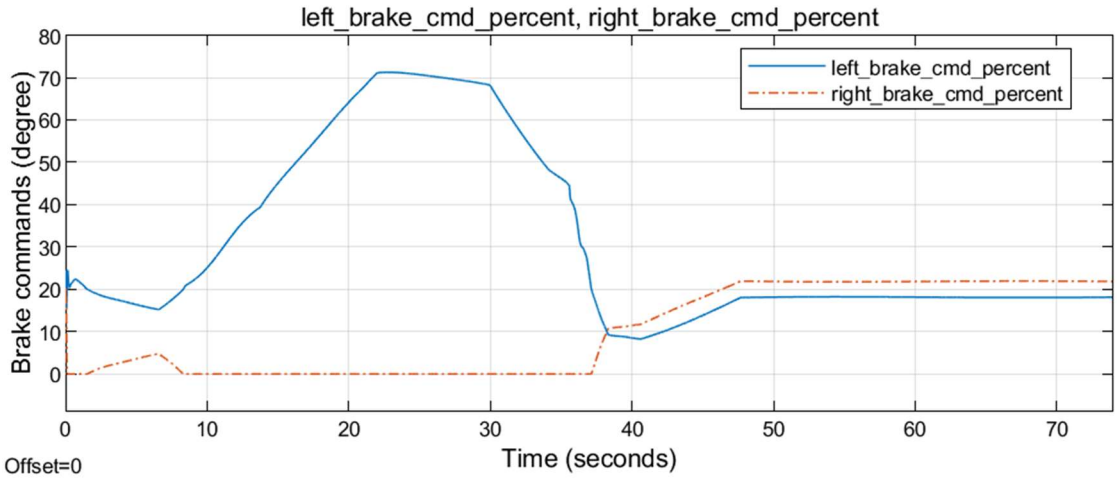

Figure 9.125 Left and right brake commands for the seventh simulation condition with PID

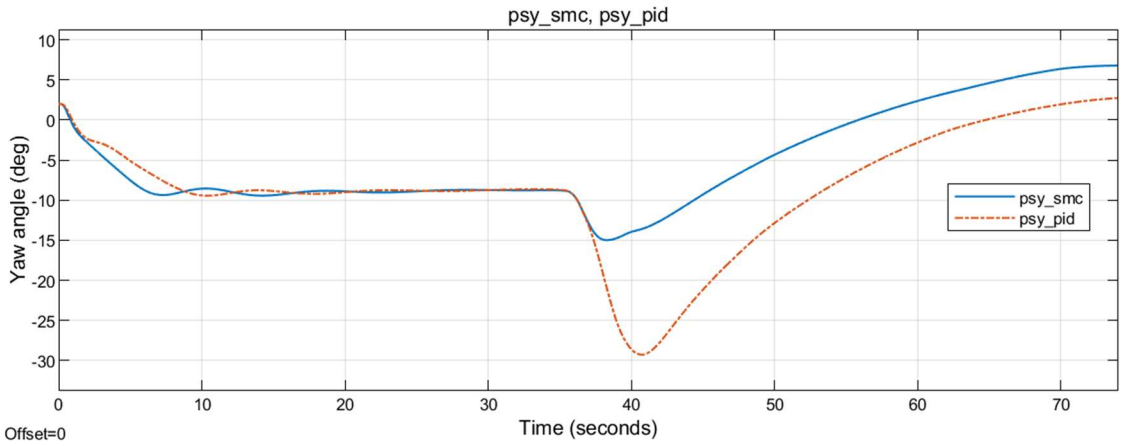

Figure 9.126 Yaw angle for the seventh simulation condition

9.8 STEERING AT CASTER

In the eighth simulation condition, the same lateral position of 2 m and track angle of 2 degrees initial conditions are given. On top of that, there is steering caster malfunction. Steering is always in caster in this condition. Results are given in Figures Figure 9.127 to Figure 9.144.

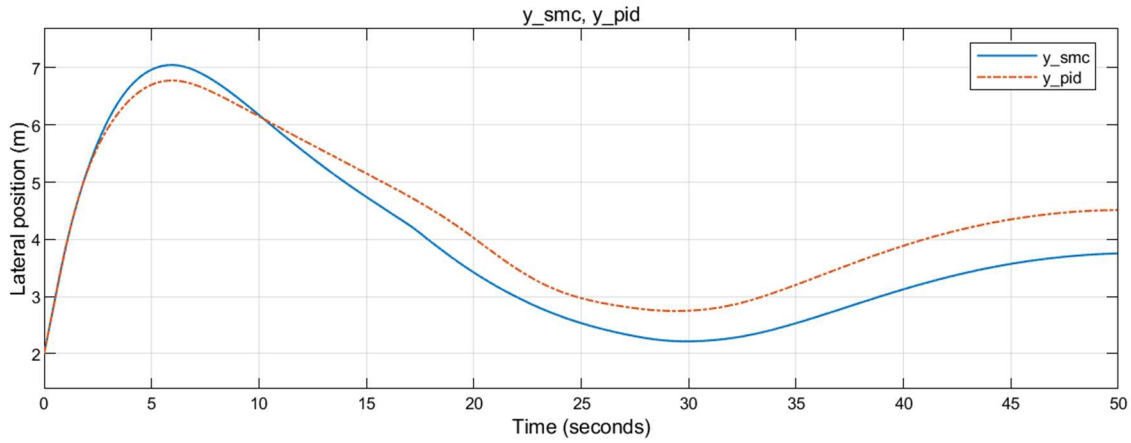

Figure 9.127 Lateral position for the eighth simulation condition

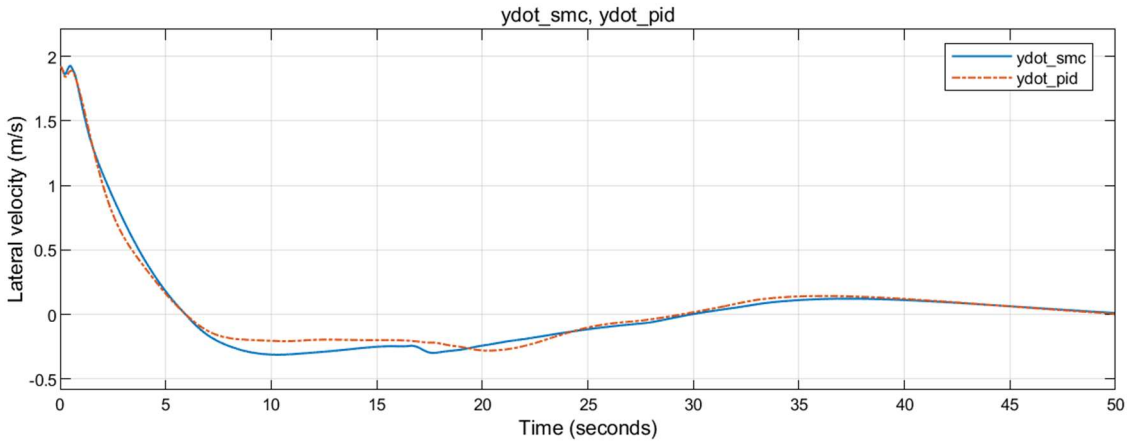

Figure 9.128 Lateral velocity with respect to runway midline for the eighth simulation condition

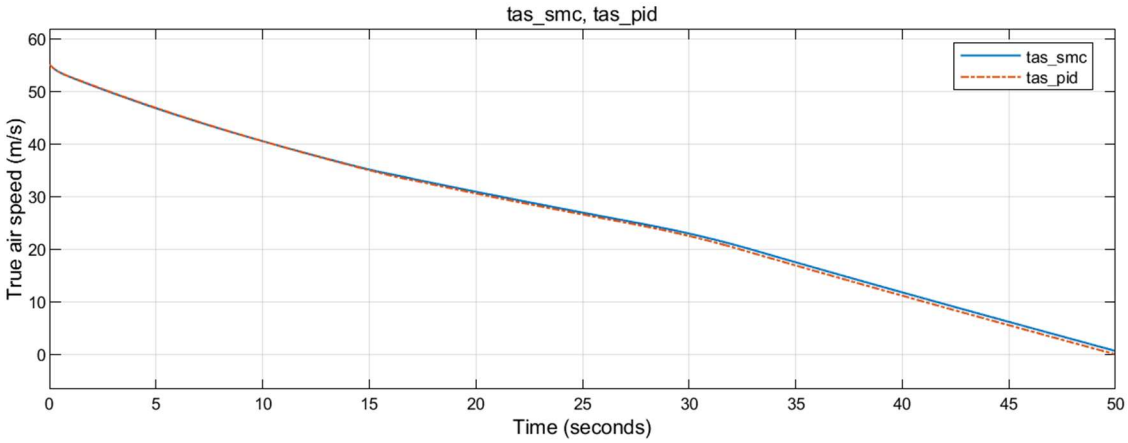

Figure 9.129 True airspeed for the eighth simulation condition

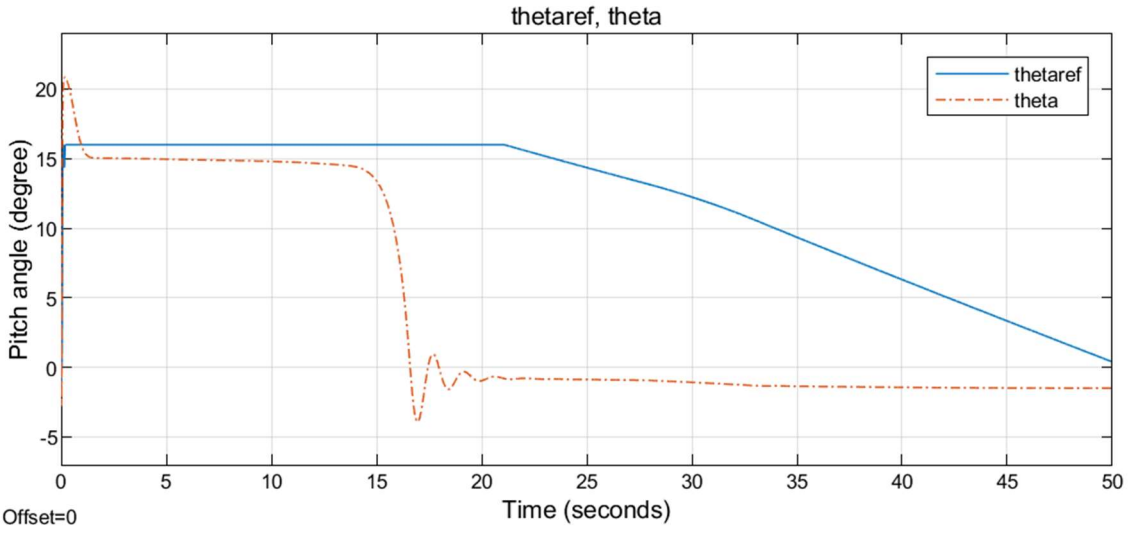

Figure 9.130 Pitch angle for the eighth simulation condition with SMC

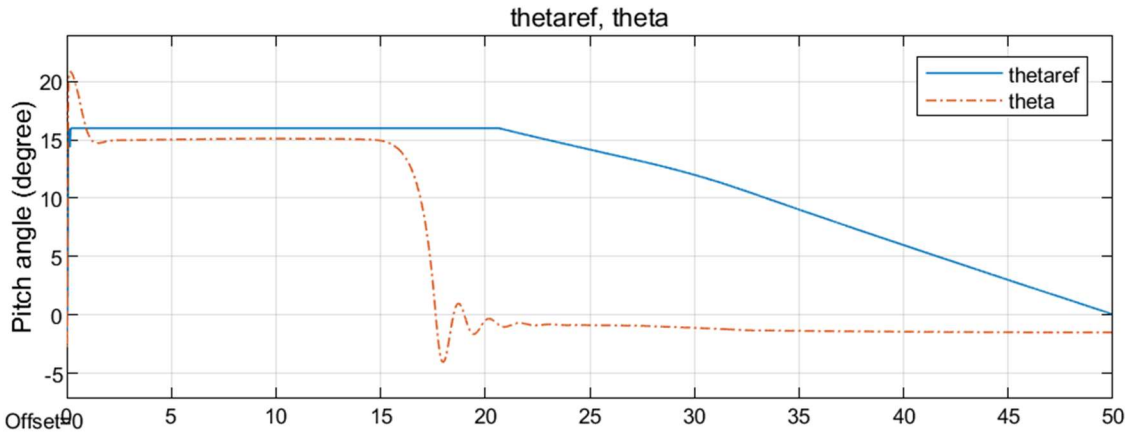

Figure 9.131 Pitch angle for the eighth simulation condition with PID

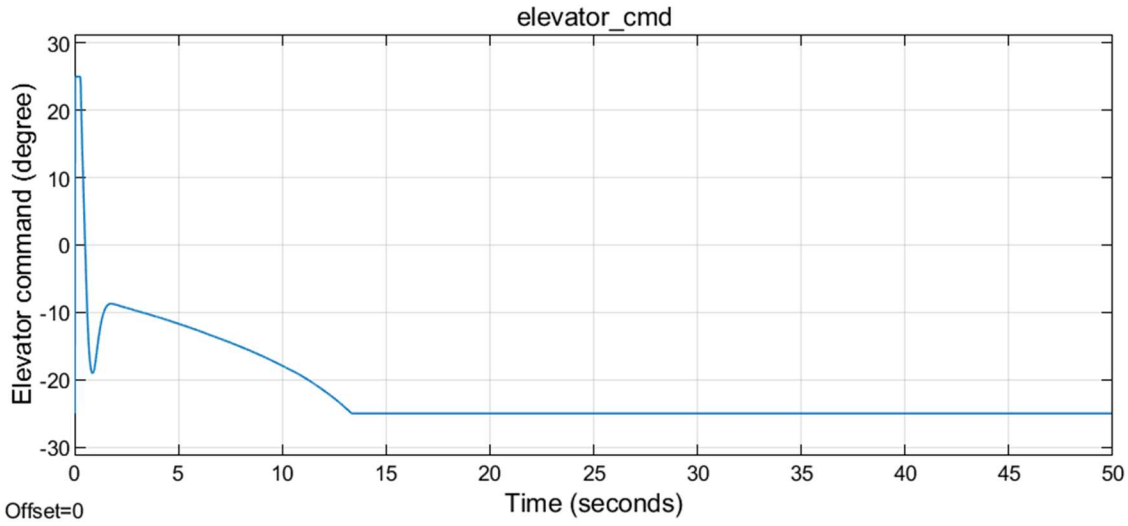

Figure 9.132 Elevator command for the eighth simulation condition with SMC

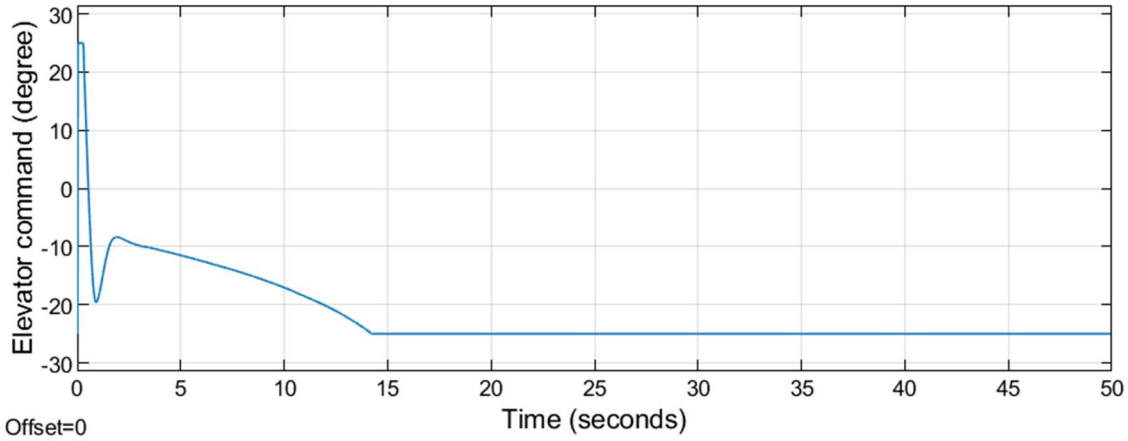

Figure 9.133 Elevator command for the eighth simulation condition with PID

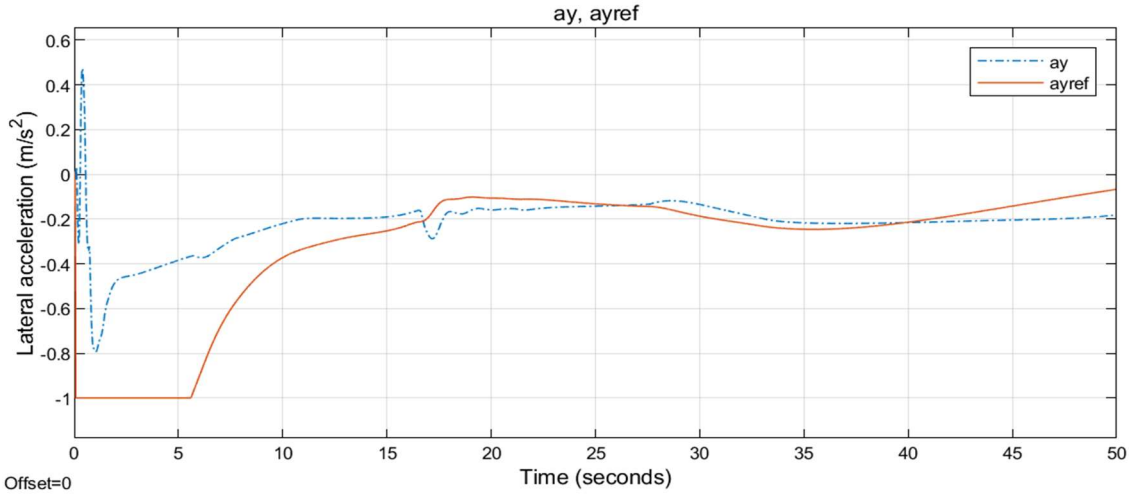

Figure 9.134 Lateral acceleration for the eighth simulation condition with SMC

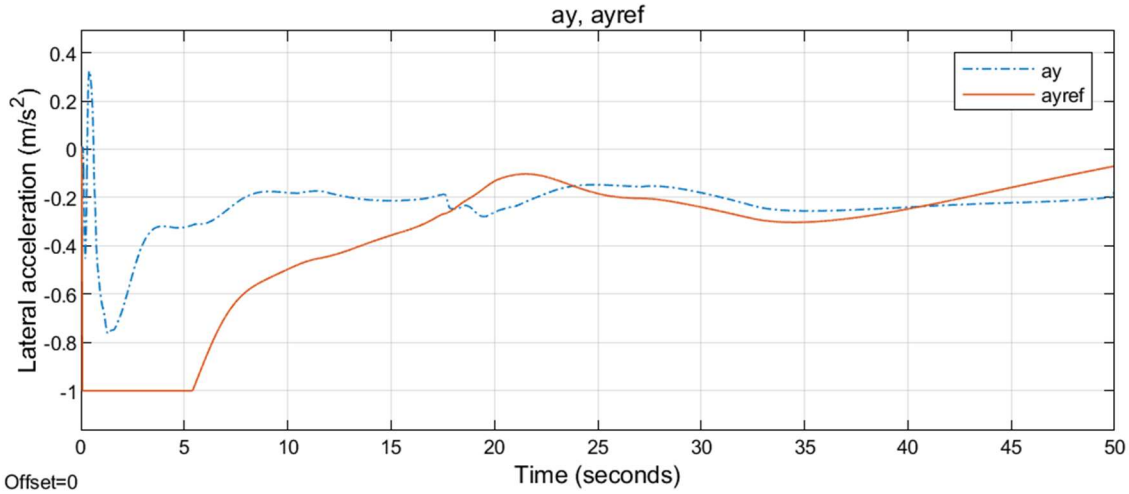

Figure 9.135 Lateral acceleration for the eighth simulation condition with PID

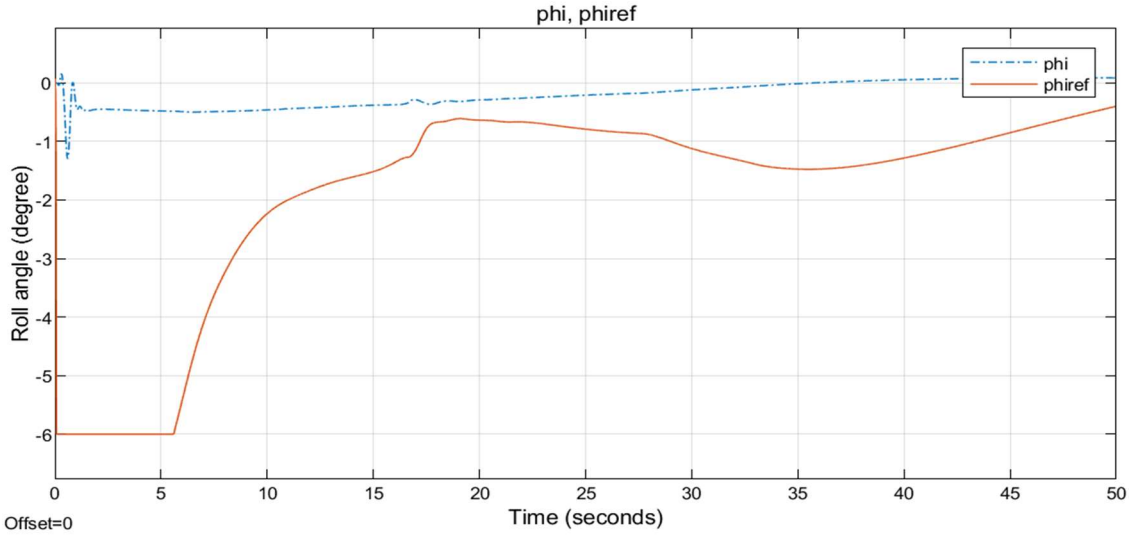

Figure 9.136 Roll angle for the eighth simulation condition with SMC

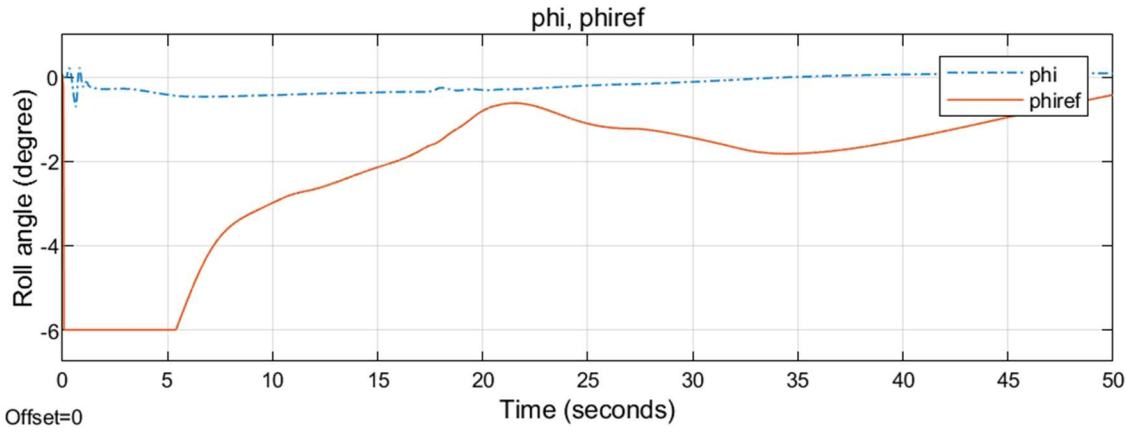

Figure 9.137 Roll angle for the eighth simulation condition with PID

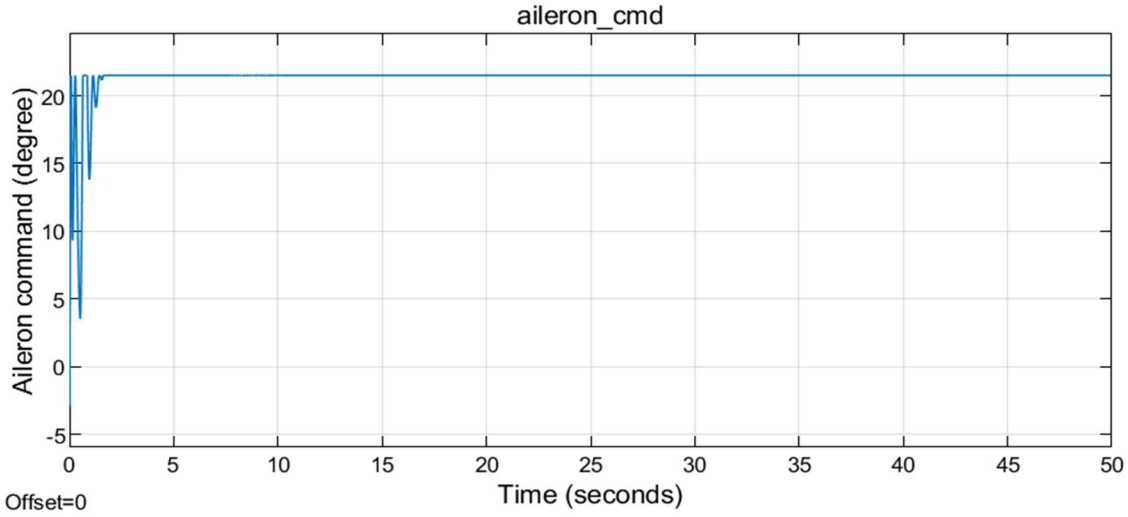

Figure 9.138 Aileron command for the eighth simulation condition with SMC

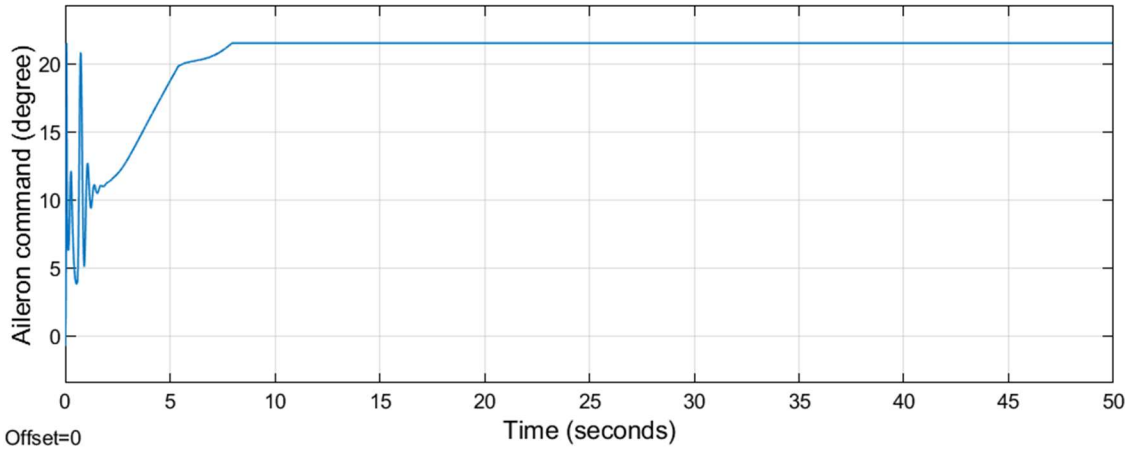

Figure 9.139 Aileron command for the eighth simulation condition with PID

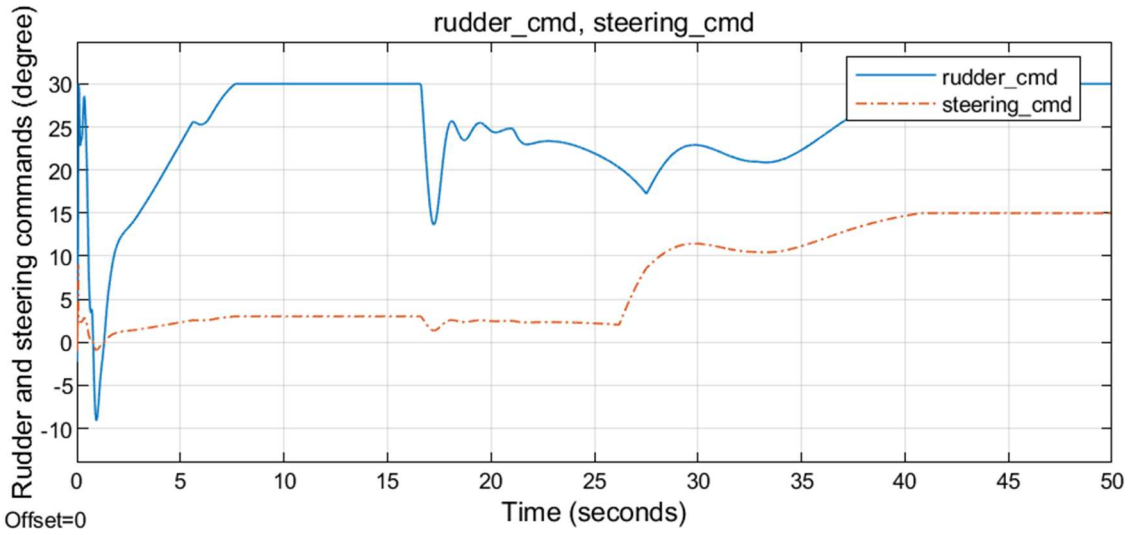

Figure 9.140 Rudder and steering commands for the eighth simulation condition with SMC

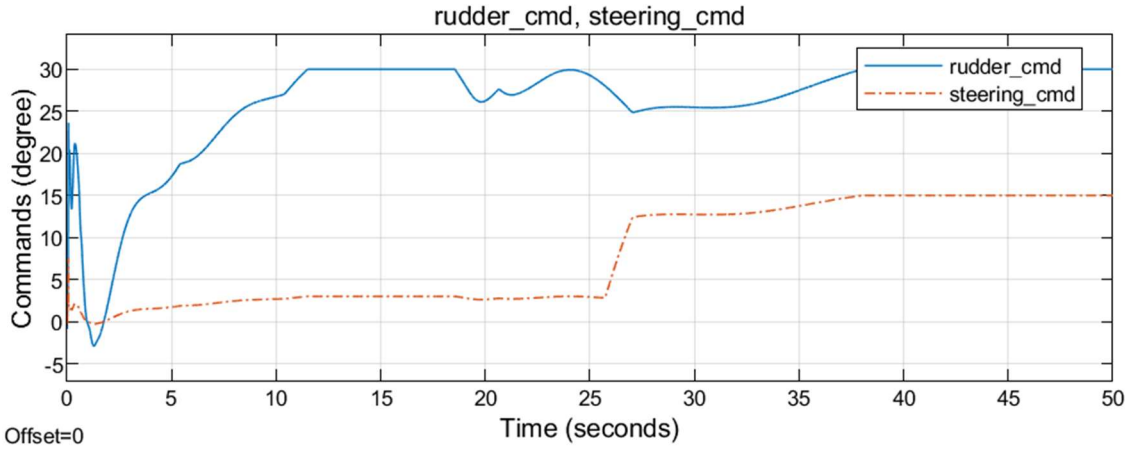

Figure 9.141 Rudder and steering commands for the eighth simulation condition with PID

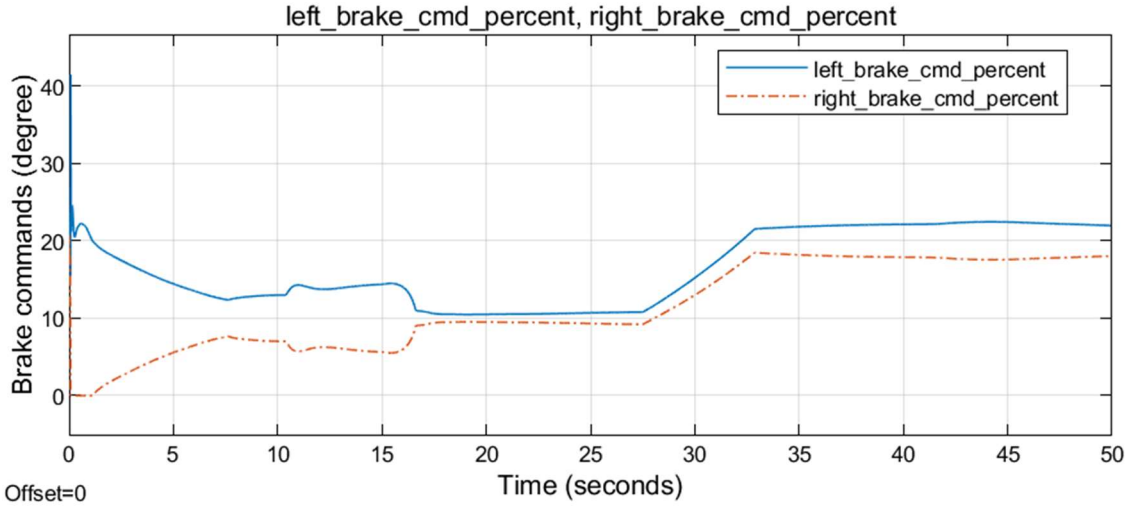

Figure 9.142 Left and right brake commands for the eighth simulation condition with SMC

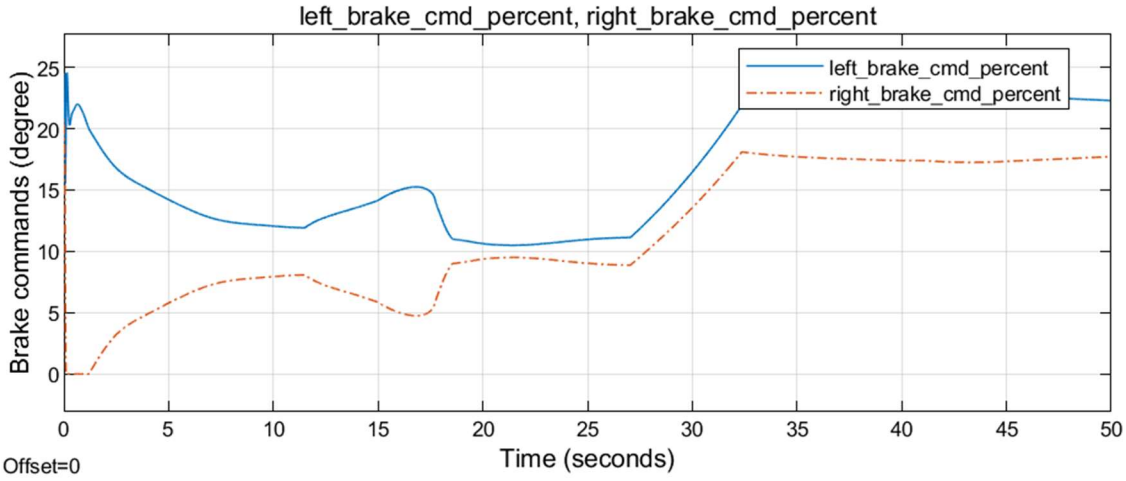

Figure 9.143 Left and right brake commands for the simulation condition with PID

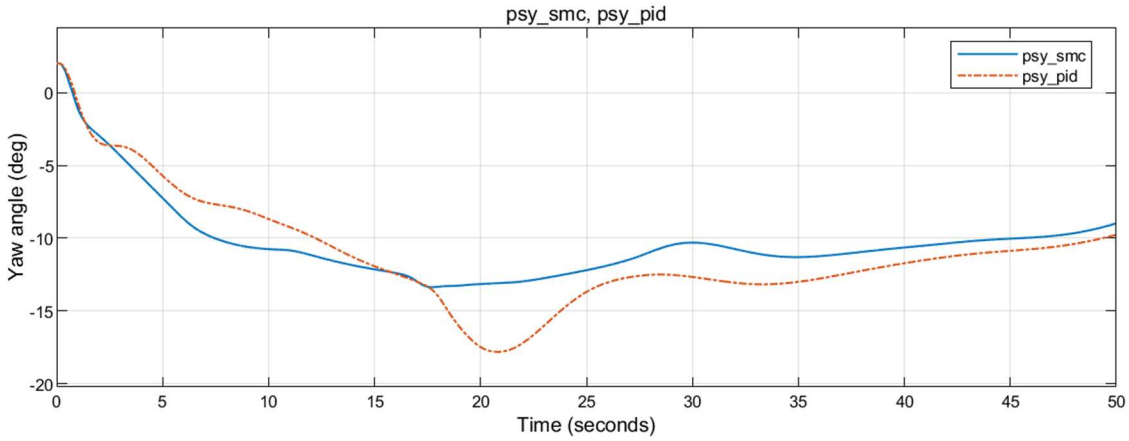

Figure 9.144 Yaw angle for the eighth simulation condition

9.9 MAIN GEAR CORNERING POWER FACTOR HALVED

In the ninth simulation condition, the same lateral position of 2 m and track angle of 2 degrees initial conditions are given. On top of that, cornering power factor of the main gear tires are halved. Results are given in Figures Figure 9.145 to Figure 9.162.

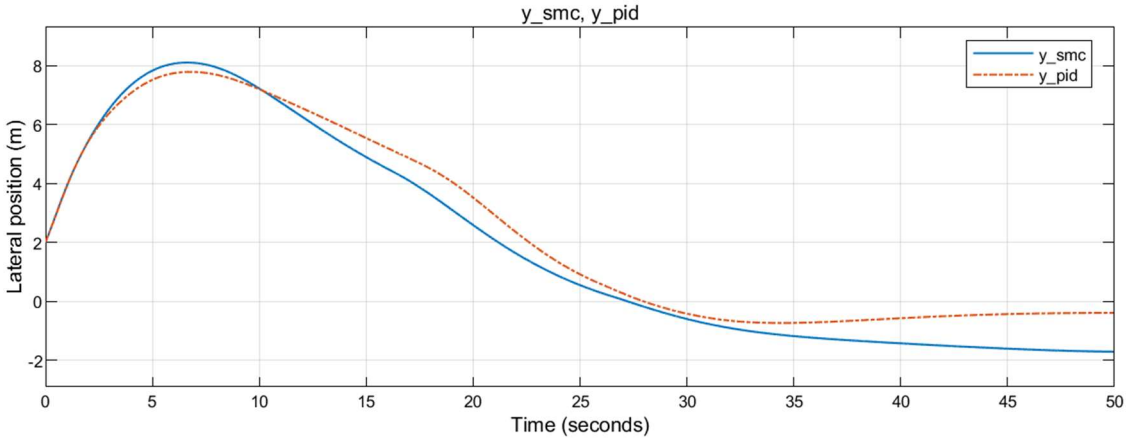

Figure 9.145 Lateral position for the ninth simulation condition

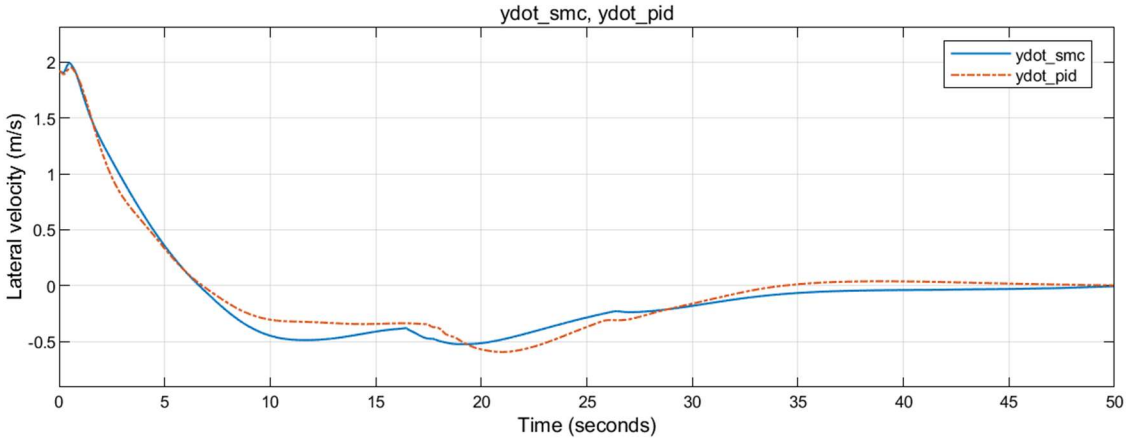

Figure 9.146 Lateral velocity with respect to runway midline for the ninth simulation condition

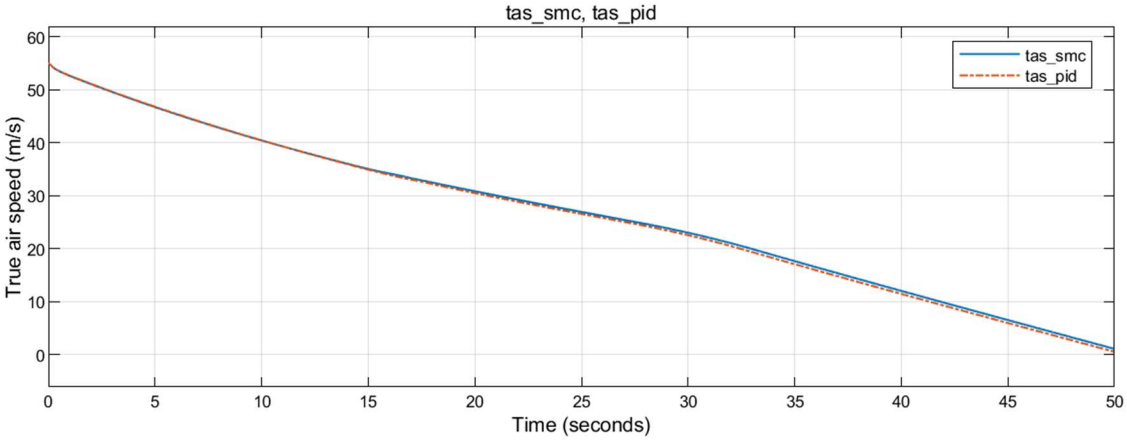

Figure 9.147 True air speed for the ninth simulation condition

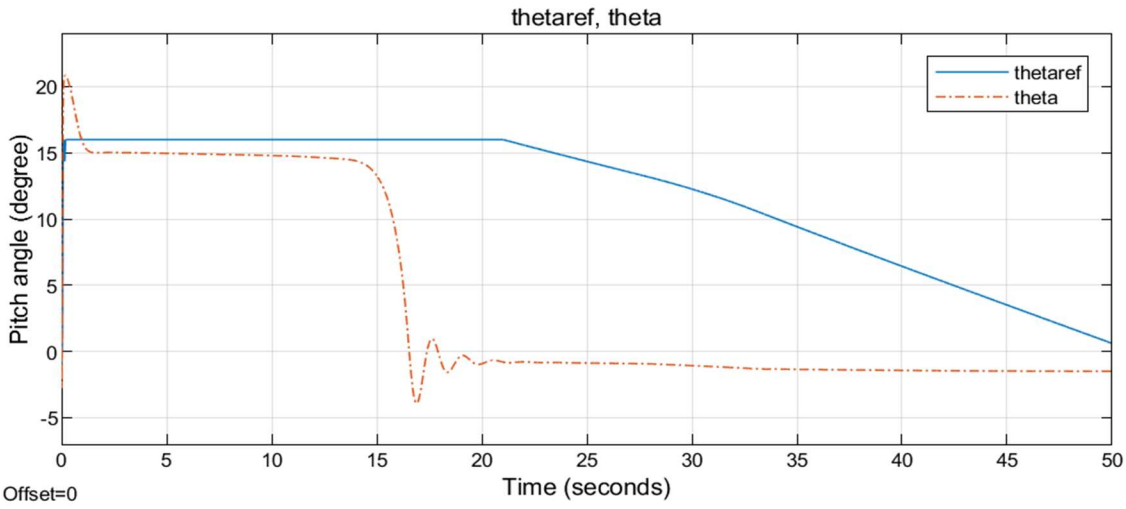

Figure 9.148 Pitch angle for the simulation condition with SMC

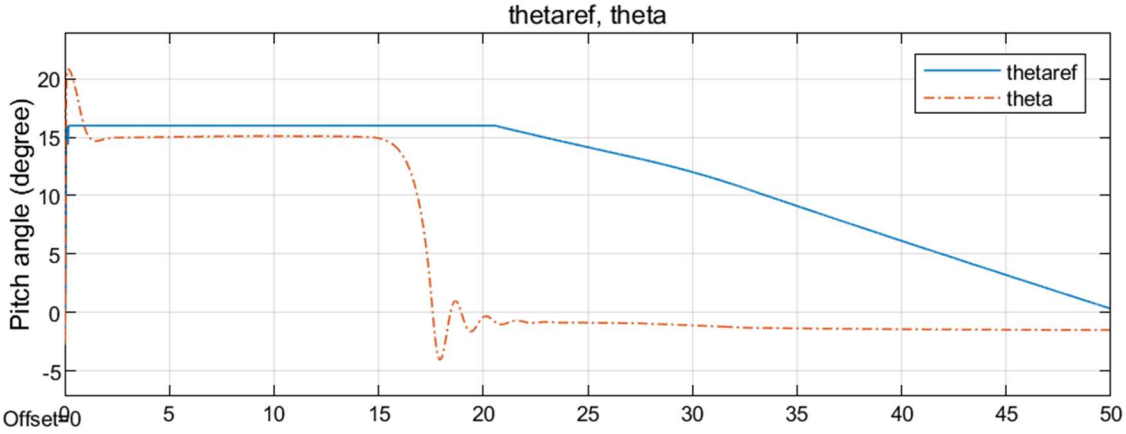

Figure 9.149 Pitch angle for the ninth simulation condition with PID

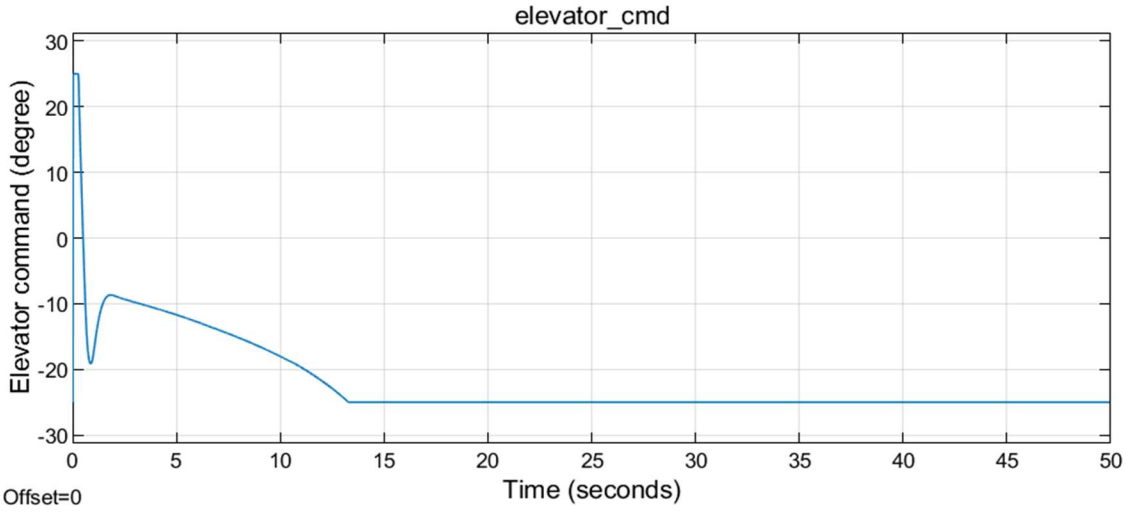

Figure 9.150 Elevator command for the ninth simulation condition with SMC

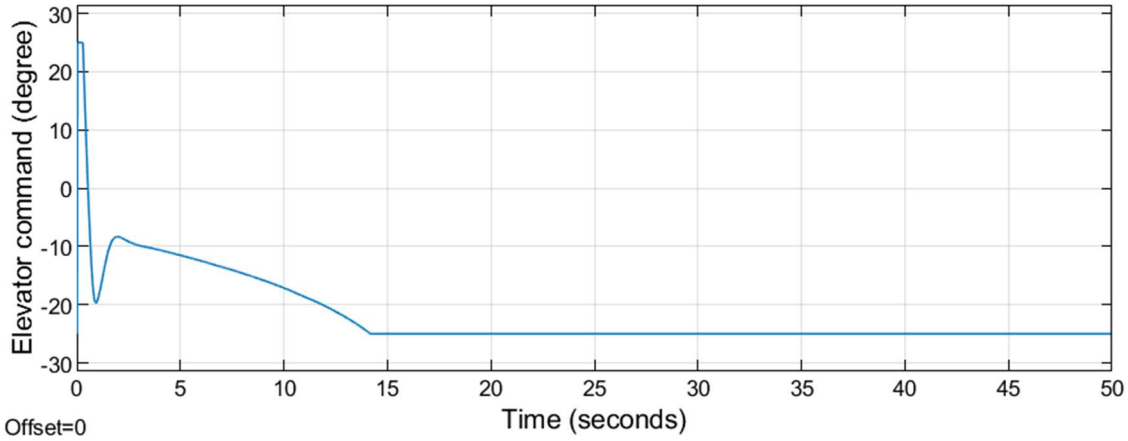

Figure 9.151 Elevator command for the ninth simulation condition with PID

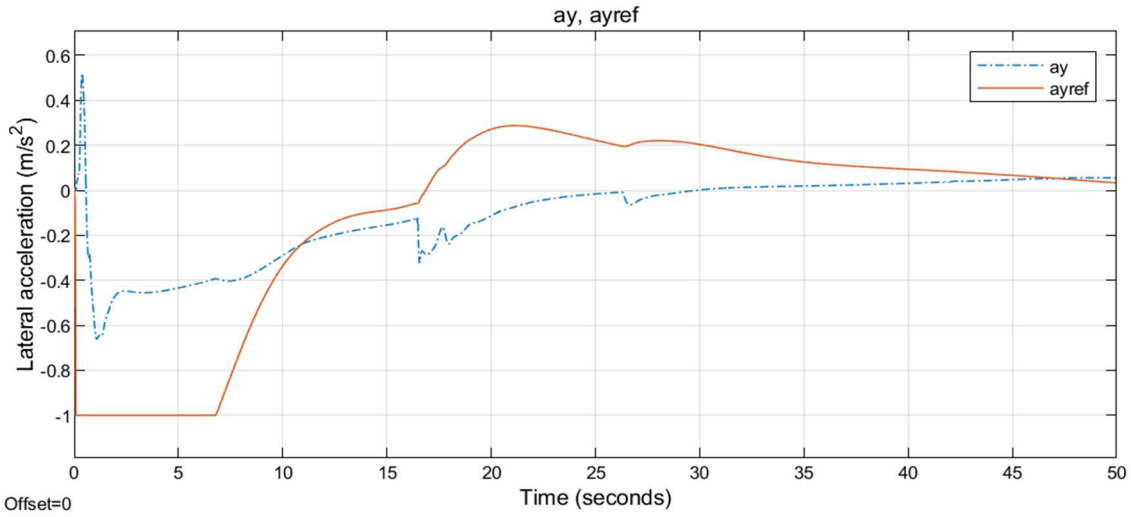

Figure 9.152 Lateral acceleration for the ninth simulation condition with SMC

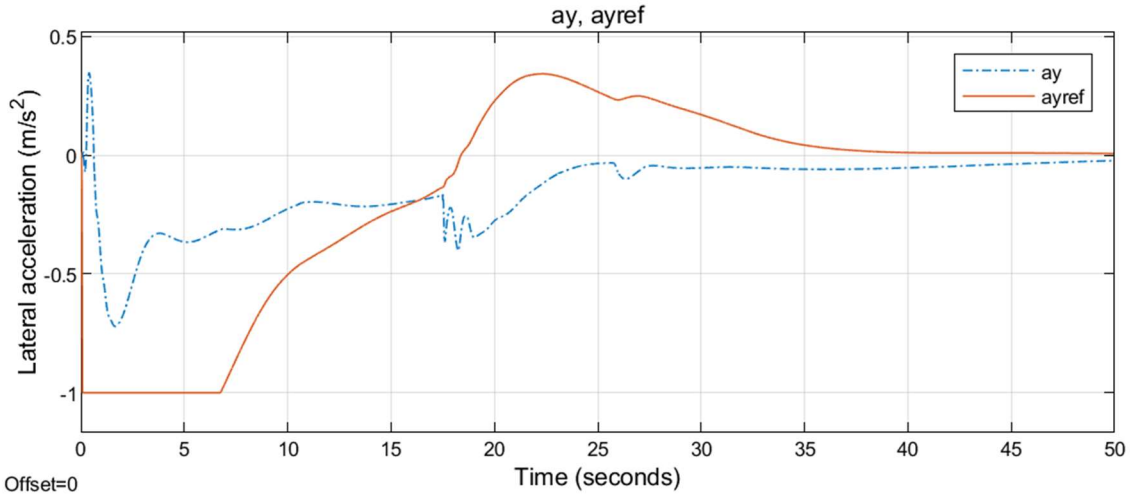

Figure 9.153 Lateral acceleration for the ninth simulation condition with PID

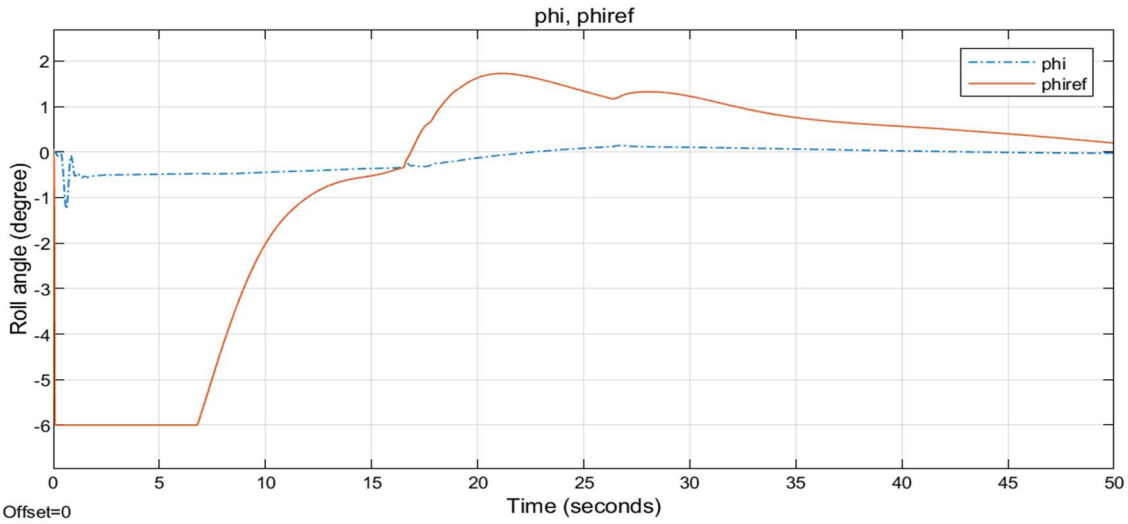

Figure 9.154 Roll angle for the ninth simulation condition with SMC

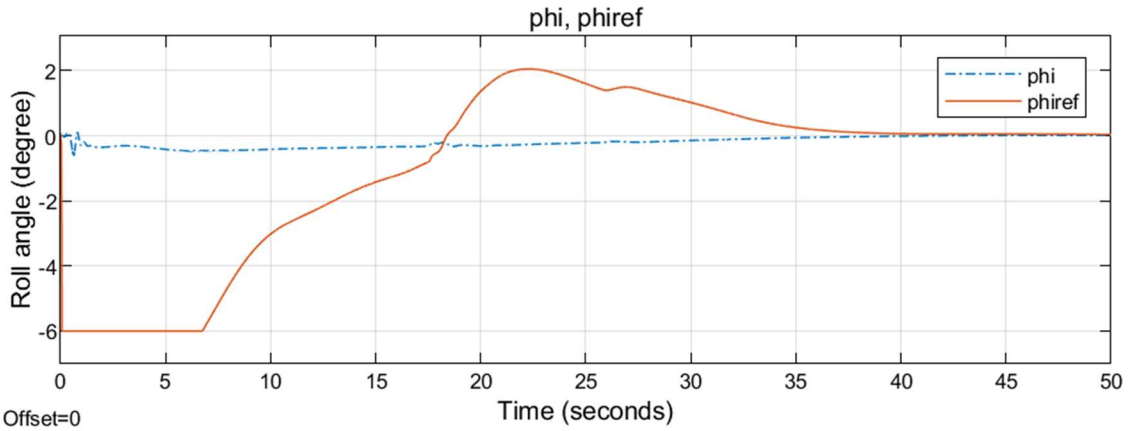

Figure 9.155 Roll angle for the ninth simulation condition with PID

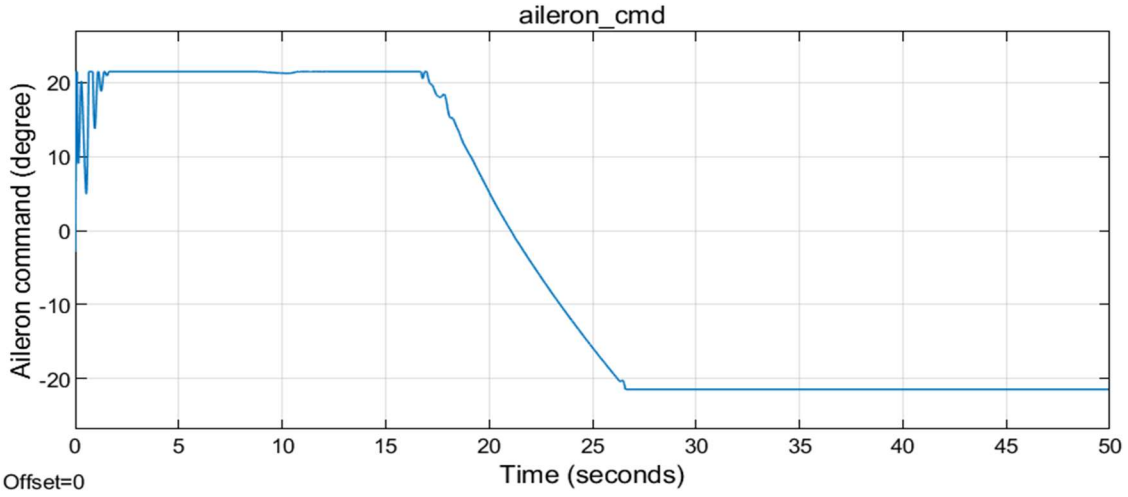

Figure 9.156 Aileron command for the ninth simulation condition with SMC

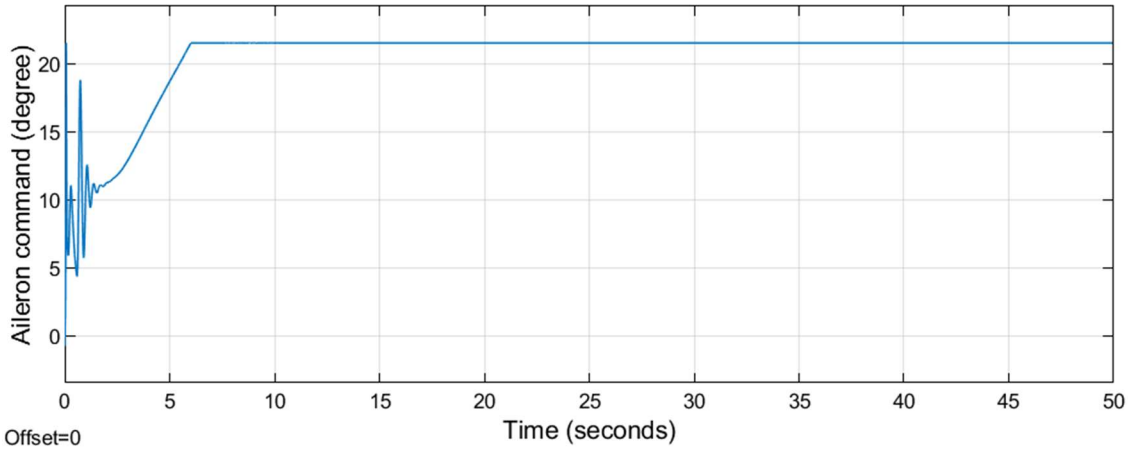

Figure 9.157 Aileron command for the ninth simulation condition with PID

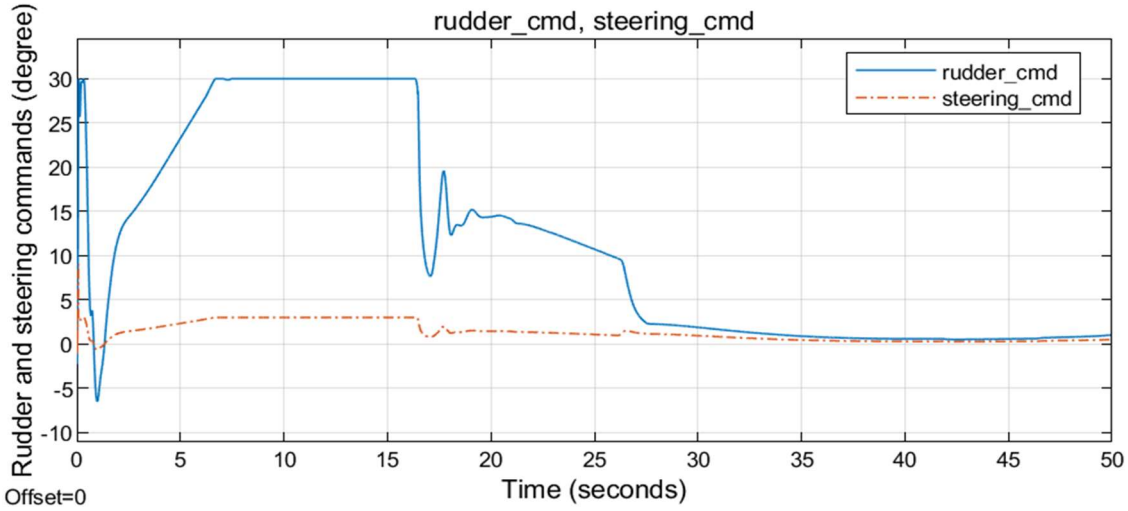

Figure 9.158 Rudder and steering commands for the ninth simulation condition with SMC

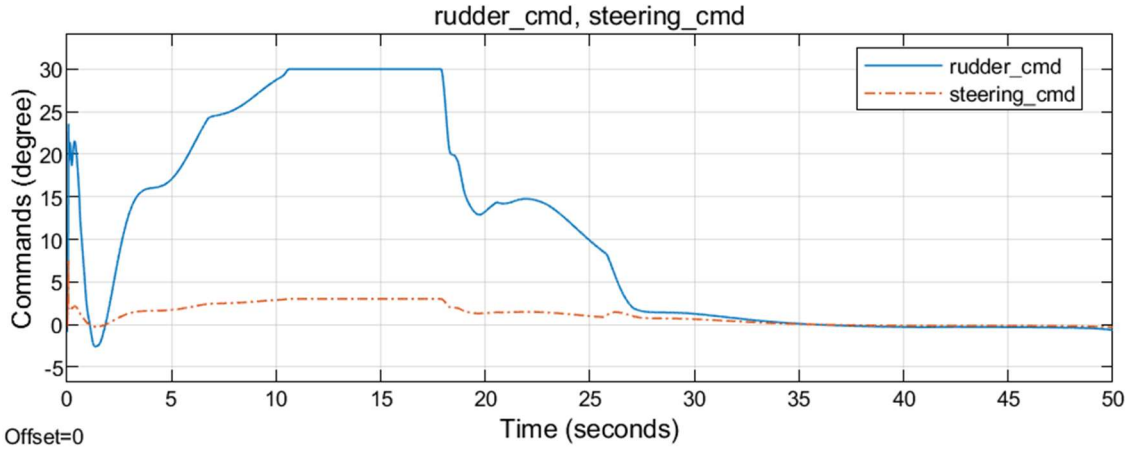

Figure 9.159 Rudder and steering commands for the ninth simulation condition with PID

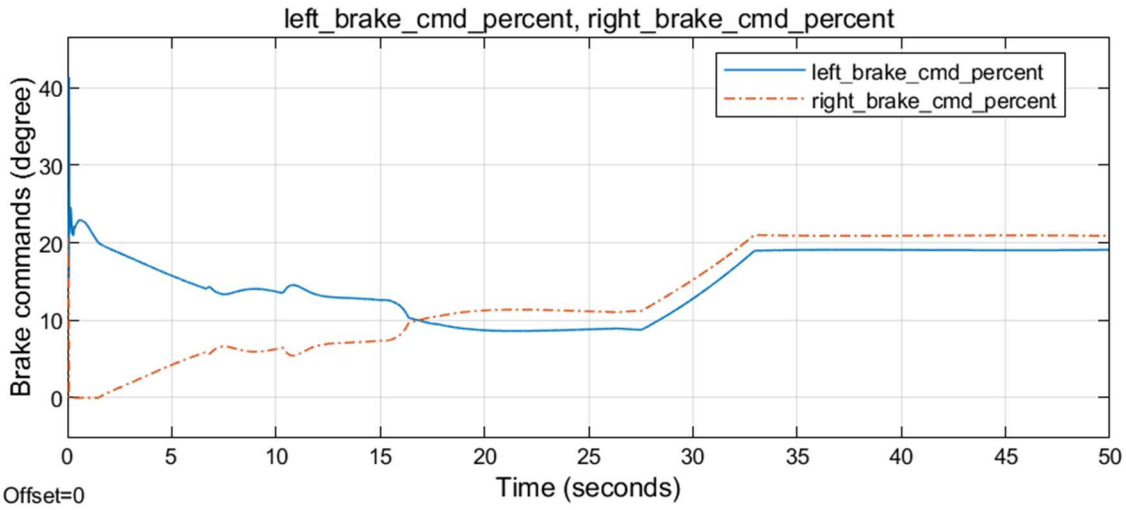

Figure 9.160 Left and right brake commands for the ninth simulation condition with SMC

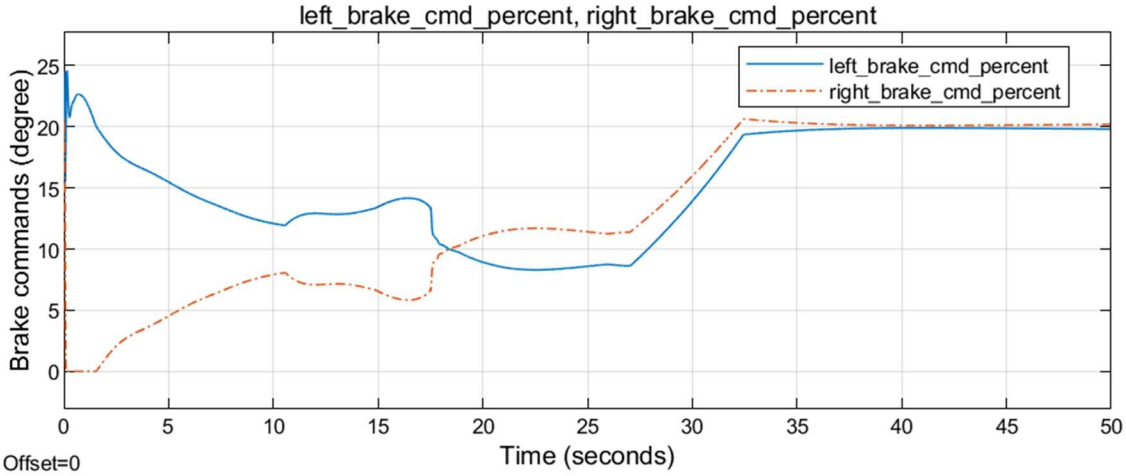

Figure 9.161 Left and right brake commands for the ninth simulation condition with PID

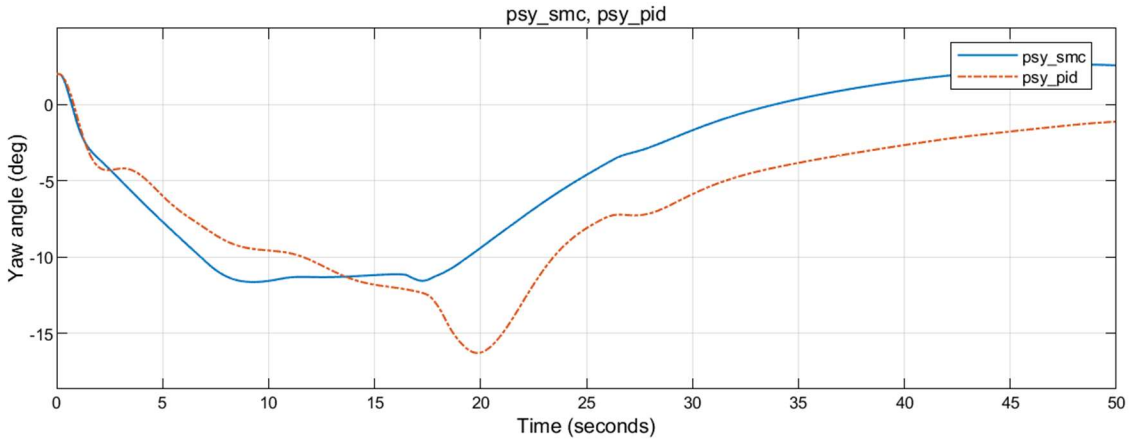

Figure 9.162 Yaw angle for the ninth simulation condition

9.10 CONCLUSION OF SIMULATION RESULTS

In this chapter, the developed aircraft ground model is tested using various disturbance and fault cases under the same initial conditions with SMC and PID regulators. Analyzing the simulation results it can be concluded that SMC and PID have similar performance in all cases. In Table 9.1 maximum lateral position overruns are summarized. SMC has smaller overrun values in third, fifth, and seventh simulation conditions. PID has smaller overrun values in the remaining simulation conditions. SMC has a slightly larger average of 9.08 while PID has an average value of 8.95 meters.

Table 9.1 Maximum lateral position overruns in simulations

MAXIMUM LATERAL POSITION (m)		
Simulation Condition #	SMC	PID
1 (No wind, no fault)	7.05	6.78
2 (Right wind, no fault)	7.4	6.99
3 (Left wind, no fault)	18.16	18.39
4 (No wind, right brake stuck at 100%)	8.5	8.13
5 (No wind, left brake stuck at 100%)	10.1	10.54
6 (No wind, right brake failure)	6.89	6.6
7 (No wind, left brake failure)	8.48	8.56
8 (No wind, steering servo failure	7.05	6.78
9 (No wind, Cornering power factor halved)	8.1	7.79
Average Values	9.08	8.95

In terms of integral absolute error of lateral position there is a similar result (Table 9.2). SMC is better in the first, fifth, seventh, and eighth simulation conditions. In the remaining simulation conditions, PID performs better. In average, PID has a smaller number of 209.4 compared to 211.5 of SMC.

In terms of stopping distance of the aircraft, the autopilot with PID controller performs better (Table 9.3). PID has an average of 1208 meters while SMC has an average of 1219 meters.

In terms of the performance of pitch hold controllers PID performs better since it has an integrator term while SMC does not have an integrator for pitch hold controller. Integral absolute values of errors in pitch angle are compared in Table 9.4.

Table 9.2 Integral absolute errors of lateral position in simulations

INTEGRAL ABSOLUTE ERROR OF LATERAL POSITION ($m \cdot s$)		
Simulation Condition #	SMC	PID
1 (No wind, no fault)	137.2	144.7
2 (Right wind, no fault)	206.3	192.6
3 (Left wind, no fault)	554.6	515.5
4 (No wind, right brake stuck at 100%)	114	108.8
5 (No wind, left brake stuck at 100%)	112.3	118.6
6 (No wind, right brake failure)	150.3	146.4
7 (No wind, left brake failure)	281	296.9
8 (No wind, steering servo failure	195.1	216.5
9 (No wind, Cornering power factor halved)	152.9	144.4
Average Values	211.5	209.4

In comparison of maximum yaw angles during simulations SMC performs better (Table 9.5). SMC has lower value of maximum yaw angle in every simulation condition. One of the reasons for this is the difference in pitch hold performances. SMC holds the high pitch angle for a smaller amount of time. Thus, nose gear drops in a shorter amount of time making it possible to correct the yaw angle and keep the aircraft going in the runway direction. This shortcoming of SMC created an advantage for lateral performance. Perhaps, a better pitch angle reference table can be created in the future by looking at this result.

In average, SMC performs better in controlling the lateral acceleration as it can be seen in Table 9.6 where SMC has an average of 10.79 and PID has an average of 11.78.

Table 9.3 Stopping distances of the aircraft in simulations

STOPPING DISTANCE OF THE AIRCRAFT (m)		
Simulation Condition #	SMC	PID
1 (No wind, no fault)	1333	1310
2 (Right wind, no fault)	1255	1250
3 (Left wind, no fault)	1160	1122
4 (No wind, right brake stuck at 100%)	427.5	449.7
5 (No wind, left brake stuck at 100%)	467.3	503.1
6 (No wind, right brake failure)	1698	1672
7 (No wind, left brake failure)	1965	1931
8 (No wind, steering servo failure	1330	1313
9 (No wind, Cornering power factor halved)	1334	1317
Average Values	1219	1208

Table 9.4 Performance comparison for pitch hold controllers

INTEGRAL ABSOLUTE ERROR OF PITCH ANGLE ($deg \cdot s$)		
Simulation Condition #	SMC	PID
1 (No wind, no fault)	1111	363.7
2 (Right wind, no fault)	1016	340.3
3 (Left wind, no fault)	891.7	280
4 (No wind, right brake stuck at 100%)	539.1	209.6
5 (No wind, left brake stuck at 100%)	589.2	233.1
6 (No wind, right brake failure)	1312	431.4
7 (No wind, left brake failure)	1093	369.7
8 (No wind, steering servo failure	1102	368.2
9 (No wind, Cornering power factor halved)	1111	371.8
Average Values	973.9	329.8

Table 9.5 Maximum yaw angles for different simulation conditions

MAXIMUM YAW ANGLE (deg)		
Simulation Condition #	SMC	PID
1 (No wind, no fault)	13.34	18.82
2 (Right wind, no fault)	24.96	24.37
3 (Left wind, no fault)	45.5	49.06
4 (No wind, right brake stuck at 100%)	9.31	14.52
5 (No wind, left brake stuck at 100%)	12.95	23.99
6 (No wind, right brake failure)	9.45	9.85
7 (No wind, left brake failure)	14.99	29.3
8 (No wind, steering servo failure	13.36	17.8
9 (No wind, Cornering power factor halved)	11.63	16.28
Average Values	17.28	22.67

Table 9.6 Performance comparison of lateral acceleration hold controllers

INTEGRAL ABSOLUTE ERROR OF LATERAL ACCELERATION ($m/s^2 \cdot s$)		
Simulation Condition #	SMC	PID
1 (No wind, no fault)	9.243	11.83
2 (Right wind, no fault)	13.36	10.85
3 (Left wind, no fault)	19.11	17.18
4 (No wind, right brake stuck at 100%)	6.233	8.415
5 (No wind, left brake stuck at 100%)	5.494	4.309
6 (No wind, right brake failure)	7.439	7.027
7 (No wind, left brake failure)	19	25.47
8 (No wind, steering servo failure	6.588	8.426
9 (No wind, Cornering power factor halved)	10.6	12.48
Average Values	10.79	11.78

10. CONCLUSION

10.1 SUMMARY OF THE THESIS

In this thesis, a robust fault-tolerant autoland system is designed for a fighter aircraft in autoland rollout.

In chapter 1, literature relevant to the autoland on the ground problem is reviewed. Topics reviewed include aircraft modelling, landing gear modelling, autoland systems, automotive lane-keeping systems, line-tracking navigation algorithms and sliding mode control.

In chapter 2, all the necessary components of the aircraft model are explained. These include aerodynamics, propulsion, mass, CG, inertia, landing gear dynamics, equations of motion and axis systems used.

In chapter 3, the model that is created in chapter 2 is verified using some simulations. Results of these simulations are included in Appendix 2.

In chapter 4, trimming and linear model derivation on the ground problem are solved. Two different trim maneuvers which are two tires on the ground and three tires on the ground maneuvers are explained. Single axis sequential secant algorithm which is used for trimming is explained. Linear model derivations are explained in detail. Both the trim points and linear models are verified, and the verification scheme is explained.

In chapter 5, dynamics and mode shapes on the ground are explained, control allocation scheme, reference pitch angle and control strategy are decided.

In chapter 6, different navigation algorithms for line tracking are explained and compared in terms of performance. The specific problem of midline tracking during landing rollout is researched and it is shown that linear sliding mode guidance performs better than most of its proposed alternatives. The proven guidance algorithm is chosen for use in the outer loop of the autoland system which is responsible for calculating the necessary lateral acceleration.

In chapter 7, a fault-tolerant, gain scheduling feedforward aided linearized sliding mode controller is designed. The theory of sliding mode control and the structure of the proposed sliding mode controller used in this thesis are explained. Performance and stability requirements are outlined and proven. The process of designing a controller is

explained in detail. These details include, adjusting the guidance law, addition of sensor delays, zero order hold, anti-windup, feedforward gains and yaw angle gains.

In chapter 8, a fault tolerant, gain scheduling feedforward aided PID controller is designed, performance and stability are proven. In this autoland system application, the same linear sliding mode guidance is used in the outer loop application as in the SMC that is designed in chapter 7.

In chapter 9, performance of SMC and PID controllers that are used in inner loops which are responsible for tracking the lateral accelerations specified by the outer loop guidance are compared by simulations. Results of the simulations show that linearized quasi-SMC is almost as good as PID in terms of inner loop performance.

10.2 CONTRUBUTION OF THE THESIS

The first contribution of the thesis is the modelling of an aircraft including the landing gear and aircraft tire models. This thesis can become a foundational reference for the researchers working on these subjects as it contains the equations and data used to create these models for F-16 aircraft which is the most used aircraft in aerospace control theory applications.

The second contribution of the thesis is the comprehensive verification routine for the aircraft and landing gear models that is proposed which can be used both in industry and academia.

The third contribution of the thesis is the trimming and linear model derivation routines for the ground dynamics of an aircraft, which were previously underexplored in the literature. The algorithm that is used in the trimming chapter can become an alternative to the widely used multi-axis Newton method.

The dynamics and mode shapes chapter also contributes to the literature by providing example linear models for the ground dynamics of the aircraft.

The outer loop guidance chapter introduces different guidance algorithms. These algorithms are also compared based on their performance. This chapter contributes to the literature by providing solutions for the specific problem of midline tracking during autoland rollout.

The major contribution of the thesis is the design of a fault-tolerant, gain scheduling feedforward-aided linearized sliding mode controller for an autoland rollout application. In the seventh chapter, sliding mode control is explained, theory and practical aspects are

described, different parts of the controller are designed. These different parts include; the outer loop, pitch hold controller, lateral controller, feedforward gains, control allocation routines, anti-windup routines and other details of the controller. One of the major contributions in this application of sliding mode controller is the usage of boundary layer control which is the usage of linear gains inside a boundary. Thus, it was possible to prove the stability margins of the controller which are necessary for aerospace applications. Another important contribution was the usage of feedforward gains coming directly from the guidance loop. These feedforward gains use differential braking to help the aircraft turn towards the desired path to track the midline. Finally, a big contribution of this thesis is the fault tolerance of the developed autoland systems. Especially, the feedforward gains that command differential braking inputs are essential for the fault tolerance of braking failures.

Although, the original sliding mode controller in theory cannot be used directly, quasi sliding mode controllers like the ones that are designed in this thesis can be used in aerospace applications. They can be designed to have sufficient performance and proven stability.

In the outer loop guidance, it is shown that SMC-based laws can perform better than many other alternatives.

The procedures that are developed in this thesis can be used in current and future autoland system design projects in the aerospace industry.

10.3 POSSIBLE IMPROVEMENTS AND FUTURE WORK

Possible improvements to this thesis include;

- A more detailed tire model,
- A more detailed verification scheme including a scheme detailing unit tests,
- Addition of different types of trim maneuvers,
- Comparison of the single-axis sequential secant algorithm with the industry standard Jacobian-based multi-axis algorithms,
- Design and comparison of different sliding mode controller methods including asymptotic sliding mode, higher order sliding mode, sliding mode differentiators and other methods,
- An automatic gain optimization tool for the sliding mode and PID controllers,
- Different simulation conditions including two malfunctions at the same time,

- Monte Carlo analysis for the model uncertainties and statistical analysis for the possibility of runway excursions,
- A detailed analysis for the effects of noise in the system,
- Better environment model including wind turbulence and gust,
- Better model of the effects of the runway surface.

Although there are a lot of possible improvement areas, this thesis can serve as a backbone for the area of ground dynamics and control of aircraft.

Possible future work in this area include;

- The same design procedure for autotakeoff applications,
- Comparison of different trimming methods and algorithms for ground trimming,
- Improvement on geometric predictive guidance algorithm,
- A different trim maneuver condition named coordinated turn on the ground,
- Design of anti-skid braking systems,
- Investigation on the effects of acceleration factor in landing gear model,
- Usage of nosewheel caster during landing for increased stability,
- Examination of different control allocation schemes such as turning the rudder and steering in the same direction for increased stability and minimum phase behavior,
- Gain optimization algorithm for SMC and PID controllers,
- Control of the nosewheel lateral force during caster,
- Usage of strut positions and velocities as feedback signals in the controller,
- Effects of sensor failures during autoland,
- Calculation of the optimum initial lateral position and track angle during a crosswind landing rollout,
- Investigation on the effect of active suspension on the landing rollout performance
- Feasibility of using thrust of the engine as an alternative input during landing rollout, especially during crosswind conditions,
- Using the full system states including position states for the design of a combined guidance and controller system design instead of cascaded loops.

11. REFERENCES

[1] BBC, "BBC," BBC, 14 January 2018. [Online]. Available: https://www.bbc.com/news/world-europe-42680238. [Accessed 12 10 2022].

[2] Onderzoeksraad, "Onderzoeksraad," Onderzoeksraad, [Online]. Available: https://www.onderzoeksraad.nl/en/page/4875/runway-excursion-maastricht-aachen-airport-11-november-2017. [Accessed 12 10 2022].

[3] IATA, "Runway Safety Accident Analysis Report 2010-2014," IATA, Montreal-Geneva, 2015.

[4] Stratejik Düşünce Enstitüsü, "sde.org.tr," 11 January 2019. [Online]. Available: https://www.sde.org.tr/savunma-guvenlik/anka-sin-ilk-siparisinde-teslimatlar-tamamlandi-haberi-9091. [Accessed 12 10 2022].

[5] TAI, "www.tai.com.tr," [Online]. Available: https://www.tusas.com/urunler/iha/yuksek-faydali-yuk-kapasitesi/aksungur. [Accessed 12 10 2022].

[6] TRT, "Turkish Radio and Television Association," 26 March 2022. [Online]. Available: https://www.trthaber.com/haber/bilim-teknoloji/tusas-malezyada-hurjet-ve-ankayi-sergileyecek-667148.html. [Accessed 12 10 2022].

[7] S. Gudeta and A. Karimoddini, "Design of a Smooth Landing Trajectory Tracking System for a Fixed-wing Aircraft," in *American Control Conference*, Philadelphia, 2019.

[8] E. A. Morelli, "GLOBAL NONLINEAR PARAMETRIC MODELING WITH APPLICATION TO F-16 AERODYNAMICS," NASA, Hampton, VA, 1997.

[9] A. F. Gabernet, Controllers for Systems with Bounded Actuators: Modeling and control of an F-16 aircraft, Irvine CA: UCA, 2007.

[10] Y. Huo, "Model of F-16 Fighter Aircraft -Equation of Motions-," Los Angeles CA.

[11] H. Georgieva and V. Serbezov, "Mathematical Model of Aircraft Ground Dynamics," in *International Conference on Military Technologies*, Brno, 2017.

[12] Q. Yin, H. Nie and X. Wei, "Dynamics and Directional Stability of High-Speed Unmanned Aerial Vehicle Ground Taxiing Process," *Journal of Aircraft,* vol. 57, no. 4, 2020.

[13] L. Bo, J. Zongxia and W. Shaoping, "Research on Modeling and Simulation of Aircraft – Taxiing Rectification," in *2006 IEEE Conference on Robotics, Automation and Mechatronics*, Bangkok, 2006.

[14] E. Coetzee, B. Krauskopf and M. Lowenberg, "Nonlinear Aircraft Ground Dynamics," in *International Conference on Nonlinear Problems in Aviation and Aerospace*, 2006.

[15] S. Pines and R. Hueschen, "Guidance and navigation for automatic landing, rollout, and turnoff using MLS and magnetic cable sensors," in *Guidance and Control Conference*, Palo Alto CA, 1978.

[16] R. F. Smiley and W. B. Horne, "Mechanical Properties Of Pneumatic Tires With Special Reference To Modern Aircraft Tires," NACA, Langley Field VA, 1958.

[17] A. De Marco, E. L. Duke and J. S. Berndt, "A General Solution to the Aircraft Trim Problem," in *AIAA Modeling and Simulation Technologies Conference and Exhibit*, Hilton Head SC, 2007.

[18] J. Luo, "MULTI-AXIS TRIM PROCESSING". United States Patent US 2008O147251A1, 19 June 2008.

[19] A. A. Pashilkar, "Algorithms for Aircraft Trim Analysis on Ground," in *AIAA Flight Simulation Technologies Conference*, Sand Diego CA, 1996.

[20] M. Millidere, U. Karaman, S. Uslu, C. Kasnakoğlu and T. Çimen, "Newton-Raphson Methods in Aircraft Trim: A Comparative Study," in *AIAA Aviation Forum*, Virtual Event, 2020.

[21] S. Ismail, A. A. Pashilkar, R. Ayyagari and S. N., "Improved autolanding controller for aircraft encountering unknown actuator failures," in *2013 IEEE*

Symposium on Computational Intelligence for Security and Defense Applications (CISDA), Singapore, 2013.

[22] C.-M. Lin and E.-A. Boldbataar, "Autolanding Control Using Recurrent Wavelet Elman Neural Network," *IEEE Transactions on Systems, Man, and Cybernetics: Systems,* vol. 45, no. 9, pp. 1281-1291, 2015.

[23] S. Ismail, A. A. Pashilkar and R. Ayyagari, "Phase compensation and anti-windup design for neural-aided sliding mode fault-tolerant autoland controller," in *2015 International Conference on Cognitive Computing and Information Processing(CCIP)*, Noida, 2015.

[24] H. Xiong, J.-q. Yi, G.-l. Fan, F.-s. Jing and R.-y. Yuan, "Autolanding of unmanned aerial vehicles based on Active Disturbance Rejection Control," in *2009 IEEE International Conference on Intelligent Computing and Intelligent Systems*, Shanghai, 2009.

[25] T. Wagner and J. Valasek, "Digital Autoland Control Laws Using Quantitative Feedback Theory and Direct Digital Design," *JOURNAL OF GUIDANCE, CONTROL, AND DYNAMICS,* vol. 30, no. 5, pp. 1399-1413, 2007.

[26] D. V. Rao and T. H. Go, "Automatic landing system design using sliding mode control," *Aerospace Science and Technology,* vol. 32, pp. 180-187, 2014.

[27] K. Lee, S. E. Li and D. Kum, "Synthesis of Robust Lane Keeping Systems: Impact of Controller and Design Parameters on System Performance," *IEEE TRANSACTIONS ON INTELLIGENT TRANSPORTATION SYSTEMS,* vol. 20, no. 8, pp. 3129-3141, 2018.

[28] M. Yamamoto, Y. Kagawa and A. Okuno, "Robust Control for Automated Lane Keeping against Lateral Disturbance," in *International Conference on Intelligent Transportation Systems*, Tokyo, 1999.

[29] N. C. Basjaruddin, F. Adinugraha, T. Ramadhan, D. Saefudin and E. Rakhman, "Lane Keeping Assist Based on Fuzzy Logic using Camera Sensor," in *2019 International Conference on Advanced Mechatronics, Intelligent Manufacture and Industrial Automation (ICAMIMIA)*, Batu, 2019.

[30] K. D. Young, V. I. Utkin and Ü. Özgüner, "A Control Engineer's Guide to Sliding Mode Control," *IEEE Transactions on Control Systems Technology,* vol. 7, no. 3, pp. 328-342, 1999.

[31] K.-K. Young, P. V. Kokotovich and V. I. Utkin, "A singular perturbation analysis of high-gain feedback systems," *IEEE Transactions on Automatic Control,* vol. 22, no. 6, pp. 931-938, 1977.

[32] J. J. Slotine and S. S. Sastry, "Tracking control of non-linear systems using sliding surfaces with application to robot manipulators," in *1983 American Control Conference*, San Francisco CA, 1983.

[33] J. A. Burton and A. S. I. Zinober, "Continuous approximation of variable structure control," *International Journal of Systems Science,* vol. 17, no. 6, pp. 875-885, 1986.

[34] A. G. Bondarev, S. A. Bondarev, N. E. Kostyleva and V. I. Utkin, "Sliding modes in systems with asymptotic state observers," *Automation and Remote Control,* vol. 46, pp. 679-684, 1985.

[35] H. G. Kwatny and K.-K. D. Young, "The variable structure servomechanism," *Systems and Control Letters,* vol. 1, no. 3, pp. 184-191, 1981.

[36] K. D. Young and S. V. Drakunov, "Discontinuous Frequency Shaping Compensation for Uncertain Dynamic Systems," *IFAC Proceedings Volumes,* vol. 26, no. 2, pp. 207-210, 1993.

[37] İ. Haskara, C. Hatipoğlu and Ü. Özgüner, "Sliding Mode Compensation, Estimation and Optimization Methods in Automotive Control," in *Variable Structure Systems: Towards the 21st Century*, Springer, 2002, pp. 155-174.

[38] B. Kürkçü, C. Kasnakoğlu and M. Ö. Efe, "Disturbance/Uncertainty Estimator Based Integral Sliding-Mode Control," *IEEE Transactions on Automatic Control,* vol. 63, no. 11, pp. 3940-3947, 2018.

[39] P. B. Sujit, S. Saripalli and J. Sousa, "An Evaluation of UAV Path Following Algorithms," in *2013 European Control Conference (ECC)*, Zurich, 2013.

[40] S. Park, J. Deyst and J. P. How, "Performance and Lyapunov Stability of a Nonlinear Path-Following Guidance Method," *Journal of Guidance, Control, and Dynamics,* vol. 30, no. 6, pp. 1718-1728, 2007.

[41] D. R. Nelson, D. B. Barber, T. W. McLain and R. W. Beard, "Vector Field Path Following for Miniature Air Vehicles," *IEEE Transactions on Robotics,* vol. 23, no. 3, pp. 519-529, 2007.

[42] A. Ratnoo, P. B. Sujit and M. Kothari, "Adaptive Optimal Path Following for High Wind Flights," in *IFAC World Congress*, Milano, 2011.

[43] H. Tiftikçi, "Vektör Alanı ile Eğrilerin Takibi ve Seyrüsefer," in *VII. ULUSAL HAVACILIK VE UZAY KONFERANSI*, Samsun, 2018.

[44] Mathworks, "mathworks.com," Mathworks, [Online]. Available: https://www.mathworks.com/help/aeroblks/about-aerospace-coordinate-systems.html. [Accessed 18 10 2022].

[45] P. Serra, Image-Based Visual Servo Control of Aerial Vehicles (Phd Thesis), Lisbon: University of Lisbon, 2016.

[46] G. Verzichelli, "Development of an Aircraft Landing Gears Model with Steering System in Modelica-Dymola," The Modelica Association, 2008.

[47] B. L. Stevens and F. L. Lewis, Aircraft Control and Simulation, New York: John Wiley and Sons Inc., 1992.

[48] J. C. D. van Zundert, "Direction cosine matrix based IMU implementation in Matlab/Simulink," Eindhoven University of Technology, Eindhoven, 2013.

[49] "depositphotos," [Online]. Available: https://tr.depositphotos.com/7305199/stock-photo-monte-real-portugal-april-7.html. [Accessed 22 01 2023].

[50] E. Muir and D. Moormann, "Description of the HIRM Model," in *Robust Flight Control Design Challenge Problem Formulation and Manual: the High Incidence Research Model (HIRM)*, Group for Aeronautical Research and Technology in Europe (GARTEUR), 1997, pp. 5-25.

[51] Mathworks Inc., "Mathworks Help Center," Mathworks Inc., [Online]. Available: https://www.mathworks.com/help/aeroblks/drydenwindturbulencemodelcontinuous.html. [Accessed 21 October 2022].

[52] İ. Gümüşboğa and A. İftar, "Aircraft Trim Analysis by Particle Swarm Optimization," *Journal of Aeronautics and Space Technologies (JAST),* vol. 12, no. 2, pp. 185-196, 2019.

[53] Wikipedia, "Wikipedia," [Online]. Available: https://en.wikipedia.org/wiki/Secant_method#/media/File:Secant_method.svg. [Accessed 25 10 2022].

[54] H. Aktan, F-16 flight control system design by using continuous time generalized predictive control (Master's Thesis), Ankara: Hacettepe University, 2018.

[55] E. Kutluay and E. Hatipoğlu, "Geometric Path Planning for Parallel Parking and Relevant Parameters," *Advances in Automotive Engineering,* vol. 2, no. 1, pp. 1-14, 2021.

[56] S. Martin, "boldmethod.com," [Online]. Available: https://www.boldmethod.com/learn-to-fly/regulations/runway-markings-and-spacing-fly-better-patterns-to-landing-explained/. [Accessed 29 March 2022].

[57] Y. Shtessel, C. Edwards, L. Fridman and A. Levant, Sliding Mode Control and Observation, New York, Heidelberg, Dordrecht, London: Springer, 2014.

[58] US Dept. of Defence, "Military Specification Flying Qualities of Piloted Airplanes (MIL-F 8785)," US Dept. of Defence, 1980.

[59] C. Brezinski and J. Van Iseghem, "Pade Approximations," in *Handbook of Numerical Analysis*, Lille, Elsevier, 2005, pp. 47-222.

[60] Mathworks, "mathworks.com," Mathworks, [Online]. Available: https://www.mathworks.com/help/control/ref/pade.html. [Accessed 5 11 2022].

[61] Mathworks, "mathworks.com," Mathworks, [Online]. Available: https://www.mathworks.com/help/simulink/slref/anti-windup-control-using-a-pid-controller.html. [Accessed 5 11 2022].

[62] W. B. Cleveland, "NASA Technical Note TN D-8331 FIRST-ORDER-HOLD INTERPOLATION DIGITAL-TO-ANALOG CONVERTER WITH APPLICATION TO AIRCRAFT SIMULATION," NASA, Moffett Field CA., 1976.

[63] B. L. Stevens and F. L. Lewis, Aircraft Control and Simulation, New York: John Wiley and Sons Inc., 1992.

12. PUBLICATIONS

[1] S. Avşar and E. Kutluay, “Muharip Hava Aracının İniş Esnasında Yer Dinamiğinin Modellenmesi” in *10. Savunma Teknolojileri Kongresi*, pp. 725-740, Ankara, Turkey, 2022.

[2] S. Avşar and E. Kutluay, “Muharip Hava Aracı Otomatik İniş Koşusu İçin Güdüm Algoritmalarının Karşılaştırılması” in *Otomatik Kontrol Türk Ulusal Kongresi*, Elazığ, Turkey, 2022.

13. APPENDIX

13.1 APPENDIX 1 (Aerodynamics Model of F-16)

Ranges of the validity of the model are shown in Figure 13.1. Model polynomials are shown in Figure 13.2. Parameter values are shown in Figure 13.3. Equations for the aerodynamics coefficients are also shown in equations 13.1 to 13.7. Here, α, β, δ_e, δ_a, and δ_r denote angle of attack, angle of sideslip, elevator deflection, aileron deflection and rudder deflection respectively. Other parameters are explained in Table 13.1.

Table 13.1 Nomenclature of aerodynamics model

α	Angle of attack
β	Sideslip angle
δ_e	Elevator deflection
δ_a	Aileron deflection
δ_r	Rudder deflection
C_x	Force coefficient in x body axis direction
C_y	Force coefficient in y body axis direction
C_z	Force coefficient in z body axis direction
C_l	Moment coefficient in x body axis direction
C_m	Moment coefficient in y body axis direction
C_n	Moment coefficient in z body axis direction
p	Angular velocity component in x body axis direction
q	Angular velocity component in y body axis direction
r	Angular velocity component in z body axis direction
b	Wingspan
$\overline{c}$	Mean aerodynamic chord
V	True airspeed

Lower Bound	Variable	Lower Bound
–0.1745 rad (–10 deg)	α	0.7854 rad (45 deg)
–0.5236 rad (–30 deg)	β	0.5236 rad (30 deg)
–0.4363 rad (–25 deg)	δ_e	0.4363 rad (25 deg)
–0.3752 rad (–21.5 deg)	δ_a	0.3752 rad (21.5 deg)
–0.5236 rad (–30 deg)	δ_r	0.5236 rad (30 deg)

Figure 13.1 Ranges of the validity of the F-16 aerodynamics model [8].

$$C_x = C_x(\alpha, \delta_e) + C_{x_q}(\alpha)\tilde{q} \tag{13.1}$$

$$C_y = C_y(\beta, \delta_a, \delta_r) + C_{y_p}(\alpha)\tilde{p} + C_{y_r}(\alpha)\tilde{r} \tag{13.2}$$

$$C_z = C_z(\alpha, \beta, \delta_e) + C_{z_q}(\alpha)\tilde{q} \tag{13.3}$$

$$C_l = C_l(\alpha, \beta) + C_{l_p}(\alpha)\tilde{p} + C_{l_r}(\alpha)\tilde{r} + C_{l_{\delta_a}}(\alpha, \beta)\delta_a + C_{l_{\delta_r}}(\alpha, \beta)\delta_r \tag{13.4}$$

$$C_m = C_m(\alpha, \delta_e) + C_{m_q}(\alpha)\tilde{q} + C_z\left(x_{cg_{ref}} - x_{cg}\right) \tag{13.5}$$

$$C_n = C_n(\alpha, \beta) + C_{n_p}(\alpha)\tilde{p} + C_{n_r}(\alpha)\tilde{r} + C_{n_{\delta_a}}(\alpha, \beta)\delta_a + C_{n_{\delta_r}}(\alpha, \beta)\delta_r - C_y\left(x_{cg_{ref}} - x_{cg}\right)\left(\frac{\bar{c}}{b}\right) \tag{13.6}$$

where,

$$\tilde{p} = pb/2V \quad \tilde{q} = q\bar{c}/2V \quad \tilde{r} = rb/2V \tag{13.7}$$

Function	Model Structure
$C_x(\alpha, \delta_e)$	$a_0 + a_1\alpha + a_2\delta_e^2 + a_3\delta_e + a_4\alpha\delta_e + a_5\alpha^2 + a_6\alpha^3$
$C_{x_q}(\alpha)$	$b_0 + b_1\alpha + b_2\alpha^2 + b_3\alpha^3 + b_4\alpha^4$
$C_y(\beta, \delta_a, \delta_r)$	$c_0\beta + c_1\delta_a + c_2\delta_r$
$C_{y_p}(\alpha)$	$d_0 + d_1\alpha + d_2\alpha^2 + d_3\alpha^3$
$C_{y_r}(\alpha)$	$e_0 + e_1\alpha + e_2\alpha^2 + e_3\alpha^3$
$C_z(\alpha, \beta, \delta_e)$	$\begin{pmatrix} f_0 + f_1\alpha + f_2\alpha^2 \\ + f_3\alpha^3 + f_4\alpha^4 \end{pmatrix}(1-\beta^2) + f_5\delta_e$
$C_{z_q}(\alpha)$	$g_0 + g_1\alpha + g_2\alpha^2 + g_3\alpha^3 + g_4\alpha^4$
$C_l(\alpha, \beta)$	$h_0\beta + h_1\alpha\beta + h_2\alpha^2\beta + h_3\beta^2 + h_4\alpha\beta^2 + h_5\alpha^3\beta + h_6\alpha^4\beta + h_7\alpha^2\beta^2$
$C_{l_p}(\alpha)$	$i_0 + i_1\alpha + i_2\alpha^2 + i_3\alpha^3$
$C_{l_r}(\alpha)$	$j_0 + j_1\alpha + j_2\alpha^2 + j_3\alpha^3 + j_4\alpha^4$
$C_{l_{\delta_a}}(\alpha, \beta)$	$k_0 + k_1\alpha + k_2\beta + k_3\alpha^2 + k_4\alpha\beta + k_5\alpha^2\beta + k_6\alpha^3$
$C_{l_{\delta_r}}(\alpha, \beta)$	$l_0 + l_1\alpha + l_2\beta + l_3\alpha\beta + l_4\alpha^2\beta + l_5\alpha^3\beta + l_6\beta^2$
$C_m(\alpha, \delta_e)$	$m_0 + m_1\alpha + m_2\delta_e + m_3\alpha\delta_e + m_4\delta_e^2 + m_5\alpha^2\delta_e + m_6\delta_e^3 + m_7\alpha\delta_e^2$
$C_{m_q}(\alpha)$	$n_0 + n_1\alpha + n_2\alpha^2 + n_3\alpha^3 + n_4\alpha^4 + n_5\alpha^5$
$C_n(\alpha, \beta)$	$o_0\beta + o_1\alpha\beta + o_2\beta^2 + o_3\alpha\beta^2 + o_4\alpha^2\beta + o_5\alpha^2\beta^2 + o_6\alpha^3\beta$
$C_{n_p}(\alpha)$	$p_0 + p_1\alpha + p_2\alpha^2 + p_3\alpha^3 + p_4\alpha^4$
$C_{n_r}(\alpha)$	$q_0 + q_1\alpha + q_2\alpha^2$
$C_{n_{\delta_a}}(\alpha, \beta)$	$r_0 + r_1\alpha + r_2\beta + r_3\alpha\beta + r_4\alpha^2\beta + r_5\alpha^3\beta + r_6\alpha^2 + r_7\alpha^3 + r_8\beta^3 + r_9\alpha\beta^3$
$C_{n_{\delta_r}}(\alpha, \beta)$	$s_0 + s_1\alpha + s_2\beta + s_3\alpha\beta + s_4\alpha^2\beta + s_5\alpha^2$

Figure 13.2 Polynomials for F-16 aerodynamics model [8].

a_0	–1.943367e–02
a_1	2.136104e–01
a_2	–2.903457e–01
a_3	–3.348641e–03
a_4	–2.060504e–01
a_5	6.988016e–01
a_6	–9.035381e–01
b_0	4.833383e–01
b_1	8.644627e+00
b_2	1.131098e+01
b_3	–7.422961e+01
b_4	6.075776e+01
c_0	–1.145916e+00
c_1	6.016057e–02
c_2	1.642479e–01
d_0	–1.006733e–01
d_1	8.679799e–01
d_2	4.260586e+00
d_3	–6.923267e+00
e_0	8.071648e–01
e_1	1.189633e–01
e_2	4.177702e+00
e_3	–9.162236e+00
f_0	–1.378278e–01
f_1	–4.211369e+00
f_2	4.775187e+00
f_3	–1.026225e+01
f_4	8.399763e+00
f_5	–4.354000e–01
g_0	–3.054956e+01
g_1	–4.132305e+01
g_2	3.292788e+02
g_3	–6.848038e+02
g_4	4.080244e+02

h_0	–1.058583e–01
h_1	–5.776677e–01
h_2	–1.672435e–02
h_3	1.357256e–01
h_4	2.172952e–01
h_5	3.464156e+00
h_6	–2.835451e+00
h_7	–1.098104e+00
i_0	–4.126806e–01
i_1	–1.189974e–01
i_2	1.247721e+00
i_3	–7.391132e–01
j_0	6.250437e–02
j_1	6.067723e–01
j_2	–1.101964e+00
j_3	9.100087e+00
j_4	–1.192672e+01
k_0	–1.463144e–01
k_1	–4.073901e–02
k_2	3.253159e–02
k_3	4.851209e–01
k_4	2.978850e–01
k_5	–3.746393e–01
k_6	–3.213068e–01
l_0	2.635729e–02
l_1	–2.192910e–02
l_2	–3.152901e–03
l_3	–5.817803e–02
l_4	4.516159e–01
l_5	–4.928702e–01
l_6	–1.579864e–02
m_0	–2.029370e–02
m_1	4.660702e–02
m_2	–6.012308e–01
m_3	–8.062977e–02
m_4	8.320429e–02
m_5	5.018538e–01
m_6	6.378864e–01
m_7	4.226356e–01

n_0	–5.159153e+00
n_1	–3.554716e+00
n_2	–3.598636e+01
n_3	2.247355e+02
n_4	–4.120991e+02
n_5	2.411750e+02
o_0	2.993363e–01
o_1	6.594004e–02
o_2	–2.003125e–01
o_3	–6.233977e–02
o_4	–2.107885e+00
o_5	2.141420e+00
o_6	8.476901e–01
p_0	2.677652e–02
p_1	–3.298246e–01
p_2	1.926178e–01
p_3	4.013325e+00
p_4	–4.404302e+00
q_0	–3.698756e–01
q_1	–1.167551e–01
q_2	–7.641297e–01
r_0	–3.348717e–02
r_1	4.276655e–02
r_2	6.573646e–03
r_3	3.535831e–01
r_4	–1.373308e+00
r_5	1.237582e+00
r_6	2.302543e–01
r_7	–2.512876e–01
r_8	1.588105–01
r_9	–5.199526e–01
s_0	–8.115894e–02
s_1	–1.156580e–02
s_2	2.514167e–02
s_3	2.038748e–01
s_4	–3.337476e–01
s_5	1.004297e–01

Figure 13.3 Parameter values for F-16 aerodynamics model [8].

13.2 APPENDIX 2 (Verification simulations of aircraft flight dynamics block)

1. Aerodynamics, propulsion, and gravity forces in the model are neglected. The aircraft simulation starts from zero velocity. The expected result is that the aircraft stays at zero velocity when there is no force and no initial velocity. As it can be seen from Figure 13.4 Verification step 1 and Figure 13.5 Verification step 1, all aircraft states remain at zero.

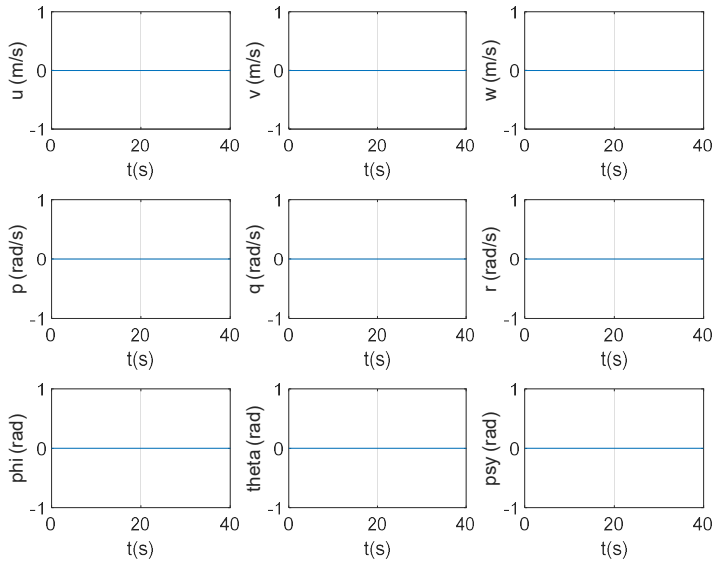

Figure 13.4 Verification step 1

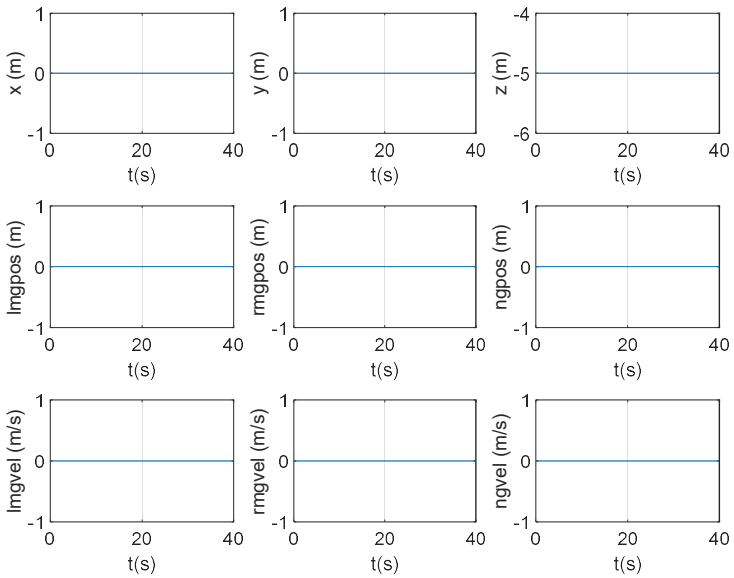

Figure 13.5 Verification step 1

2. Aerodynamics, propulsion, and gravity forces in the model are neglected. The aircraft starts with a translational velocity component. The expected result is that the aircraft stays at the initial velocity when there is no force or moment. As it can be seen from Figure 13.6 and Figure 13.7, the aircraft remains at the initial velocity when there is no force or moment present.

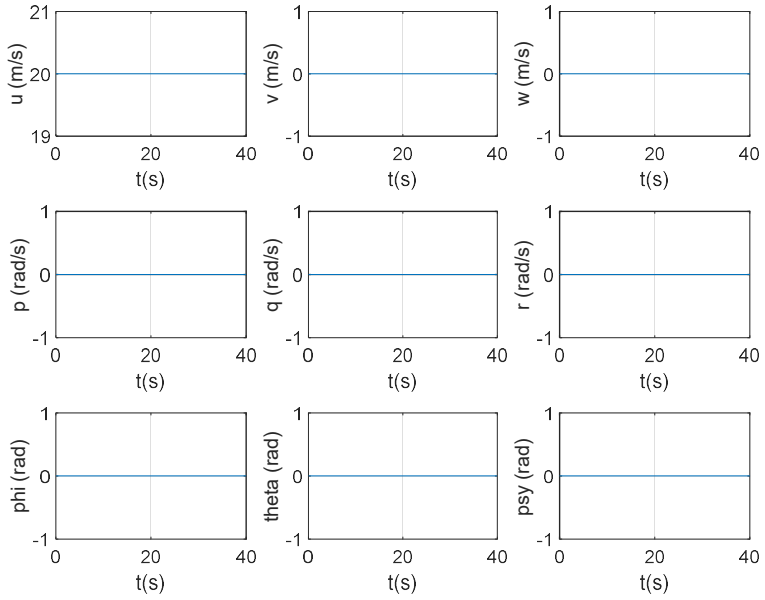

Figure 13.6 Verification step 2

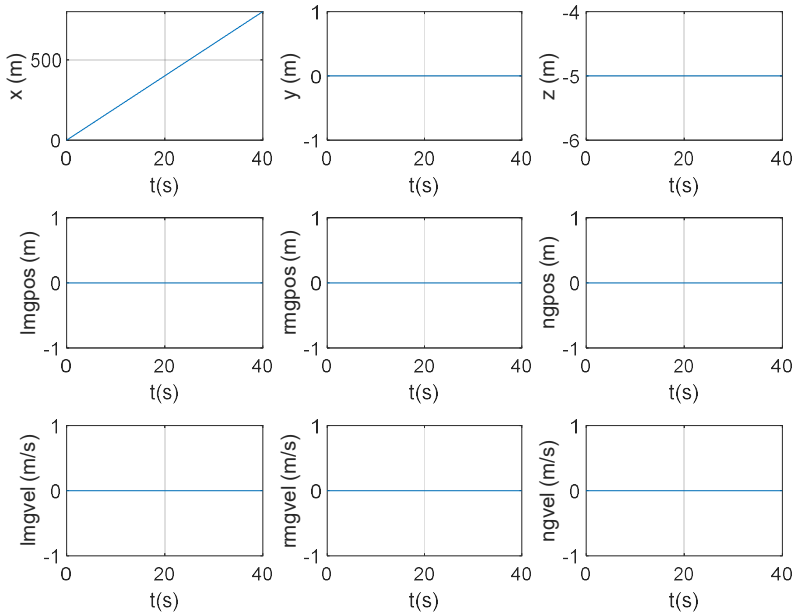

Figure 13.7 Verification step 2

3. Aerodynamics, propulsion, and gravity forces in the model are neglected. The aircraft starts with an angular velocity component. The expected result is that the aircraft stays at the initial angular velocity when there is no force or moment present. In Figure 13.8 and Figure 13.9, the aircraft stays at the initial angular velocity when there is no external force or moment present.

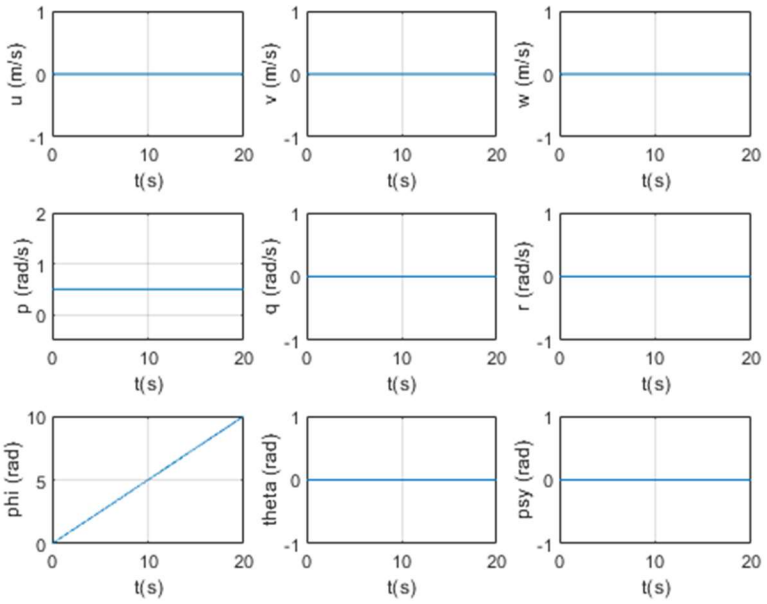

Figure 13.8 Verification step 3

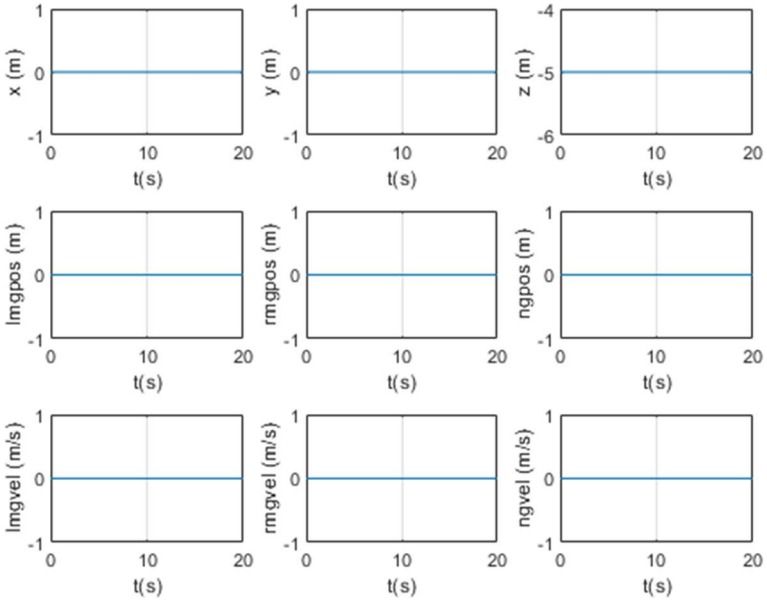

Figure 13.9 Verification step 3

4. Aerodynamics, propulsion, and gravity forces in the model are neglected. The aircraft starts with both translational velocity and angular velocity components. The expected result is that the aircraft stays at the initial angular velocity, and it stays at the initial NED axis velocity when there is no force or moment. In Figure 13.10 and Figure 13.11, the aircraft stays at the initial angular velocity and initial NED axis velocity.

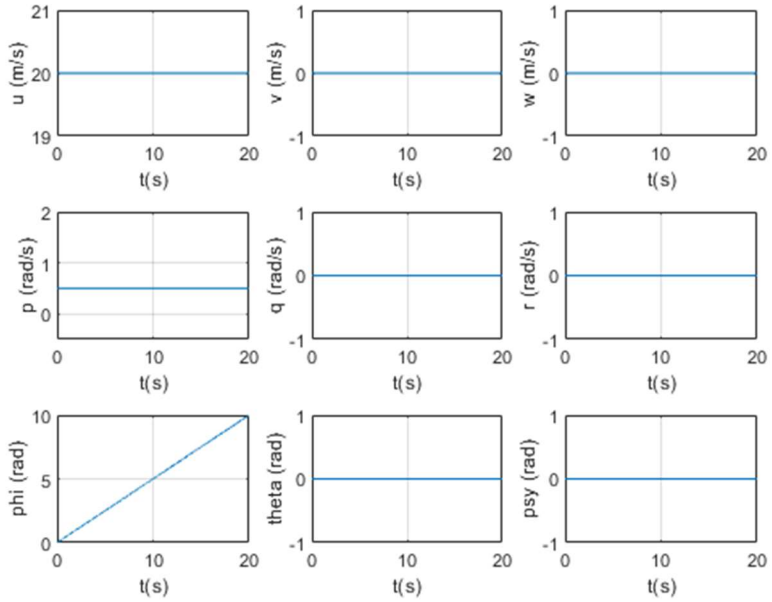

Figure 13.10 Verification step 4

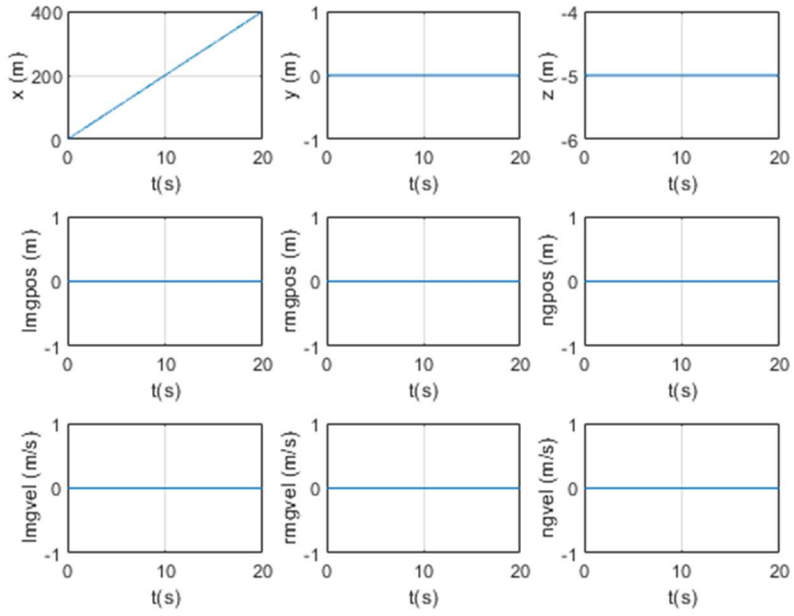

Figure 13.11 Verification step 4

5. Aerodynamics and propulsion blocks in the model are neglected. Gravity block is set working. The aircraft starts from zero velocity. The expected result is that the aircraft accelerates downwards with gravitational acceleration. In Figure 13.12 and Figure 13.13 the aircraft makes a free falling motion just as expected.

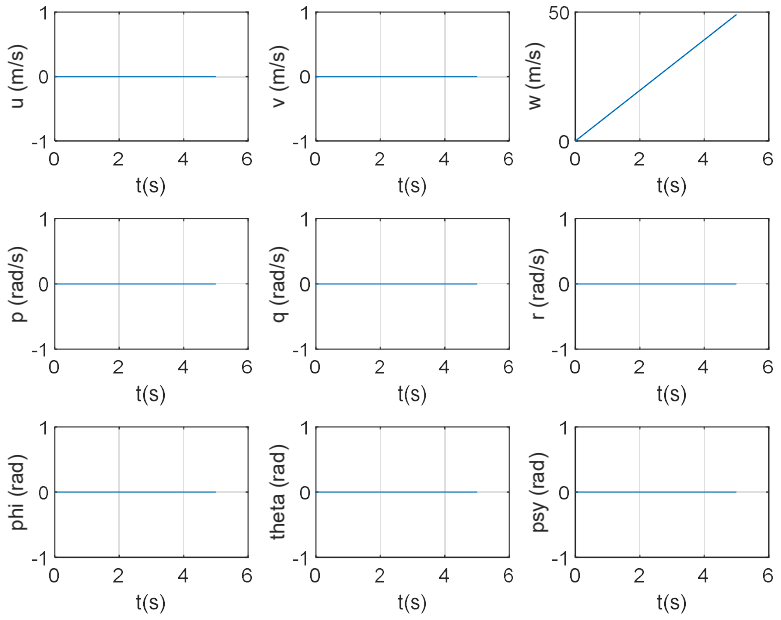

Figure 13.12 Verification step 5

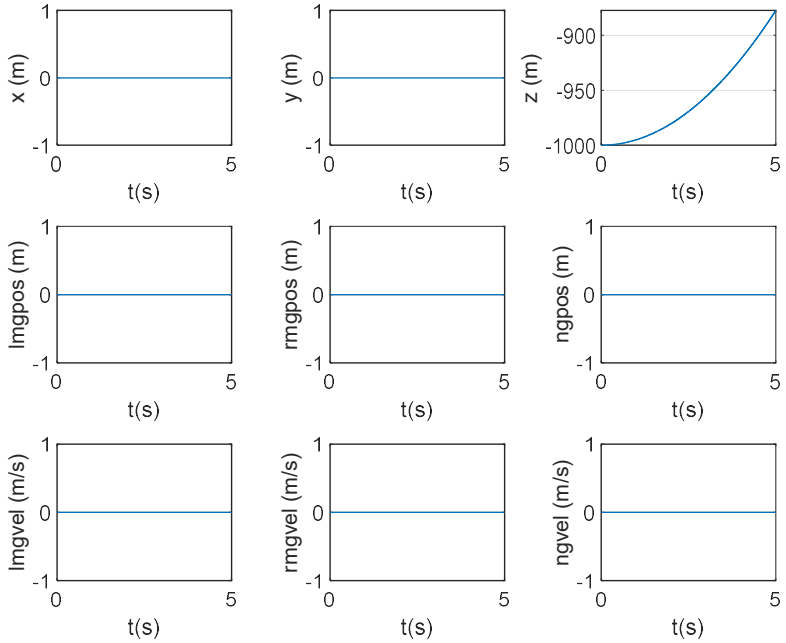

Figure 13.13 Verification step 5

6. Aerodynamics and propulsion blocks in the model are neglected. Gravity block is set working. The aircraft starts with a forward translational velocity parallel to the ground. The expected result is that the aircraft accelerates downwards with gravitational acceleration and the forward NED velocity component stays as the initial value. Results are the same as expected as it can be seen in Figure 13.14 and Figure 13.15.

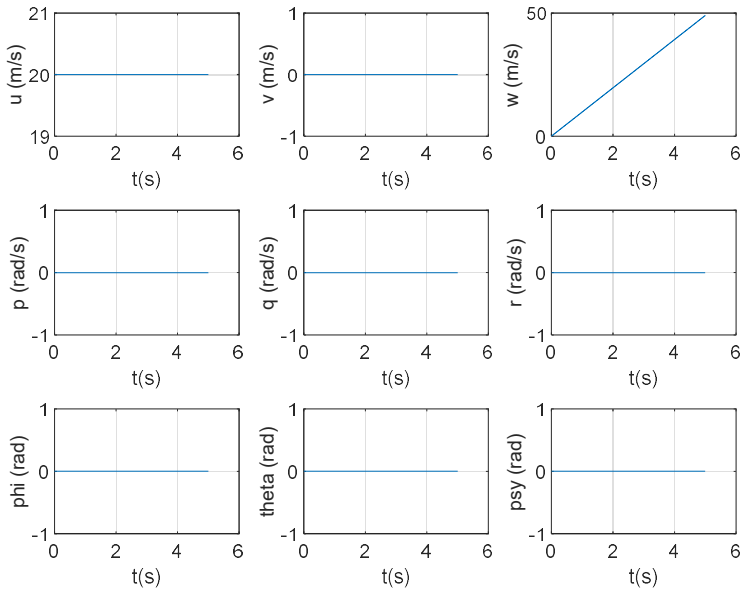

Figure 13.14 Verification step 6

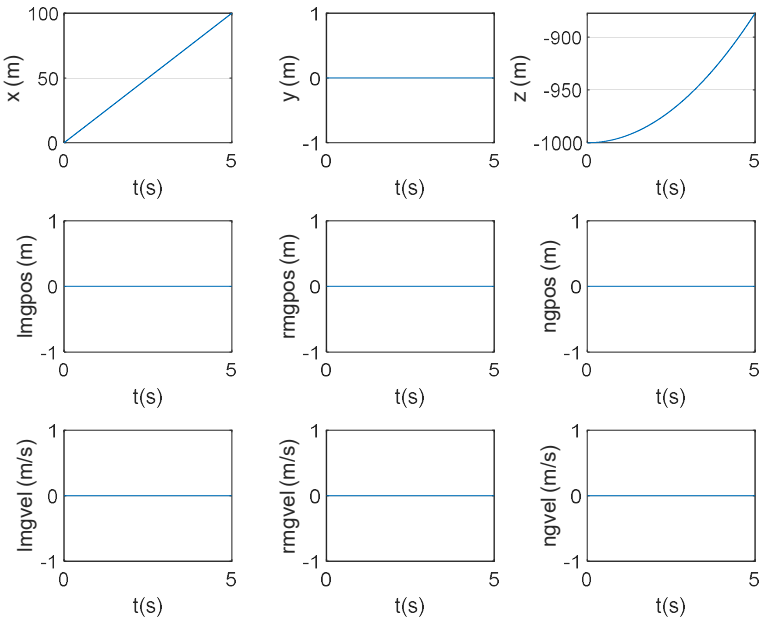

Figure 13.15 Verification step 6

7. Aerodynamics and gravity blocks in the model are neglected. Propulsion forces are set working. Propulsive moments are neglected. The aircraft starts with zero initial velocity and a propulsion force. The expected result is that the aircraft accelerates in the forward direction. Simulation results match the expected results as it can be seen in Figure 13.16 and Figure 13.17.

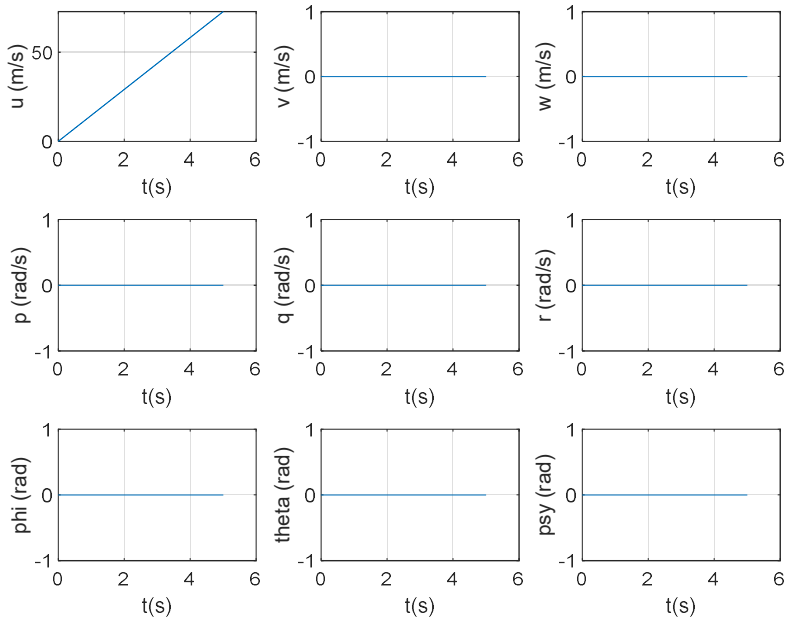

Figure 13.16 Verification step 7

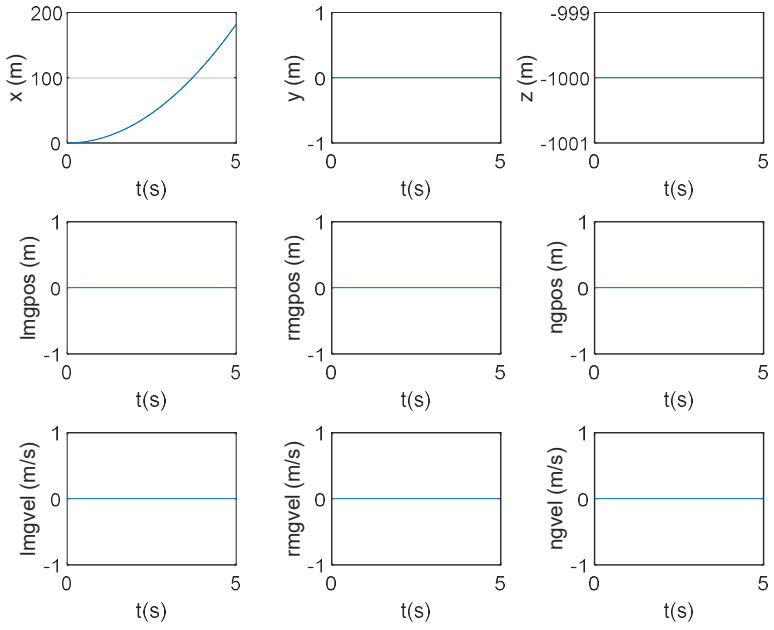

Figure 13.17 Verification step 7

8. Propulsion and gravity blocks in the model are neglected. Aerodynamics forces and moments are set working. The aircraft starts with an initial forward velocity. The expected result is that the aircraft slows down due to the drag force. The aircraft slows down due to the drag force as it is seen in Figure 13.18.

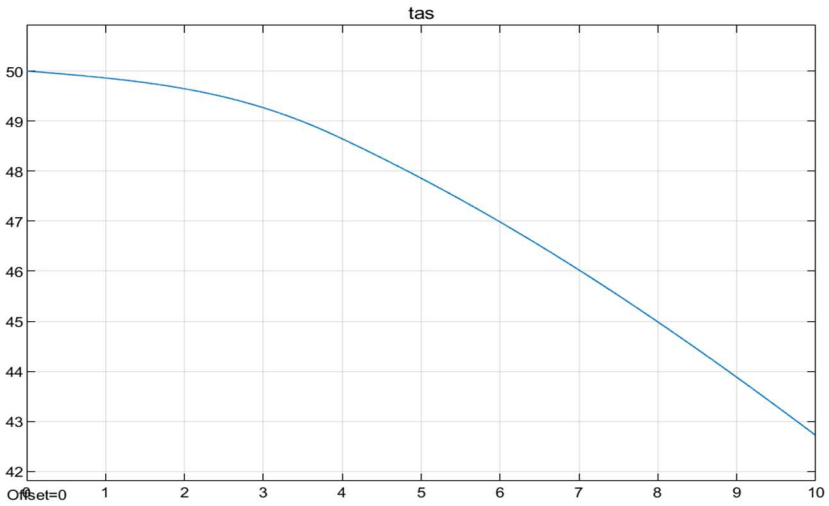

Figure 13.18 Verification step 8

9. Propulsion and gravity blocks in the model are neglected. Aerodynamics forces and moments are set working. The aircraft starts with a forward velocity parallel to the ground and a high angle of attack. The expected result is that the altitude increases and the angle of attack decreases. Results of the simulations are congruent with the expected results as it is seen in Figure 13.19, Figure 13.20, and Figure 13.21.

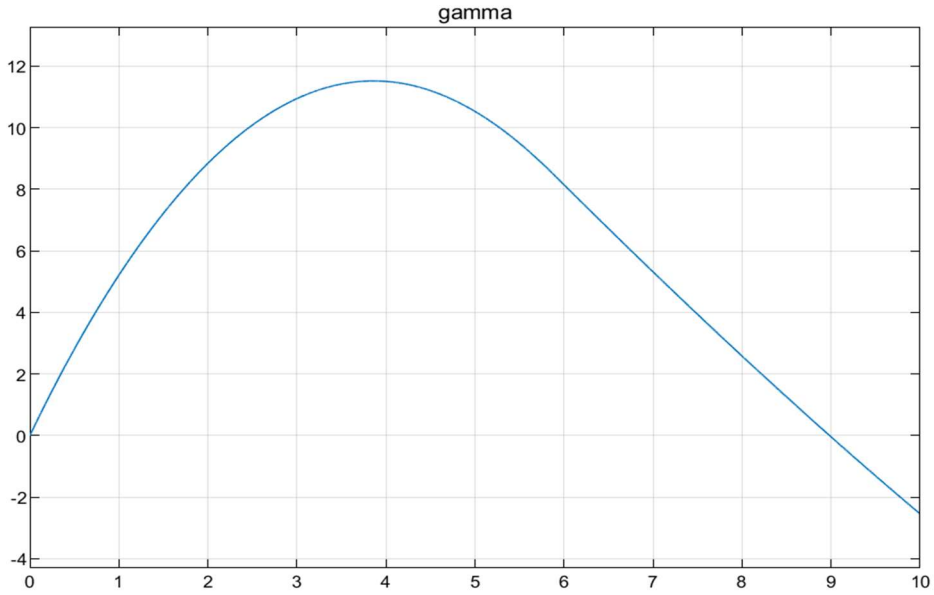

Figure 13.19 Verification step 9

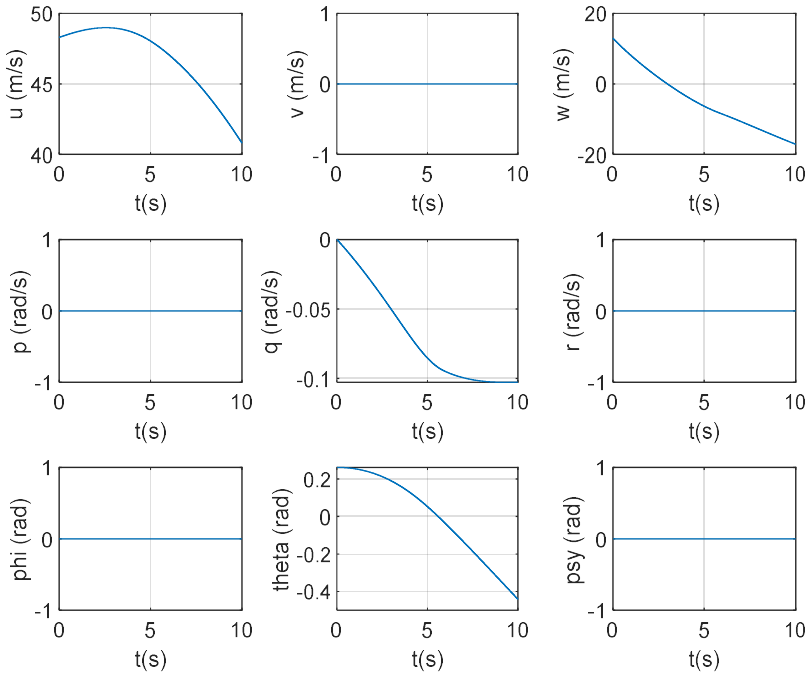

Figure 13.20 Verification step 9

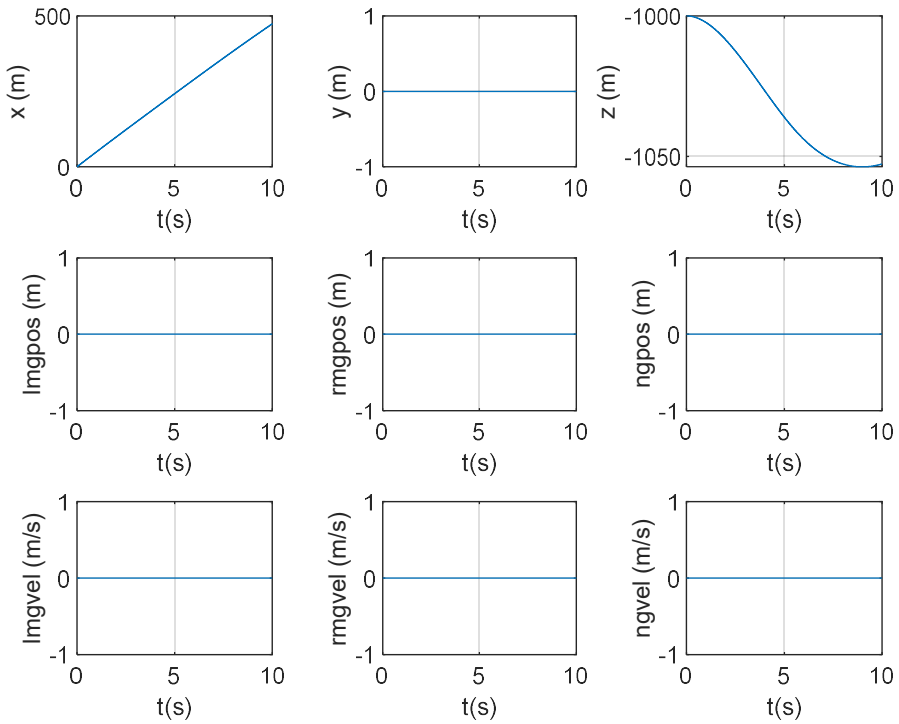

Figure 13.21 Verification step 9

10. Propulsion and gravity blocks in the model are neglected. Aerodynamics forces and moments are set working. The aircraft starts with a forward velocity parallel to the ground and a high angle of sideslip. The expected result is that the heading angle increases, and the sideslip angle decreases. Results are congruent with the expected as it is seen in Figure 13.22.

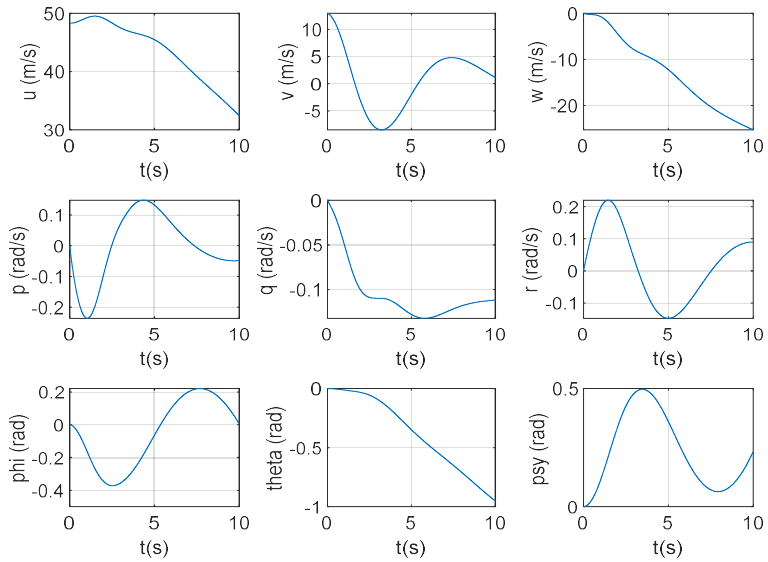

Figure 13.22 Verification step 10

11. Aerodynamics, propulsion, and gravity blocks are set working. The aircraft starts with a positive roll angle and a positive angle of attack. The expected result is that the heading and track angles increase. Results match with the expected as it is seen in Figure 13.23 and Figure 13.24.

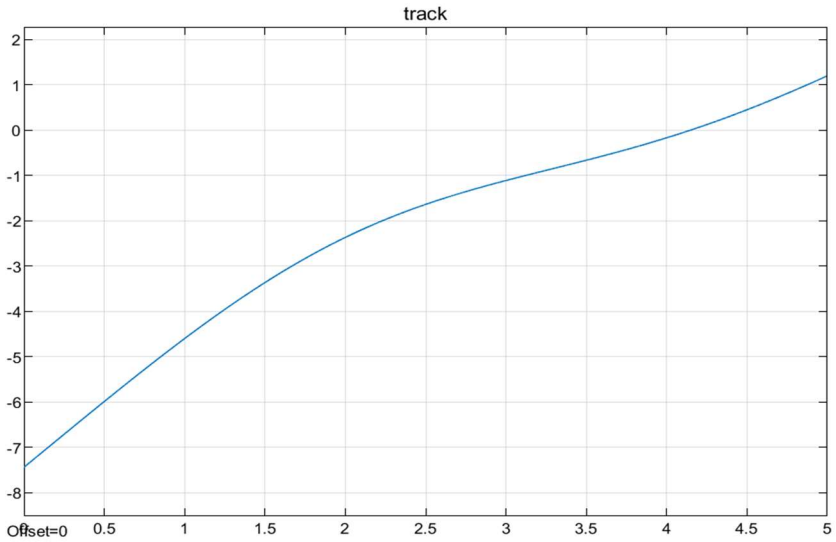

Figure 13.23 Verification step 11

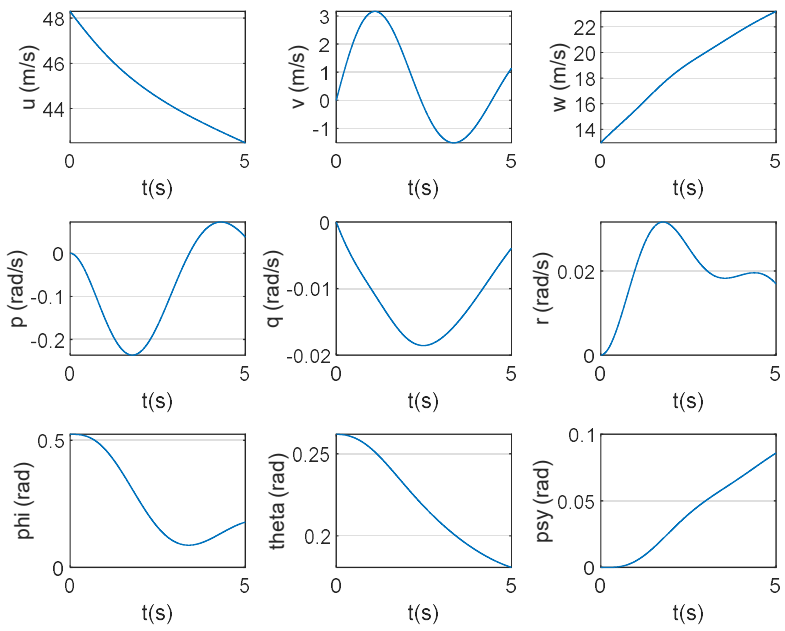

Figure 13.24 Verification step 11

12. Aerodynamics, propulsion, and gravity blocks are set working. The aircraft starts with a forward velocity parallel to the ground. Negative elevator command is given. The expected result is that the pitch angle increases. In Figure 13.25 and Figure 13.26 the pitch angle increases.

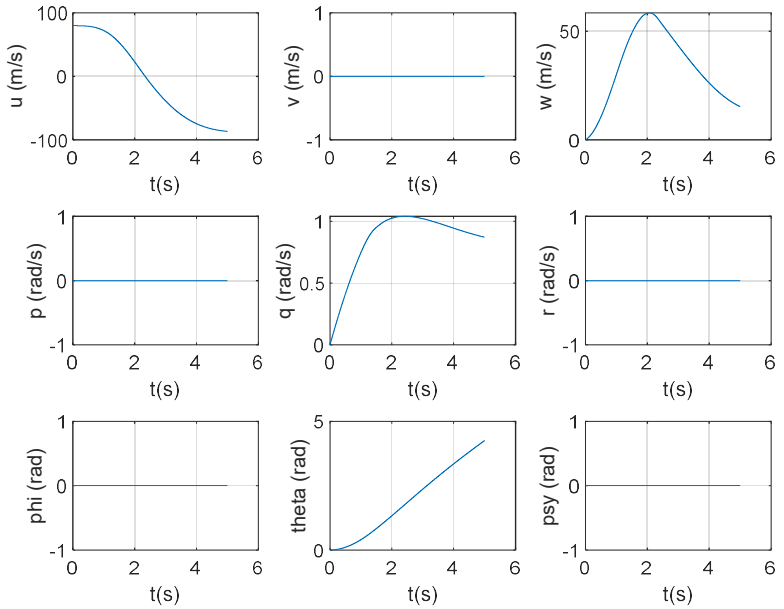

Figure 13.25 Verification step 12

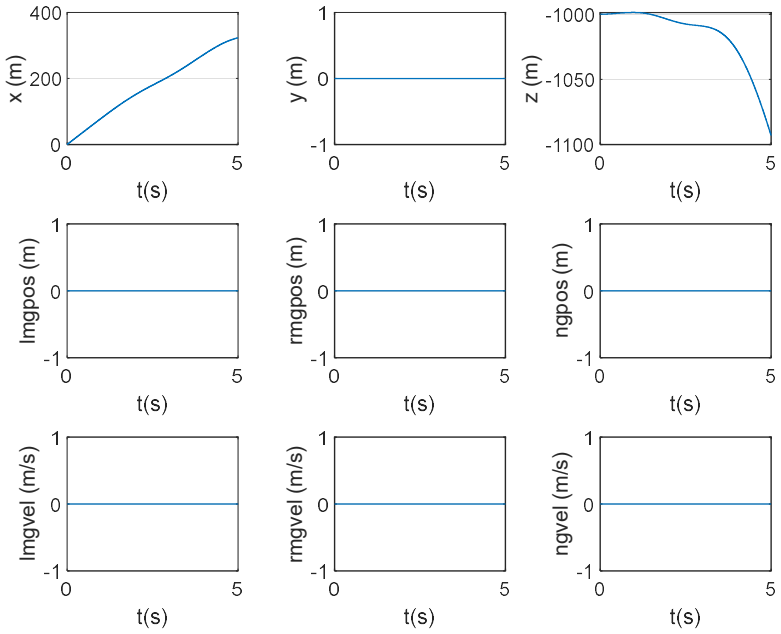

Figure 13.26 Verification step 12

13. Aerodynamics, propulsion, and gravity blocks are set working. The aircraft simulation starts with a forward velocity parallel to the ground. Negative aileron command is given. The expected result is that the roll angle increases. In Figure 13.27, the roll angle increases.

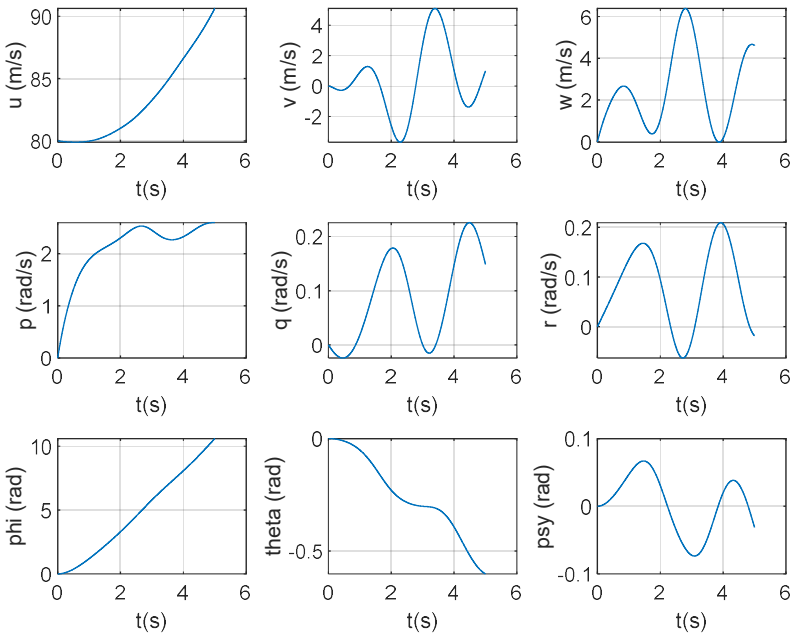

Figure 13.27 Verification step 13

14. Aerodynamics, propulsion, and gravity blocks are set working. The simulation starts with a forward velocity parallel to the ground. Negative rudder command is given. An increase in yaw angle is expected. The yaw angle increases as expected. It can be seen in Figure 13.28 and Figure 13.29.

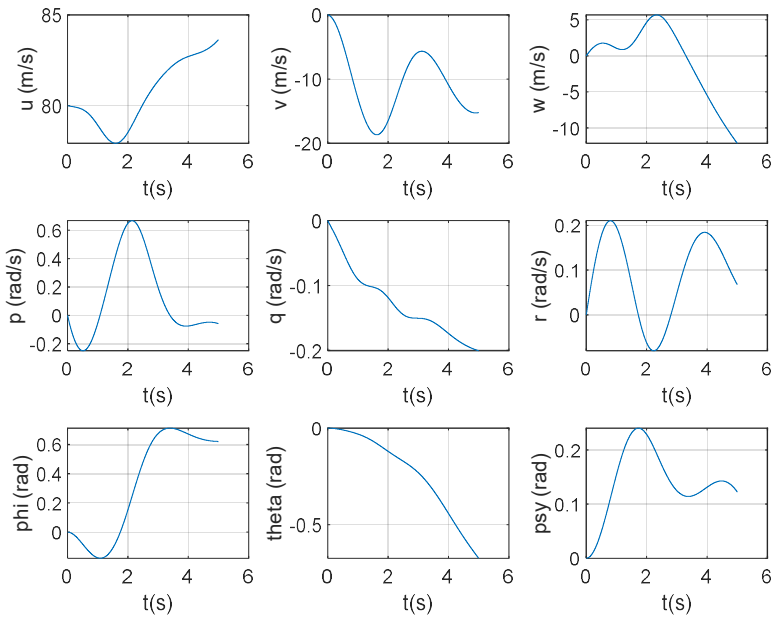

Figure 13.28 Verification step 14

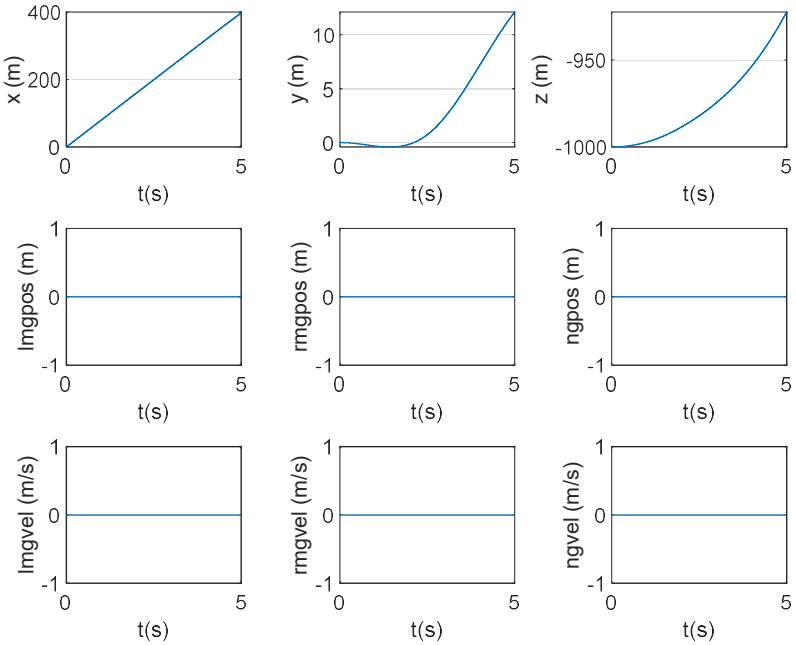

Figure 13.29 Verification step 14

15. Aerodynamics, propulsion, landing gear and gravity blocks are set working. The aircraft simulation starts with zero initial velocity and its landing gears just above the ground. The expected result is that the aircraft falls to the ground, bounces from the ground, and eventually stops. Simulations are coherent with the expected results as they are seen in Figure 13.30 and Figure 13.31.

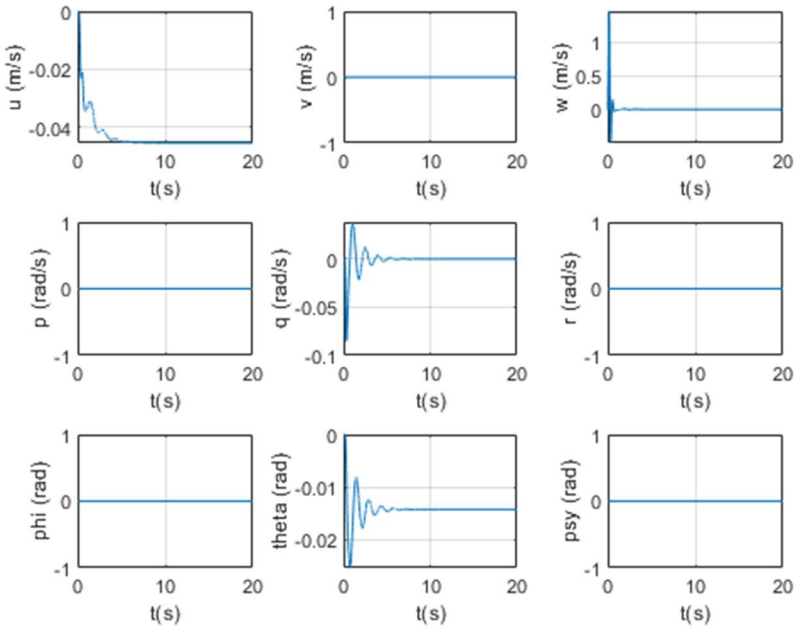

Figure 13.30 Verification step 15

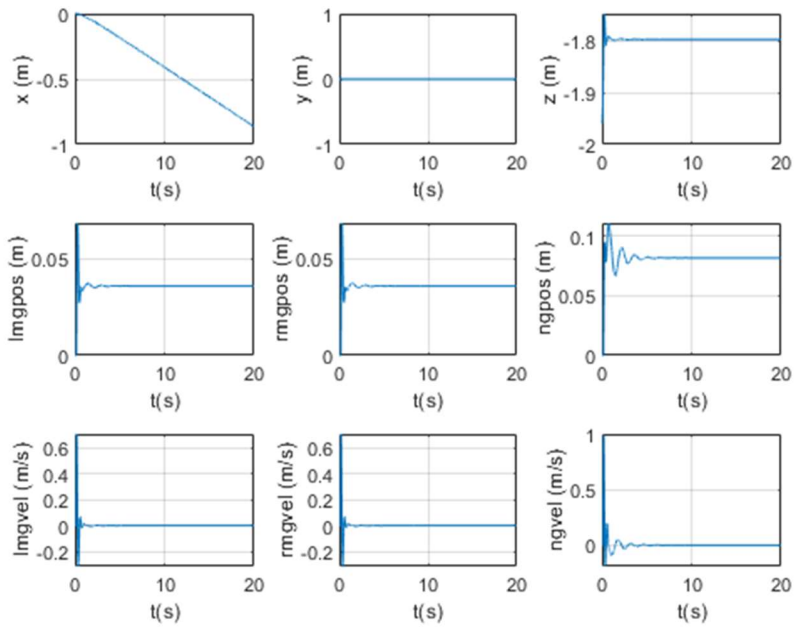

Figure 13.31 Verification step 15

16. Aerodynamics, propulsion, landing gear, and gravity blocks are set working. The aircraft starts with a forward velocity and its landing gears just above the ground. The expected result is that the aircraft falls to the ground and bounces from the ground. Forward velocity should decrease due to the rolling resistance. Results are congruent with the expected behavior as they are seen in Figure 13.32, Figure 13.33 and Figure 13.34.

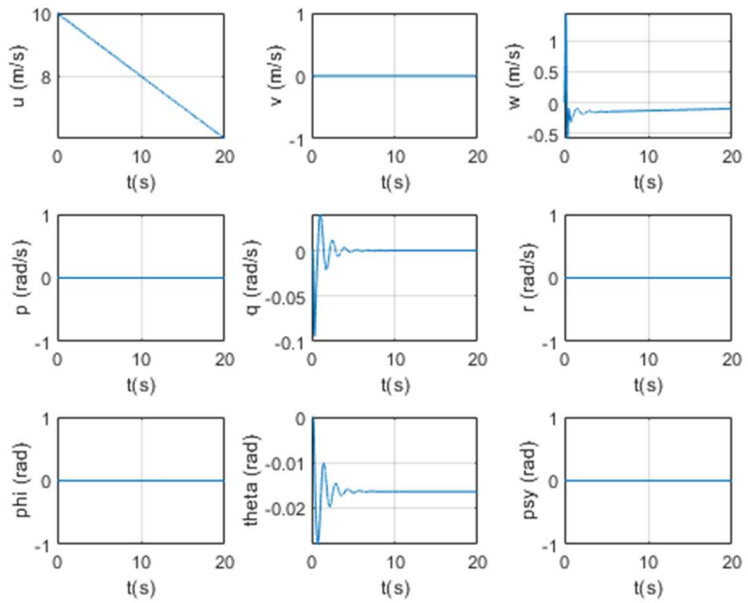

Figure 13.32 Verification step 16

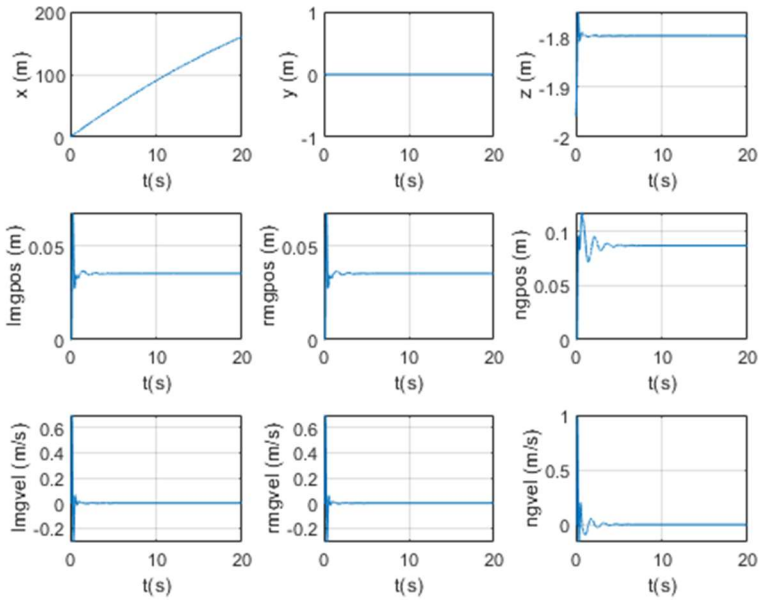

Figure 13.33 Verification step 16

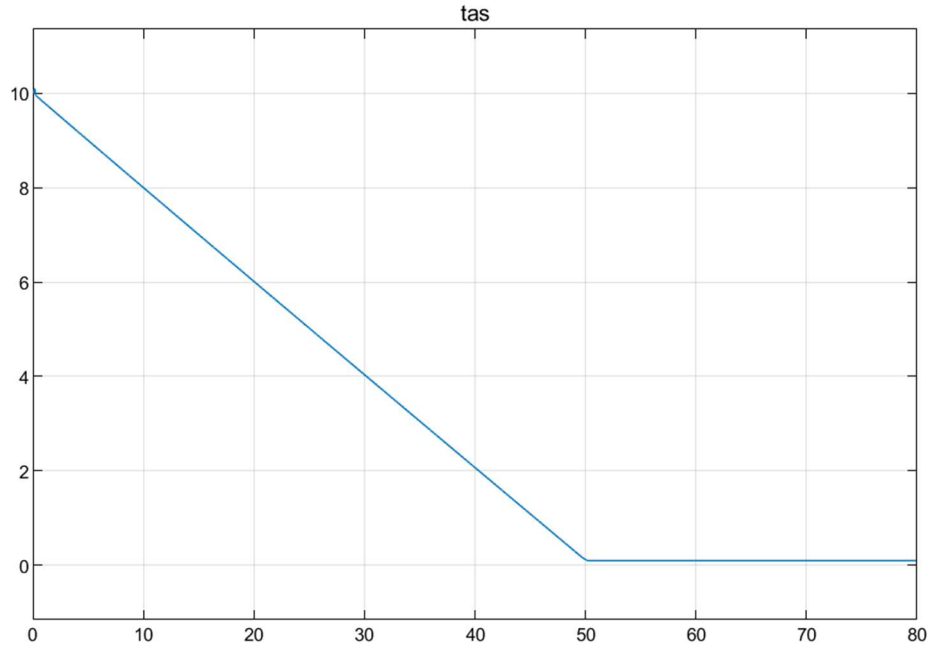

Figure 13.34 Verification step 16

17. Aerodynamics, propulsion, landing gear and gravity blocks are set working. The aircraft starts with a forward velocity on ground. Brakes are activated. Expected result is that the aircraft slows down and stops due to the brakes. The aircraft does indeed slow down and stop as it is seen in Figure 13.35, Figure 13.36 and Figure 13.37.

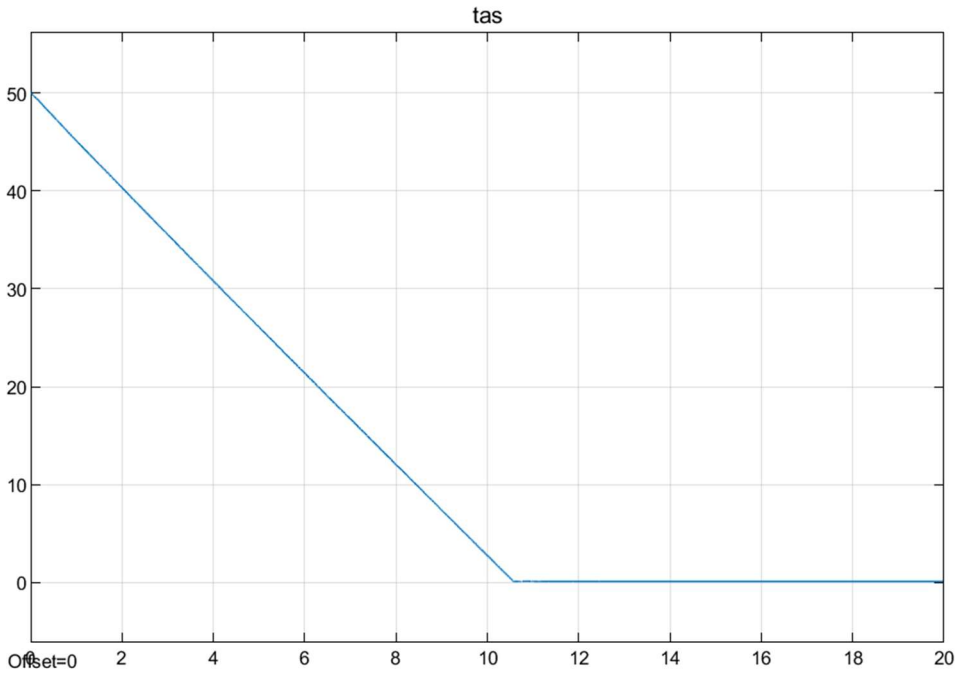

Figure 13.35 Verification step 17

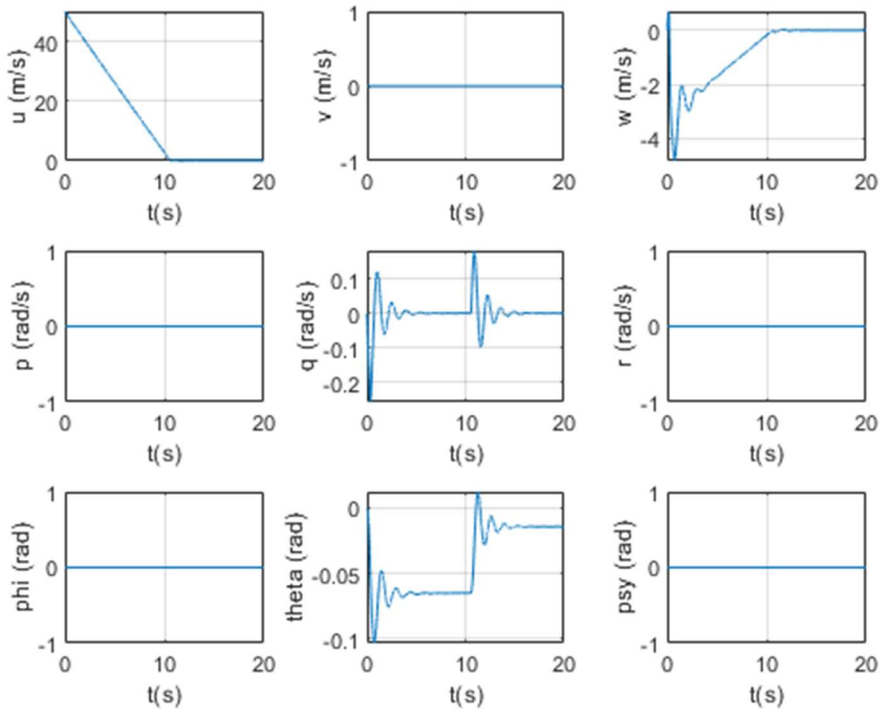

Figure 13.36 Verification step 17

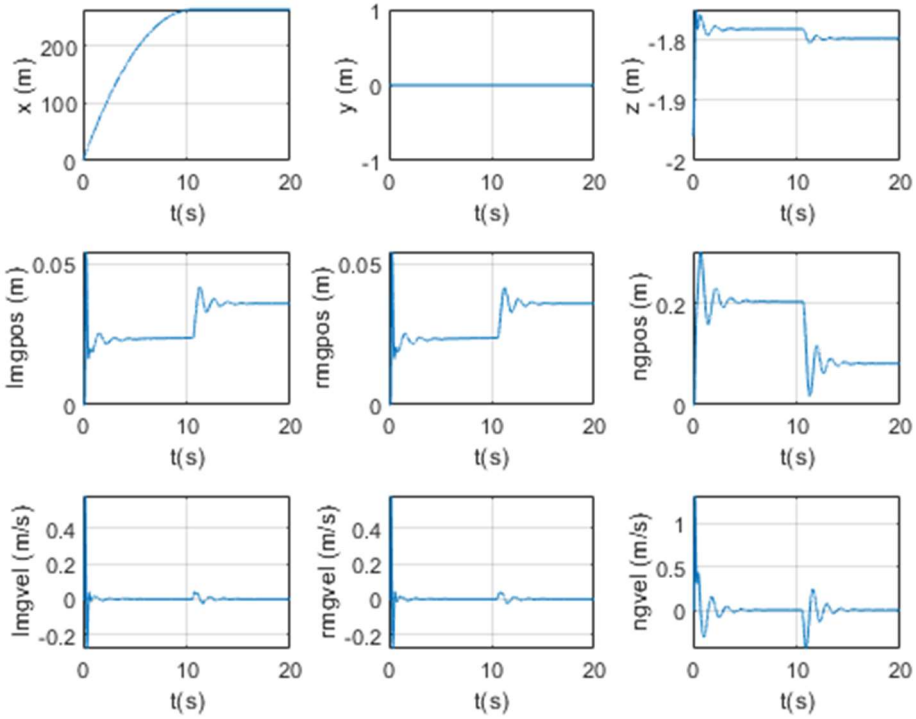

Figure 13.37 Verification step 17

18. Aerodynamics, propulsion, landing gear and gravity blocks are set working. The aircraft starts with a forward velocity on the ground. One of the brakes is activated. The expected result is that the aircraft slows down and stops due to the brake and the aircraft maneuvers to the side with a yaw rate and change its heading and track angle. Results agree with the expectations as they can be seen in Figure 13.38, Figure 13.39 and Figure 13.40.

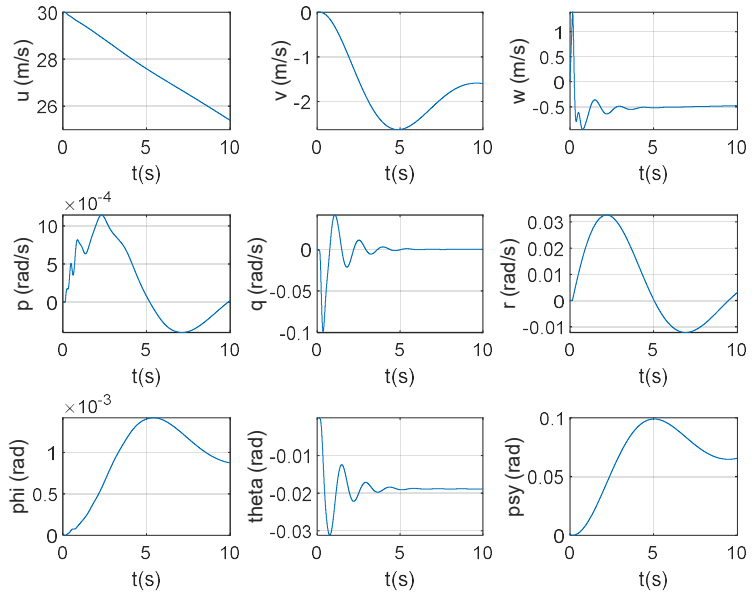

Figure 13.38 Verification step 18

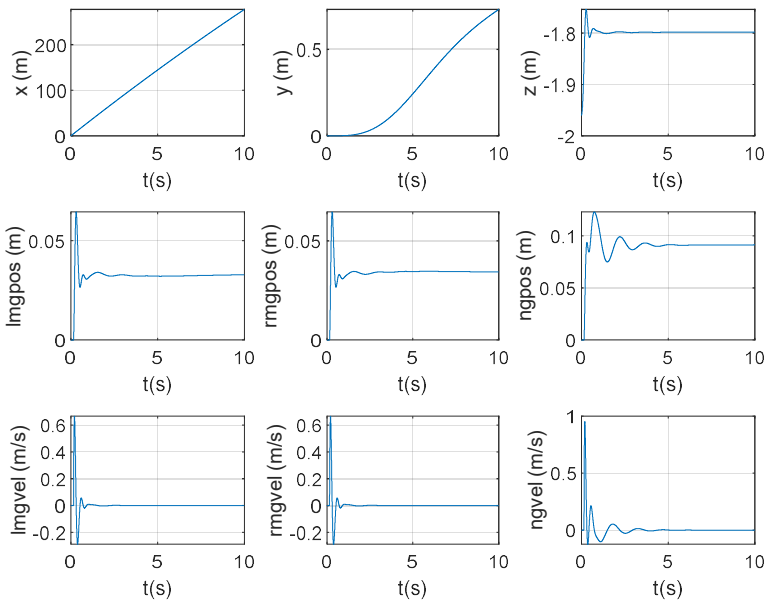

Figure 13.39 Verification step 18

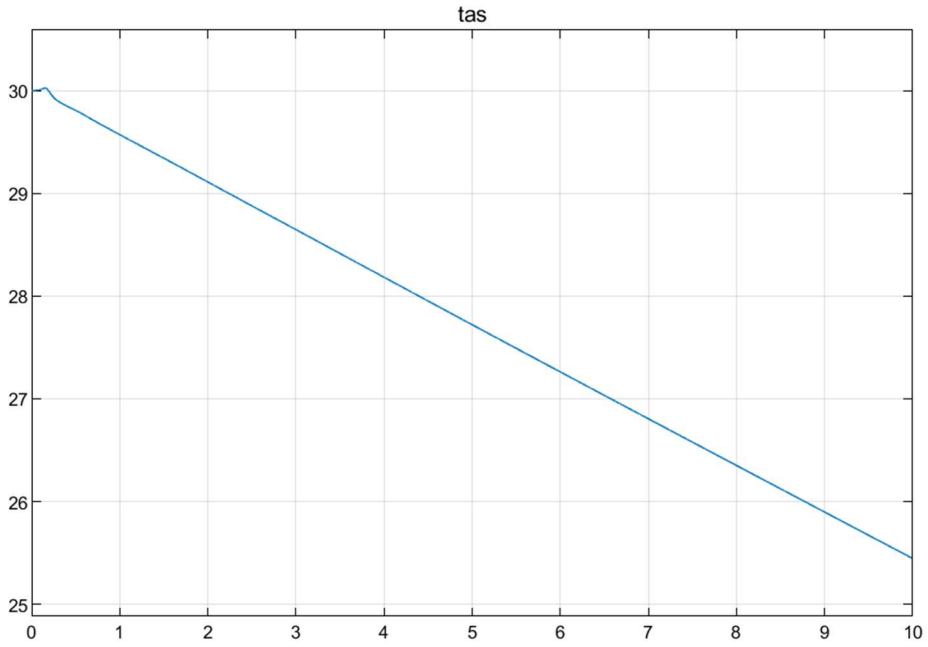

Figure 13.40 Verification step 18

19. Aerodynamics, propulsion, landing gear and gravity blocks are set working. The aircraft starts with a forward velocity on ground. Steering angle input is given. The expected result is that the aircraft maneuvers to the side with a yaw rate and change its heading and track angle. Results are congruent with the expected behavior as they are seen in Figure 13.41 and Figure 13.42.

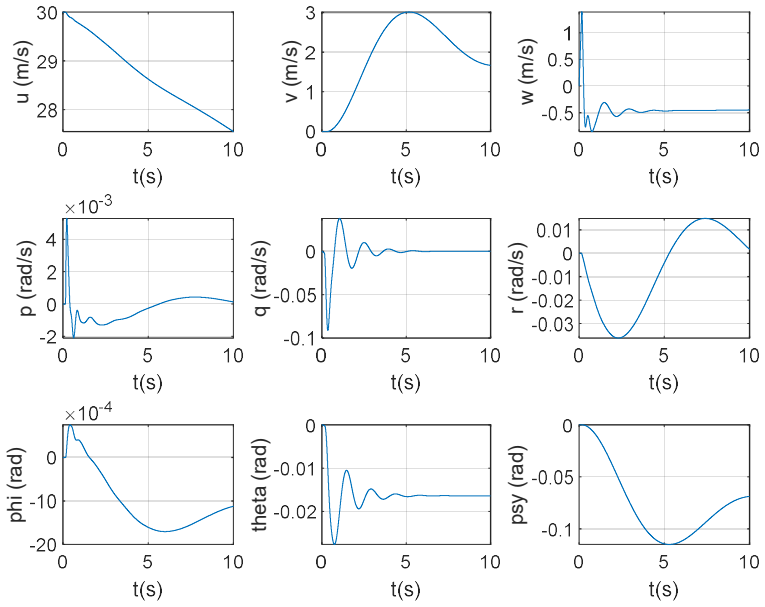

Figure 13.41 Verification step 19

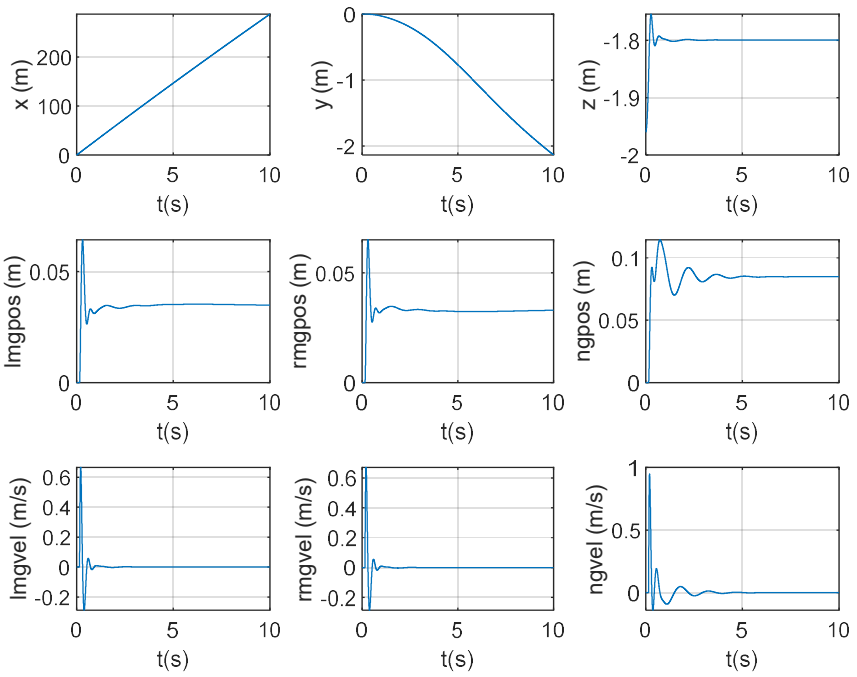

Figure 13.42 Verification step 19

20. Aerodynamics, propulsion, landing gear and gravity blocks are set working. The aircraft starts with a forward velocity on the ground. Throttle input is given. The expected result is that the aircraft accelerates. Results agree with the expected behavior as they are seen in Figure 13.43, Figure 13.44 and Figure 13.45.

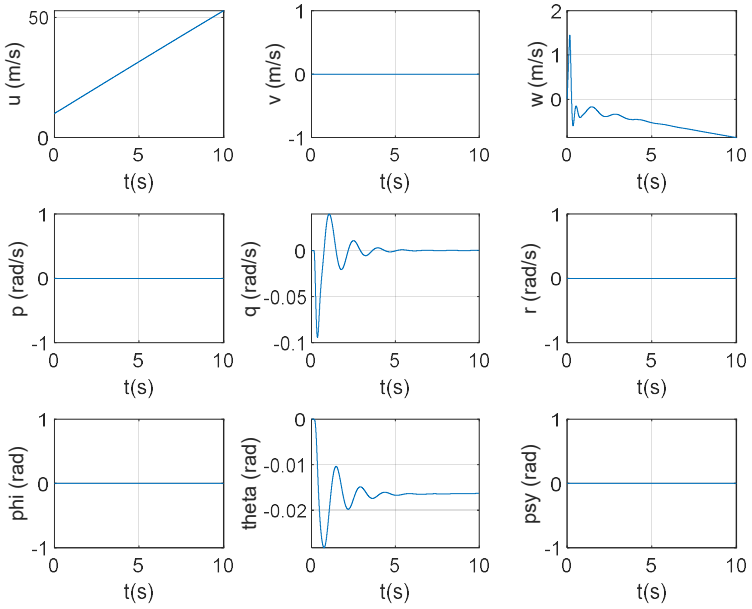

Figure 13.43 Verification step 20

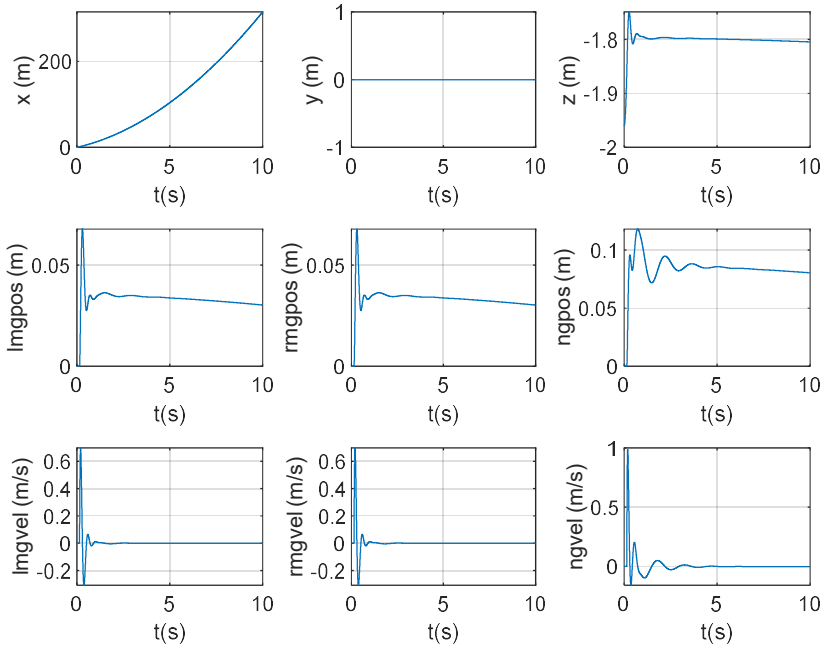

Figure 13.44 Verification step 20

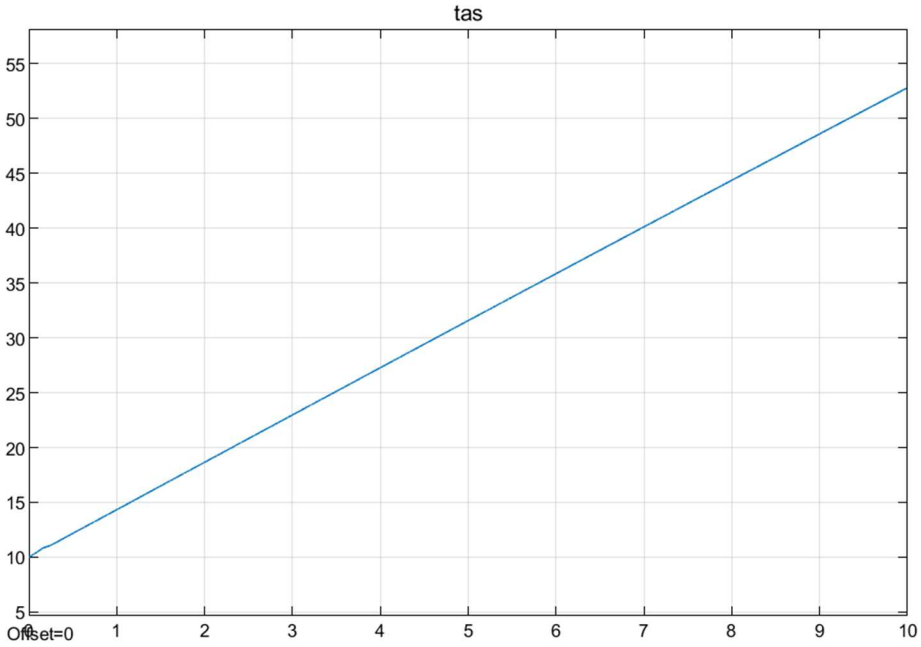

Figure 13.45 Verification step 20

13.3 APPENDIX 3 (Proof of Stability for Pitch SMC)

An example loopbreak is shown in Figure 13.46. Nichols charts for q, θ, and elevator servo loops are shown in Figures Figure 13.47, Figure 13.48, and Figure 13.49.

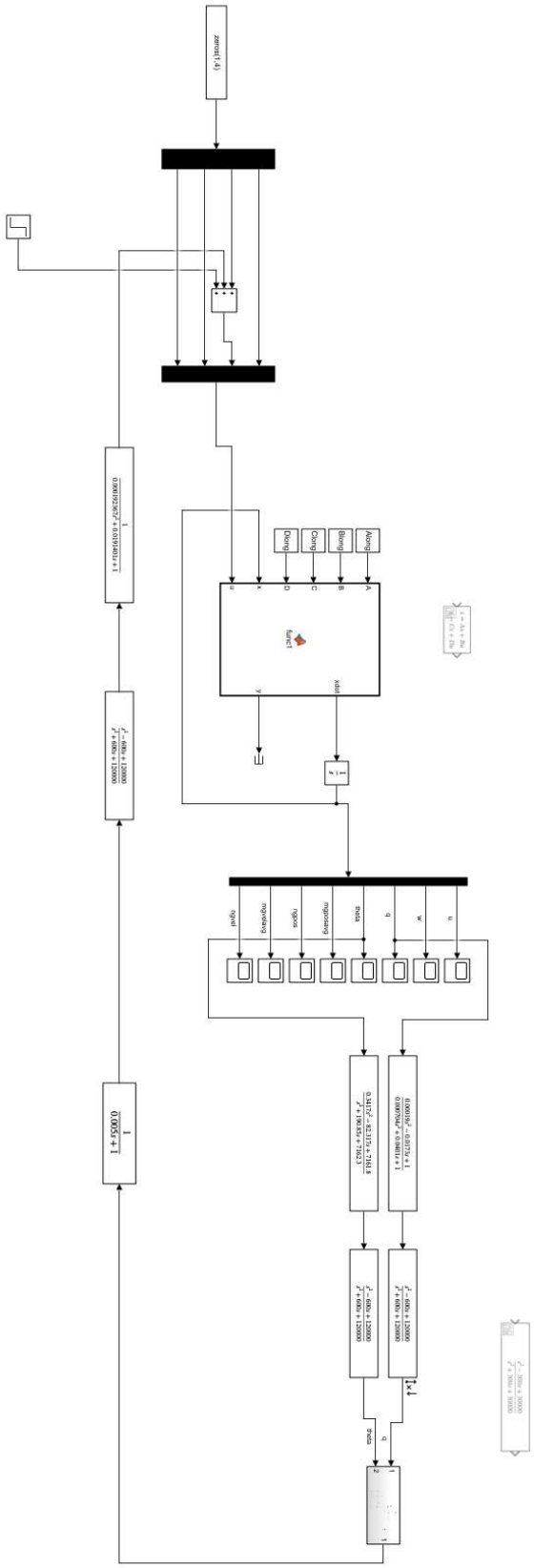

Figure 13.46 q loopbreak for pitch SMC controller

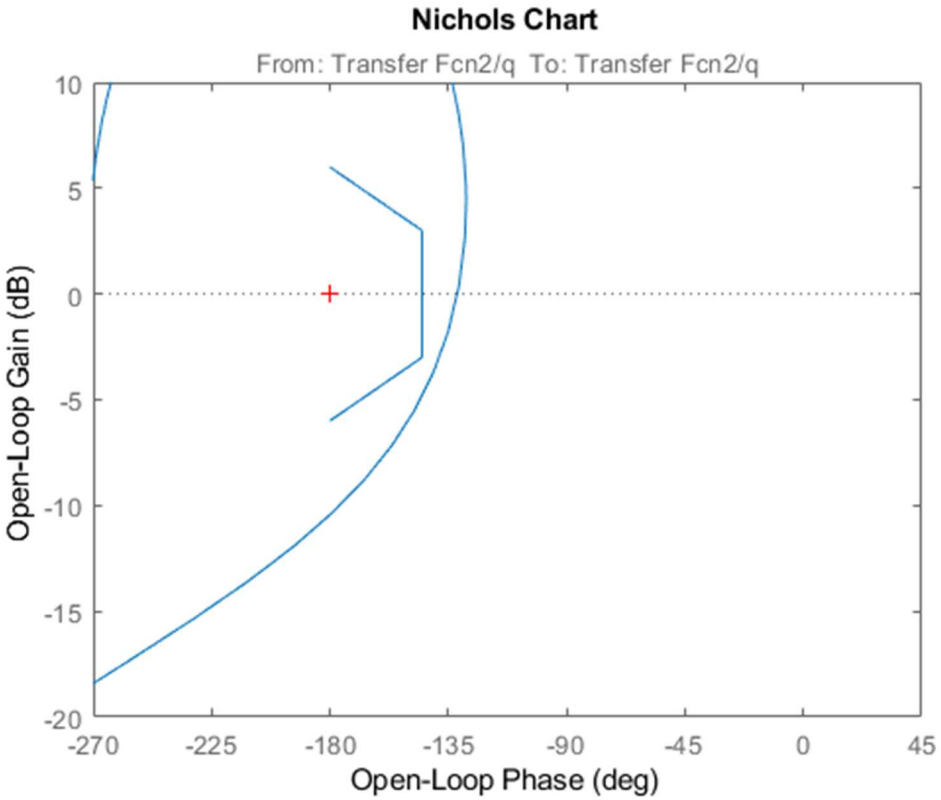

Figure 13.47 q loop for pitch SMC controller

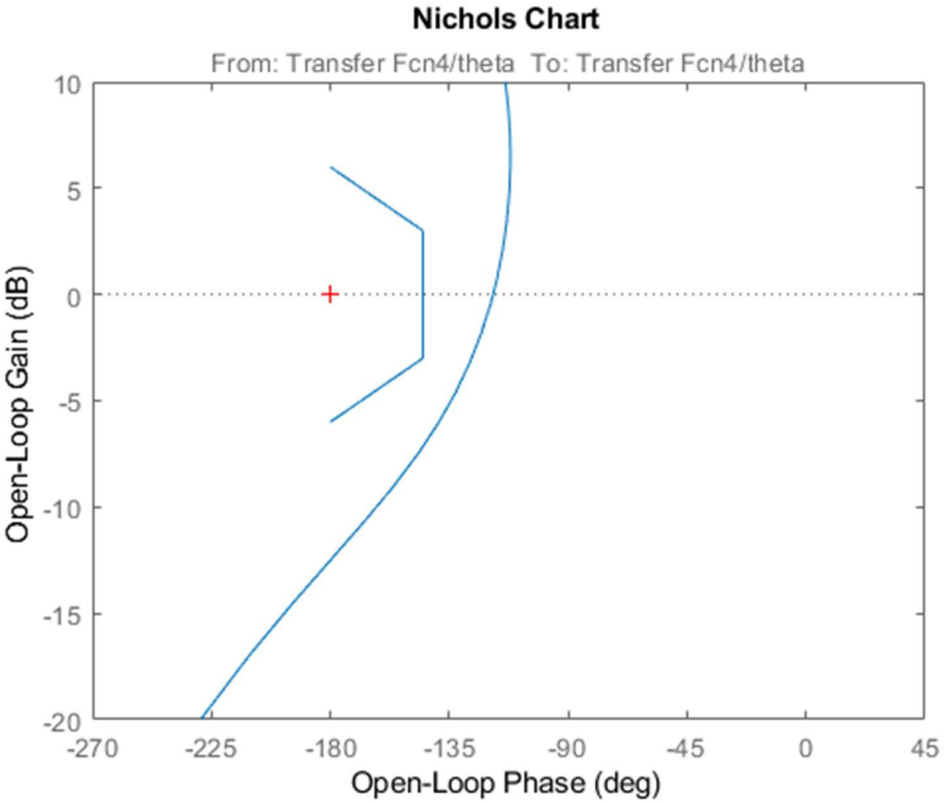

Figure 13.48 theta loop for pitch SMC controller

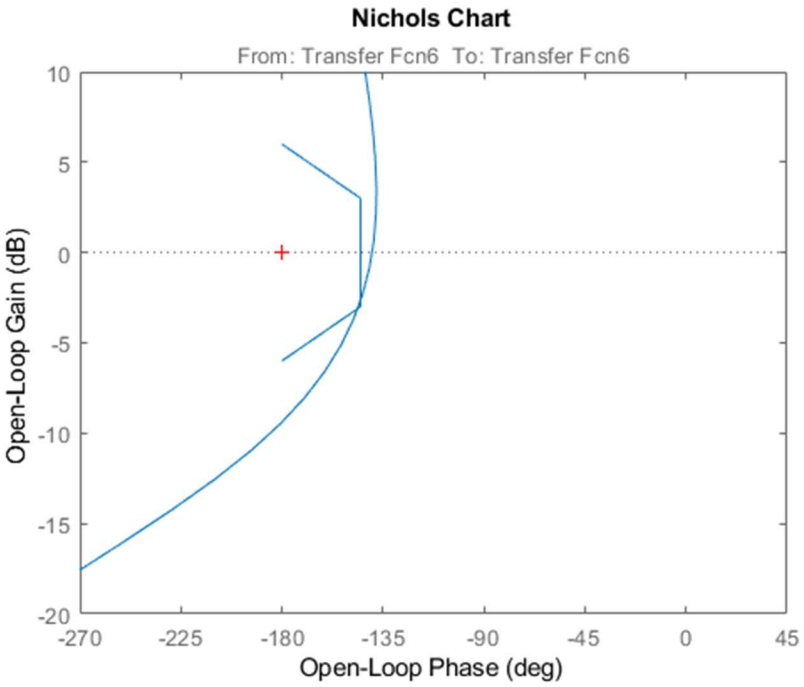

Figure 13.49 Elevator servo loop for pitch SMC controller

13.4 APPENDIX 4 (Proof of Stability for Lateral Acceleration SMC)

Stability is checked again using the Nichols Charts. Nichols Charts for p, r, ϕ, a_y, rudder and aileron loopbreaks are shown in Figures Figure 13.50, Figure 13.51, Figure 13.52, Figure 13.53, Figure 13.54, and Figure 13.55.

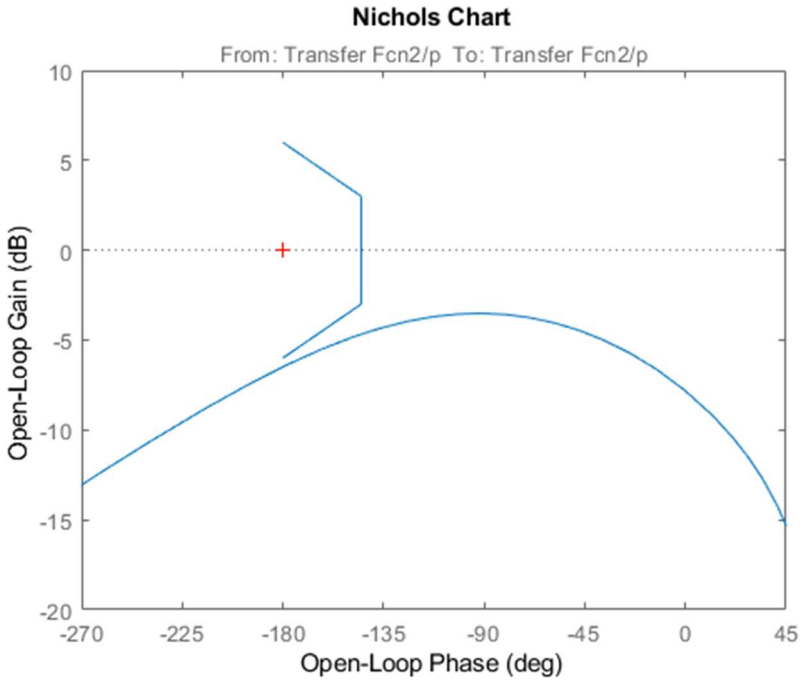

Figure 13.50 p loop for lateral SMC controller

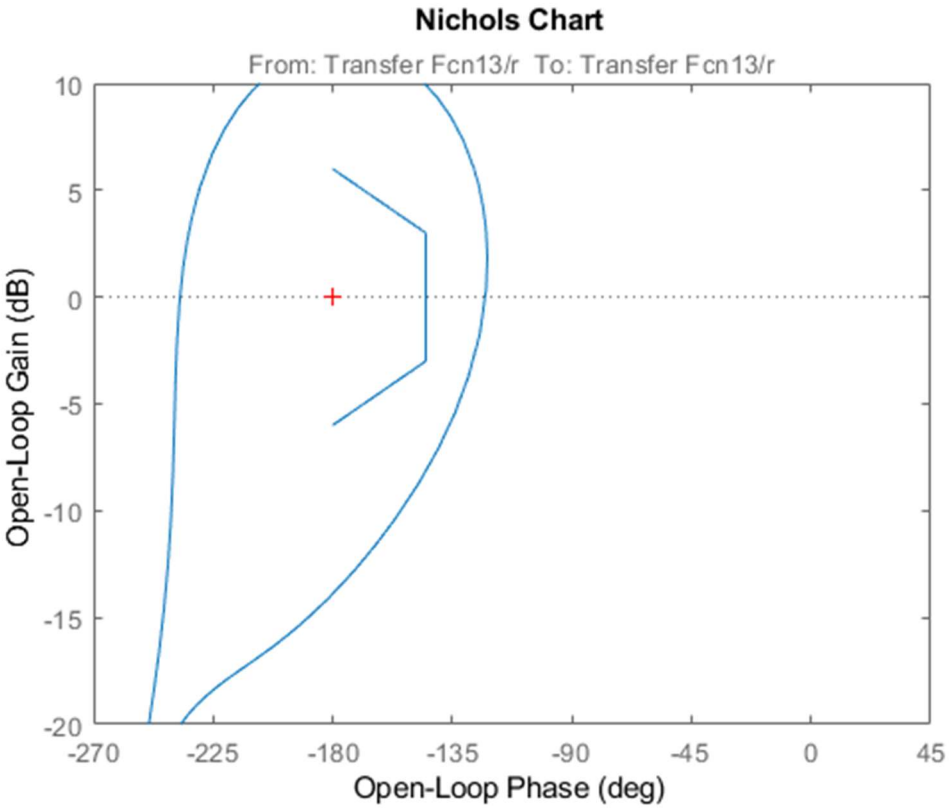

Figure 13.51 r loop for lateral SMC controller

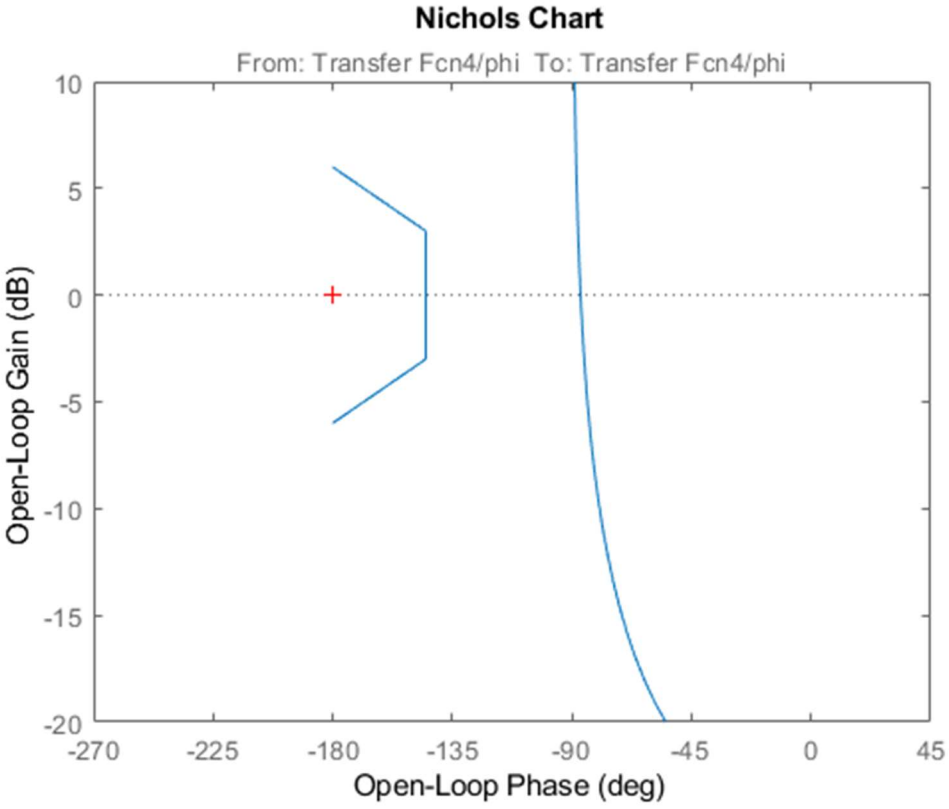

Figure 13.52 phi loop for lateral SMC controller

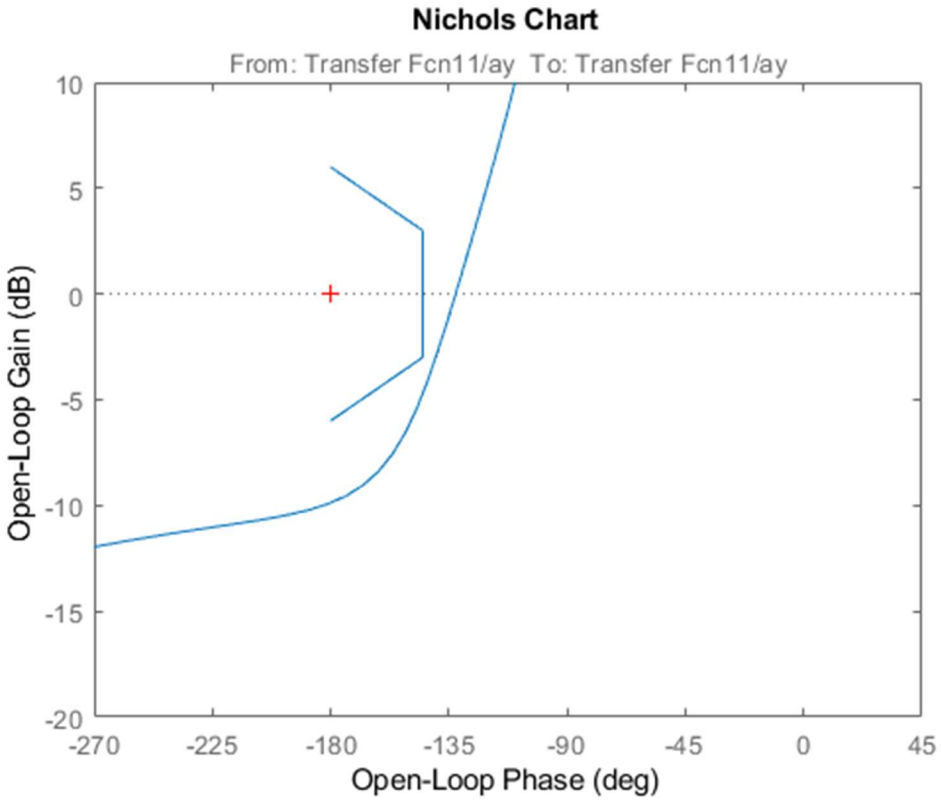

Figure 13.53 ay loop for lateral SMC controller

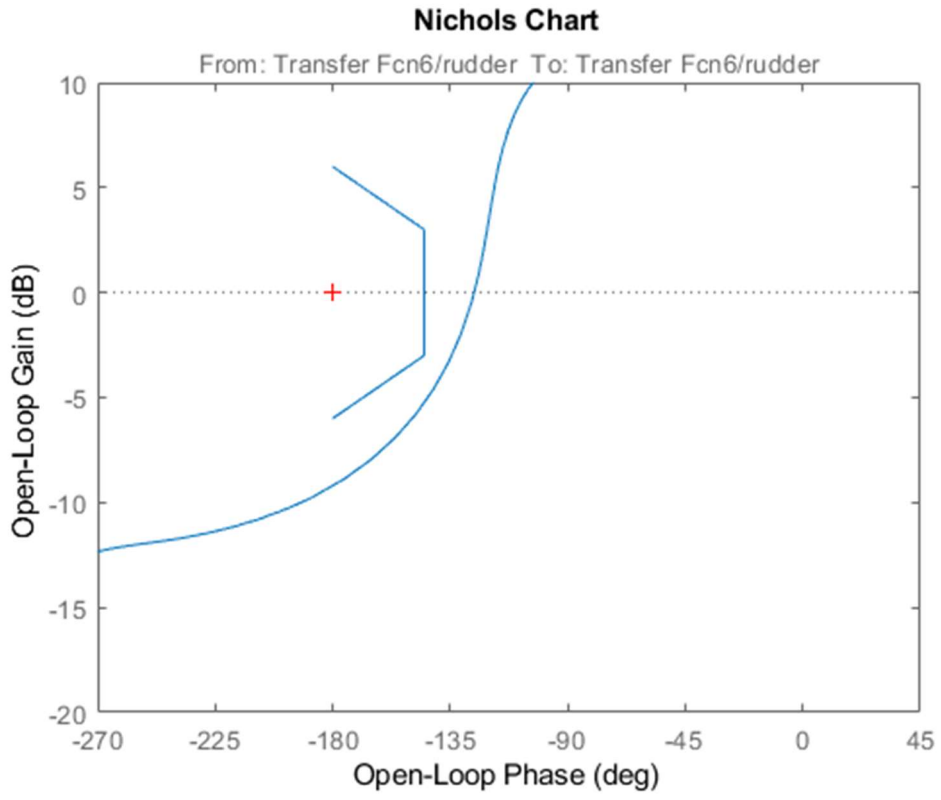

Figure 13.54 Rudder servo loop for lateral SMC controller

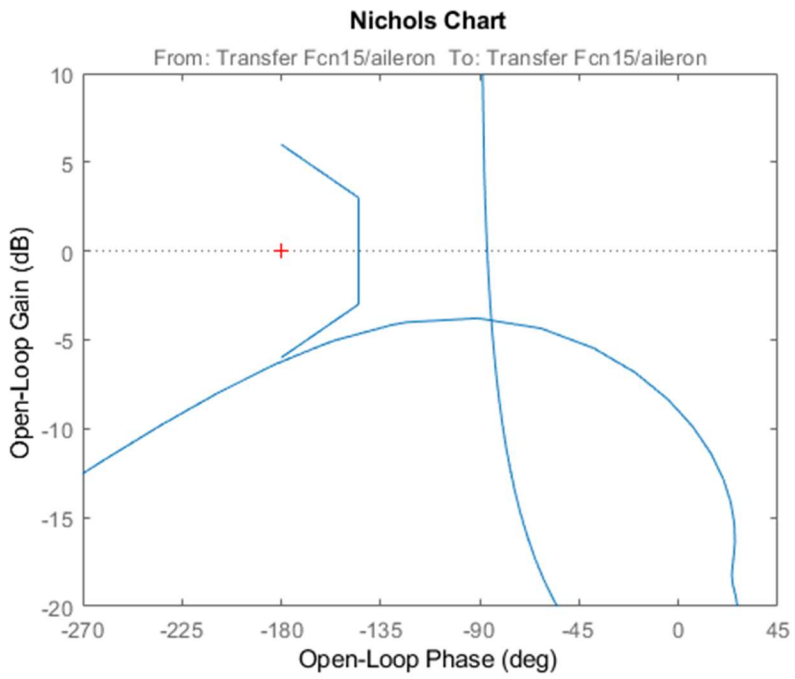

Figure 13.55 Aileron servo loop for lateral SMC controller

13.5 APPENDIX 5 (Proof of Stability for pitch angle PID controller)

Nichols charts for proof of stability of pitch PID controller are included in Figures Figure 13.56, Figure 13.57, and Figure 13.58. These charts are obtained by loopbreaks of q, θ, and elevator signals.

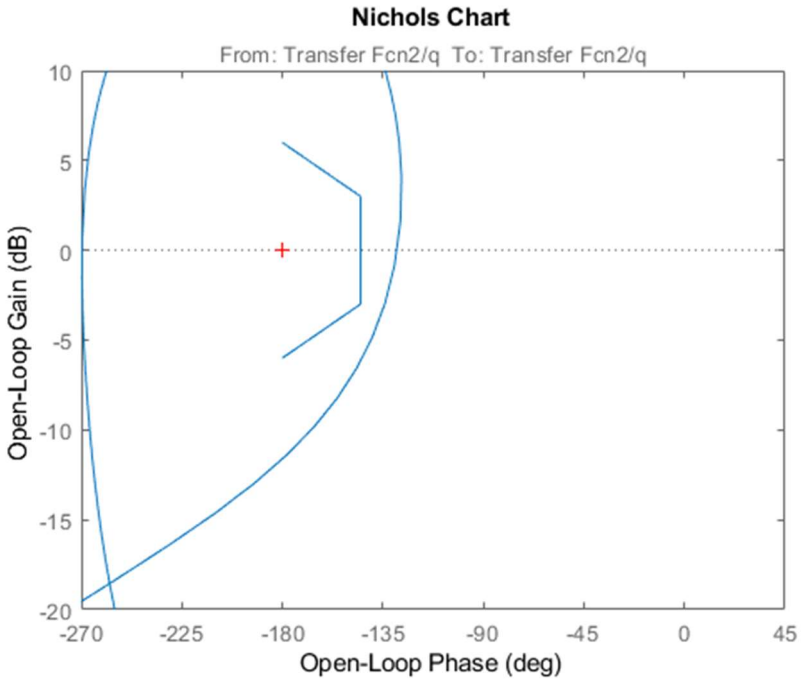

Figure 13.56 q loop for pitch PID controller

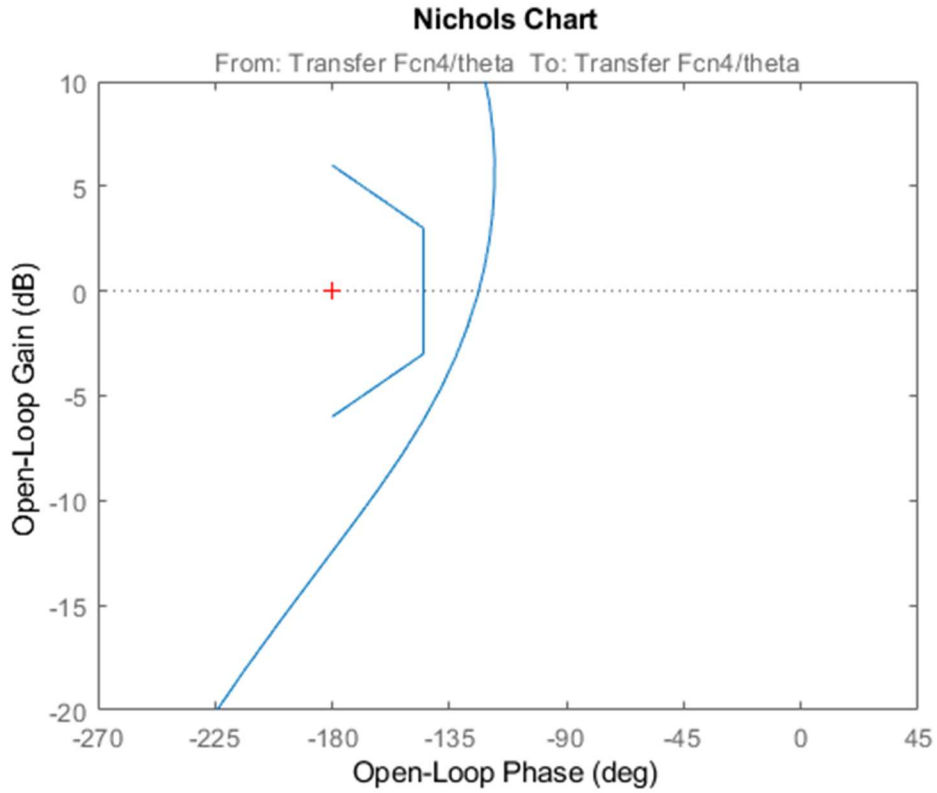

Figure 13.57 theta loop for pitch PID controller

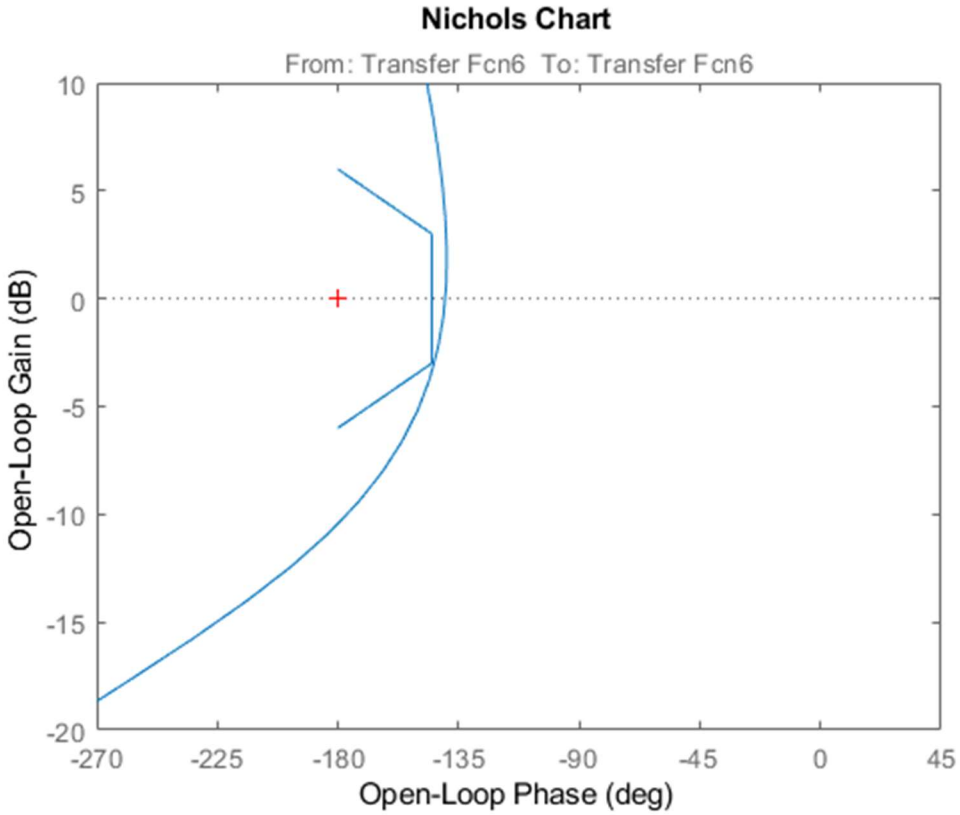

Figure 13.58 Elevator servo loop for pitch PID controller

13.6 APPENDIX 6 (Proof of Stability for Lateral PID Controller)

Nichols charts for proof of stability of pitch PID controller are included in Figures Figure 13.59, Figure 13.60, Figure 13.61, Figure 13.62, Figure 13.63, and Figure 13.64. These charts are obtained by loopbreaks of p, r, ϕ, a_y, rudder and aileron signals.

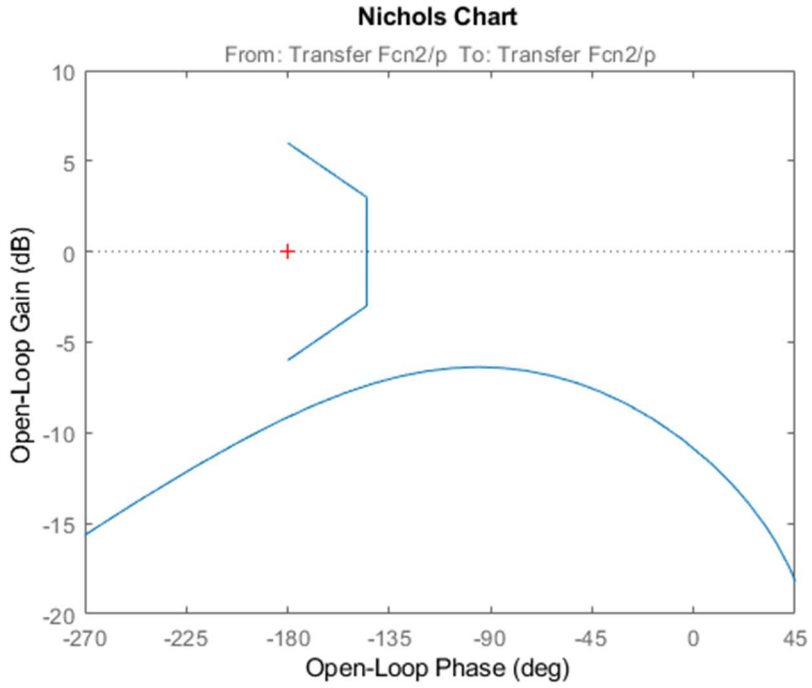

Figure 13.59 p loop for lateral PID controller

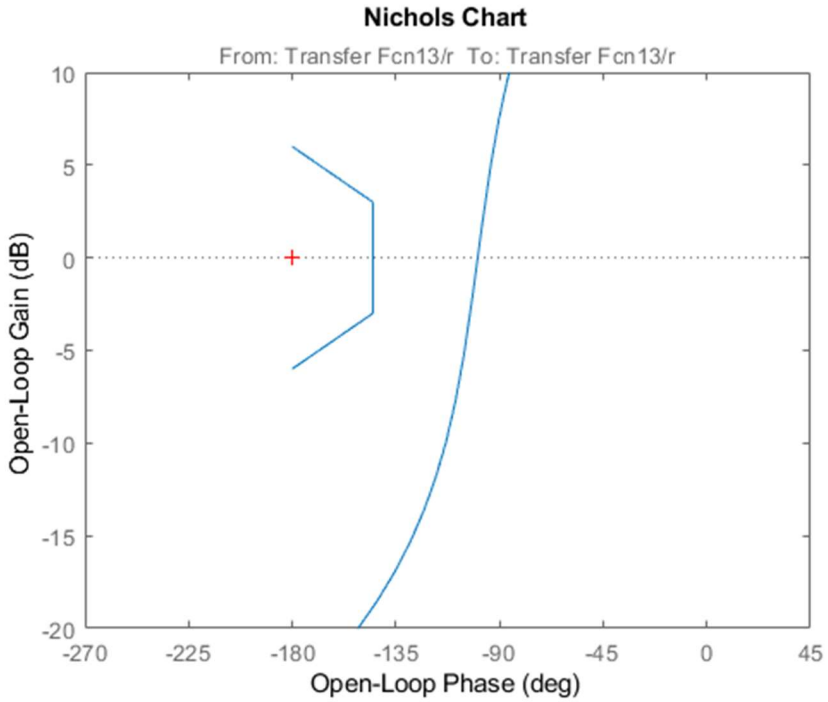

Figure 13.60 r loop for lateral PID controller

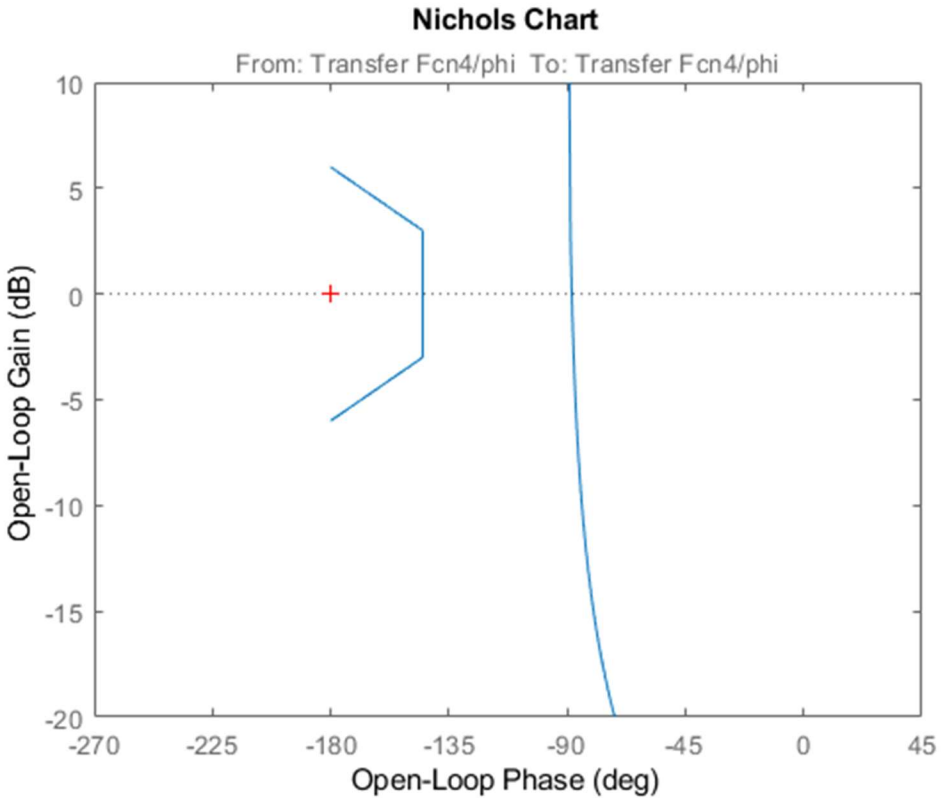

Figure 13.61 phi loop for lateral PID controller

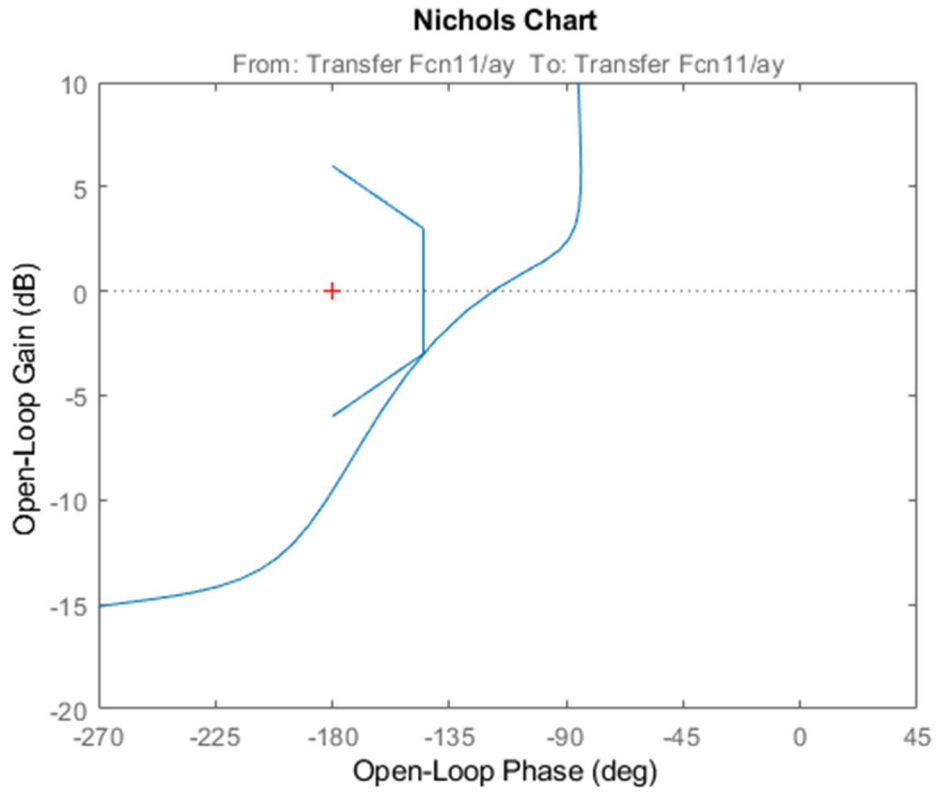

Figure 13.62 ay loop for lateral PID controller

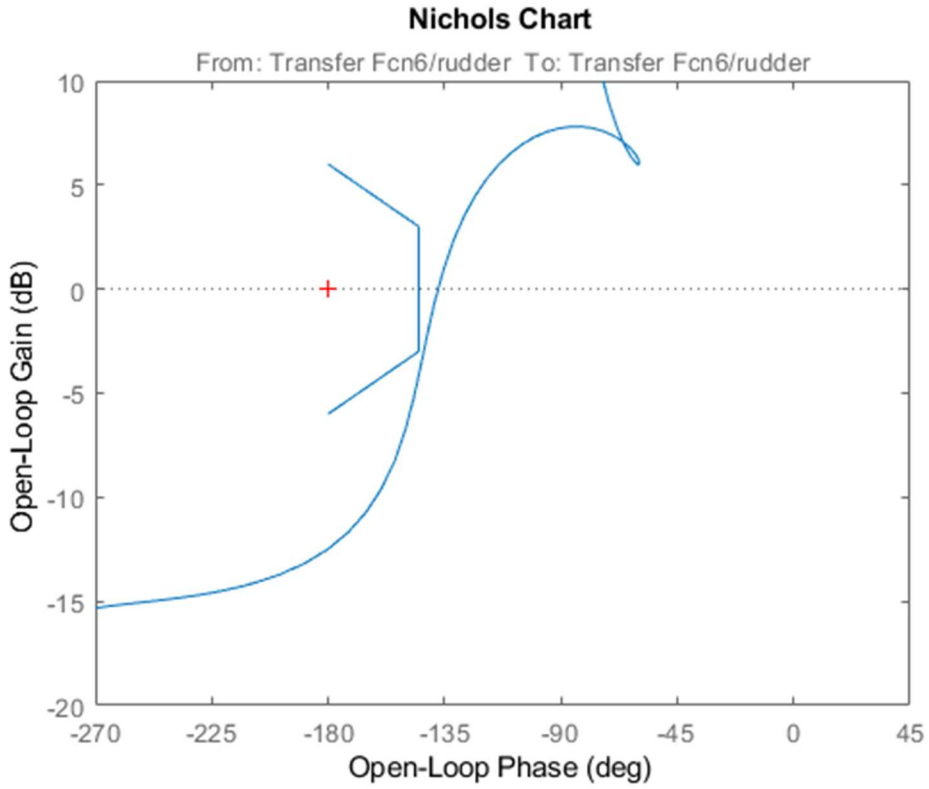

Figure 13.63 rudder servo loop for lateral PID controller

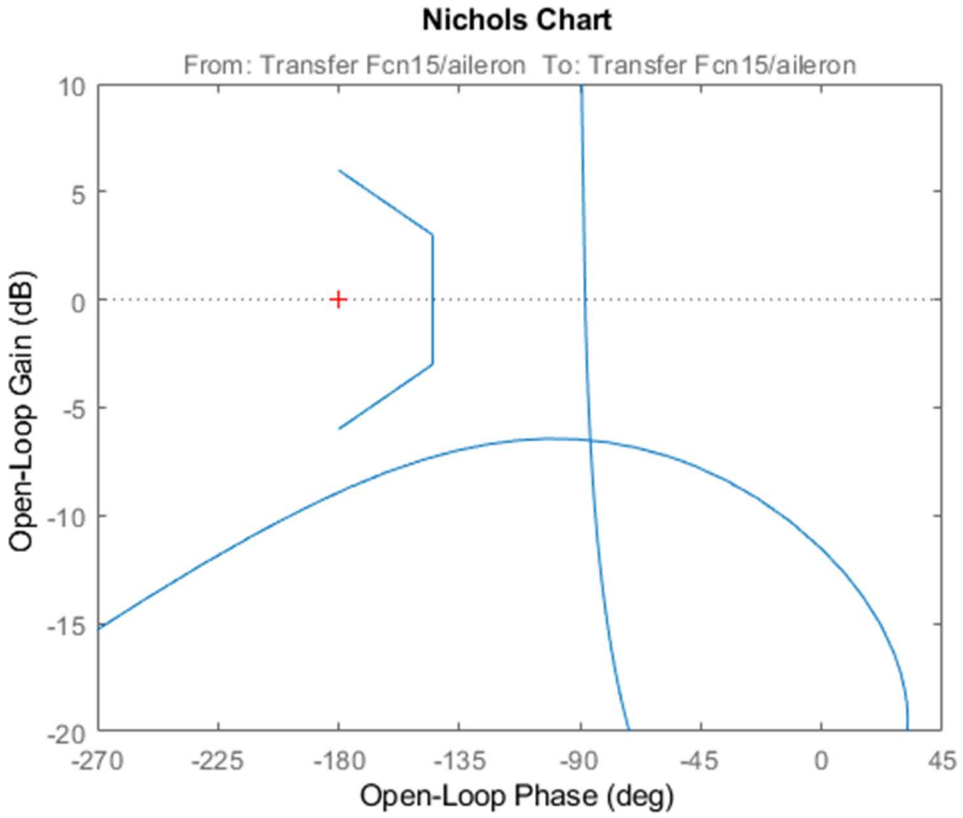

Figure 13.64 aileron servo loop for lateral PID controller

13.7 APPENDIX 7 (Variations of longitudinal two tires on the ground poles)

Variations of poles can be seen in Figures Figure 13.65 and Figure 13.66.

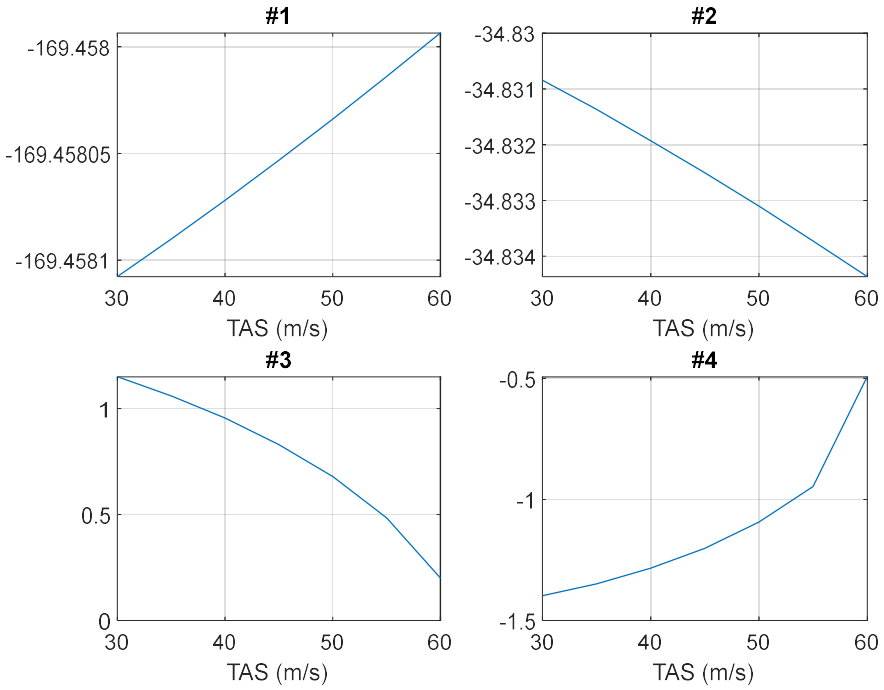

Figure 13.65 Poles of longitudinal 2 tires on the ground aircraft

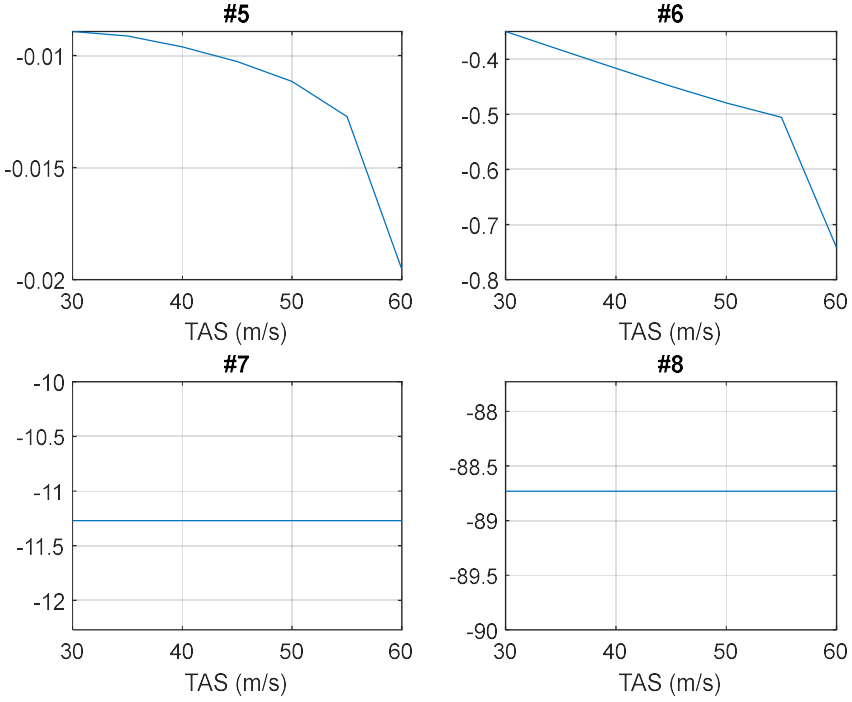

Figure 13.66 Longitudinal poles of 2 tires on the ground aircraft

13.8 APPENDIX 8 (Variations of lateral two tires on the ground poles)

Variations of poles can be seen in Figure 13.67.

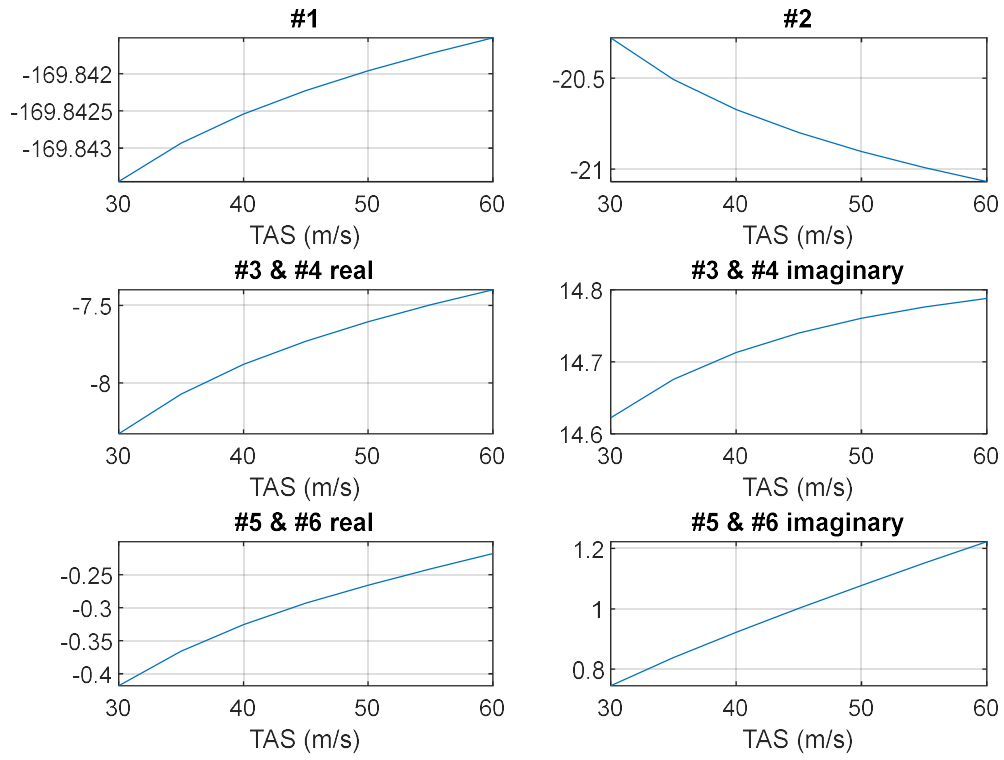

Figure 13.67 Lateral poles of 2 tires on the ground aircraft

13.9 APPENDIX 9 (Variations of longitudinal three tires on the ground poles)

Variations of poles can be seen in Figures Figure 13.68 and Figure 13.69.

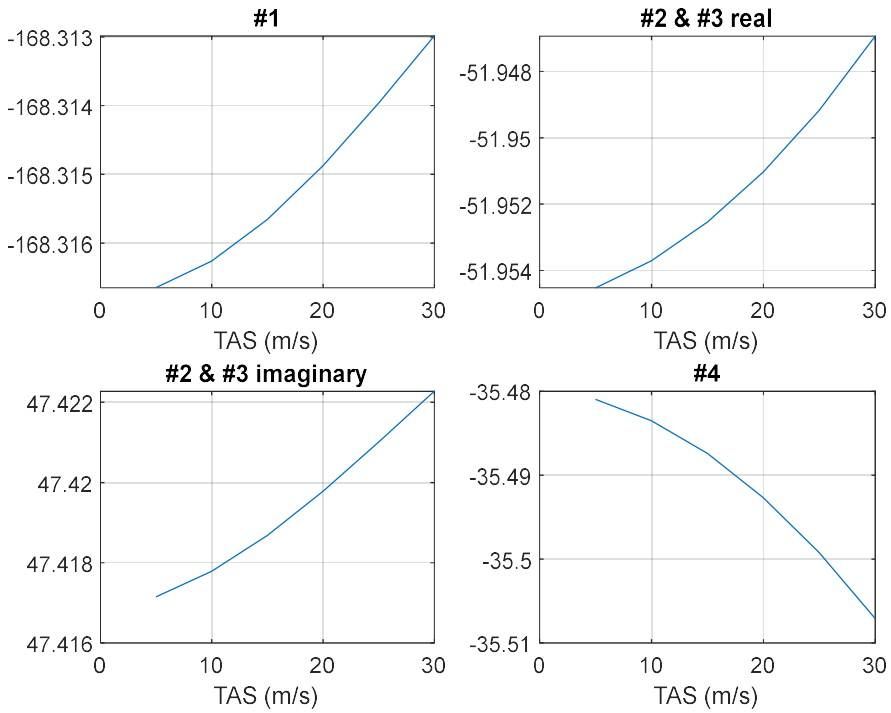

Figure 13.68 Longitudinal poles of 3 tires on the ground aircraft

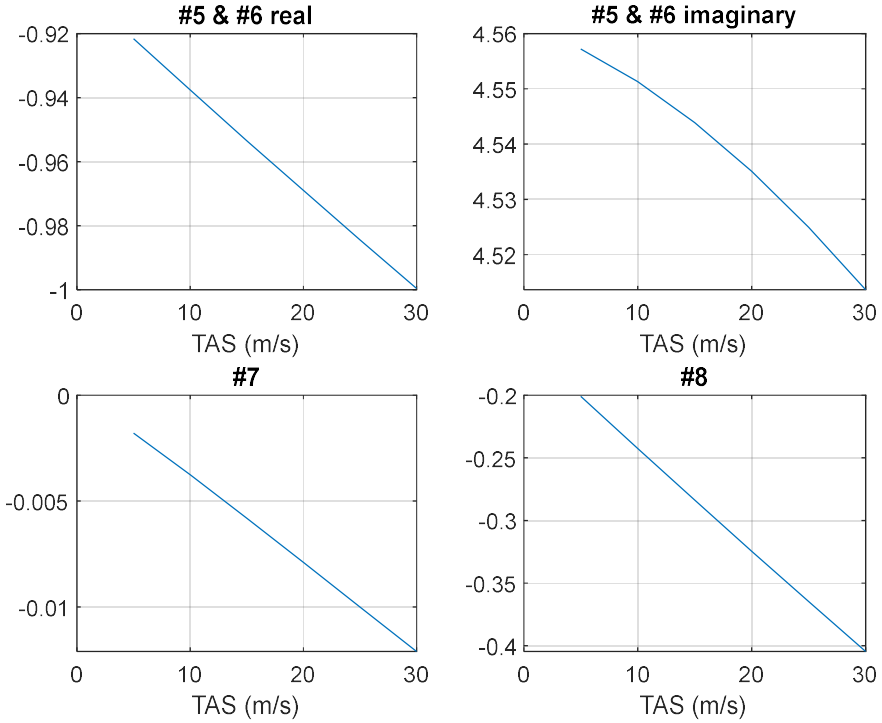

Figure 13.69 Longitudinal poles of 3 tires on the ground aircraft

13.10 APPENDIX 10 (Variations of lateral three tires on the ground poles)

Variations of poles can be seen in Figure 13.70.

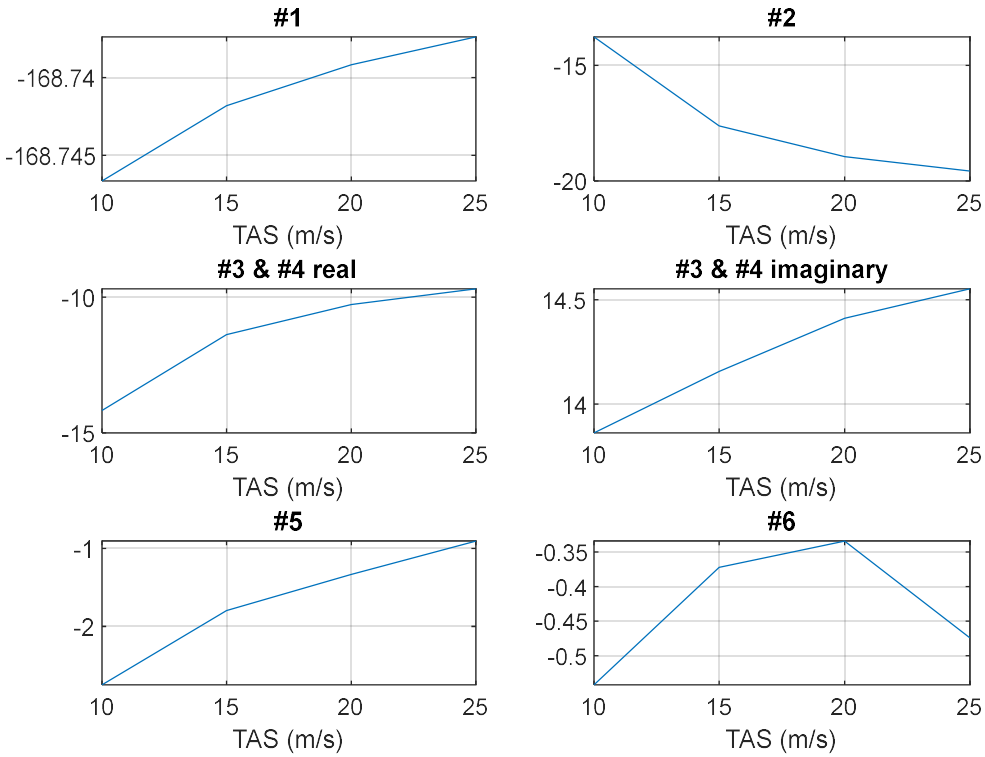

Figure 13.70 Lateral poles of 3 tires on the ground aircraft